

Table of content

Plenary talks	2
Talks	
Bio-Crystallography I: Signalling, macromolecular interactions and other new structures	4
Inorganic crystal structures I	6
Micro- and nanocrystalline materials (powder diffraction, EM, ...).....	9
in situ/in operando studies	12
Bio-Crystallography II: Crystallographic and hybrid methods	15
Small molecules at large facilities	17
Solid state physics in crystallography.....	19
Inorganic crystal structures II	22
Organic molecules and coordination compounds	25
Bio-Crystallography III: Enzymes.....	28
Bio-Crystallography IV: Structure-based drug design.....	31
Structure-property-relationships	33
Disordered Materials	36
Bio-Crystallography V: Instrumentation and methods	40
Extreme/non-ambient conditions	43
Instrumentation.....	46
Spectroscopy	49
Complex and aperiodic structures.....	52
Young Crystallographers: Lightning talks I.....	55
Young Crystallographers: Lightning talks II	63
Poster	
Bio-Crystallography I: Signalling, macromolecular interactions and other new structures	70
Bio-Crystallography III: Enzymes.....	71
Bio-Crystallography IV: Structure-based drug design.....	72
Bio-Crystallography V: Instrumentation and methods	74
Complex and aperiodic structures.....	76
Disordered Materials	79
Extreme/non-ambient conditions	80
in situ/in operando studies	82
Inorganic crystal structures.....	85
Instrumentation.....	105
Micro- and nanocrystalline materials (powder diffraction, EM, ...).....	109
Organic molecules and coordination compounds	112
Small molecules at large facilities	116
Solid state physics in crystallography.....	117
Spectroscopy	120
Structure-property-relationships	121
Author index.....	126

Plenary talks

P1

Development of electron diffraction techniques for *ab initio* crystal structure determination and phase analysis – from small molecules to proteinsX. Zou¹¹Stockholm University, Department of Materials and Environmental Chemistry, Stockholm, Sweden

Electron diffraction (ED) has unique advantages in studying nano- and micrometer-sized crystals, which are too small for X-ray diffraction [1]. Although *ab initio* structure solution using ED has already been demonstrated on inorganic and organic crystals since 1990s [2-3], it has not been widely used because of the concern about dynamical effects/multiple scattering and the difficulty to collect complete 3D data. The development of precession electron diffraction (PED) by Vincent & Midgley 1994 brought new insights in structure determination by ED [4]. Integrated intensities can be obtained by PED and the effects of dynamical effects were reduced when electron beam is tilted from zonal axes. Since 2007, new techniques for collecting integrated 3D microcrystal electron diffraction (MicroED) data have been developed; automated diffraction tomography (ADT) [5,6], rotation electron diffraction (RED) [7,8], continuous rotation electron diffraction [9-11]. They are used not only for *ab initio* structure solution of many novel inorganic [12-13] and organic [14-15] structures, but also for structure determination of protein microcrystals [9,10,16].

Here I will give an overview on the development of electron diffraction techniques, and show the current state-of-the-art ED techniques and their power for structure determination of novel inorganic, organic and protein crystals. Today, a complete dataset can be obtained in less than a minute on a standard TEM. The data processing, structure solution and refinement are performed using standard X-ray crystallography software. The data can be treated as kinematical data, and the refined structure models can reach better than 0.10 Å in accuracy for all non-H atoms. Using dynamical refinement, more accurate atomic positions can be determined and even hydrogen atoms can be located [17].

To further speed up and automate data collection, we have developed serial electron diffraction (*SerialED*) by taking ED patterns (snapshots) of individual particles [18]. ED patterns from more than > 3000 particles can be collected automatically in less than one hour! This provides new possibilities for studying very beam sensitive crystals. We developed methods and software for automated particle detection, data collection and processing, and indexing. The large number of particles makes it possible for phase analysis, and for detection of minor phases that may not be detectable even by X-ray diffraction. The development of new ED techniques has made large breakthroughs in science, which has recently gained enormous attentions [19].

[1] X. Zou, S. Hovmöller, P. Oleynikov, Electron Crystallography - Electron microscopy and electron diffraction, Oxford University Press, 2011. ISBN 978-0-19-958020-0.

[2] D.L. Dorset, Structural Electron Crystallography, Plenum Press, New York, 1995. ISBN 0-306-45049-6.

[3] T.E. Weirich, X. Zou, R. Ramlau, A. Simon, G. L. Cascarano, C. Giacovazzo, S. Hovmöller, Acta Cryst. 2000, A56, 29.

[4] Vincent, R. & Midgley, P. A. *Ultramicroscopy*, 1994, 53, 271.

[5] U. Kolb, T. Gorelik, C. Kübel, M.T. Otten, D. Hubert, *Ultramicroscopy*, 2007, 107, 507.

[6] U. Kolb, T. Gorelik, M.T. Otten, *Ultramicroscopy* 2008, 108, 763.

[7] D. Zhang, S. Hovmöller, P. Oleynikov, X. Zou, *Z. Kristallogr.* 2010, 225, 94.

[8] W. Wan, J.L. Sun, J. Su, S. Hovmöller, X. Zou, *J. Appl. Cryst.* 2013, 46, 1863.

[9] I. Nederlof, E. van Genderen, Y. Li, J.P. Abrahams. *Acta Crystallogr.* 2013, D69, 1223.

[10] B.L. Nannenga, D. Shi, A.G.W. Leslie, T. Gonen, *Nat. Methods* 2013, 11, 927-930.

[11] M. Gemmi, M.G.I. La Placa, A.S. Galanis, E.F. Rauch, S. Nicolopoulos, *J. Appl. Crystallogr.* 2015, 48, 718.

[12] D. Denysenko, M. Grzywa, M. Tonigold, B. Schmitz, E. Mugnaioli, U. Kolb, D. Volkmer et al. *Chem. Eur. J.* 2010, 17, 1837.

[13] R. Martínez-Franco, M. Moliner, Y. Yun, J. Sun, W. Wan, X. Zou, A. Corma, *Proc. Natl. Acad. Sci.* 2013, 110, 3749.

[14] U. Kolb, E. Mugnaioli, T. Gorelik, A. Stewart *Polymer Reviews*, 2010, 50, 385.

[15] Y. Zhang, J. Su, H. Furukawa, Y. Yun, F. Gándara, A. Duong, X. Zou, O. Yaghi, *J. Am. Chem. Soc.* 2013, 135, 16336.

[16] H. Xu, H. Lebrette, T. Yang, V. Srinivas, S. Hovmöller, M. Högbom, X. Zou, *Structure*, 2018, 26, 1.

[17] L. Palatinus, P. Brázda, P. Boullay, O. Perez, M. Klementová, S. Petit, V. Eigner, M. Zaarour, S. Mintova *Science* 2017, 355, 166.

[18] S. Smeets, X. Zou, W. Wan, *J. Appl. Cryst.* 2018, 51, 1262.

[19] <https://vis.sciencemag.org/breakthrough2018/>; A. Brown, J. Clardy, *Nature* 2018, 564, 348-349.

P2

Order in 'disorder': a modulation wave approach to the crystal chemical understanding, modelling and interpretation of structured diffuse scattering.R. Withers¹¹The Australian National University, Research School of Chemistry, College of Science, Acton, Canberra, Australia

The widespread class of 'disordered' crystalline materials are often characterized by weak, highly anisotropic, structured diffuse scattering accompanying the strong Bragg reflections of well-defined, underlying average structures (see *e.g.* [1]). Such diffuse scattering comes in all shapes, sizes and complexities, from all types of materials (organic, inorganic, biological) and for a myriad of different reasons. Examples include compositionally 'disordered' solid solutions, inherently flexible framework structures, solid electrolytes, ferroic phases, materials susceptible to electronically driven structural instabilities *etc.* exemplified below by <-110> electron diffraction patterns (EDP's) of (a) K3MoO3F3 and (b) SiO2-tridymite (above 250°C) and (c) the [001] zone axis EDP characteristic of ThAsSe. The physical and phase transition properties of many such materials are often intimately connected with the 'disorder' so it is important, and rewarding, to take it into account, particularly with the rapid development of new detectors and new tomographic approaches to data measurement.

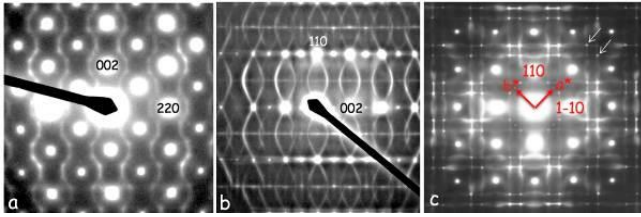
To gain insight into both the very local order, as well as the much longer range order hidden in disordered materials of this type it is very helpful to use the language of modulated structures. Such an approach automatically emphasizes the close relationship between the crystallography of disordered structures and aperiodic crystallography in general. In this contribution, the use of such an approach will be exploited to understand, model and interpret the often highly structured 3-D shapes of such diffuse distributions as well as to describe what it tells us about the underlying crystal chemistry and real space ordering rules responsible. Several such systems of the type mentioned in para 1 above will be discussed in detail.

References:

[1] Withers, R. *IUCrJ* 2(1) (2015) 74-84.

Fig. Legend: EDP's of (a) $K_3MoO_3F_3$ and (b) SiO_2 -tridymite (above $250^\circ C$). (c) an $[001]$ EDP of ThAsSe.

Figure 1



Bio-Crystallography I: Signalling, macromolecular interactions and other new structures

S01-01

Of rats and men: Insight into homologous cytomegalovirus IE1 structures

J. Schweininger¹, Y. A. Muller¹

¹Friedrich-Alexander-Universität Erlangen-Nürnberg, Division of Biotechnology, Erlangen, Germany

Introduction

Cytomegalovirus (CMV) infections are a threat to newborn children and immunocompromised patients, while infections in healthy individuals are usually asymptomatic. CMV has evolved strategies to evade antiviral defense systems and to persist in the host for life [1]. CMV replication is initially antagonized by intrinsic immune defense mechanisms mediated by nuclear domain 10 (ND10) structures within the nucleus. The formation of these complexes is, however, dependent on SUMO modification of its main component PML (promyelocytic leukemia protein) [2]. To counteract the ND10-mediated immunity, the CMV immediate early protein 1 (IE1) is expressed and transferred to the nucleus. The globular CORE domain of IE1 interacts with the coiled-coil region of PML and inhibits its *de novo* SUMOylation. This leads to a loss of functional ND10 bodies and the associated antiviral effects [3]. With the crystal structure of the rhesus monkey CMV IE1 CORE domain, our group has previously solved the first structure of a CMV IE1 protein ([2], PDB: 4WID).

Objectives

This work is aimed to further our understanding of the CMV IE1 structure and thereby the molecular determinants of its function and specificity.

Results

We have solved crystal structures of the rat and human cytomegalovirus IE1 CORE domains at 3.4 and 3.0 Å resolution, respectively. The structures were solved using Se-MAD and molecular replacement. Methionine and cysteine positions in the final models were further validated with anomalous maps derived from Se peak and 6 keV X-ray data. Despite sequence identities as low as 16 % between rat and human/rhesus monkey CMV IE1, the three structures show a common overall shape, size and architecture.

Conclusions

Our results give further insight into the structure of CMV IE1 from different species and will provide a framework for future *in vivo* and *in vitro* studies by us and our collaborators (group of Prof. Dr. Thomas Stamminger, Ulm University).

[1] M. Scherer, T. Stamminger (2014), *Fut Virol.* **9**, 415-430

[2] M. Scherer, S. Klingl, M. Sevvana, V. Otto, E-M. Schilling, J. D. Stump, R. Müller, N. Reuter, H. Sticht, Y. A. Muller, T. Stamminger (2014), *PLoS Pathog.* **10**(11): e1004512

[3] E-M. Schilling, M. Scherer, N. Reuter, J. Schweininger, Y. A. Muller, T. Stamminger (2017), *J Virol.* **91**, e02049-16.

S01-03

A molecular embrace – crystal structure of a DNA repair factor complex

J. Jia¹, E. Absmeier¹, A. J. Pietrzyk-Brzezinska^{1,2}, M. C. Wahl^{1,3}

¹Freie Universität Berlin, Department of Biology, Chemistry, Pharmacy, Berlin, Germany

²Lodz University of Technology, Institute of Technical Biochemistry, Lodz, Poland

³Helmholtz-Zentrum Berlin, Macromolecular Crystallography, Berlin, Germany

Human activation signal cointegrator complex (ASCC) is composed of four subunits, ASC-1, ASCC1, ASCC2 and ASCC3^{1,2}. It was originally identified as coactivator of nuclear receptors³ and later found to be involved in down-tuning of cellular anti-viral responses⁴, regulation of myogenic differentiation⁵ and DNA dealkylation repair^{2,6}. For DNA dealkylation repair, the ASCC3 subunit, a member of the superfamily 2 nucleic acid helicases with 3"-5" DNA helicase activity, is thought to provide single-stranded DNA as a substrate for dealkylation by the α -ketoglutarate-dependent dioxygenase, ALKBH3². Except for an unpublished NMR structure of a CUE domain in ASCC2 (PDB ID 2DIO), the structures and modes of interactions among the ASCC subunits are presently unknown. We experimentally delineated interacting regions among the components and determined a crystal structure of a portion of the ASCC2 subunit in complex with a fragment of ASCC3. The ASCC3 fragment comprises a central helical domain and two terminals, extended arms with which it embraces the compact ASCC2 unit. Based on the structure, we delineated which residues and regions of the interacting protein portions are required for complex formation. While the ASCC2 subunits has previously been implicated in the recruitment of the repair complex to damage sites⁶, our results have implications for how ASCC2 might also directly regulate ASCC3 helicase activity, and thus DNA dealkylation repair by ALKBH3.

References

[1] Jung DJ *et al.* (2002) Novel transcription coactivator complex containing activating signal cointegrator 1. *Mol Cell Biol* **22**, 5203-5211.

[2] Dango S *et al.* (2011) DNA unwinding by ASCC3 helicase is coupled to ALKBH3-dependent DNA alkylation repair and cancer cell proliferation. *Mol Cell* **44**, 373-384.

[3] Kim HJ *et al.* (1999) Activating signal cointegrator 1, a novel transcription coactivator of nuclear receptors, and its cytosolic localization under conditions of serum deprivation. *Mol Cell Biol* **19**, 6323-6332.

[4] Li J *et al.* (2013) A short hairpin RNA screen of interferon-stimulated genes identifies a novel negative regulator of the cellular antiviral response. *MBio* **4**.

[5] Knierim E *et al.* (2016) Mutations in subunits of the activating signal cointegrator 1 complex are associated with prenatal spinal muscular atrophy and congenital bone fractures. *Am J Hum Genet* **98**, 473-489.

[6] Brickner JR *et al.* (2017) A ubiquitin-dependent signalling axis specific for ALKBH-mediated DNA dealkylation repair. *Nature* **551**, 389-393.

S01-04

Solute Binding Proteins and their cognate ligands: Structure, Function and their role in functional annotation

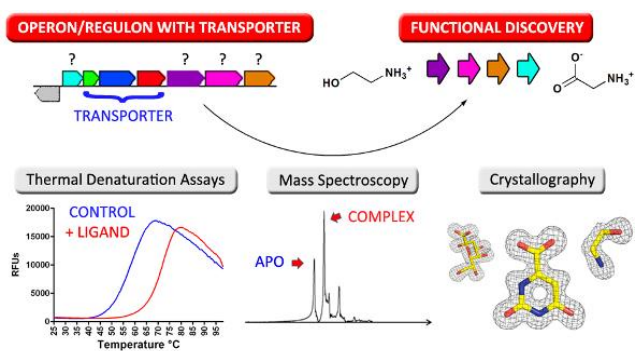
U. Yadava¹

¹DDU Gorakhpur University, Physics, gorakhpur, India

The uptake of exogenous solutes are mediated by transport systems embedded in the plasma membrane and drive active transport even at μ M to nM solute concentrations. In many of these systems a periplasmic Solute-Binding Protein (SBP) is utilized to bind their

cognate ligands with high affinity and deliver them to the membrane bound translocator subunits. Knowledge of the cognate ligand for the SBP component of the transporter can provide crucial data for functional assignment of co-located or co-regulated genes. In the present study, the structural and functional characterizations of several solute binding proteins have been carried out. Proteins were cloned from genomic DNA, expressed by autoinduction, and purified by a combination of Ni-NTA and size exclusion chromatography. The purified SBPs were screened using differential scanning fluorometry (DSF) and about 400 compounds ligand library. Two of the SBPs exhibited DSF hits that were novel for their respective transport family. Crystallization trials of proteins have been conducted with their respective DSF ligand hits. Those SBPs that have structures determined and their respective interactions with co-crystallized ligands will be presented. Co-crystallization with DSF determined ligands resulted in structures of Avi_5305 in complex with D-glucosamine and D-galactosamine, the first structure of an ABC SBP with an amino sugar.

Figure 1



S01-05

X-ray and cryo-EM structural studies of viral hijacking of the Cullin4-RING ligase ubiquitin-proteasome pathway

S. Banchenko¹, F. Krupp¹, C. Gotthold¹, C. Spahn¹, D. Schwefel¹
¹Charité - Universitätsmedizin Berlin, Institut für Medizinische Physik und Biophysik, Berlin, Germany

Lentiviruses use the host's ubiquitination machinery to overcome the effect of cellular defense proteins that inhibit virus replication. One such restriction factor, SAMHD1, inhibits HIV-1 infection of myeloid-lineage cells and resting T cells by depleting their dNTP pool. Certain lentiviruses, such as HIV-2 and some SIVs, encode the accessory proteins x (Vpx) or r (Vpr) that recruit SAMHD1 to the host's Cullin4-RING E3 ligase to target SAMHD1 for ubiquitination and proteasomal degradation [1].

Cullin-RING E3 ligases (CRLs) are the largest family of E3 ligases in eukaryotes. CRLs consist of a Cullin scaffold protein and a catalytic RING subunit, Rbx1 or Rbx2 [2, 3]. Additionally, CRLs recruit different adaptor proteins, which in turn bind to exchangeable substrate receptors. Previous X-ray structural studies of protein complexes Vpx/DCAF1/SAMHD1 C-terminus and Vpr/DCAF1/SAMHD1 N-terminus shed light on the structural basis of the interaction between host restriction factor, CRL4 and virus protein [4, 5]. However, they do not fully explain the molecular mechanism by which these viral proteins are able to usurp the host cell's ubiquitination machinery. In our current studies, we explore these mechanisms, focusing on the SIV Vpr/CRL4 complex by combining the X-ray crystallography, cryo-electron microscopy (cryo-EM), and proteomics.

To date we crystallized a DDB1/DCAF1/Vpr complex, and solved the structure at 2.6 Å resolution. Currently we are crystallizing DDB1/DCAF1/Vpr/SAMHD1 complexes. We also collected initial negative stain and cryo-EM low-resolution micrographs of CRL4 scaffold and catalytic subunit, but high-resolution cryo-EM data analysis is ongoing.

Ultimately, we do not restrict our research to viral hijacking of CRL4. We also explore a variety of CRL4 substrate receptors and their endogenous and non-endogenous interaction partners, to obtain molecular insights into the principles of substrate-specific recognition in the CRL4 system.

[1] H. Baldauf, X. Pan, E. Erikson, S. Schmidt, ... O. T. Keppler, *Nat Med*, **18**, (2012), 16-82-1689
 [2] M. B. Metzger, V. A. Hristova, A. M. Weissman, *J Cell Sci*, **125**, (2012), 531-537. 1. 3. E. S. Zimmermann, B. A. Schulman, N. Zheng, *Curr Opin Struct Biol*, **20**, (2010), 714-721. 4. D. Schwefel, H. C. T Groom, V. C. Boucherit, E. Christodoulou, P. A. Walker, J. P. Stoye, K. N. Bishop, I. A. Taylor, *Nature*, **505**, (2014), 234-238. 5. D. Schwefel, V. C. Boucherit, E. Christodoulou, P. A. Walker, J. P. Stoye, K. N. Bishop, I. A. Taylor, *Cell Host Microbe*, **17**, (2015), 489-499.

S01-06

Activation mechanism of the receptor tyrosine kinase MET: New crystallographic support for ligand-mediated receptor dimerization

H. Niemann¹
¹Universität Bielefeld, Fakultät für Chemie, Bielefeld, Germany

Receptor tyrosine kinases (RTKs) are single-pass transmembrane proteins. The paradigm of RTK activation suggests that resting RTKs are monomeric while binding of agonistic ligands to the extracellular domain results in RTK dimerization that enables autophosphorylation of the intracellular kinase domains. The receptor tyrosine kinase MET plays a pivotal role in vertebrate development and tissue regeneration; its deregulation contributes to cancer. The structural basis of ligand-induced MET dimerization by its natural ligand hepatocyte growth factor (HGF) is not well understood. MET is also targeted by the facultative intracellular bacterium *Listeria monocytogenes* during infections. Interesting insight into the molecular mechanism of MET dimerization has emerged from crystal structures of MET in complex with the bacterial agonist, the invasion protein internalin B (InIb).

Data from different experimental methods including X-ray crystallography, small angle X-ray scattering, cellular receptor activation assays and super resolution fluorescence microscopy converge on a model, in which the monomeric bacterial MET agonist InIb binds with high affinity to membrane-bound MET receptors on the cell. The 1:1 MET:InIb complexes then diffuse within the plane of the membrane and form low-affinity 2:2 complexes facilitated by reducing the dimensionality of diffusion from three to two dimensions. Formation of the 2:2 complex is mediated by a small homodimerization contact of InIb that is too weak to drive dimerization in solution. Due to the high protein concentration in crystals, crystallography is ideally suited to visualize such low-affinity interactions as in the signalling-active 2:2 MET:InIb complex. A recent low-resolution (6.5 Å) crystal structure of MET in complex with InIb and a crystallization chaperone corroborates our structural model of receptor dimerization. The new structure further suggests that the receptor also contributes to homodimerization through formation of an additional low-affinity contact in a membrane-proximal domain.

Inorganic crystal structures I

S02-01

The $[\text{Ag}_2\text{Hg}_2]^{4+}$ cluster cation in rudabányaite, a new mineral from the Rudabánya ore depositH. Effenberger¹, S. Szakáll², B. Fehér³, T. Váczi^{4,5}, N. Zajzon²¹Universität Wien, Institut für Mineralogie und Kristallographie, Wien, Austria²University of Miskolc, Institute of Mineralogy and Geology, Miskolc-Egyetemváros, Hungary³Herman Ottó Museum, Department of Mineralogy, Miskolc, Hungary⁴Eötvös Loránd University, Department of Mineralogy, Budapest, Hungary⁵Hungarian Academy of Sciences, Wigner Research Centre for Physics, Budapest, Hungary

Recently the new mineral rudabányaite, $[\text{Ag}_2\text{Hg}_2][\text{AsO}_4]\text{Cl}$, was found in cavities of siliceous sphaerosiderite and limonite rocks at the Rudabánya ore deposit (North-East Hungary). The crystal-structure investigation was performed on single-crystal X-ray data (refinements on F^2 , $wR2(F^2) = 0.068$, $R1(F) = 0.031$ for 972 unique data, 53 variable parameters; space group $F\bar{4}3c$, $a = 17.360(3)$ Å, $V = 5231.8$ Å³, $Z = 32$).

The crystal structure is characterized by two crystallographically different tetravalent 4-center 2-electron bonded cluster cations $[\text{M}_4]^{4+}$; $M = (\text{Ag}, \text{Hg})$, $\text{Ag}:\text{Hg} \sim 1:1$, $M-M = 2.62$ to 2.75 Å. Small amounts of the M atoms are displaced by ~ 0.5 Å. Obviously it correlates with some slow change of the colour in natural light. Raman spectra taken in distinctly coloured areas showed some differences mainly for the band at ~ 119 cm⁻¹.

Topologically, the barycentres of the $[\text{M}_4]^{4+}$ clusters and the $[\text{AsO}_4]$ tetrahedra form a cubic primitive lattice with $a' = \frac{1}{2}a = 8.68$ Å; half of the voids are occupied by Cl atoms. Thus, rudabányaite is related to half Heusler compounds. Rudabányaite exhibits strong crystal chemical, structural, and topological similarities to tillmannsite, $[\text{Ag}_3\text{Hg}][(\text{V}, \text{As})\text{O}_4]$ [1,2]. Even in both minerals Ag and Hg atoms are disordered, $\text{Ag}:\text{Hg}$ is stoichiometric. In kuznetsovite ($[\text{Hg}_3][\text{AsO}_4]\text{Cl}$, space group $P2_13$, $a = 8.3983(6)$ Å), trigonal $[\text{Hg}_3]^{4+}$ clusters substitute the larger $[(\text{Hg}, \text{Ag})_4]^{4+}$ metal clusters of rudabányaite [3,4]. The two synthetic compounds exhibiting tetrahedral cationic clusters, *i.e.*, $[\text{Ag}_2\text{Hg}_2]_3[\text{VO}_4]_4$ and $[\text{Ag}_2\text{Hg}_2]_2[\text{HgO}_2][\text{AsO}_4]$, display stoichiometry but disorder of the M atoms [5]. However, in the double-tetrahedron $[\text{Ag}_2\text{Hg}_4]$ in $[\text{Ag}_2\text{Hg}_4][\text{XO}_4]_2$ ($X = \text{P}, \text{As}$) the Ag and Hg atoms are ordered [6]. New in rudabányaite is the partial displacement of the M atoms.

[1] H Sarp *et al.*: Eur J Mineral **15** (2003) 177[2] LP Solov'eva *et al.*: Kristallografiya **36** (1991) 1292[3] GV Romanenko *et al.*: J Struct Chem **40** (1999) 270[4] M Weil: Z Naturforsch **56b** (2001) 753[5] M Weil *et al.*: Inorg Chem **44** (2005) 1443[6] M Weil: Z Naturforsch **58b** (2003) 1091

S02-02

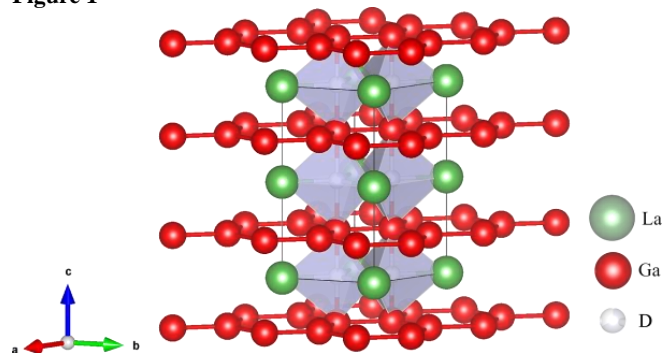
The Zintl-Phase hydride $\text{LaGa}_2\text{D}_0.71$ A. Werwein¹, H. Kohlmann¹, C. Benndorf², M. Bertmer³, A. Franz⁴, O. Oeckler²¹Universität Leipzig, Institut für Anorganik, Leipzig, Germany²Universität Leipzig, Fakultät für Chemie und Mineralogie, Leipzig, Germany³Universität Leipzig, Fakultät für Physik und Geowissenschaften, Leipzig, Germany⁴Helmholtz-Zentrum Berlin, Berlin, Germany

Zintl phases are polar intermetallic compounds formed by alkaline, alkaline earth metals or lanthanides M , and a main group element of group 13-16, X , forming polyanions X_n^- . The hydrogenation of

Zintl phases has attracted considerable interest recently, since the incorporation of hydrogen can influence the structure and the physical properties in manifold ways. Hydrogen may oxidize the polyanions, *e. g.* from X_n^- to $X_{(n-1)}^-$, thus increasing the number of covalent bonds of X atoms. SrAl_2H_2 was the first example, where the polyanion forms covalent element-hydrogen bonds. The aluminium atoms are arranged in hexagonal puckered layers and are terminated by hydrogen [1]. Many further AlB_2 related Zintl phase hydrides MX_2H_2 and MXEH ($M = \text{Ca}, \text{Sr}, \text{Ba}$; $X = \text{Al}, \text{Ga}$; $E = \text{Si}, \text{Ge}$) are known [2-4]. LaGa_2 (AlB_2 type) can be described by the limiting ionic formula $\text{La}^{3+}(\text{Ga}^-)_2$. In contrast to the electron-precise SrAl_2 , the compound LaGa_2 can be called a metallic Zintl phase or not electron-precise. The hydrogenation of LaGa_2 at 2 MPa hydrogen pressure and 573 K yields a new phase, with nearly identical X-ray powder diffraction pattern. A Rietveld refinement based on the structure model of LaGa_2 shows a reduced c lattice parameter ($4.4267(3) \rightarrow 4.33730(11)$ Å) while the a lattice parameter slightly increases. The neutron powder diffraction pattern of the deuteride of LaGa_2 shows superstructure reflections, which were not observed in X-ray data, indicating a doubling of c . Hydrogen atoms are located in trigonal-bipyramidal La_3Ga_2 voids and the Ga-D distances are $2.099(3)$ and $2.247(3)$, thus it can not be called covalent anymore, rather it should be described as a interstitial hydride. The superstructure can be explained by an ordering of the deuterium atoms. Density functional theory calculations revealed that the density of states at the Fermi level is dominated by d electrons from lanthanum, emphasizing the metallic character of LaGa_2 , while LaGa_2H shows a small pseudo gap at the Fermi level suggesting a small band semiconductor.

[1] F. Gingl, T. Vogt, E. Akiba, *J. Alloys Compd.* **2000**, *306*, 127-132[2] T. Björling, D. Noréus, U. Häussermann, *J. Am. Chem. Soc.* **2006**, *128*, 817-824[3] U. Häußermann, *Z. Kristallogr.* **2008**, *223*, 628-635[4] M. H. Lee, T. Björling, B. C. Hauback, T. Utsumi, D. Moser, D. Bull, D. Noréus, Otto F. Sankey, U. Häussermann, *Phys. Rev. B* **2008**, *78*, 195209

Figure 1



S02-03

The New Trisilicide BaSi_3 : High Pressure Synthesis, Crystal Structure and Chemical BondingJ. M. Hübnér¹, L. Akselrud¹, W. Schnelle¹, U. Burkhardt¹, M. Bobnar¹, Y. Prots¹, Y. Grin¹, U. Schwarz¹¹Max Planck Institute for Chemical Physics for Solids, Dresden, Germany

Electron counting rules and their dependence on chemical bonding for compounds of the element semiconductors silicon or germanium with alkaline-, alkaline earth- and rare-earth metals can be well understood within the Zintl-Klemm concept [1]. This works successfully for compounds like BaSi_2 [2] assuming a complete charge transfer from the metal to the tetrel and the formation of covalent $2c-2e$ interactions. The violation of the

classical electron count because of unusual coordinations often yields more exotic bonding properties [3]. Quite a few of these so-called covalent metals are accessible by high-pressure high-temperature methods.

A variety of motifs with the composition MT_3 exceed the scope of the 8- N rule and show interesting physical properties. Although germanium forms two $BaGe_3$ modifications, $hP8$ [4] and $tI32$ [5], a corresponding silicon phase remained clandestine to date.

$BaSi_3$ was synthesized under high-pressure high-temperature conditions between 12(2) and 15(2) GPa and 800(80) to 1050(105) K. At ambient pressure and 570(5) K, the compound decomposes exothermally. It crystallizes in the space group $I-42m$ and adopts a unique atomic arrangement related to the $CaGe_3$ type. Chemical bonding analysis reveals a covalent silicon partial structure and polar multicenter interactions. Electrical resistivity and magnetic susceptibility measurements indicate metallic behaviour.

- [1] (a) Zintl, E.; Brauer, G.Z. *Phys. Chem.* **1933**, *B* 20, 245-271.
 (b) Zintl, E. *Angew. Chem.* **1939**, 52, 1-6.
 [2] Gladyshevskii, E.I. *Dopov Akad Nauk Ukr RSR* **1959**, 294-297.
 [3] (a) San-Miguel, A.; Toulemonde, P. *Adv. High Pressure Res.* **2005**, 25, 159-185. (b) Flores-Livas, J.A.; Debord, R.; Botti, S.; San-Miguel, A.; Pailhès, S.; Marques, M.A.L. *Phys. Rev. B*, **2011**, 84, 184503.
 [4] Castillo, R.; Baranov, A.; Burkhardt, U.; Cardoso-Gil, R.; Schnelle, W.; Bobnar, M.; Schwarz, U. *Inorg. Chem.* **2016**, 55, 4498-4503.
 [5] Fukuoka, H.; Tomomitsu, Y.; Inumaru, K. *Inorg. Chem.* **2011**, 50(13), 6372-6377.

S02-04

On the crystal structures of long-chain polysulfates

D. J. van Gerven¹, S. Wolf¹, M. S. Wickleder¹

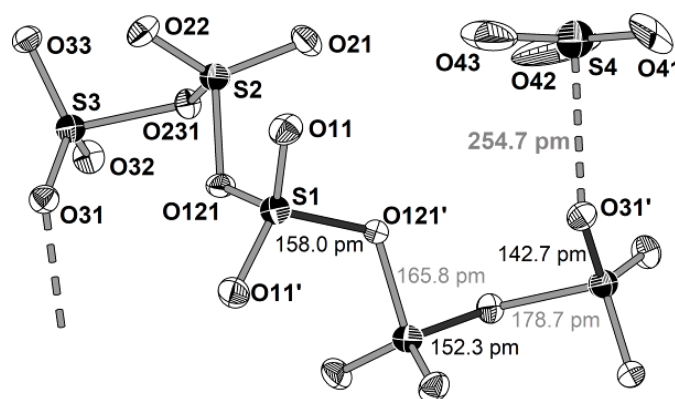
¹University of Cologne, Institute of Inorganic Chemistry, Cologne, Germany

In recent years, using neat SO_3 in reactions with various starting materials, we were able to synthesize a series of different polysulfates.^[1-4] The structural characterization of these compounds revealed a great variety of crystal structures. Based on supporting theoretical calculations predictions on the stability and the maximum chain length of polysulfates (S_nO_{3n+1})²⁻ could be made.^[2,4] According to these calculations, the Gibbs free enthalpy ΔG for the reaction $(S_5O_{16})^{2-} + SO_3 \rightarrow (S_6O_{19})^{2-}$ is already slightly positive.^[3] Nevertheless, the hexasulfates $(NH_4)_2(S_6O_{19})$,^[3] $Rb_2(S_6O_{19})$,^[3] $K_2(S_6O_{19})$ and $Cs_2(S_6O_{19})$ could be gained as longest polysulfates known so far. Characteristic for these structures is the alternation of long and short bond lengths between sulfur atoms and bridging oxygen atoms within the chain. Particularly, the terminal oxygen bridges show a significant asymmetry (Fig. 1).^[3] Thus, according to this significantly elongated distance O-S, hexasulfates may also be described as Lewis acid/base adduct according to $(S_5O_{16})^{2-} \cdot SO_3$.^[3,4] A good measure for the interaction of the terminal oxygen atom with the sulfur atom of the SO_3 molecule is the planarity of the latter. In the respect, the new compound $Rb_2(S_5O_{16}) \cdot SO_3$ is the perfect adduct displaying a completely planar SO_3 molecule located between two pentasulfate anions. Accordingly the S-O distance of more than 254.7 pm is by far longer than bond lengths observed so far. In contrast, the recently determined crystal structure of a second polymorph of $(NH_4)_2(S_6O_{19})$ shows the shortest terminal S-O bridging bonds up to now. This example demonstrates the immense influence of the corresponding counter cations and may be a route forward to stabilize even longer polysulfates.

Figure 1: Structure and atom labeling of the $(S_5O_{16})^{2-} \cdot SO_3$ unit in the crystal structure of $Rb_2(S_5O_{16}) \cdot SO_3$. Thermal ellipsoids are set at 70% probability.

- [1] Logemann, M. S. Wickleder, *Z. Anorg. Allg. Chem.* **2010**, 636, 11, 2075.
 [2] Logemann, T. Klüner, *Angew. Chem.* **2012**, 124, 5082-5085; *Angew. Chem. Int. Ed.* **2012**, 51, 4997-5000.
 [3] V. Schindler, A. Becker, M. Wieckhusen, T. Klüner, M. S. Wickleder, *Angew. Chem.* **2016**, 128, 16399-16401; *Angew. Chem. Int. Ed.* **2016**, 55, 16165-16167.
 [4] V. Schindler, M. Struckmann, A. Becker, M. S. Wickleder, *Eur. J. Inorg. Chem.* **2017**, 5, 958-964.

Figure 1



S02-05

Crystal structure and thermodynamic behavior of $Bi_6Te_2O_{15}$: the likely structure of the rare mineral pingguite

G. Nénert¹, M. Schreyer¹, H. Lian², G. R. Blake²

¹Malvern Panalytical, Almelo, Netherlands

²University of Groningen, Zernike Institute for Advanced Materials, Groningen, Netherlands

Introduction:

Pingguite is a rare mineral reported for the first time in 1994 [1]. However no report of its crystal structure was reported, only cell parameters and the existence of a phase transition around 800°C [1, 2].

Objectives

With this contribution, we aim to shed some new light onto this rare mineral by investigating in detail the structural properties at room temperature and as function of temperature coupled to detailed TGA/DSC experiment.

Results

We synthesized $Bi_6Te_2O_{15}$ using a solid-state reaction according to literature [3]. We were able to solve its crystal structure using laboratory powder diffraction data (see Fig. 1a). The system crystallizes in space group $Pnma$ with $a = 10.61156(7)$ Å, $b = 22.7446(2)$ Å and $c = 5.39906(4)$ Å. We note that those cell parameters are in good agreement with the initial report on pingguite where the multiplication of the cell parameter of the b axis is required to be able to index weak reflections. In addition, we confirm the existence of a phase transition from $Bi_6Te_2O_{15}$ to the cubic phase $Bi_6Te_2O_{13}$ around 840°C as illustrated in Fig. 1b.

Conclusion

We investigated the crystal structure of synthetic pingguite as

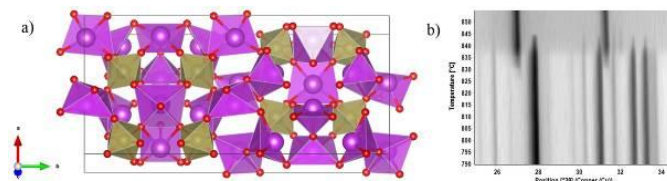
function of temperature and were able to solve its crystal structure and demonstrate the existence of the reduction of Te+VI to Te+IV around 840°C giving rise to the cubic phase Bi₆Te₂O₁₃ at high temperature.

Figure 1: a) Crystal structure of Bi₆Te₂O₁₅ and b) Phase transition from Bi₆Te₂O₁₅ to Bi₆Te₂O₁₃.

References

- [1] Sun Zhifu, Luo Keding, Tan Falan, and Zhang Jingyi (1994) Pinguite; a new bismuth tellurite mineral. Acta Mineralogica Sinica, 14(4), 315–321
- [2] John L. Jambor, Nikolai N. Pertsev, Andrew C. Roberts, American Mineralogist, Volume 81, pages 766-770, 1996
- [3] Hiroshi Sakai, Mihoko Yamamoto, Satoru Nakashima, Yutaka Maeda, Hyperfine Interactions 90 (1994), pp 401-405

Figure 1



S02-06

Chemical preparation, crystallographic characterization and vibrational study of a new condensed phosphate CaKP3O9.H2O

R. Oubouaza¹, M. Tridane², M. Belhabra¹, S. Belaaouad¹
¹Hassan II University of Casablanca, Faculty of Sciences/ Laboratory of Chemistry-Physics of Materials, Casablanca, Morocco
²Centre Régional des métiers d'éducation et de formation Casablanca Anfa, Bd Bir Anzarane Casablanca. Maroc., Laboratory of Chemistry-Physics of Materials, Casablanca, Morocco

Cyclophosphates are the simplest terms of condensed phosphates. Their anions correspond to the general formula P_nO_{3n}, those with n = 3, 4, 5, 6, 8, 10 and 12. For each family of cyclophosphates, corresponding to a particular value of n, the methods of chemical preparation are very specific, and with a few exceptions, the development of these methods required the optimization of a procedure for the chemical preparation of an appropriate starting material. The present work concerns the Chemical preparation of CaKP3O9.H2O which was prepared by the method of ion exchange resin and its thermal evolution was followed by and IR and X-ray experiments. A vibration study was also made on the title compound by IR and Raman.

Keywords: Condensed phosphates, cyclotriphosphates, method of ion exchange resin, Chemical preparation, crystallographic characterization, infrared spectrometry.

Figure 1

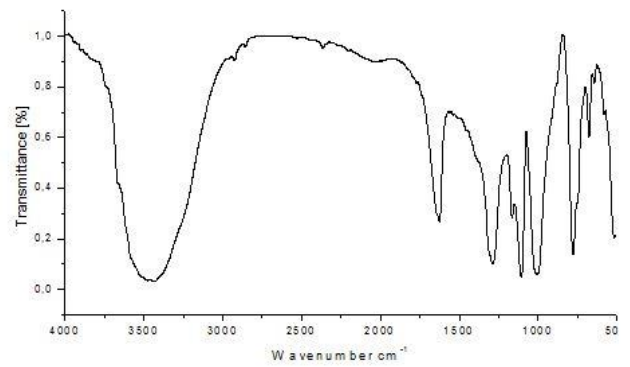


Figure 2

Fréquences observées ν(cm ⁻¹)	Vibration
3469	νO-H
1626	ν ₂ HOH
1288.77	ν _{as} OPO ⁻
1164.00	ν _s OPO ⁻
1105.14	
1006.54	ν _{as} POP
677.40	ν _s POP
780.00	
643.31	δOPO- ρ OPO- δPOP
579.17	
515	

Micro- and nanocrystalline materials (powder diffraction, EM, ...)

S03-01

Transformation strains to evaluate domain orientations by electron backscatter diffraction

A. Leineweber¹, H. Becker¹, M. J. Krieger¹, S. Martin¹¹Technische Universität Bergakademie Freiberg, Freiberg, Germany

Ferroelastic, martensitic, ordering and many other phase transformations involving domain formation are accompanied by spontaneous strains breaking the symmetry with respect to a high-symmetry state. Scanning-electron microscopy (SEM) in combination with electron-backscatter diffraction (EBSD) is frequently able to provide a mesoscopic picture of the domain microstructure, which complements with Powder-X-ray diffraction and transmission electron microscopy.

One frequent issue is the pseudosymmetry exhibited by the Kikuchi patterns complicating application of the EBSD analysis in combination with Hough-transform based indexing. It will be explored how to make systematic use of the symmetry breaking strains to differentiate between domain orientations and similar phases in EBSD. It is in particular worked out how one can assess the lattice parameters with respect to the likelihood that symmetry-breaking strain is sufficiently large to allow reliable distinction between different domain orientations.

Model cases involving domain microstructures in Al-rich Al-Mo-Ti phases and ordered η -Al₅Fe₂ are presented. The amount of symmetry breaking strain usable to distinguish between domain orientations and different phases is assessed based on concepts for assessing spontaneous strain in ferroelectrics [1] and the effects of such strains on reflection splitting or broadening in powder diffraction [2]. The Figure shows SEM/EBSD data from η -Al₅Fe₂ with two different monoclinic η' orientation states in an orthorhombic matrix.

It has been shown how symmetry breaking strains can be successfully employed. The evaluated strain tensors can further be used to predict the orientation of domain and interphase boundaries, which are accessible from the SEM/EBSD analysis, too.

Figure 1

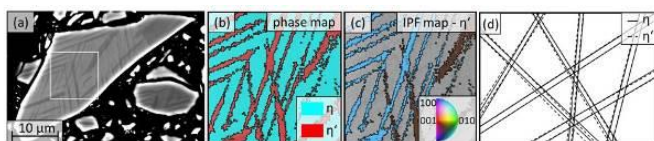


Figure: SEM/EBSD results from partially ordered Al₅Fe₂ alloy. (a) Backscatter electron contrast of a polished powder particle. (b) EBSD phase map distinguishing between orthorhombic η phase and monoclinically distorted η' phase where the inverse pole figure (IPF) map (c) reveals presence of two orientation variants of η' . (d) Simulated Kikuchi bands of η and η' illustrating the effect of the of the symmetry breaking monoclinic strain allowing for distinction between η and η' but also between the two variants of η' .

S03-02

Electron Diffraction Tomography and X-ray Powder Diffraction on Photoredox Catalyst PDI

A. Bodach¹, H. Zhao², N. W. Liu³, E. Alig¹, G. Manolikakes^{3,4}, L. Fink¹, U. Kolb²¹Goethe-Universität Frankfurt am Main, Anorganische und Analytische Chemie, Frankfurt am Main, Germany²Johannes Gutenberg Universität Mainz, Institute of Inorganic Chemistry and Analytical Chemistry, Mainz, Germany³Goethe-Universität Frankfurt am Main, Organic Chemistry and Chemical Biology, Frankfurt am Main, Germany⁴TU Kaiserslautern, Department of Chemistry, Kaiserslautern, Germany

In order to solve a crystal structure of a nano crystalline material in the bulk X-ray powder diffraction (XRPD) is nowadays used routinely. In the last decade, as a complementary method, three-dimensional electron diffraction data collected tomographically evolved as a method for crystal structure analysis of a single nanocrystal¹. XRPD is limited by reliable indexing, which may become problematic with increasing peak overlap and the exact knowledge of the molecular constitution is crucial. With the development of automated electron diffraction tomography (ADT) the hitherto existing problem of strong dynamical scattering for electron diffraction is significantly reduced allowing for ab-initio structure analysis². Nevertheless, electron beam damage and missing diffraction data due to preferred orientation may provide problems especially in the case of organic compounds^{3, 4}. A major improvement is the reduction of data acquisition time by using high speed cameras or improving the data collection strategy by working in scanning -TEM (STEM-NED) mode¹.

With the combination of ADT and XRPD the structure of *N,N*-Bis(2,6-diisopropylphenyl)-perylene-3,4,9,10-bis(dicarboximide) (PDI) was determined. PDI is starting to be widely used as a metal-free homogeneous photoredox catalyst. The mechanism is still under discussion and insight into its structural features may provide further understanding. ADT delivered the crystal structure including all non-H atoms, while X-ray powder diffraction determined the lattice parameters, followed by Rietveld refinement of the ADT model. Surprisingly, the crystal structure of PDI exhibits small empty voids leading to a remarkable solubility. To validate these empty voids further DFT-D calculations and additional analytics were performed.⁵

[1] U. Kolb, T. Gorelik, C. Kübel, M. Otten, D. Hubert, *Ultramicroscopy*, 2007, **107**, 507-513 and 2008, **108**, 763-772.

[2] E. Mugnaioli, T. Gorelik, U. Kolb, *Ultramicroscopy*, 2009, **109**, 758-765.

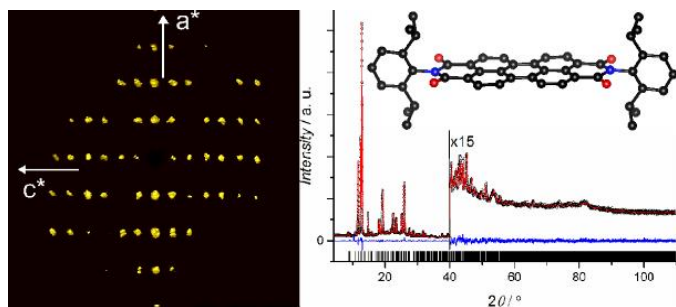
[3] U. Kolb, T. Gorelik, E. Mugnaioli, A. Stewart, *Polymer Reviews*, 2010, **50**, 385-409.

[4] M. B. Mesch, K. Bärwinkel, Y. Krysiak, Ch. Martineau, F. Taulelle, R. B. Neder, U. Kolb, J. Senker, *Chem. Eur.J.*, 2016, **22**(47), 16878 –16890.

[5] presented results submitted to *CrystEngComm*.

Fig. 1 Reconstructed electron diffraction volume of PDI obtained from ADT data, view along b^* (left) Rietveld-Plot and molecular structure of PDI (right).

Figure 1


S03-03
Structure determination of rare-earth vanadium selenide oxides by combination of transmission electron microscopy and microfocused synchrotron radiation

 F. Gehlhaar¹, C. Bennndorf¹
¹Universität Leipzig, Institut für Mineralogie, Kristallographie und Materialwissenschaft, Leipzig, Germany

Mixed oxide chalcogenides ($Ch = S, Se$) of rare-earth (RE) and transition metals (T) exhibit a large variety of crystal structures with different compositions. Building units like chains of edge-sharing $\infty^1[Ch_4/2O_2]$ octahedra are characteristic for quaternary rare-earth transition metal chalcogenide oxides, e.g. $RE_4Ti_4Se_4O_4$ [1], $RE_7VSe_8O_4$ [2], $RE_4Ti_4S_4O_9$ [3] and $RECrSe_2O$ [4]. In general, the compositions of these compounds correspond to $RE_2Ch_3 \cdot xT_2^{(n+1)} + Ch^{2-n+1}$ ($n = 1, 2, 3$), depending on the transition metal's oxidation state. In a combined study using transmission electron microscopy (TEM) and microfocused synchrotron radiation [5], a new series of quaternary rare-earth vanadium selenide oxides $RE_3VSe_3O_3$ has been characterized. The compounds appear as opaque, brownish-orange needles. They crystallize with a new structure type (space group $P2_1/m$) representing a structural variant of quaternary selenide oxides. It is characterized by chains of $\infty^1[VSe_4/2O_2]$ rods of edge sharing octahedra separated by $[RECh_6/2]$ building blocks yielding a network with channel along [010] (see Figure: Left: Crystal structure of $RE_3VSe_3O_3$ projected along [010]. The $\infty^1[VSe_4/2O_2]$ octahedra are emphasized. Right: Bright field TEM image and SAED along [101] of a $Nd_3VSe_3O_3$ single-crystal.).

[1] A. J. Tuxworth, J. S. O. Evans, *J. Solid State Chem.* **2014**, *210*, 188-194.

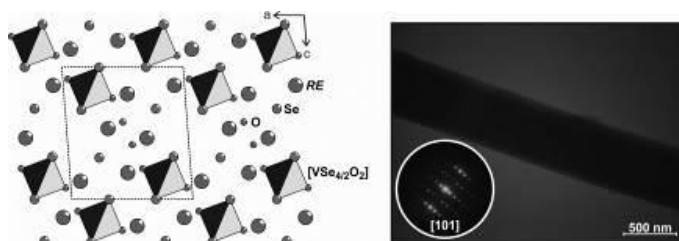
[2] O. Tougait, J. A. Ibers, *J. Solid State Chem.* **2000**, *154*, 564-568.

[3] C. Guillot Deudon, V. Meignen, L. Cario, A. Lafond, A. Meerschaut, *J. Solid State Chem.* **2004**, *177*, 2464-2469.

[4] V. V. Tien, N. H. Dung, *C. R. Seances Acad. Sci.* **1981**, *293*, 933-936.

[5] F. Fahrnbauer, T. Rosenthal, T. Schmutzler, G. Wagner, G. B. M. Vaughan, J. P. Wright, O. Oeckler, *Angew. Chem.* **2015**, *127*, 10158-10161.

Figure 1


S03-04
Thermal transformation of amorphous HfO₂ nanoparticles followed by *in-situ* powder diffraction and *in-situ* transmission electron microscopy

 O. Prymak¹, P. D. Nallathamby², M. Epple¹, S. Rouvimov³, R. K. Roeder²
¹University of Duisburg-Essen, Inorganic Chemistry, Essen, Germany

²University of Notre Dame, Department of Aerospace and Mechanical Engineering, Notre Dame, United States

³University of Notre Dame, Department of Electrical Engineering, Notre Dame, United States

Hafnium oxide (HfO_2) nanoparticles have attracted considerable interest in biomedicine as novel radiographic contrast agent. Due to its enhanced X-ray absorption in the energy region of Au and Gd_2O_3 nanoparticles, a simultaneous spectral (color) imaging is possible^[1]. However, commercially available HfO_2 nanoparticles with a comparative large density and diameter (>50 nm) are not colloidal stable in dispersion. Therefore, a novel templated synthesis was developed^[2] in order to produce well-dispersible HfO_2 nanoparticles with a diameter below 10 nm. In this synthetic pathway, amorphous HfO_2 seeds of about 1.5 nm were subjected to calcination (>650 °C), resulting in the formation of crystalline HfO_2 nanoparticles with a diameter of about 6 nm (Fig. 1, left). X-ray powder diffraction (XRD) and transmission electron microscopy (TEM) were used *in situ* to investigate the recrystallization of the seeds at elevated temperature. An extensive crystallographic investigation combined with Rietveld refinement (Fig. 1, right) gave the phase proportions, the lattice parameters, the crystallite size, and thermal expansion coefficients. The amorphous seeds recrystallized into the cubic HfO_2 phase at 700 °C and then transformed into monoclinic phase. During this calcination process (up to 1200 °C) the crystallite size of cubic HfO_2 remained constant (5 nm), whereas the crystallite size of monoclinic HfO_2 increased from 17 to 22 nm, indicating a coalescence of the particles.

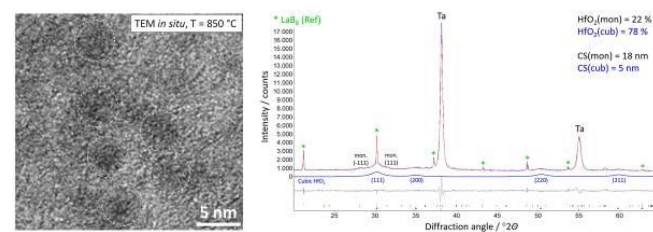
Figure 1: Representative TEM (left) at 850 °C and *in situ* XRD with Rietveld refinement (right) at 800 °C of HfO_2 nanoparticles, transformed from amorphous into cubic (cub) and monoclinic (mon) crystalline phases. Further diffraction peaks belong to the tantalum sample holder (Ta) and to LaB_6 added as internal reference (*).

References:

[1] T.L. McGinnity, et al., *Nanoscale* **8** (2016) 13627

[2] P.D. Nallathamby, et al., *J. Mater. Chem. B* **4** (2016) 5418

Figure 1



S03-05

Simultaneous Study of Periodic and Local-Structural Features of Polycrystalline Samples – An Upgrade of the Powder Diffraction and Total Scattering Beamline P02.1 at PETRA III, DESY

M. Wharmby¹, M. Etter¹, A. Schökel¹, J. C. Tseng¹, M. Wendt², S. Wenz²

¹DESY, P02.1/FS-PE, Hamburg, Germany

²DESY, FS-PE, Hamburg, Germany

Powder X-ray diffraction (PXRD) is a standard tool for characterisation of periodic solids across a wide range of fields in the physical sciences: from materials science and metallurgy, to chemistry and solid state physics. In recent years, the analysis of Pair Distribution Functions (PDFs) to understand the local structure of compounds of interest – from crystalline to amorphous – in these same research fields has seen significantly wider application. Using the high-energy X-rays available at the PETRA III third generation synchrotron light source (DESY, Hamburg) and through the recent addition of an extra detector, the Powder Diffraction and Total Scattering beamline, P02.1, is now able to offer simultaneous collection of PXRD and PDF data. With a fixed energy of 60 keV, the beamline is able to collect total-scattering data for PDF data with a Q_{Max} of at least 20 \AA^{-1} , whilst PXRD data can be collected with a resolution of 0.005° ($\Delta Q \sim 2.65 \times 10^{-3} \text{ \AA}^{-1}$) over an angular range of $0\text{-}12^\circ 2\theta$ (equivalent to more than $100^\circ 2\theta$ with standard Cu $K\alpha$ radiation), more than adequate for Rietveld refinement. Moreover, the beamline offers a wide range of non-ambient sample environments, including variable temperatures (hot-air blower – RT-1100 K; cryostream – 90-500 K; cryostat – 10-300 K), gas sorption (up to 1 bar pressure) and electrochemistry, which may be used to understand the behaviour of samples in situ or operando. A robot is also now available for automated beamline operation.

This talk will detail the new and significant upgrade to the beamline which has just been completed, including case studies of user experiments in the field of battery research and in situ crystallisation, which would benefit from the new joint total scattering/powder diffraction set-up. Moreover, we will present upcoming improvements and soon to be available facilities which will be of interest to the wider crystallographic community.

Figure: *Left* - the new twin detector set-up with forward detector for total scattering and rear for powder diffraction; *right* - the sample change robot.

Figure 1



in situ/in operando studies

S04-01

Dynamic observation of gas-solid interactions of porous iridium/ iridium dioxide nanoparticles by *in situ* TEM heating in different gaseous environments

K. Loza¹, K. Pappert¹, R. Schierholz², M. Heggen³, M. Eppl¹

¹University of Duisburg-Essen, Institut für Anorganische Chemie, Essen, Germany

²Forschungszentrum Jülich GmbH, Institut für Energie- und Klimaforschung–Grundlagen der Elektrochemie, Jülich, Germany

³Forschungszentrum Jülich GmbH, Ernst Ruska-Centre and Peter Grünberg Institute, Jülich, Germany

Question

In conventional transmission electron microscopy (TEM) heating stages, thermal studies can be conducted at very low pressure. This may not reflect the real environment a functional material experiences in *operando* mode, *i.e.* during a chemical reaction. This is particularly true for thermally activated reactions including heterogeneous catalysis (combustion, steam reforming, etc.), corrosion, or materials synthesis by thermolysis. Oxidizing or reducing conditions may change the surface properties of supported metal nanoparticles used in heterogeneous catalysis. This can cause a thermal deactivation and also lead to enhanced sintering.

Methods

Here, we report on the dynamic morphological evolution of dispersed porous iridium/iridium dioxide nanoparticles (crystallite size ca. 2 nm), prepared by a colloid-chemical route. TEM heating studies were performed under different gas environments (oxygen, nitrogen or argon/hydrogen) to follow their shape, internal crystal structure (like polycrystallinity) and composition up to 1000 °C.

Results

Thermal treatment of the sample resulted in a temperature-dependent crystallite growth. The hollow structures turned into solid nanoparticles. Neither disintegration nor generation of smaller particles were observed. Bright-field *in situ* TEM and *ex situ* HAADF-STEM images showed the influence of the gas of interest on the particle end morphology. In oxygen flow at 1 bar the edges became more rounded. In contrast to O₂ atmosphere, a mixture of Ar/4% H₂ at 1 bar caused pronounced particle faceting.

S04-02

In situ structural vacancy ordering phenomena observed by in situ TEM heating experiments and relation to electrical properties for Ge₆Sn₂Sb₂Te₁₁

T. Dankwort¹, C. Koch², A. L. Hansen¹, D. Johnson³, M. Wuttig⁴, W. Bensch¹, L. Kienle¹

¹Christian-Albrechts Universität zu Kiel, Kiel, Germany

²University of Applied Science Bremerhaven, Bremerhaven, Germany

³University of Oregon, Eugene, United States

⁴RWTH Aachen University, Aachen, Germany

Introduction

Thin films of ternary Ge-Sb-Te compounds are also referred to as Phase Change Materials (PCMs) due to their unique ability to be easily switched between a high resistive amorphous phase and a low resistive metastable crystalline phase.

Objectives

Our study focuses on the micro- and nanostructural changes occurring by heating an amorphous Ge₆Sn₂Sb₂Te₁₁ thin film. Especially the ordering of the structural vacancies and their effect on electrical properties will be discussed.

Results

Three different crystalline phases could be identified which can be separated by their unique degree or structural vacancy ordering.

At 112 °C the films started to crystallize. In the temperature range of 112 °C – 130 °C a so far for Ge₆Sn₂Sb₂Te₁₁ unreported (pseudo) cubic phase with statistically distributed structural vacancies was observed.

At 130 °C structural vacancies start to order associated with the formation of a primitive trigonal layered phase which form coherent nanoscale domains in the (pseudo) cubic matrix. As it will be demonstrated structural vacancies increasingly order at elevated temperatures. Intuitively this process can be explained by a nucleation and growth model. Between 240 °C – 260 °C a gradual phase transition to another trigonal phase with altered layered structure could be recognized. Further, the order in the latter phase is increased by in plane movement of so-called bi layer defects, which are of major interest in the field of interfacial PCMs (figure 1). This mechanism was recently proposed but could not be observed directly by means of in situ observations.

The heat dependent resistance measurements revealed an extra intermediate resistive state which appears in the same temperature region with sole presence of the strongly disordered (pseudo) cubic phase.

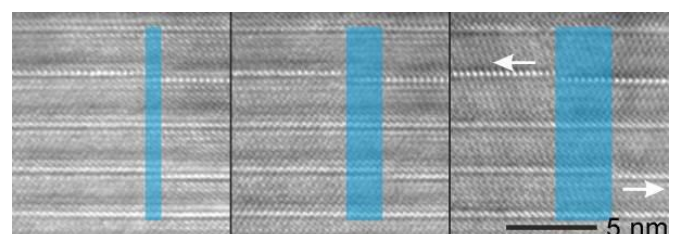
Conclusion

In summary, Ge₆Sn₂Sb₂Te₁₁ shows an extra intermediate resistive state between the amorphous and metastable crystalline phases supposedly due to the formation and stable presence in that temperature regime of a (pseudo) cubic phase.

Reference

[1] C.Koch, T.Dankwort et al., Acta Materialia, 152, 2018

Figure 1



S04-03

Hydrogenation steps to perovskite-type hydride CaRhH₃ and in situ investigations of its intermediates CaRh₂H_x

*A. Götze¹, H. Kohlmann¹, J. Möllmer²

¹Universität Leipzig, Anorganische Chemie, Leipzig, Germany

²Universität Leipzig, Institut für Nichtklassische Chemie, Leipzig, Germany

Several hydrides are known in the system Ca-Rh ranging from K₂PtCl₆ type Ca₂RhH₅ with RhH₅⁴⁻ complexes to Ca₈Rh₅H₂₃ and Ca₈Rh₆H₂₄, which mark a transition to the cubic perovskite type [1, 2]. However, the perovskite CaRhH₃ was not found yet and a solid state synthesis by calcium hydride and rhodium was not successful [1]. An alternative access to this hydride was found by hydrogenation of the cubic Laves phase CaRh₂ [3]. Three hydrogenation intermediates CaRh₂H_x were investigated based on *in situ* thermal analysis (DSC), *in situ* powder X-ray (PXRD) and neutron diffraction (PND) and hydrogen sorption measurements. The Laves phase CaRh₂ absorbs a small amount of hydrogen at room temperature to form cubic α-CaRh₂H_{0.05} (ZrCr₂H_{3.08} type)

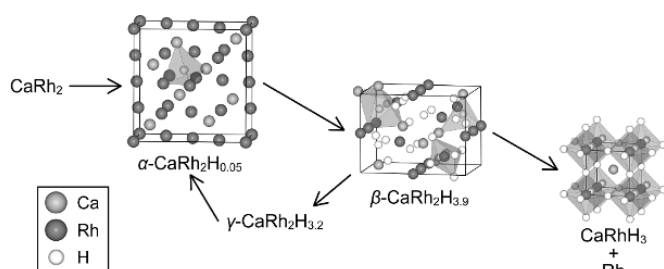
with hydrogen in tetrahedral $[\text{Ca}_2\text{Rh}_2]$ voids. This hydride reacts further to the hydrogen-rich $\beta\text{-CaRh}_2\text{H}_{3.93(5)}$ (own structure type) with an orthorhombically distorted Laves-phase type. Hydrogen occupies also tetrahedral $[\text{Ca}_3\text{Rh}_2]$ and additionally bipyramidal $[\text{Ca}_3\text{Rh}_2]$ voids. The third intermediate $\gamma\text{-CaRh}_2\text{H}_{3.20(10)}$ ($\beta\text{-CaRh}_2\text{H}_{3.9}$ type) is formed during the hydrogen desorption of the hydrogen-rich β -phase. The perovskite-type hydride CaRhH_3 ($a = 3.6512(2)$ Å) is formed at 560 K and 5 MPa hydrogen pressure by decomposition of the intermediate $\beta\text{-CaRh}_2\text{H}_{3.93(5)}$. Nanocrystalline rhodium is formed as side-product during the decomposition.

Figure: Reaction pathway of the hydrogenation of the Laves-phase hydride CaRh_2 .

References:

- [1] W. Bronger, L. Breil, *Z. Anorg. Chem.* **1998**, *624*, 1819-1822.
- [2] W. Bronger, K. Jansen, L. Breil, *Z. Anorg. Allg. Chem.* **1998**, *624*, 1477-1480.
- [3] A. Götze, J. Möllmer, H. Kohlmann, *Inorg. Chem.* **2018**, *57*, 10925-10934.

Figure 1



S04-04

Study of proton conductivity on powder samples using XRD

J. Plocek¹, *D. Havlíček²

¹Czech Academy of Sciences, Institute of Inorganic Chemistry, Department of Materials Chemistry, ež, Czech Republic

²Charles University Prague, Department of Inorganic Chemistry, Faculty of Science, Prague, Czech Republic

The study of proton conductivity is important in many different fields and disciplines, like materials for so called "Proton Exchanging Membranes" (PEM) in hydrogen fuel cells or "Solid Oxide Fuel Cells" (SOFC). The large family of proton conductors includes also salts of oxoacids, which have been studied in our department for several years. The conductivities, whilst not high, were still several orders of magnitude higher than for insulators. We have prepared and described these new compounds, studied their structural properties by single crystal X-ray and neutron and measured proton conductivity. We were able to define the direction of conductivity in these crystals.

Proton transfer could occur via either the vehicle mechanism or the Grotthus mechanism. In anhydrous salts, the lack of water molecules excludes application of vehicle mechanism. But the application of Grotthus mechanism should cause disorders of the ions through which the protons are transferred at the conditions of proton conductivity.

For the first information, about existence of proton conductivity in any compound, we have tried to study this property by measurement on powder samples. The results are given in this presentation. Among our (mostly first prepared) samples we have also studied well known proton conductor CsHSO_4 . This sample

exhibit proton conductivity in powder form, and the value is comparable with measurement on single crystal. We have adapted our sample holder to be possible to keep the sample under high voltage (DC) during measurement.

On approx. 60 % diffraction lines we have observed broadening and in some cases also the significant shift of diffraction lines both to higher and smaller angles. The analysis of such pattern can show, which lines are affected by proton transfer and define the "direction" of conductivity in the crystal, even the measurement is made on powder sample. The results of CsHSO_4 were compared with the study of non-conductive reference material: Cs_2SO_4 .

Keywords: proton conductivity, powder samples, in situ XRD measurement

S04-05

Complementarity of operando XRD and XAS for a deep understanding of $\text{Na}_x\text{Ni}_{0.5}\text{Ti}_{0.5}\text{O}_2$ as Na-ion battery cathode material

S. Maletti¹, A. Sarapulova², D. Mikhailova¹

¹Leibniz Institute for Solid State and Materials Research Dresden, Electrochemical Energy Storage, Dresden, Germany

²Karlsruhe Institute of Technology (KIT), Institute of Applied Materials, Karlsruhe, Germany

Sodium-ion batteries (SIBs) represent a promising alternative to lithium technology for economical and ecological reasons. Presently, research on possible cathode materials for SIBs focuses on layered oxides. Oxides with only one transition metal in the structure exhibit numerous transformations upon desodiation and are therefore unfavorable [1]. By incorporating a second metal, these structures can be stabilized, yielding a smooth potential curve and an increased cycle life. Recently, $\text{O}3\text{-Na}_x\text{Ni}_{0.5}\text{Ti}_{0.5}\text{O}_2$ has been reported for its remarkable performance but the occurring structural changes are still unknown [2]. However, a profound insight into these changes is essential in order to improve its characteristics and pave the way towards applicability. We carried out *operando* synchrotron diffraction and *operando* X-Ray absorption spectroscopy in order to elucidate structural changes as well as the redox mechanism upon sodium removal and insertion. These methods have become a standard toolbox for researchers, but are usually not fully utilized. We demonstrate the mutual complementation of both methods with an in-depth data analysis. Firstly, structural transformations were clarified. Secondly, three independent values of the sodium content are available by monitoring the current flow along with the refinement of sodium occupancy numbers and an analysis of the transition metal oxidation states. Thus, the plausibility of the reaction mechanisms could be significantly increased, and a conclusion regarding parallel oxidizing processes was made. Moreover, interatomic distances, calculated from both the Rietveld analysis and EXAFS fits are well in accordance, further demonstrating advantages of a comprehensive multi-technique *operando* characterization. Finally, *ex situ* magnetization measurements yielded additional information of the present nickel oxidation states.

[1] M. H. Han et al., *J. Power Sources* **2014**, *258*, 266-271.

[2] H. Yuet et al., *Chem. Commun.* **2014**, *50*(4), 457-459.

Figure 1

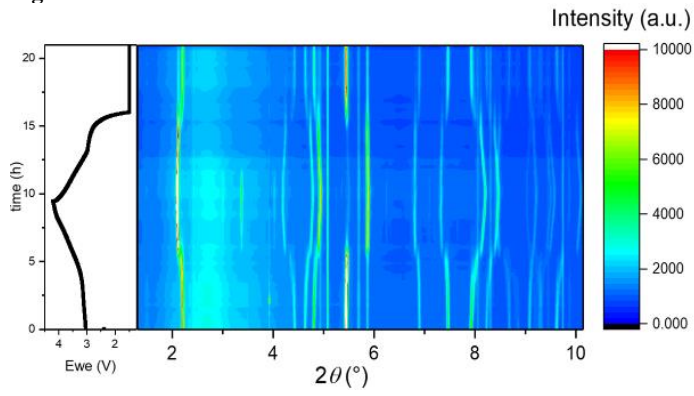
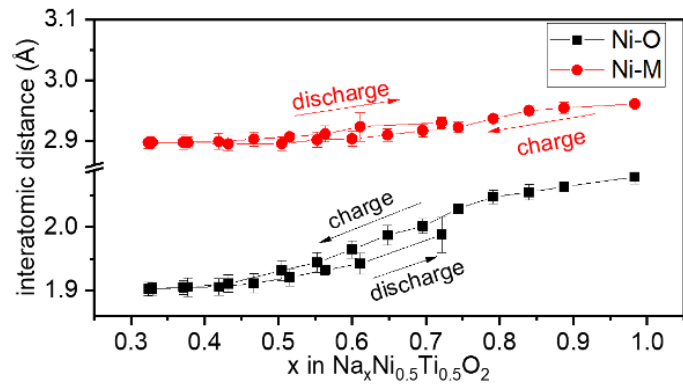


Figure 2



Bio-Crystallography II: Crystallographic and hybrid methods

S05-01

Structural basis of ribosomal RNA synthesis

Y. Huang¹, T. Hilal², N. Said¹, B. Loll¹, M. Wahl^{1,3}

¹Freie Universität Berlin, Institut für Chemie und Biochemie, Berlin, Germany

²Freie Universität Berlin, Research Center for Electron Microscopy, Berlin, Germany

³Helmholtz-Zentrum Berlin, Macromolecular Crystallography, Berlin, Germany

Competition between transcription termination and continued transcription (anti-termination) is a pervasive gene regulatory principle in bacteria. During the synthesis of ribosomal RNAs (rRNAs) in *Escherichia coli*, RNA polymerase (RNAP) is modified by an RNA signal sequence encoded in the leader and spacer regions of rRNA operons (containing stem-loop structure *boxB* and linear elements *boxA* and *boxC*), transcription factors NusA, B, E and G, ribosomal (r-) proteins, in particular S4, and a recently identified component, inositol-monophosphatase SuhB1-3. The RNA and proteins build up a complex ribonucleoprotein particle (RNP) on the surface of RNAP that renders the enzyme resistant against ρ -dependent transcription termination and that supports rRNA folding and maturation^{1,3}. We used various assays to show (i) that SuhB directly binds the C-terminal AR2 domain of NusA and the RNA signal element; (ii) that SuhB is required for stable integration of the NusB/E dimer and of r-protein S4 into the transcription complex; (iii) that SuhB is crucial for counteracting ρ -dependent termination; (iv) that SuhB can also subdue intrinsic termination; and (v) that SuhB-AR2 contacts contribute to these effects. Furthermore, we delineated the structural basis of these effects by an integrative structural biochemical approach that involved X-ray crystallography and cryo-electron microscopy. Our results reveal how SuhB organizes the modifying RNP on RNAP during rRNA synthesis and how it thereby reprograms the transcriptional machinery and supports rRNA folding and maturation.

References

- [1] Condon C, Squires C, Squires CL (1995) Control of rRNA transcription in *Escherichia coli*. *Microbiol Rev* **59**, 623-645.
- [2] Torres M *et al.* (2001) Ribosomal protein S4 is a transcription factor with properties remarkably similar to NusA, a protein involved in both non-ribosomal and ribosomal RNA antitermination. *EMBO J* **20**, 3811-3820.
- [3] Singh N *et al.* (2016) SuhB associates with Nus factors to facilitate 30S ribosome biogenesis in *Escherichia coli*. *MBio* **7**, e00114.

S05-02

Characterization of biohybrid nanomaterials with diffraction methods

M. Künzle¹, M. Lach¹, T. Beck¹

¹RWTH Aachen University, Institute of Inorganic Chemistry, Aachen, Germany

Self-organization is a key tool for the construction of functional nanomaterials. In nature, biomolecules can function as a matrix to organize inorganic components into hybrid materials. Such materials have inspired researchers to create novel materials based on biomolecules and inorganic building blocks. We have recently established a novel method for the self-organization of biomolecular building blocks and nanoparticles. Here, protein containers, engineered with opposite surface charge, are used as an atomically precise ligand shell for the assembly of inorganic nanoparticles.[1] The assembly of these protein-nanoparticle composites yields highly ordered nanoparticle superlattices with

unprecedented precision. The structure of the protein scaffold can be tuned with external stimuli such as metal ion concentration.[2] Importantly, these composite materials show catalytic activity inside the porous material.[3] Along these lines, the protein containers used as a scaffold offer a viable route towards renewable materials.[4-5]

For the structural characterizations of the synthesized biohybrid materials, we employ a range of methods. The structure of protein scaffolds is elucidated with protein X-ray crystallography. The nanoparticle superlattice is structurally characterized with single crystal and ensemble small angle X-ray scattering. For the nanoparticle building block characterization, we employ electron microscopy and electron diffraction methods.

References:

- [1] M. Künzle, T. Eckert, T. Beck, *J. Am. Chem. Soc.* **2016**, *138*, 12731-12734.
- [2] M. Künzle, T. Eckert, T. Beck, *Inorg. Chem.* **2018**, *57*, 13431-13436.
- [3] M. Lach, M. Künzle, T. Beck, *Chem. Eur. J.* **2017**, *23*, 17482-17486.
- [4] M. Künzle, M. Lach, T. Beck, *Dalton Transactions* **2018**, *47*, 10382-10387.
- [5] M. Lach, M. Künzle, T. Beck, *Biochemistry* **2018**, 10.1021/acs.biochem.8b00966.

S05-04

On the possibility of utilizing the Fourier Shell Correlation for validation of crystal structures

P. Neumann¹, R. Ficner¹

¹Georg-August-Universität Göttingen, Molekulare Strukturbiologie, Göttingen, Germany

One of the most fundamental task of evaluating the quality of an X-ray crystal structure is comparison of the build atomic model to various electron density maps. Calculation of these maps usually necessitates employment of model phases without or with phase combination. The latter requires the availability of an additional source providing the phase information, however, these phases are often inaccurate and/or of a limited resolution. The necessity of utilizing model phases in electron density map calculation results in the unavoidable model bias which needs to be minimized in order to provide a good quality atomic model. As a consequence, numerous maps are being calculated during the structure determination process. The performed electron density map calculations utilize diverse algorithms in order to reduce bias and support model rebuilding as well as its validation, e.g.: *prime-and-switch* phasing, composite omit map combined with refinement or simulated annealing, *ping-pong* map, standard density modification procedure, *iterative-build* OMIT map, *"Feature-Enhanced"* Map (*FEM*), *sigma-A* weighting. However, regardless of the employed model building/refinement protocol and availability of experimental phases, at the final stage of refinement the model is usually inspected against the calculated 2mFo-DFc electron density map which is the *Sigma-A weighted* map generated by all modern refinement programs.

In order to check the applicability of the above-mentioned electron density maps for validation purposes using the Fourier Shell Correlation (FSC), a set of about 260 crystal structures, determined using SAD approach, has been analyzed. The availability of experimentally determined phases provides an opportunity to compare the quality of the above-mentioned maps for each individual crystal structure as well as to estimate the level of model bias. Application of the FSC for estimation of the quality of the

crystal structure as well as the pros and cons of the proposed approach will be discussed.

S05-05

A crystallographic "superstructure" of a phytochrome photosensory core module reveals pronounced structural flexibility of this protein in the dark state

P. Scheerer¹, S. Nagano², K. Zubow³, N. Michael⁴, K. Inomata⁵, T. Lamparter⁶, N. Krauß⁶

¹Charité - Universitätsmedizin Berlin, Institut für Medizinische Physik und Biophysik, Berlin, Germany

²Justus-Liebig-Universität Gießen, Institut für Pflanzenphysiologie, Gießen, Germany

³Queen Mary University of London, School of Biological and Chemical Sciences, London, United Kingdom

⁴Technische Universität Berlin, Institut für Chemie, Berlin, Germany

⁵Kanazawa University, Division of Material Sciences, Graduate School of Natural Science and Technology, Kanazawa, Japan

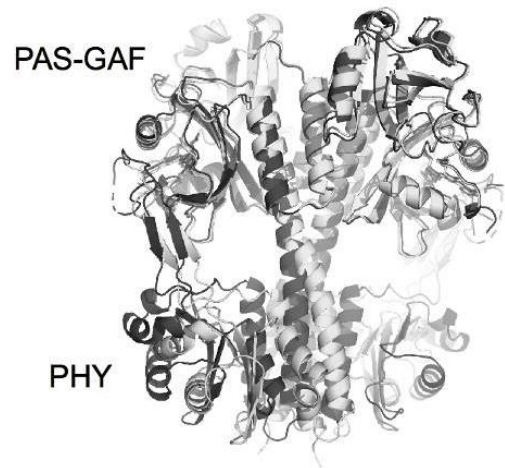
⁶Karlsruhe Institute of Technology (KIT), Botanical Institute, Karlsruhe, Germany

Phytochromes are photoreceptors in plants, bacteria and fungi that respond to light in the red/far-red range of the visible spectrum. We use the biliverdin-binding phytochromes Agp1 and Agp2 from *Agrobacterium fabrum* to study the molecular mechanisms underlying photoreceptor functions in these proteins. We solved various crystal structures of the photosensory core module (PCM), a PAS-GAF-PHY tridomain, of Agp1 in its red-absorbing dark state (*Pr*). The first structure to be solved was that of a mutant crystal (space group $P4_32_12$) diffracting to 1.85 Å resolution, followed by the crystal structure of the wild-type protein (space group I422, one molecule per asymmetric unit) which was refined to 2.7 Å resolution [1]. The SeMet derivative of wild-type Agp1-PCM assembled with a "locked" chromophore which stabilises a *Pr*-like state (15Za-Agp1-PCM_{SeMet}) crystallises in the same space group with essentially identical unit cell parameters as the crystals of the wild-type protein that has bound the native chromophore. Only a few crystals of 15Za-Agp1-PCM_{SeMet} were found to belong to the same space group but have a four times larger unit cell. The two structures of the locked chromophore adducts are closely related; the structure with the larger unit cell is a crystallographic "superstructure" of the one with the smaller cell. In the superstructure, four molecules in the asymmetric unit form two dimers of pronounced non-crystallographic symmetry (NCS). In one dimer the PHY domains adopt significantly different positions with respect to the PAS-GAF bidomains than in the other dimer (Figure 1). The observed flexibility of the PCM may be indicative of a highly dynamic structure of this protein in *Pr* in solution, which would be relevant for the mechanism by which the activity of the effector module of this phytochrome is modulated by light. Similar crystallographic superstructures of proteins may form more frequently than is apparent from the literature. Analysis of such structures may reveal otherwise inaccessible evidence of structural heterogeneity, flexibility and dynamics.

[1] Nagano, S., Scheerer, P., Zubow, K., Michael, N., Inomata, K., Lamparter, T., and Krauß, N. (2016) *J. Biol. Chem.* **291**, 20674-20691.

Figure 1: The superposed structures of the two dimers in the crystallographic "superstructure" of 15Za-Agp1-PCM_{SeMet}. Superpositioning of the PAS-GAF bidomains only, one dimer in light grey, the other in dark grey.

Figure 1



Small molecules at large facilities

S06-01

The Chemical Crystallography Beamline P24 at DESY / Petra III

N. Nöthling¹, R. Goddard¹¹Max-Planck-Institut für Kohlenforschung, Chemical Crystallography, Mülheim an der Ruhr, Germany

Following the shutdown of the DORIS storage ring in 2013, an extension of Petra III was planned and this has led to the creation of ten additional beamlines, one of which is the chemical crystallography beamline P24. Located in the Ada Yonath hall, the beamline was designed and has been equipped in a close collaboration between DESY and a BMBF funded consortium. The P24 beamline has been developed by groups from LMU Munich, Bergakademie Freiberg, University of Bayreuth and MPI Kohlenforschung under the leadership of U. Bismayer (University of Hamburg). Presently the beamline offers monochromatic synchrotron radiation with a continuous energy range from 15 to 40 keV plus a small window around 8 keV, using a water cooled C-type monochromator. A set of beryllium compound refractive lenses, ready to be installed, allows focusing of the beam down to a few micrometers in diameter. The beamline comprises two experimental hutches, one of which is equipped with a heavy duty kappa goniometer and the other with a four circle Eulerian cradle goniometer. A Pilatus 3 X CdTe one megapixel detector has been recently installed in addition to two Mar 165 CCD-detectors as well as point detectors. Designed for small molecule crystallography, the experimental set-up is complemented by low temperature gas stream devices, operating as low as 10 K, an optional closed cycle cryostat, a heating device and a diamond anvil cell. Most importantly, a small sample preparation laboratory including a fume hood is provided which enables users to mount air-sensitive samples directly at the beamline. The beamline commenced user operation in Spring 2018 and currently calls for proposals are issued twice a year. In the future a sample changer will become available and a rapid access scheme is planned for single data sets. Further experimental environments for non-ambient conditions, including magnetic fields are planned. With the focusing beam in place, it should also be possible to do spatially resolved crystallography.

S06-02

Neutrons know better: characterization of the short intramolecular hydrogen bond in substituted acetylacetones by temperature dependent diffraction

K. N. Truong¹, M. Meven², U. Englert¹¹RWTH Aachen University, Institute of Inorganic Chemistry, Aachen, Germany²Forschungszentrum Jülich GmbH at Heinz Maier-Leibnitz Zentrum (MLZ), Jülich, Germany

Ligands with two different coordination sites offer a systematic route to mixed-metal coordination polymers. N donor substituted acetylacetones combine the hard and chelating O,O' acac moiety with a softer N donor site and represent a particularly successful class [1] among these ditopic ligands. Two such potential linkers are shown in the scheme. In the crystalline state these neutral molecules exist as enol tautomers with a short intramolecular hydrogen bond between a hydroxy and a keto group. This O-H...O moiety may be associated with different bonding models: the bridging H can occupy a single site or be disordered about a double minimum with equal or different potential energies. A correct description must take displacement and temperature dependence into account.

Single crystals of **1** and **2** were investigated by neutron diffraction on the HEiDi instrument [2] in order to avoid the X-ray inherent H contrast problem. Intensity data were collected at different temperatures and complemented by temperature-dependent in house single crystal and powder diffraction.

1 and **2** show different crystal chemistry: **1** undergoes a phase transition; in the high temperature phase, the bridging H is disordered over two symmetry equivalent sites. The phase transition leads to twins, and the bridging H atom becomes ordered [3]. In contrast, **2** shows proton disorder over two general positions in the whole temperature range between 300 and 2.5 K, with only a minor preference for one site [4]. In both **1** and **2**, the hydrogen occupancies deduced by neutron diffraction match the distance pattern between the non-hydrogen atoms, with longer C-O and shorter C=O bonds.

The temperature-dependent description of the short hydrogen bond apart, the phase transition in **1** matches predictions from microwave spectroscopy on the unsubstituted parent compound acetylacetone: spectroscopists expect coupling between methyl group rotation and H atom tunneling.

Caption: substituted acetylacetone derivatives with a short intramolecular hydrogen bond in their enol tautomeric form.

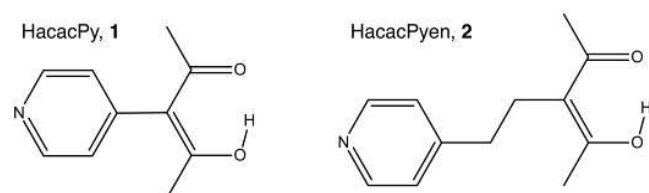
[1] M. Kremer, U. Englert, Z. Kristallogr. 233, 437-452 (2018).

[2] M. Meven, A. Sazonow, Heinz Maier-Leibnitz Zentrum, J. Large-Scale Res. Facil. 1, A7, (2015); <http://dx.doi.org/10.17815/jlsrf-1-20>.

[3] K.-N. Truong, C. Merkens, M. Meven, B. Faßbänder, R. Dronskowski, U. Englert, Acta Crystallogr. B73, 1172–1178 (2017).

[4] K.-N. Truong, C. Merkens, U. Englert, Acta Crystallogr. C74, 1635-1640 (2018).

Figure 1



S06-03

Supramolecular Crystallography Beamline (BL2D-SMC) for the Chemical Crystallography at Pohang Accelerator Laboratory in Korea.

D. Moon¹¹Pohang Accelerator Laboratory, Beamline Department, Pohang, Gyeongbuk, South Korea

Single crystal X-ray crystallography is very powerful technique for determining the atomic or molecular structure of crystalline material. This technique determines the atomic positions, and the corresponding bond distances and angles within materials as well as the correlation between structural features and chemical or physical properties.

The supramolecular crystallography beamline (BL2D-SMC) is the unique dedicated crystallography beamline for the structure solution of crystalline materials both small and supramolecule using synchrotron radiation in Korea. The beamline is located at

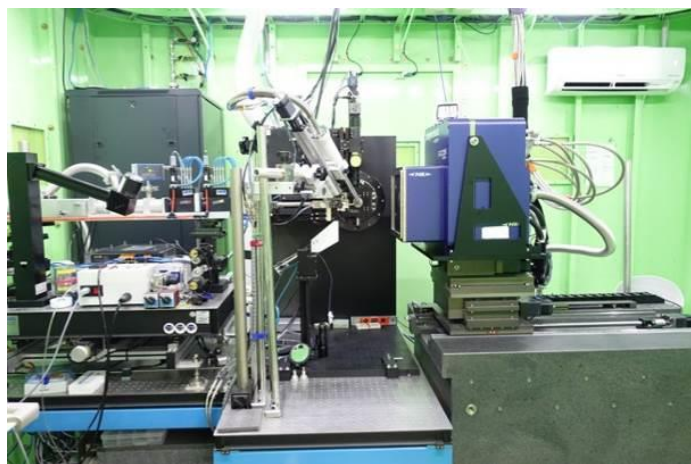
the 2D bending magnet port in the 3GeV storage ring (400mA, top-up mode) of Pohang Light Source II. The optics of BL2D-SMC are consist of two mirrors (one vertical collimating and one toroidal focusing) and a Si (111) double crystal monochromator to operate in the tunable energy range between 8 and 20 keV (1.5 and 0.6 Å). Diffraction data are collected by a Rayonix MX225HS CCD area detector (installed in Mar. 2018). This CCD detector is performed both very fast (10 image per sec, 2x2 binned, 16 bits standard) data collection and high quality with high dynamic range (1x1 non-bin, 18 bits HDR). It will give a chance to get the structural change of the single crystals or to get the high resolution image data. The beamline control and data collection is controlled by custom BL2D-supramolecular data collection software (BL2D-SMDC). The software has an interactive GUI and is designed to run on a Windows operating system. HKL3000sm is used for cell refinement and data reduction.

BL2D is performing not only general single crystal data collection such as hollow molecular structure (MOFs, cage structure, and very tiny size crystal (< 10 μm³)) but also non-ambient crystallography with variable temperature, gas sorption and photo-excitation to the crystal.

The instruments, status and diverse application of BL2D will be introduced in this presentation.

Figure 1. BL2D-SMC end-station

Figure 1



S06-04

Giant Supramolecules Meet Synchrotron Radiation

A. Virovets^{1,2}, E. Peresykina^{1,2}, M. Scheer¹

¹University of Regensburg, Institute of Inorganic Chemistry, Regensburg, Germany

²Novosibirsk State University, Novosibirsk, Russian Federation

During last decades we have been using pentaphosphaferrocenes, [Cp^RFe(η⁵-P₅)] (Cp^R = η⁵-C₅R₅, R = Me, CH₂Ph, PhC₄H₉), as building blocks for the rational design of giant supramolecules, up to 4.6 nm in size [1-3]. Solving the crystal structures at atomic resolution requires the diffraction data up to $d_{\min} = 0.84 \text{ \AA}$. This resolution can be easily reached with laboratory X-ray sources for small molecules, but not for giant supramolecules consisting of hundreds of heavy atoms. Being formally "small molecules" they however demonstrate some features of biological macromolecules like weak scattering power and disorder. The use the high-flux synchrotron sources is sometimes the only remedy.

Typical in-house diffraction experiment of modest $I/\sigma \sim 10$ requires at least 2-4 days and is frequently accompanied by icing of the crystal. To obtain quality data at $d_{\min} > 1 \text{ \AA}$ we use DESY PETRA III P11 beamline [4]. The most critical is to choose radiation energy as a compromise between d_{\min} and quantum efficiency (QE) of a PILATUS 6M detector. Thus, usage of the 20 keV radiation allows to obtain data up to $d_{\min} = 0.69 \text{ \AA}$, at the cost of rather low QE = 25%. Decreasing to 16.5 keV improves the QE to 42%, but disimproves the d_{\min} to 0.84 Å. Optimization of the experimental strategy allowed us obtaining high-quality diffraction data even from weakly scattering crystals with the cell constant of ~91 Å (Fig.) and investigate such unusual structural effects as superstructural ordering.

This work was supported by the SELFPHOS grant ERC AdG-339072. Parts of this study were carried out at PETRA III synchrotron source at DESY.

[1] E. Peresykina, C. Heindl, A. Virovets, M. Scheer (2016)

Structure and Bonding **174**, 321.

[2] E. Peresykina, C. Heindl, E. Mädl, et al (2018) *Chem.-A Eur. J.* **24**, 2503 – 2508.

[3] C. Heindl, E.V. Peresykina, A.V. Virovets, et al (2017)

Angew. Chem. Int. Ed. **56**, 13237.

[4] A. Burkhardt, T. Pakendorf, B. Reime, et al (2016) *Eur. Phys. J. Plus*, **131**, 56.

Figure 1

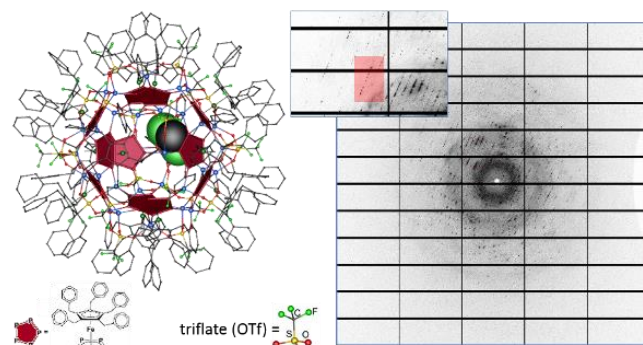


Fig. Diffraction from [(Cp^{Rh}FeP₅)₁₂(AgOTf)₂₀], $a = 46.54$, $b = 32.12$, $c = 91.79 \text{ \AA}$, $\beta = 97.72^\circ$, $E = 20 \text{ keV}$

S07-01

Discovery of the wave nature of crystals

G. Shpenkov¹

¹Retired, Bielsko-Biala, Poland

The derivation of characteristic angles of crystals, determining their shape, was and still is an unsolvable problem of modern physics. This means that the nature of the formation of the definite geometrical configuration of facets in the crystals is not properly understood so far. Actually, until now the characteristic angles of crystals are determined only experimentally, because none of the modern physical theories, including quantum mechanics, adhering to the Standard Model (SM) [1], is unable, in principle, directly derive them. So that the above problem still remains one of the most important unsolved problems of theoretical quantum chemistry and crystal chemistry, which are based on abstract-mathematical postulates of quantum mechanics being its fundamental concepts.

In contrast to the SM, the Wave Model (WM) that we develop have solved this problem. In the framework of the WM, there were revealed the wave shell-nodal structure of the atoms, the main role of the specific spatial arrangement of the nodes and internodal strong bonds in the atoms at the formation of chemical bonds, secondary role of electrons at this (which define the strenght of chemical bonds but not their directions), the nature of symmetry and periodicity in the properties and structure of atoms, and much more (see, for example, Ref. [2]). It is therefore not suprising that the WM led us also to the right theoretical solution concerning characteristic angles of crystals, stipulating their shape.

Obviously, since, in accordance with the WM, we recognize the wave nature of all objects and phenomena in Nature, including atoms, hence, the wave origin of natural crystalline formations, consisting of atoms, also did not cause our doubts. Therefore, we began seeking the characteristic angles of crystals in solutions of

the general („classical”) wave equation, $\Delta\hat{\Psi} - \frac{1}{c^2} \frac{\partial^2 \hat{\Psi}}{\partial t^2} = 0$, as this equation is applicable to the description of all wave objects and processes. Our expectations were fully met [3]. Indeed, as we found out, the angles that determine the position of the planes of the faces in crystals, are really contained in the well-known particular solutions of the mentioned above wave equation, moreover, in the same its solutions that define the shell-nodal structure of the atoms. The experimentally data confirmed, convincingly enough, the validity of this discovery, which we intend to discuss at the conference.

References

- [1] G. P. Shpenkov, “Some Words about Fundamental Problems of Physics: Constructive Analysis”, LAMBERT Academic Publishing, pages 116 (2012).
- [2] G. P. Shpenkov, An Elucidation of the Nature of the Periodic Law, Chapter 7 in "The Mathematics of the Periodic Table", edited by Rouvray D. H. and King R. B., Nova Science Publishers, NY, 119-160, 2006.
- [3] [5] G. P. Shpenkov, DIALECTICAL VIEW OF THE WORLD, The Wave Model (Selected Lectures), Vol. 6 Topical Issues (2015), Supplementary Data, I. The wave nature of minerals, pages -130-155; <http://shpenkov.com/pdf/Vol.6.TopicalIssues.pdf>

Figure 1

TABLE
Characteristic angles of crystals of natural minerals (fragment of Table 2, taken from [3]).

Characteristic angles of $\hat{\Theta}_{e,s}(\theta)$ (theoretical values first calculated and published by L. Kreidlik and G. Shpenkov [2-4])	The angles of crystal minerals (measured by R. Häfky [5], N. Kokscharov [6, 7], and others [8-23])
$\hat{\Theta}_{2,0}(\theta) = \cos^2 \theta - \frac{1}{3}$	
a) Zeros:	
$\Theta_1(2,0) = \arccos \sqrt{\frac{1}{3}} = 54^\circ 44' 8.''20$	54° 44' 8.''20
$\Theta_2(2,0) = \arccos \left(-\sqrt{\frac{1}{3}}\right) = 125^\circ 15' 51.''80$	125° 15' 52.'' [5: Part I, Vol. III, p.364, 1853]
b) Sectors:	
$2\Theta_1(2,0) = 109^\circ 28' 16.''40$	Häfy: 109° 28' 16'' [5: p.29; 1*]
$\Theta_1(2,0) - \Theta_2(2,0) = 70^\circ 31' 43.''60$	Häfy: 70° 31' 44'' [5: p.29; 1*]
$2(\Theta_1(2,0) - \Theta_2(2,0)) = 141^\circ 03' 27.''20$	141° 03' [6: Part. III, Vol. VII, p.26, 1844]
c) Extremes: $\theta_1(2,0) = 0^\circ$, $\theta_2(2,0) = 90^\circ$, and $\theta_3(2,0) = 180^\circ$	characteristic angles of crystals
$\hat{\Theta}_{1,1} = \cos \theta \sin \theta$	
Zeros and extremes of 45° and 90°	characteristic angles of crystals
$\hat{\Theta}_{1,0} = \cos \theta (\cos^2 \theta - \frac{3}{5})$	
a) Zeros:	
$\Theta_1(3,0) = \arccos \left(\sqrt{\frac{3}{5}}\right) = 39^\circ 13' 53.''47$	Häfy: 39° 13' 53'' [5: p.85; 2*]
$\Theta_2(3,0) = 90^\circ$,	
$\Theta_3(3,0) = \arccos \left(-\sqrt{\frac{3}{5}}\right) = 140^\circ 46' 06.''53$	Häfy: 140° 46' 07'' [5: p.86; 2*]
.....	
$\hat{\Theta}_{e,s}(\theta) = \sin^2 \theta \cos \theta$	
.....	

S07-02

Density functional theory calculations of merohedric twinning in KLiSO₄

H. Grimmer¹, B. Delley¹

¹Paul Scherrer Institut, Research with Neutrons and Muons, Villigen PSI, Switzerland

For many years, KLiSO₄ crystals have been grown and investigated at the institute for crystallography of RWTH Aachen. The crystals have space group *P6₃* at ambient temperature and show various kinds of twinning by merohedry [1].

In order to understand the observed twinning frequencies, density functional theory (DFT) calculations were performed on four models of periodic, polysynthetic twin interfaces. The models represent the three merohedric twin laws (reflection twin *m*//*z*, rotation twin *2*⊥*z* and inversion twin *-1 = m*⊥*z*), all with boundary plane (1 0 -1 0), and, in addition, with boundary plane (0 0 0 1) for the reflection twin *m*. The models satisfy stoichiometry at the boundary plane and maintain the fourfold coordination of the Li and S atoms and the twofold coordination of the oxygen atoms.

Relaxed lattice parameters and atomic positions were determined by DFT, using the DMol³ code with functional PBEsol. The energy difference between polysynthetic twin and single crystal per primitive cell of the twin is 0.0009 eV for *m*(0 0 0 1), 0.09 eV for *-1*(1 0 -1 0), 0.58 eV for *m*(1 0 -1 0) and 0.55 eV for *2*(1 0 -1 0) [2]. In the KLiSO₄ crystals grown from aqueous solutions at RWTH Aachen the first twin was frequently observed, similarly also the second twin in Cr-doped crystals, whereas the third twin appeared only rarely and the fourth was not observed [1, 3]. This roughly corresponds to the sequence of their calculated DFT energies.

Not only for KLiSO_4 but also for quartz, the energy of twins and the frequency of their occurrence are closely connected for crystals grown from aqueous solutions, whereas for the formation of transformation twins the availability of twin nuclei plays a major role.

Dedicated to: Prof. emerit. Theo Hahn, RWTH Aachen University, Germany († 12 Feb. 2016).

[1] H. Klapper, Th. Hahn, S. J. Chung, *Acta Cryst. B* **43** (1987) 147-159.

[2] H. Grimmer and B. Delley, *Z. Kristallogr.* (2018) <https://doi.org/10.1515/zkri-2018-2126>.

[3] Chr. Scherf, N. R. Ivanov, S. J. Chung, Th. Hahn, H. Klapper, *Z. Kristallogr.* **232** (2017), 415-434.

S07-03

Intrinsic point defects in kesterite-type $\text{Cu}_2\text{ZnGeSe}_4$ compound semiconductors

D. Fritsch¹, S. Schorr^{1,2}

¹Helmholtz-Zentrum Berlin, Structure and Dynamics of Energy Materials, Berlin, Germany

²Freie Universität Berlin, Institut für Geologische Wissenschaften, Berlin, Germany

In recent years, kesterite-type compound semiconductors such as $\text{Cu}_2\text{ZnSnS}_4$ and $\text{Cu}_2\text{ZnSnSe}_4$ (CZTSSe) received a lot of attention due to their possible application as absorber layers in low-cost thin-film solar cells. However, substituting Ge^{4+} for Sn^{4+} in CZTSSe kesterite-type absorber layers has been shown to improve the optoelectronic properties [1].

Here, we address the computational modelling of intrinsic point defects in kesterite-type $\text{Cu}_2\text{ZnGeSe}_4$ employing density functional theory together with the PBE and the more accurate hybrid functional HSE06. Details of the intrinsic defects' characteristics will be discussed, as well as their influence on the electronic and optical properties.

This work made use of computational resources provided by the North-German Supercomputing Alliance (HLRN), and the Soroban and Dirac HPC facilities of the Freie Universität Berlin and the Helmholtz-Zentrum Berlin, respectively.

[1] R. Gunder, J. A. Márquez-Prieto, G. Gurieva, T. Unold, and S. Schorr, *Cryst. Eng. Comm.* **20**, 1491 (2018).

S07-04

Crystal growth and characterization of metal (M^{II})-guanidinium formates $[\text{C}(\text{NH}_2)_3]M^{\text{II}}(\text{HCOO})_3$ ($M^{\text{II}}=\text{Cu, Zn, Mn, Co}$)

J. Büscher¹, L. Bayarjargal¹, R. Luchitskaia¹, B. Winkler¹, E. Haussühl¹

¹Goethe-Universität Frankfurt am Main, Institut für Geowissenschaften, Frankfurt am Main, Germany

Metal-organic framework (MOF) compounds allow the variation of their physical properties by substitution of their constituents. Here, the physical properties of guanidinium-metal formates, $[\text{C}(\text{NH}_2)_3]M^{\text{II}}(\text{HCOO})_3$ ($M^{\text{II}}=\text{Cu, Zn, Mn, Co}$), are investigated. These compounds crystallize in space group $Pnna$, except for Cu ($Pna2_1$), and exhibit ferroic phase transitions for the Cu, Mn and Co-bearing compounds [1].

Crystals with dimensions of three to ten millimeters and optical quality were grown from aqueous solutions by evaporation at

ambient temperature and by lowering the temperature from 38 to 32 °C. The role of several parameters on crystal growth, such as the ratio and composition of the educts, the pH-value, and the presence of modifiers, were investigated. The samples were characterized by x-ray diffraction and Raman spectroscopy at ambient temperature. Complementary DFT calculations were carried out to quantitatively interpret the lattice dynamics and to predict the elastic behavior.

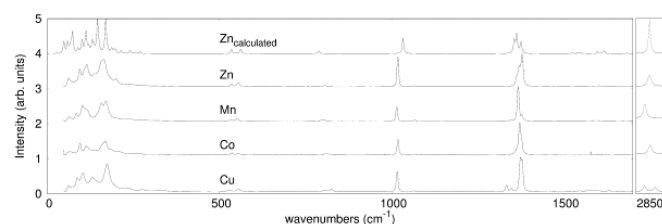
Typical Raman spectra are shown in Fig. 1. The ν_1 , ν_2 and ν_3 modes shift systematically to lower wavenumbers with increasing radius of the M^{II} cation. The DFT calculations reproduce the observed spectra well (Fig. 1) and therefore now allow an unambiguous assignment of the observed Raman bands. Further physical properties, such as low temperature, heat capacities and the elastic behavior will be discussed at the conference.

The authors gratefully acknowledge the Deutsche Forschungsgemeinschaft (DFG) for financial support of this study (HA 5137-5).

Fig. 1: Comparison of the Raman spectra of metal ($M^{\text{II}}=\text{Cu, Mn, Zn, Co}$)-guanidinium formate measured at ambient conditions to a spectrum of Zn-guanidinium formate calculated by DFT showing good agreement. The calculated data were scaled differently for both plots. The experimental data were collected in backscattering geometry, $\lambda_0=532.14$ nm.

[1] Hu, K. L. et al., *Chem. Eur. J.* **15** (2009) 12050 - 12064.

Figure 1



S07-05

Effect of thermal annealing on mechanical properties of radiation-damaged allanite-(Ce)

C. E. Reissner¹, U. Bismayer², H. Pöllmann¹, T. Beirau¹

¹Martin-Luther-Universität, Institut für Geowissenschaften und Geographie Mineralogie/Geochemie, Halle (Saale), Germany

²Universität Hamburg, Hamburg, Germany

Understanding the change in properties of condensed matter through nuclear radiation is increasingly important given the interest in secure long-term disposal of actinides from e.g. nuclear power plants. Investigating long-term effects can be achieved by analysing minerals containing natural U and Th and thus having experienced radiation exposure over geological timescales [1].

In this study, the effect of thermal annealing on allanite-(Ce) containing natural actinides on mechanical properties will be presented. Structure and long-range order have been damaged by alpha-decay resulting from incorporated ThO₂. Through step-wise thermal annealing, recrystallization and decomposition the structural properties of the mineral are altered.

On three samples from different locations, hardness and elastic modulus were analysed by the means of nanoindentation. Earlier studies have shown beginning recrystallization at about

600°C (~873K) [2] or even 650°C (~923K) [3]. It can be shown now, that hardness and elastic modulus show significant increases as early as 700K. Initial, partial recrystallization is therefore assumed to start already at thermal treatment below 700K.

[1] Ewing et al. (1988) *Nuc. Instr. Met. Phys. Res. B* 32, 487–497

[2] Janeczek & Eby (1993) *Phys Chem Minerals* 19, 343–356[3]

Čobić et al. (2010) *Can Mineral* 48: 513–521

S07-06

Determination of the H₂O content from refractive indices of crystals

R. X. Fischer¹, M. Burianek¹, R. D. Shannon²

¹Universität Bremen, Fachbereich Geowissenschaften, Bremen, Germany

²University of Colorado, Department of Geosciences/CIRES, Boulder, United States

Usually, the H₂O content in crystals is determined by thermogravimetry, recording the weight loss due to dehydration. This works well if sufficient amount of material is available. If only small crystals exist, the exact determination usually is not possible and may be just estimated from single-crystal structure refinements. This, however, might have large errors if the H₂O positions cannot be totally determined as it is often the case for zeolites. We have found that the number of H₂O molecules in compounds where only one or a few single crystals exist can be determined from the mean refractive indices if the chemical composition is known.

The determination is done according to the following procedure:

(1) The refractive indices of the crystal are measured, e.g., using the immersion method on a spindle stage mounted on a petrographic microscope.

(2) The anhydrous chemical composition is determined, e.g., by microprobe analysis.

(3) The total polarizability α_T of the anhydrous compound is calculated from the sum of the individual electronic polarizabilities α_{ei} of the ions (from [1]) according to the chemical composition. This can be easily done using, e.g., the program POLARIO [2].

(4) The observed total polarizability of the hydrous compound is calculated from the measured mean refractive index using the relationship (see [1]) $\alpha_{AE} = ((n^2 - 1)V_m) / (4\pi + (4\pi/3 - 2.26)(n^2 - 1))$.

(5) The amount of H₂O molecules can then be calculated from the difference $(\alpha_{AE} - \alpha_T) / \alpha(\text{H}_2\text{O})$ with $\alpha(\text{H}_2\text{O})$ from [1].

Following the procedure described above, the H₂O content of crystals can be determined with high accuracy. Preliminary studies of 14 different zeolites with known water content show that the mean deviation between observed and calculated H₂O content is less than 6%.

References

[1] Shannon, R.D and Fischer, R.X., *Amer. Mineral.* 101, 2016, 2288.

[2] Fischer, R.X., Burianek, M., Shannon, R.D., *Amer. Mineral.* 103, 2018, 1345.

We thank the DFG for funding (FI442/21-2)

Inorganic crystal structures II

S08-01

Oxygen's oxidation state at very high pressures

L. Dubrovinsky¹, E. Koemets¹, S. Khandarkhaeva¹, E. Bykova¹, M. Bykov¹, N. Dubrovinskaia¹

¹University of Bayreuth, Bayerisches Geoinstitut (BGI), Bayreuth, Germany

Oxygen and iron interactions control oxygen fugacity and thus most of the global geochemical processes on Earth. Extreme pressures and temperatures characteristic for deep planetary interiors are known to drastically affect the chemistry of both iron and oxygen, and promote the formation of oxides unknown at ambient conditions, such as a homologous series of $n\text{FeO} \cdot m\text{Fe}_2\text{O}_3$ and FeO_2 . To elucidate the chemistry of oxygen and crystal chemistry of iron-oxygen compounds in detail, we use *in situ* single-crystal X-ray diffraction and Mössbauer spectroscopy in diamond anvil cells. We found that at extreme pressure-temperature conditions the oxidation state of oxygen in FeO_2 is equal to 1.5- and in major phases, which constitute the lower mantle and the core-mantle boundary, it deviates from 2-. The crystal chemistry of Fe,Al-bearing silicate perovskite (bridgmanite, Brg) and post-perovskite (PPv) considerably change: iron enters octahedral structural position, the amount of iron in pure iron silicate perovskite and post-perovskite can be larger than the amount of silicon, and the quantity of iron in co-existing Brg and PPv may be significantly different.

S08-02

High-pressure high-temperature synthesis of transition-metal polynitrides

M. Bykov¹, E. Bykova², G. Aprilis³, E. Koemets¹, T. Fedotenko³, K. Glazyrin², H. P. Liermann², N. Dubrovinskaia³, L. Dubrovinsky¹

¹University of Bayreuth, Bayerisches Geoinstitut (BGI), Bayreuth, Germany

²DESY, FS-PE, Hamburg, Germany

³University of Bayreuth, Laboratory of Crystallography, Hamburg, Germany

The high-pressure chemistry of nitrogen and nitrogen-rich compounds have been in a focus of many studies in the recent years due to both fundamental and practical interest and due to the improvement of high-pressure synthetic and characterization techniques. Poly-nitrogen compounds are usually considered as potential high energy density materials (HEDM) due to the remarkable difference in the average bond energy between the single N–N bond (160 kJ/mol), the double N=N bond (418 kJ/mol), and the triple N≡N bond (945 kJ/mol). Application of pressure is one of the ways to synthesize and stabilize poly-nitrogen compounds. Several polymeric nitrogen polymorphs were obtained at high pressure and are considered as one the best HEDM known [1]. Numerous polynitrogen compounds with various nitrogen polymeric networks were theoretically predicted, but there are only a very few experimental attempts to obtain such compounds [2].

In the present work, through direct reactions between Fe, Re and N_2 in a laser-heated diamond anvil cell, we synthesized two novel nitrogen-rich compounds FeN_4 and $\text{ReN}_8 \cdot \text{N}_2$ and characterized them using single-crystal X-ray diffraction [3,4]. Both compounds feature polymeric nitrogen chains within their crystal structures (Figure 1). FeN_4 , synthesized at 106 GPa, contains catena-poly[tetraz-1-ene-1,4-diyl] anions with the ratio between double and single nitrogen-nitrogen bonds 1:3 and ratio between sp^2 and sp^3 -bonded nitrogen atoms 1:1. $\text{ReN}_8 \cdot \text{N}_2$, first obtained at 110 GPa, contains conjugated catena-poly[1,2-diazendiyl] anions with all nitrogen atoms having sp^2 hybridization. Interestingly, this

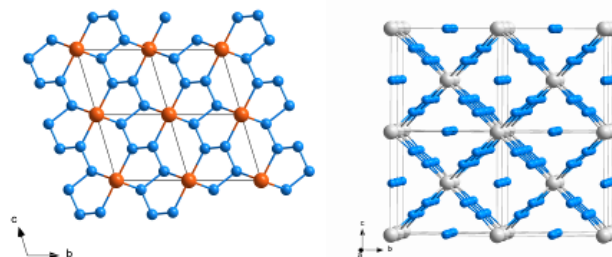
compound also contains nitrogen molecules trapped in the square-shape channels running along the [100] direction of the crystal. Moreover, syntheses conducted at lower pressures resulted in several novel compounds with stoichiometries Fe_3N_2 , FeN_2 and ReN_2 .

Figure 1 Crystal structures of FeN_4 at 135 GPa (left) and $\text{ReN}_8 \cdot \text{N}_2$ at 110 GPa (right). Fe, Re and N atoms are represented by orange, grey and blue balls respectively.

References

- [1] M. I. Eremets, *et al. Nat. Mater.* **3**, 558 (2004).
- [2] B. A. Steele, *et al. Chem. Mater.* **29**, 735 (2017)
- [3] M. Bykov *et al. Nat. Commun*, **9**, 2756 (2018)
- [4] M. Bykov *et al. Angew. Chemie. Int Ed.* **57**, 9048 (2018)

Figure 1



S08-03

Structural distortion and Eu(II) luminescence in perovskite-type $\text{KCaH}_{3-x}\text{F}_x$ ($0.5 \leq x \leq 3$)

C. Pflug¹, H. Kohlmann¹

¹Universität Leipzig, Inorganic Chemistry, Leipzig, Germany

The structural chemistry of ionic metal hydrides of alkaline and alkaline earth metals often resembles that of the corresponding fluorides, sometimes enabling the formation of solid-state solutions.[1] For instance, $\text{KCaH}_{3-x}\text{F}_x$ with $x = 1, 1.5, 2, 2.5$ was described with an orthorhombic unit cell suggesting the GdFeO_3 type ($Pnma$).[2] $\text{KCaH}_{3-x}\text{F}_x$ ($0.5 \leq x \leq 3$) can be synthesised by solid-state reactions under hydrogen gas pressure from the binary ionic hydrides and fluorides. Rietveld refinement based on powder X-ray diffraction data confirms the GdFeO_3 type ($Pnma$) for compounds rich in fluorine. However, lattice parameters a and c converge with increasing hydride content indicating a tetragonal lattice for compounds rich in hydrogen. The crystal structure of $\text{KCaH}_{3-x}\text{F}_x$ with $x \leq 1.4$ is thus better described by the SrTiO_3 type ($I4/mcm$).

Alkaline and earth alkaline earth hydrides and fluorides have been widely examined as host lattices for photoluminescence active rare earth ions.[3] Photoluminescence measurements on europium(II) substituted $\text{KCaH}_{3-x}\text{F}_x$ revealed a significant red shift of the emission wavelength ($\lambda_{em} = 728 \text{ nm}$ for $\text{KCaH}_{0.5}\text{F}_{2.5}:\text{Eu}$ and $\text{KCaH}_2\text{F}:\text{Eu}$) in comparison to violet emitting $\text{KCaF}_3:\text{Eu}$ ($\lambda_{em} = 431 \text{ nm}$ [4]) due to the strong nephelauxetic effect of hydrogen as a ligand.

- [1] A. J. Maeland, W. D. Lahar, *Z. Phys. Chem.*, **1993**, 179, 181-185
- [2] A. Bouamrane, J.-P. Soulié, J. P. Bastide, *Thermochim. Acta* **2001**, 375, 81-84
- [3] N. Kunkel, H. Kohlmann, *J. Phys. Chem. C*, **2016**, 120, 10506-10511
- [4] J. M. Garcia, W. A. Sibley, C. A. Hunt, J. M. Spaeth, *J. Lumin.* **1988**, 42, 35-42

S08-04

Is MAPbI₃ centrosymmetric? A crystallographic approach.

J. Breternitz¹, S. Barnett², H. Nowell², F. Lehmann^{1,3}, S. Schorr^{1,4}

¹Helmholtz-Zentrum Berlin, Structure and Dynamics of Energy Materials, Berlin, Germany

²Diamond Light Source Ltd, Didcot, United Kingdom

³Universität Potsdam, Institute of Chemistry, Potsdam, Germany

⁴Freie Universität Berlin, Institut für Geologische Wissenschaften, Berlin, Germany

The recent reports of piezoelectric and ferroelectric effects in the signature hybrid halide solar absorber material methylammonium lead iodide (MAPbI₃) at room temperature [1] are contradictory to the generally accepted crystal structure in the space group *I4/mcm*. While the latter is centrosymmetric, a polar space group, i.e. the breaking of inversion symmetry in the structure, would be a necessary prerequisite for ferroelectricity. A convenient explanation for this apparent discrepancy would be a symmetry breaking due to the non-symmetric molecular cation orientation and dynamics, as has been suggested in the past. [2] Since the molecule is heavily disordered, [3] a non-linear effect would probably disappear on a macroscopic scale if it is only caused by this. In order to resolve the cause of the measured non-linear effects, we performed anomalous single crystal X-ray diffraction at the lead absorption edge using the I19 beamline at Diamond Light Source, which allowed us to determine the atom positions in the inorganic part of the structure to a most accurate level. Herein, we will describe the consequences of atom shifting for the symmetry breaking in the room temperature structure of MAPbI₃ and discuss some of the causes for this behaviour. We will highlight the consequences of the symmetry breaking for the extraordinary performance of the class of hybrid halide solar cell materials.

References

- [1] e.g. Y. Rakita, O. Bar-Elli, E. Meirzadeh, H. Kaslasi, Y. Peleg, G. Hodes, I. Lubomirsky, D. Oron, D. Ehre, D. Cahen, *PNAS* (2017), 114, E5504-E5512.
 [2] e.g. S. Govinda, B. P. Kore, M. Bokdam, P. Mahale, A. Kumar, S. Pal, B. Bhattacharyya, J. Lahnsteiner, G. Kresse, C. Franchini, A. Pandey, D. D. Sarma, *J. Phys. Chem. Lett.*, 2017, 8, 4113-4121.
 [3] A. Franz, D. M. Töbrens, S. Schorr, *Cryst. Res. Technol.* (2016), 51, 534–540.

S08-05

Intergrowth of the β - and δ -Al-Fe-Si intermetallic phase and polytypes of the β phase

H. Becker^{1,2}, T. Bergh³, P. E. Vullum³, A. Leineweber¹, Y. Li²

¹Technische Universität Bergakademie Freiberg, Institute of Materials Science, Freiberg, Germany

²Norwegian University of Science and Technology, Materials Science and Engineering, Trondheim, Norway

³Norwegian University of Science and Technology, Department of Physics, Trondheim, Norway

Frequently occurring plate-shaped particles in Fe-containing Al-Si alloys have a crucial effect on the cast and mechanical properties. These particles form during solidification and consist of the intermetallic β and/or δ phase depending on the formation conditions. Hence, their distinction within the microstructures is too superficial by their morphology only. However, also the crystal structures of the β and δ phase are closely related and represent two extreme types of regular stacking of layers of edge connected bicapped antiprisms. Furthermore, the crystal structure of the β phase is still under discussion lacking a systematic analysis of ordered stacking of the layers that leads to polytype formation.

The objective of the present study is to give detailed insight into similarities and differences of the crystal structure characteristics of

the β and δ phase, show their clear distinction and to reanalyse the crystal structure of the β phase in view of its polytypes.

The analysis employs an intermetallic alloy with 60.4at% Al, 24.2at% Si and 15.4at% Fe consisting predominantly of the β and δ phase and plate-shaped intermetallic particles in a secondary Al_{7.1}Si_{1.2}Fe_{0.3}Mn model alloy. The investigation is based on SEM including EBSD, TEM and XRD.

The β and δ phase consist of the same *basic layers* while all cap atoms are shared in the δ phase but terminate every second layer, forming *double layers*, in the β phase. Due to the good fit along the (001) planes both actually distinct phases can be severely intergrown. The β phase exhibits polytypes based on ordering of the double layers being shifted by $\mathbf{a}/2$ or $\mathbf{b}/2$ displacements leading to 4 different double layer positions A, B, C, and D. An AB polytype with idealized *Acam* symmetry actually shows a monoclinic distortion towards *A12/a1* symmetry. An ABCD polytype with idealized *I41/acd* symmetry has been observed. Next to the ordered polytypes, stackings with non-periodic sequences of A, B, C and D double layers exist.

S08-06

Packings of Sphere Packings – Pushing Ahead

M. Petrik¹, W. Hornfeck²

¹Philipps-Universität Marburg, Marburg, Germany

²Czech Academy of Sciences, Prague, Czech Republic

Sphere packings lie at the heart of structural inorganic chemistry. They provide a rationale for the classification of crystal structures. Both homogeneous [1] and heterogeneous [2] sphere packings are currently being compiled. Recently, we realized that a higher level of categorization is possible by considering *packings of sphere packings* (PSPs). [3] PSPs emerge whenever two (or more) sphere packings interpenetrate and thereby establish contact, provided the contiguity (network of contacts) in either of them is not disrupted. These two conditions set them apart from most of the known interpenetrating structures like Cu₂O, MgCu₂ or metal-organic frameworks (MOFs), in which the two substructures fail to establish contact. PSPs not only serve for the classification of crystal structures, they may also show remarkable new characteristics in their own right, e.g. quasirandomness. [3-5] Therefore, in 2017, we initiated a search for PSPs. [6] Up to now, 41 have been discovered, for the most part previously unrecognized. One example, named PSP-9, is shown in **Figure 1** to illustrate how a PSP arises when two concatenated sphere packings establish contact while at the same time maintaining their individual connectivity.

Among the insights gained by considering PSPs may be mentioned the following. The structure of a novel sphere packing isopointal with β -manganese [4] consists of two interpenetrating sphere packings, or nets, forming a PSP: on the one hand the three-connected Laves net, on the other a related net obtained by placing vertices in the centers of the bonds of the former. The Laves net may be viewed as a three-dimensional variant of the graphene net. Then, by analogy, the second net is a kind of three-dimensional Kagome net (vertices in place of bonds of the graphene net). Thus, the novel PSP (and consequently β -manganese also) is found to derive from two most simple and fundamental motifs: graphene and the Kagome net extrapolated into three dimensions!

References:

- [1] H. Sowa, *Acta Cryst.* **2018**, A74, 143.

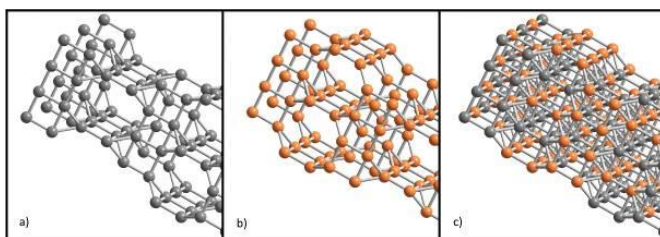
[2] M. O'Keeffe, M. A. Peskov, S. J. Ramsden, O. M. Yaghi, *Acc. Chem. Res.* **2008**, *41*, 1782.

[3] M. Petrik, W. Hornfeck, *Z. Anorg. Allg. Chem.* **2016**, *642*, 1023.

[4] M. Petrik, W. Hornfeck, B. Harbrecht, *Z. Anorg. Allg. Chem.* **2014**, *640*, 2328.

[5] W. Hornfeck, P. Kuhn, *Acta Cryst.* **2014**, *A70*, 441. [6] M. Petrik, *Call for Contributions of PSPs, Hako conference, Augsburg, Germany, March 16-18, 2017*; <https://spherepacker.github.io/welcome.html>.

Figure 1



Organic molecules and coordination compounds

S09-01

Synthesis, Crystal Structures and Thermodynamic Relations in Polymorphic Coordination Compounds

C. Näther¹, T. Neumann¹, I. Jess¹, L. S. Germann², R. E. Dinnebier², F. Pielhofer²¹Christian-Albrechts Universität zu Kiel, Institut für Anorganische Chemie, Kiel, Germany²Max Planck Institute for Solid State Research, Scientific Facility X-ray diffraction, Stuttgart, Germany

Polymorphism is a widespread phenomenon for coordination compounds but in most cases the thermodynamic relations are not investigated, because they usually decompose before they melt or transform and helpful thermodynamic rules like the heat of transition or the melting enthalpy rule cannot be used.

In our ongoing project on the synthesis of thiocyanate coordination compounds we obtained two polymorphic modifications (**I-Co** and **II-Co**) of a discrete complex with the composition $\text{Co}(\text{NCS})_2(4\text{-dimethylamino-pyridine})_2$ [1]. Both modifications are related by enantiotropism with **I-Co** as the HT form. From the melting points and the heats of fusion the transition temperature was estimated to 153°C, in very good agreement with that determined by annealing experiments of 145°C.

For the compound with $\text{Zn}(\text{NCS})_2$ similar modifications were found, with **I-Zn** isotypic to **I-Co** and **II-Zn** isotypic to **II-Co**, together with a third form (**III-Zn**), that is not observed with cobalt. Investigations on their thermodynamic relations reveal, that **I-Zn** and **II-Zn** are also related by enantiotropism with **I-Zn** as the HT form. **III-Zn** and **I-Zn** are related by monotropism, whereas **III-Zn** and **II-Zn** are related by enantiotropism, with the energy temperature curves crossing at a temperature where **I-Zn** is already stable. The thermodynamic transition temperature between **II-Zn** and **I-Zn** was experimentally determined to be below about -35°C, which is in rough agreement with that estimated from the melting points and melting enthalpies. The extremely huge difference in thermodynamic stability between the Co(II) and the Zn(II) forms is surprising, because each pair is isotypic, the cations exhibit the same charge and similar ionic radii and the intermolecular interactions should be comparable.

[1] T. Neumann, I. Jess, F. Pielhofer, C. Näther, *Eur. J. Inorg. Chem.*, **2018**, doi:10.1002/ejic.201800741.[2] T. Neumann, I. Jess, L. E. Germann, R.E. Dinnebier, C. Näther, *Cryst. Growth. Des.*, **2018**, submitted.

S09-02

Organometallic cavities as functional pores and building blocks

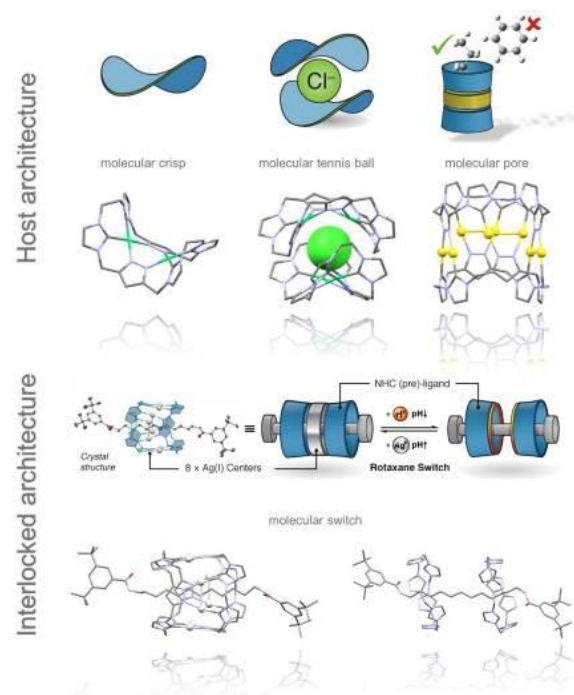
A. Pöthig¹¹Technische Universität München, München, Germany

Porous materials have been applied in a variety of different fields, especially for separation and storage applications. One approach to design new materials towards desired properties is to build up multi-dimensional frameworks out of organic building blocks. These are connected either covalently to form supramolecular organic polymeric frameworks (COFs) or via metal nodes to form porous coordination polymers (MOFs). Additionally, also discrete molecules with cavities – so-called cavitiands – can be used as single pores for a variety of applications. However, in contrast to their rather projectable topology, the (post-synthetic) inclusion of further functionality into these materials is often difficult.

To overcome these limitations we design and employ organometallic complexes, which exhibit defined cavities and additionally possess intrinsic functionality, e.g. photoluminescence, selective guest recognition, easily adjustable polarity/solubility and catalytic activity.¹⁻³ Furthermore, the complexes can be employed as building blocks in mechanically-interlocked molecules, namely rotaxanes, forming a pH-responsive molecular switch.⁴ Depending on the metal, the organometallic cavitiands show different bio activity.⁵ The compounds have been characterized using single crystal X-ray diffraction and the structures are discussed in detail.

[1] P. J. Altmann, C. Jandl, A. Pöthig, *Dalton Trans.*, **2015**, 44, 11278-11281.[2] P. J. Altmann, A. Pöthig, *Chem. Commun.*, **2016**, 52, 9089-9092.[3] P. J. Altmann, A. Pöthig, *J. Am. Chem. Soc.*, **2016**, 138(40), 13171-13174.[4] P. J. Altmann, A. Pöthig, *Angew. Chem., Int. Ed.* **2017**, 129(49), 15939-15942.[5] A. Pöthig*, S. Ahmed, H. C. Winther-Larsen, S. Guan, P. J. Altmann, J. Kudermann, A. M. Santos-Andresen, T. Gjøen, O. A. Høymoen-Åstrand*, *Front. Chem.* **2018**, asap.

Figure 1



S09-03

From Pentagons to Squares: Giant Supramolecules Based on $[\text{Cp}^R\text{Ta}(\text{CO})_2(\eta^4\text{-P}_4)]$ Organometallic Building BlockE. Peresyphkina^{1,2}, A. Virovets^{1,2}, M. Scheer¹¹University of Regensburg, Regensburg, Germany²Novosibirsk State University, Novosibirsk, Russian Federation

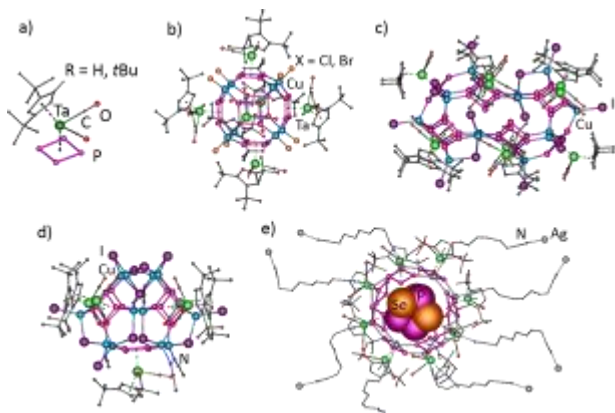
Since 2003, we have been using organometallic complexes $[\text{Cp}^R\text{Fe}(\eta^5\text{-P}_5)]$ ($\text{Cp}^R = \eta^5\text{-C}_5\text{R}_5$, $\text{R} = \text{Me}, \text{CH}_2\text{Ph}, \text{PhC}_4\text{H}_9$) as building blocks to obtain giant supramolecules [1-4]. The atoms of the planar P_5 -rings of $[\text{Cp}^R\text{Fe}(\eta^5\text{-P}_5)]$ coordinate to Cu^+ and Ag^+ cations resulting in self-assembled spherical supramolecules of 2.1 – 4.6 nm in diameter. The central metallophosphorus core is sometimes able to encapsulate various guest molecules [2].

The extension of the same principle to η^4 -P₄ complexes as [Cp^RTa(CO)₂(η^4 -P₄)] (**1**: Cp^R = η^5 -C₅H₃tBu₂, C₅H₃tBu₃) leads to various supramolecules (Fig.) [5, 6]. Thus, the self-assembly of **1** with CuX (X = Cl, Br) allows to obtain [({**1**})₆{CuX}]₈ spheres with non-classical fullerene topology. The inorganic cores of 24 P and 8 Cu atoms represent the carbon-free analog of C₃₂, where six P₄ squares instead of six C₅ pentagons are isolated by alternating Cu₂P₄ hexagons (isolated-square rule, Fig.b). Using CuI results in unprecedented supramolecules with non-fullerene topologies [({**1**})₁₀{CuI}]₁₄ and [({**1**})₅{CuI}]₁₂(MeCN)₅ (Fig.c,d). Recently we succeeded in obtaining of the first 2D coordination polymers based on **1**, AgSbF₆ and flexible dinitrile NC(CH₂)₇CN linkers, where supramolecular donut-like nodes [({**1**})₈Ag₈]⁸⁺ (Fig.e) encapsulate P₄S₃ and P₄Se₃ molecules in the central cavity.

Financial support from the ERC grant AdG-339072 is gratefully acknowledged. The research was partly done at the light source PETRA III at DESY.

- [1] J. Bai, A. Virovets, M. Scheer (2003), *Science*, **300**, 781
 [2] E. Peresyphkina, C. Heindl, A. Virovets, M. Scheer (2016) *Structure and Bonding* (2016) **174**, 321
 [3] C. Heindl, E.V. Peresyphkina, A.V. Virovets, et al (2017) *Angew. Chem. Int. Ed.* **56**, 13237
 [4] E. Peresyphkina, C. Heindl, A.V. Virovets, et al (2018). *Chem. – A Eur. J.* **24**, 2503
 [5] B. P. Johnson, F. Dielmann, G. Balázs, et al (2006), *Angew. Chem. Int. Ed.*, **45**, 2473
 [6] F. Dielmann, E.V. Peresyphkina, B. Krämer, et al (2017) *Angew. Chem. Int. Ed.* **55**, 14833

Figure 1



S09-04

Towards crystal structure solution of organic compounds without prior knowledge of space group and lattice parameters by fit to the pair distribution function

D. Prill¹, C. Schlesinger¹, S. Habermehl¹

¹Goethe-Universität Frankfurt am Main, Anorganische und Analytische Chemie, Frankfurt am Main, Germany

Local structures in crystalline, nanocrystalline and amorphous organic compounds can be investigated using pair distribution functions (PDFs). The experimental determination of the PDF curves of organic compounds is very similar to that of inorganic compounds. However, the fit of structural models to the PDF curve has rarely been done for organic compounds. In our previous research, the method developments for structure determination from PDF were successful with determination of molecular position and orientation starting from random values[1]. Experimental lattice parameters and space group have been given

as an input. For many nanocrystalline organic compounds the space group and lattice parameters are unknown. Therefore, a global procedure in which the lattice parameters, the space group, the molecular position and orientation are determined from PDF-Data has been developed[2]. The calculations initiate with creating a large set of random starting structures in various space groups using FIDEL Software[3]. The space groups are chosen according to the space group frequency of the corresponding compound class, regarding the chemical class and the molecular symmetry[4]. The optimisation of lattice parameters starts from random values within the sensible range. The ranges are automatically chosen depending on the size of the investigated molecule and space group in which the calculations are performed. The optimisation calculations are carried out using TOPAS Software[5]. At this stage of the method development, the chosen investigated molecules are small and rigid and therefore treated as rigid bodies during the calculations.

- [1] D. Prill, P. Juhás, S. J. L. Billinge, M. U. Schmidt, *Acta Cryst. A*, 2015, **72**, 62.
 [2] D. Prill, C. Schlesinger, S. Habermehl, *in preparation*.
 [3] S. Habermehl, P. Mörschel, P. Eisenbrandt, S. M. Hammer, M. U. Schmidt, *Acta Cryst. B*, 2014, **70**, 347.
 [4] E. Pidcock, W. D. S. Motherwell, J. C. Cole, *Acta Cryst. B*, 2003, **59**, 634.
 [5] A. A. Coelho, *J. Appl. Cryst.*, 2018, **51**, 210.

S09-05

IDEAL – Invariom Derived Electron AnaLysis in APEX3

H. Ott¹, J. Lübben¹, M. Ruf², C. B. Hübschle³

¹Bruker AXS GmbH, Application, Karlsruhe, Germany

²Bruker AXS Inc, Madison, United States

³University of Bayreuth, Bayreuth, Germany

With the introduction of large shutterless detectors, data quality to high resolution has dramatically improved over the last few years. Data to 0.5 Å and beyond can be collected with only one detector setting, with short exposure times, and short overall experiment times. Traditionally, structures are refined using an Independent Atom Model (IAM), although good data beyond the traditional 0.8 Å reveals additional electron density that cannot be modeled appropriately. Often practitioners choose to cut data to preserve a low structure reliability criteria *R*₁, sacrificing additional information and overall structure quality.

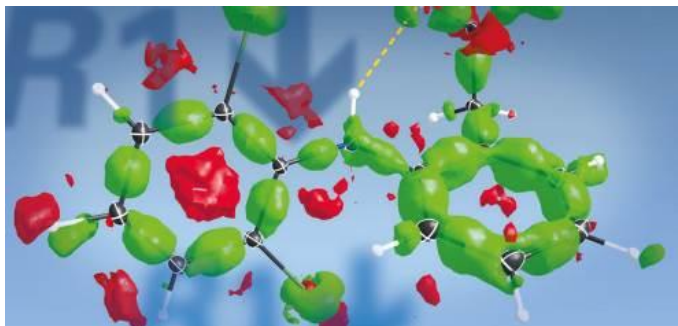
IDEAL lets you have the cake and eat it too! This APEX3 feature uses a database of bond-oriented deformation density parameters derived from the INVARIOM¹ database of *ab initio* calculations of model compounds. BEDE (Bond Electron DEnsity) and LONE (LONe pair Electron density) parameters are automatically assigned for the refinement with an extended version of XL. This uses IAM scattering factors and, in addition, models scattering contributions of bonds and lone pairs.²

IDEAL delivers structures with increased model accuracy and provides access to more detailed model properties. It is easy to use and seamlessly integrated with APEX3 in the Refine Structure plug-in (SHELXle).

The presentation will introduce the details of the method and describe the application of a number of examples.

- [1] B. Dittrich, C. B. Hübschle, K. Pröpper, F. Dietrich, T. Stolper, J. J. Holstein, *Acta Crystallogr. Sect. B* **2013**, **69**, 91.
 [2] J. Lübben, C. Wandtke, C. B. Hübschle, M. Ruf, B. Dietrich, *Acta Crystallogr. Sect. A*, **2019**, **75**,
<https://doi.org/10.1107/S2053273318013840>.

Figure 1



S09-06

Crystalline Sponges by Merck: bringing an exciting new method to a wider audience

C. von Essen¹, C. Kühn¹, A. Khutia¹, K. Kawata¹, W. Hierse¹

¹Merck KGaA, Darmstadt, Germany

The Crystalline Sponge method developed by Prof. Fujita facilitates the crystal structure determination of non-crystalline analytes in low quantity by using a porous complex that can absorb small to medium size molecules.¹ The molecules arrange uniformly within the pores making them observable by conventional X-ray crystallography. The initial publication has gained strong interest throughout the scientific community² as the method promises to ease absolute structure determination of e.g. impurities and natural compounds.³

However, many labs around the world found it difficult to reproduce the technique as it requires a certain level of experience and expert knowledge despite the fact, that the Fujita group published a revised method with more detailed experimental description.⁴

At the science and technology company Merck, we run a project to help the Crystalline Sponge method to a broader application. We licensed the technology from the University of Tokyo and the Japanese Science and Technology Agency and are engaged in a Japanese consortium aiming for the development of the Crystalline Sponge method.

We are currently setting up an analytical service and are developing processes and consumables around the method to enable non-expert scientists to successfully apply the Crystalline Sponge method.

References

- [1] Y. Inokuma, S. Yoshioka, J. Ariyoshi, T. Arai, Y. Hitora, K. Takada, S. Matsunaga, K. Rissanen, M. Fujita, *Nature* **2013**, 495, 461–466.
- [2] B. Halford, *Chemical & Engineering News* **2015**, 97, 29-30.
- [3] S. Urban, R. Brkljača, M. Hoshino, S. Lee, M. Fujita, *Angew. Chem. Int. Ed.* **2016**, 55, 2678–2682.
- [4] M. Hoshino, A. Khutia, H. Xing, Y. Inokuma, M. Fujita, *IUCrJ* **2016**, 3, 139–151.

Bio-Crystallography III: Enzymes

S10-01

Structure-based insights into molybdenum cofactor biosynthesis, transport and insertion

J. Krausze¹

¹Braunschweig University of Technology, Institute of Plant Biology, Braunschweig, Germany

The transition metal molybdenum (Mo) is essential for all life as it bestows redox activity on two key enzymes of the biogenic nitrogen and sulfur cycles, i.e. nitrate reductase and sulfite oxidase. Yet, in its abundant form – molybdate – it is chemically inert unless complexed by the dithiolene motif of a specific pterin compound to form molybdenum cofactor (Moco, Figure 1). With the sole exception of nitrogenase, Moco is the prosthetic group of all Mo-dependent enzymes. Its highly conserved biosynthesis pathway comprises four steps, the first three of which are already well understood. In contrast, the last biosynthesis step – the insertion of molybdate into the dithiolene motif – is still in the focus of research. Also, the implementation and regulation of the transport of mature Moco to its target enzymes is still to be elucidated. It is assumed that Moco, which is not stable in free form, binds to Moco carrier proteins (MCPs) that are in control of its protection and trafficking within the cell. For a better understanding of Moco biosynthesis, transport and insertion, we aimed for the characterization of the Mo-insertase from *Arabidopsis thaliana* (AtCnx1E) and MCPs from various organisms by means of x-ray crystallography. The structure of AtCnx1E in complex with molybdate allowed us to identify two oxo-anion binding sites (Figure 2), which are fundamental for the initiation of the insertion reaction and for the substrate selectivity of AtCnx1E. Through site-directed mutagenesis, we were able to generate and crystallize an AtCnx1E variant that accumulates a hitherto unknown intermediate that has broad implications for the elucidation of the enzymatic mechanism. The structures of MCP combined with docking experiments allowed us to unambiguously identify the site of Moco binding in a shallow cavity at the protein surface, which was confirmed by mutagenesis studies. These results confirm the role of MCP as a mediator between Mo-insertase and the target enzymes and complete the picture of the interplay between the proteins of Moco biosynthesis.

Figure 1

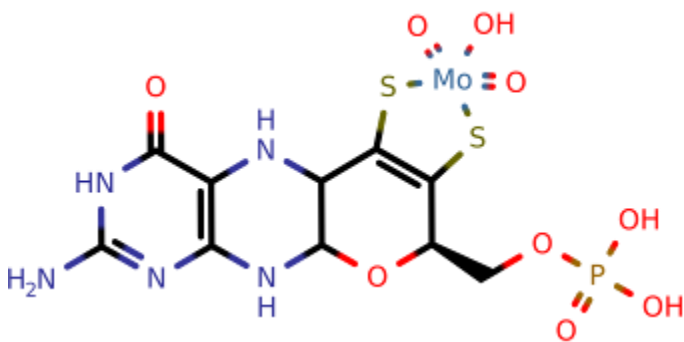
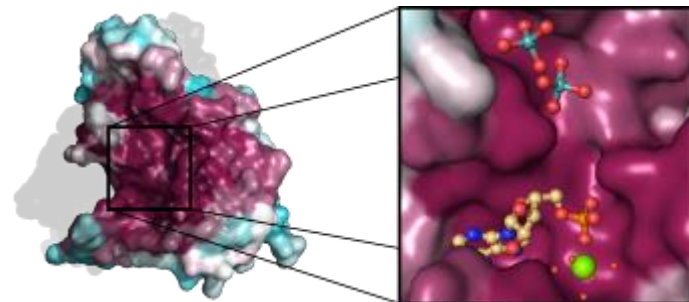


Figure 2



S10-02

Structural characterization of cold-adapted β -D-galactosidase mechanism

M. Rutkiewicz^{1,2}, M. S. Weiss¹, A. Bujacz²

¹Helmholtz-Zentrum Berlin für Materialien und Energie, Macromolecular Crystallography (HZB-MX), Berlin, Germany

²Lodz University of Technology, Institute of Technical Biochemistry, Lodz, Poland

The majority of enzymes used in industry originate from mesophilic organisms, however nowadays extremophilic enzymes tend to compete for its place in various branches of industry. β -D-galactosidases (β DG) are enzymes widely used in food processing to hydrolyze lactose, naturally occurring in milk. Depending on type of the available acceptor, the enzyme can perform either hydrolysis or transglycosylation.

The aim of this study is to structurally characterize differences between cold adapted β DG from *Arthrobacter* sp. 32cB (*Arth* β DG) and mesophilic homologues, that result in change in enzyme's optimal temperature.

The crystal structures of *Arth* β DG and its complexes with ligands collected on BL14.2 line of BESSY Berlin, Germany enable analysis of subsequent stages of reaction mechanism. The diffraction data were processed in trigonal space group P 31 2 1 up to the resolutions varying in range of of 1.7 – 2.8 Å. Careful analysis of the obtained crystal structures shows that the movement of Phe581 is the sole conformational change accompanying reaction mechanism. In fact, the 10-aa loop restricting access to the active site in mesophilic GH2 β DGs, in *Arth* β DG is stabilized in a position allowing an unrestricted access of substrate to active site by a number of strong interactions with other parts of Domain 5.

The analysis of a series of crystal structures of *Arth* β DG complexes highlights differences in active site architecture that aim into making its active site more open. Such a design, promotes substrate association and product dissociation resulting in higher turnover rate, which is one of the main factors promoting efficient hydrolysis at low temperature.

This project was funded by National Science Centre Poland (2016/21/B/ST5/00555) (AB).

MR's PhD scholarship was financed by National Science Centre Poland (2018/28/T/ST5/00233).

S10-03

Elucidation of cd₁ nitrite reductase NirS maturation of *Pseudomonas aeruginosa* by NirF and NirN with x-ray crystallography

T. Klünemann¹, A. Preuß², G. Layer², W. Blankenfeldt¹

¹Helmholtz Centre for Infection Research, Structure and Function of Proteins, Braunschweig, Germany

²Albert-Ludwigs-Universität Freiburg, Institut für Pharmazeutische Wissenschaften, Freiburg i. Br., Germany

Introduction

Many bacteria are capable of switching from oxygen to nitrate as terminal electron acceptor in the respiratory chain. One central step during this "denitrification" is the reduction from nitrite to nitric oxide by the cd₁ nitrite reductase NirS, which uses an uncommon isobacteriochlorin "heme d₁" in its catalytic center. Although the nitrite reduction mechanism is quite well understood, the maturation of the nitrite reductase NirS and the biosynthesis of heme d₁ are still elusive. The last biosynthesis step is catalyzed by NirN, a dehydrogenase, which introduces a double bond in the propionate sidechain of dihydro heme d₁ by a novel electron bifurcation mechanism. Another protein involved in the biosynthesis is NirF, but its function in this process is unknown. Both NirN and NirF have been shown to interact with NirS in vivo and might be involved in the insertion of heme d₁.

Methods

To get insight into the unique reaction mechanism of NirN, the function of NirF and the conformation of apo NirS, we determined their crystal structures. The importance of d₁-type heme-interacting residues was investigated by activity assays.

Results

Similar to cd₁-nitrite reductase, the monomeric NirN is composed of a cytochrome c domain and an eight-bladed β-propeller binding heme d₁, but their relative orientation is different. The central iron ion of heme d₁ is coordinated by His147 at its proximal side, and a flexible loop on the other side (residue 317-327) contributes His323 as ligand. Tyr461 and His417 are in close proximity to the hydrogens removed during dehydrogenation, suggesting a function as catalytic base. The homodimeric NirF consists of two eight-bladed β-propellers that each present His62 and His252 as ligands for the central iron of heme d₁. The homodimeric nitrite reductase NirS without bound heme d₁ occupies a conformation, where the two cytochrome C domains are moved away from each other as compared to the heme d₁ bound conformation.

Conclusion

The necessity of His147, His323 and Tyr461 for the catalytic activity NirN was identified, giving first insight into its uncommon dehydrogenation activity. NirS takes a different conformation without bound heme d₁, revealing a possible loading state, that may be crucial for the maturation of this enzyme. The structure of NirF revealed two histidines important for heme d₁ binding, but its function during heme d₁ biosynthesis remains elusive.

S10-04

Structure of the c-di-AMP synthesising diadenylate cyclase CdaA

J.L. Heidemann¹, P. Neumann¹, A. Dickmanns¹, R. Ficner¹

¹Georg-August Universität Göttingen, Molekulare Strukturbiologie, Institut für Mikrobiologie & Genetik, GZMB, , Göttingen, Germany

Cyclic di-AMP (c-di-AMP) is the only known essential second messenger mainly found in gram-positive bacteria of which several are known as human pathogens (1). It is involved in many cellular processes like cell wall metabolism and DNA integrity scanning. c-

di-AMP is synthesised by proteins containing diadenylate cyclases (DAC) domain. CdaA is the sole DAC in the human pathogen *Listeria monocytogenes*, which is also conserved in many other human pathogenic bacteria. Since c-di-AMP is also essential for the growth of these pathogenic bacteria CdaA seems to be an attractive target for the development of novel antibiotic compounds.

Here, we report new crystal forms of CdaA from *Listeria monocytogenes* in its apo-state, post-catalytic state with bound c-di-AMP and two catalytic Co²⁺ ions as well as in complex with AMP. The comparison of the determined crystal structures revealed a tyrosine side chain (Tyr187) positioned in different orientations, but locking the adenine ring after ATP binding. A mutation of Tyr187 to Ala unveiled its essential role during catalysis.

In order to identify potential compounds that reduce the CdaA activity we used crystallographic fragment screening. This approach requires well diffracting (~ 2.0 Å) crystals of CdaA in its apo-state. Obtained apo CdaA crystals belong to the space group P212121 and diffracted up to 1.7 Å resolution. Furthermore the active site of apo CdaA in the crystal is exposed to solvent channels making it suitable for fragment screening. Analysis of the mFo-DFc difference Fourier electron density map unveiled an excess electron density corresponding to a small molecule bound to apo CdaA. This density was interpreted as a sucrose molecule, which was added to the crystal during soaking in the cryo-protectant solution.

[1] Commichau, F. M., Dickmanns, A., Gundlach, J., Ficner, R., Stülke, J. 2015. A jack of all trades: the multiple roles of the unique essential second messenger cyclic di-AMP. *Mol. Microbiol.* 97: 189-204.

S10-05

Legumain inhibitory cystatin E transforms to multimers with distinct function

E. Dall¹, J. Hollerweger¹, S. O. Dahms¹, H. Brandstetter¹

¹University of Salzburg, Biosciences, Salzburg, Austria

Altering the oligomerization state is an established strategy to regulate protein activity. In this context, domain swapping is a mechanism by which proteins exchange part of their structure and thereby form long-lived dimers or multimers. Domain swapping was specifically observed in amyloidogenic proteins, a prominent example thereof is the cystatin superfamily of cysteine protease inhibitors. Cystatins are twin-headed inhibitors, simultaneously targeting the lysosomal cathepsins and legumain, with important roles in cancer progression and Alzheimer's diseases. Although cystatin E is the most potent legumain inhibitor identified so far, nothing is known about its propensity to oligomerize. In this study we show that conformational destabilization of cystatin E led to the formation of a domain-swapped dimer with increased conformational stability. While the hCE dimer was active as a legumain inhibitor by forming a trimeric complex, it lost its inhibitory function towards papain-like enzymes. Additionally, we provide evidence that the dimer can further convert to amyloid fibrils. Unexpectedly, cystatin E amyloid fibrils contained functional protein, inhibiting both legumain and papain-like enzymes. Together these findings suggest that cystatin amyloid fibrils might serve as a binding platform to stabilize the pH-sensitive legumain and cathepsins in the extracellular environment, thereby increasing their lifetime for (patho-)physiologic function.

S10-06

Adaptation of a Bacterial Multidrug Resistance System Revealed by the Structure and Function of AlbA

J. A. Köhnke^{1,2}

¹Helmholtz Center for Infection Research, Structural Biology of Biosynthetic Enzymes, Saarbrücken, Germany

²Helmholtz Institute for Pharmaceutical Research Saarland, Saarbrücken, Germany

To combat the rise of antimicrobial resistance, the discovery of new antibiotics is paramount. Albicidin and cystobactamid are related natural product antibiotics with potent activity against Gram-positive and, crucially, Gram-negative pathogens. AlbA has been reported to neutralize albidin by binding it with nanomolar affinity. To understand this potential resistance mechanism, we determined structures of AlbA and its complex with albidin. The structures revealed AlbA to be comprised of two domains, each unexpectedly resembling the multi-antibiotic neutralizing protein TipA. Binding of the long albidin molecule was shared pseudosymmetrically between the two domains. The structure also revealed an unexpected chemical modification of albidin, which we demonstrate to be promoted by AlbA, and to reduce albidin potency; we propose a mechanism for this reaction. Overall, our findings suggest that AlbA arose through internal duplication in an ancient TipA-like gene, leading to a new binding scaffold adapted to the sequestration of long-chain antibiotics.

Bio-Crystallography IV: Structure-based drug design

S11-01

Rational Identification of Allosteric Regulation Sites in

Biocatalysts: A Way to New Therapies

R. Fedorov¹, J. Cramer^{1,2}, J. Fühling², P. Baruch¹, J. Lieske^{1,2,3}, O. Zeymer¹, X. Zhou¹, O. Prakash², B. Feddersen¹, J. Lohöfener¹, N. Steinke¹, P. Kay-Fedorov⁴, C. Goffinet⁵, U. Curth¹, C. Brütting⁶, H. J. Knölker⁶, F. Routier², D. Manstein¹, R. Gerardy-Schahn²

¹Hannover Medical School, Institute for Biophysical Chemistry / Research Division for Structural Biochemistry, Hannover, Germany

²Hannover Medical School, Institute of Clinical Biochemistry, Hannover, Germany

³Center for Structural Systems Biology, Hamburg, Germany

⁴Hannover Medical School, Institute of Virology, Hannover, Germany

⁵Center for Experimental and Clinical Infection Research, Hannover, Germany

⁶Technische Universität Dresden, Department of Chemistry, Dresden, Germany

Biocatalysts utilize allosteric mechanisms to control selectivity, catalytic activity and the transport of reaction components¹. The allosteric control of enzymatic catalysis has a high potential for the development of drugs and biotechnologies. In particular, it opens the way to specific regulation of vital enzymes with conserved active sites. Using the central metabolic enzyme UDP-glucose pyrophosphorylase from the pathogen *Leishmania major* (LmUGP), we demonstrate how specific allosteric inhibition sites and their links to the catalytic center can be revealed rationally, through analysis of molecular interfaces along the enzymatic reaction cycle^{1,2}. Two previously unknown allosteric inhibition sites in LmUGP were rationally identified and experimentally verified. These sites are specific for the *Leishmania* enzyme and are coupled with the catalytic center via allosteric networks¹⁻³. The molecular scaffold for allosteric inhibitor targeting the pathogen's enzyme was developed. This led to the identification of murrayamine-I as an allosteric inhibitor that selectively blocks LmUGP¹. The presented approach opens up the possibility of using central metabolic enzymes with highly conserved active sites as allosteric drug targets, thus solving the cross-reactivity problem. In particular, it paves the ways to anti-microbial treatments. Currently, we are extending the presented approach to other pathogens of the Trypanosomatidae family and towards the development of specific modulators of the innate immune sensors OAS and cGAS⁴, which can provide potent agents in the treatment of infectious diseases and autoinflammation.

[1] Cramer JT, Fühling JI, Baruch P, Brütting C, Knölker H-J, Gerardy-Schahn R, and Fedorov R. (2018) *ACS Catalysis*. **8**:2683-2692.

[2] Fühling J, Cramer JT, Routier FH, Lamerz A-C, Baruch P, Gerardy-Schahn R and Fedorov R. (2013) *ACS Catalysis*. **3**:2976-2985.

[3] Fühling JI, Cramer JT, Schneider J, Baruch P, Gerardy-Schahn R, and Fedorov R. (2015) *Sci. Rep.* **5**:9618.

[4] Lohöfener J, Steinke N, Kay-Fedorov P, Baruch P, Nikulin A, Tishchenko S, Manstein DJ, and Fedorov R. (2015) *Structure*. **23**(5):851-862.

S11-02

Crystal Structures of Gephyrin in Complex with Antimalarial Artemisinins: Molecular Basis for Inhibitory Neurotransmission Regulation by Artemisinins

V. Kasaragod¹, H. Schindelin¹

¹Universität Würzburg, Rudolf-Virchow-Zentrum für Experimentelle Biomedizin, Würzburg, Germany

The frontline anti-malarial drug artemisinin and its derivatives have also been implicated in modulating multiple mammalian cellular

pathways including the recent identification of targeting γ -aminobutyric acid type A receptor (GABA_AR) signaling in the pancreas. Their molecular mechanism of action, however, remains elusive. Here we present crystal structures of gephyrin, the central organizer at inhibitory postsynapses, in complex with artesunate and artemether at 1.5 Å resolution. These artemisinins target the universal inhibitory neurotransmitter receptor-binding epitope of gephyrin, thus inhibiting critical interactions between gephyrin and glycine receptors (GlyRs) as well as GABA_ARs. Electrophysiological recordings reveal a significant inhibition of gephyrin-mediated neurotransmission by artemisinins. Furthermore, clustering analyses in primary neurons demonstrate a rapid inhibition and a time-dependent regulation of gephyrin and GABA_AR cluster parameters. Our data not only provide a comprehensive model for artemisinin-mediated modulation of inhibitory neurotransmission but also establish artemisinins as potential lead compounds to pharmacologically interfere with this process.

S11-03

Structure-based Design of Broad-Spectrum Antivirals Targeting Coronaviruses and Enteroviruses

L. Zhang^{1,2}, D. Lin^{1,2,3}, Q. Ma¹, Y. Kusov^{1,2}, R. Hilgenfeld^{1,2}

¹University of Lübeck, Institute of Biochemistry, Lübeck, Germany

²German Center for Infection Research (DZIF), Hamburg - Lübeck - Borstel - Riems Site, Lübeck, Germany

³Changchun Discovery Sciences Ltd., Changchun, China

Despite the devastating consequences of emerging viruses such as Ebola virus or SARS coronavirus (SARS-CoV) for the affected patients, the development of antiviral drugs against these pathogens is not commercially viable in view of the comparatively low patient numbers. We are attempting to circumvent this problem for SARS-CoV and related coronaviruses (CoVs) by designing and developing antiviral drugs that target the large genus *Enterovirus* in addition to CoVs. The main protease of coronaviruses and the 3C protease of enteroviruses share a similar active-site architecture and a unique requirement for glutamine in the P1 position of the substrate, even though they are otherwise quite different. In order to obtain near-equipotent, broad-spectrum antivirals against alphacoronaviruses, betacoronaviruses, and enteroviruses, we pursue structure-based design of peptidomimetic alpha-ketoamides as inhibitors of main and 3C proteases. Six crystal structures of protease:inhibitor complexes were determined as part of this study. Compounds synthesized were tested against the recombinant proteases as well as in viral replicons and virus-infected cell cultures; most of them were not cell-toxic. Optimization of the P2 substituent of the alpha-ketoamides proved crucial for achieving near-equipotency against the three virus genera. The best near-equipotent inhibitors, **11u** (P2 = cyclopentyl methyl) and **11r** (P2 = cyclohexyl methyl), display low-micromolar EC₅₀ values against enteroviruses, alphacoronaviruses, and betacoronaviruses in cell cultures. In Huh7 cells, **11r** exhibits the highest activity of any antiviral described against Middle East Respiratory Syndrome coronavirus (MERS-CoV). This compound is now undergoing pre-clinical optimization.

S11-04

Crystallographic Fragment Screening at HZB - Workflow for Efficient User Experiments

J. Wollenhaupt^{1,2}, A. Metz², T. Barthel^{1,3}, M. Gerlach¹, C. Feiler¹, S. Glöckner², D. Wallacher⁴, G. Klebe², M. S. Weiss¹

¹Helmholtz-Zentrum Berlin, Macromolecular Crystallography, Berlin, Germany

²Philipps-Universität Marburg, Drug Design Group, Marburg, Germany

³Freie Universität Berlin, AG Strukturbiochemie, Berlin, Germany

⁴Helmholtz-Zentrum Berlin, Sample Environments, Berlin, Germany

Small molecule compounds are useful tools to study and modulate protein function. Crystallographic fragment screening is an established method to develop these compounds, allowing to initiate a structure-based compound development without the necessity of elaborate pre-screens. The fragments, i.e. small (<300 Da), low affinity organic molecules are used as probes to explore starting points for compound design. Crystals of the protein or protein-complex of interest are soaked or co-crystallized with the fragments and can then be detected by X-ray crystallographic analysis. As fragments cover a large chemical space, the experiments comprise reasonable sample amounts, e.g. a screen of 96 fragments.

At HZB we provide users with an efficient workflow to realize successful fragment screening campaigns and additionally support first steps to advance the initial hits to more strongly binding follow-up compounds. Pending optimized conditions for crystal treatment, one 96-fragment campaign (crystal treatment, X-ray experiments and data processing) can be carried out within less than a week.

We provide diverse 96-fragment starting screens as well a large library of over 1000 fragments dispensed by acoustic liquid transfer. In-house developed tools for sample handling as well as highly-efficient beamline set-ups with robot-assisted throughput of samples speed up the experiments. Data processing and refinement is fully automated and thus enables rapid evaluation of the results. Downstream optimization of fragment hits can include a rational sub-selection of the 1000-fragment library or can be guided by a web service to choose purchasable, diversified compounds. We show examples of fragment hits that were substantially increased in affinity to the target protein using our follow-up compound design strategy.

S11-05

Discovery of fragments that stabilize the KRAS-SOS1 interaction

R. Hillig¹

¹Bayer AG, Structural Biology, Berlin, Germany

Over the last 30 years, mutations in the RAS gene have been established as major oncogenes with a high occurrence rate in human cancers. The mutations reduce the ability of the small GTPase RAS to hydrolyse GTP, keeping this molecular switch in a constitutively active GTP-bound form that drives unchecked, oncogenic downstream signalling. One strategy to reduce the levels of active RAS is to target guanine nucleotide exchange factors, which allow RAS to cycle from the inactive GDP-bound state to the active GTP-bound form. Here, we describe the discovery of fragments which bind to SOS1 and stabilize the KRAS-SOS1 interaction. They were identified in an NMR fragment screen and the binding modes were elucidated by co-crystallization with the KRAS-SOS1 complex.

S11-06

Structural Biology for Antibody Design at Roche

A. Ruf¹

¹F. Hoffmann-La Roche AG, pRED Innovation Center Basel, Basel, Switzerland

This review includes examples from more than a decade of structural biology work on antibodies at Roche. It will show how structural biology contributions evolved from mere epitope determination for patenting or differentiation from competitor's products to various applications in support of the design of new antibody formats. The examples include structures that helped in the humanization of antibodies, structures that informed libraries for antibody maturation, or structures that illustrated the mechanism of action of therapeutic antibodies or glyco-engineered antibodies. Also the application of structural biology methods in analyzing antibody side products is exemplified. The use of structural biology in understanding and designing novel complex conjugated antibody molecules is shown. The structural biology methods covered are X-ray crystallography, negative stain EM and cryo-EM.

[1] Bohrmann et al. Gantenerumab: a novel human anti-A β antibody. *Journal of Alzheimer's disease: JAD*; 2012;28(1):49-69 PMID:21955818.

[2] Ferrara et al. Unique carbohydrate-carbohydrate interactions are required for high affinity binding between Fc γ RIII and antibodies lacking core fucose. *PNAS*; 2011 Aug 2;108(31):12669-74 PMID:21768335

[3] Rieset et al. Targeting tumor-associated macrophages with anti-CSF-1R antibody reveals a strategy for cancer therapy. *Cancer cell*; 2014 Jun 16;25(6):846-59 PMID:248985494.

[4] Dengl et al. Hapten-directed spontaneous disulfide shuffling: a universal technology for site-directed covalent coupling of payloads to antibodies. *FASEB journal*; 2015 May;29(5):1763-79 PMID:256702344

[5] Bujotzek et al. MoFvAb: Modeling the Fv region of antibodies. *mAbs*; 2015;7(5):838-52 PMID:261768125.

[6] Bujotzek et al. VH-VL orientation prediction for antibody humanization candidate selection: A case study. *mAbs*; 2016;8(2):288-305 PMID:266370544.

[7] Plathet et al. Characterization of mAb dimers reveals predominant dimer forms common in therapeutic mAbs. *mAbs*; 2016 Jul;8(5):928-40 PMID:27031922

[8] Klein et al. Cergutuzumab amunaleukin (CEA-IL2v), a CEA-targeted IL-2 variant-based immunocytokine for combination cancer immunotherapy. *Oncoimmunology*; 2017;6(3): e1277306 PMID:28405498.

[9] Kuglstatter et al. Structural differences between glycosylated, disulfide-linked heterodimeric Knob-into-Hole Fc fragment and its homodimeric Knob-Knob and Hole-Hole side products. *Protein engineering, design & selection: PEDS*; 2017 Sep 1;30(9):649-656 PMID:28985438

Structure-property-relationships

S12-01

Vacancy distributions, optical properties and switching mechanisms in epitaxial Ge₂Sb₂Te₅ thin film

M. Behrens¹, A. Lotnyk¹, J. W. Gerlach¹, B. Rauschenbach¹

¹Leibniz Institute of Surface Engineering (IOM), Leipzig, Germany

Introduction

The fast and reversible switching phase change materials of the pseudobinary (GeTe)_{1-x} – (Sb₂Te₃)_x system are regarded to be excellently suited for non-volatile memory and thermoelectric applications [1,2]. An advantageous feature of the Ge-Sb-Te (GST) alloys is the ordering of intrinsic vacancies into periodically arranged vacancy layers which leads to an enhancement of the thermoelectric efficiency and triggers an insulator-to-metal transition [3].

Objectives

The objective of this work is to fabricate epitaxial GST thin films of high phase purity in order to reliably investigate the impact of vacancy ordering on physical properties separated by structural phase transitions. Furthermore, possible vacancy order-disorder pathways within epitaxial GST thin films are explored. The material of choice is the prototypical compound Ge₂Sb₂Te₅.

Results

Epitaxial growth of Ge₂Sb₂Te₅ thin films with different phases and vacancy distributions is demonstrated. In addition, a classification of the optical reflectivity contrast of the epitaxial thin films is provided [4]. Moreover, structural transitions in epitaxial thin films induced by single ns-laser pulse and ion irradiation are reported [5].

Conclusions

In conclusion, distinct differences in optical reflectivity between different epitaxial Ge₂Sb₂Te₅ thin films are presented which demonstrates the impact of texture and vacancy distributions on optical properties. Additionally, unconventional switching pathways are presented by inducing transitions from highly vacancy ordered to vacancy disordered epitaxial Ge₂Sb₂Te₅ structures.

[1] N. Yamada et al., *Jpn. J. Appl. Phys.*, 1987, **26**, 61-66.

[2] M. N. Schneider et al., *Z. Kristallogr.*, 2010, **225**, 463-470.

[3] Siegrist et al., *Nature Materials*, 2011, **10**, 202-208.

[4] M. Behrens et al., *Crystengcomm*, 2018, **20**, 3688-3695.

[5] M. Behrens et al., *Nanoscale*, 2018, DOI:

10.1039/C8NR06567E.

S12-02

Structural complexity in the Cu₂ZnGeSe₄ – Cu₂ZnSiSe₄ solid solution series

S. Schorr¹, S. Niedenzu^{2,1}, A. Franz², G. Gurieva²

¹Freie Universität Berlin, Institut für Geologische Wissenschaften, Berlin, Germany

²Helmholtz-Zentrum Berlin, Structure and Dynamics of Energy Materials, Berlin, Germany

Photovoltaics (PV), the direct conversion of sunlight into electrical energy, plays a key role within renewable energies. Thin film solar cells using compound semiconductors as absorber material are foreseen as one of the most promising and cost-efficient technology. To achieve further cost reductions in PV module efficiency must be increased beyond the single-junction limit (Shockley-Queisser limit). Therefore, there is an increasing interest

in semiconductor materials which are potentially suitable for wide-bandgap applications such as absorber layers in the top cell of multi-junction solar cells.

Quaternary chalcogenide semiconductors, like Cu₂ZnGeSe₄, Cu₂ZnGeSe₄ or Cu₂ZnSiSe₄ contain only earth abundant, non-toxic elements. Cation and anion substitution offer the possibility of flexible band gap tuning between 1.5 eV and 2.2 eV which made the material an excellent candidate for band gap engineering.

The focus of our research is on the investigation of structure-function relations in the Cu₂ZnGeSe₄ – Cu₂ZnSiSe₄ solid solution series. Polycrystalline samples were grown by solid state reaction of the elements in evacuated silica tubes. As revealed by wavelength dispersive spectroscopy (WDX) Cu₂Zn(Ge_xSi_{1-x})Se₄ mixed crystals were successfully synthesized. Rietveld analysis of X-ray diffraction data show that Cu₂ZnSiSe₄ and Si-rich mixed crystals adopt the orthorhombic wurtz-stannite type structure, whereas Ge-rich mixed crystals crystallize in a tetragonal structure. In between 0.45 ≤ x ≤ 0.55 an orthorhombic and a tetragonal phase, both with the same chemical composition, coexist. The continuous change in the band gap energy within the Cu₂Zn(Ge_xSi_{1-x})Se₄ series was studied by photoluminescence (PL) spectroscopy and diffuse reflectance.

The differentiation between the isoelectronic cations Cu⁺, Zn²⁺, and Ge⁴⁺ and thus between the tetragonal structure types is only possible by neutron diffraction. Detailed simultaneous Rietveld analysis of neutron and X-ray diffraction data revealed the complex structural transition from the orthorhombic to the tetragonal crystal structure within the Cu₂Zn(Ge_xSi_{1-x})Se₄ solid solution.

S12-03

Hexagonal Bariumtitanate stabilized as ultra-thin film on Pt(111): An X-ray diffraction and electron-energy-loss spectroscopy study

H. Meyerheim¹, K. Mohseni¹, S. Förster², E. M. Zollner², F. Schumann², R. Felici³, W. Hergert², W. Widra²

¹MPI Halle, Halle, Germany

²Martin-Luther-Universität, Institut f. Physik, Halle (Saale), Germany

³ESRF, Grenoble, France

Bariumtitanate (BaTiO₃) is one of the most intensely studied oxides. Besides the perovskite- (PV) type low-temperature phases with cubic, tetragonal, orthorhombic, and rhombohedral symmetry, a high-temperature hexagonal (h) phase exists, which is stable above 1705 K. The structure of the latter is distinctly different from the PV-type, since it contains TiO₆ octahedra linked by common faces rather than by common corners. In the past many attempts have been made to stabilize h-BaTiO₃ at ambient conditions e.g. by reducing the crystallite size [1], but thus far only a mixture of PV-type (83%) and h-type (17%) BaTiO₃ could be obtained in microcrystals of approximately 140 nm in size.

Here we present an x-ray diffraction (XRD) and electron-energy loss spectroscopy (EELS) study carried out in combination with theoretical simulations which shows that h-BaTiO₃ can be prepared in pure form as a 7 nm thick film on the (111) surface of a platinum single crystal by using radiofrequency magnetron sputtering followed by annealing at 1050 K as reported in Ref. [2]. The film forms a (2x2) superstructure with respect to the Pt(111) surface unit cell. XRD experiments carried out at the European Synchrotron Radiation Facility in Grenoble indicate that the h-BaTiO₃ unit cell parameters are in-plane contracted by -3.04% and vertically expanded by +3.89% relative to the bulk parameters (a=b=5.724 Å, c=13.965 Å). Based on the fitting of the intensities of 14 symmetry independent reflections the formation of h-BaTiO₃

in unambiguously confirmed. Along the c-axis the film is structurally disordered by the presence of two terminations of the h-BaTiO₃ unit cell at the Pt(111) surface. In parallel, comparison of EELS spectra collected for PV-type BaTiO₃ and for the film with simulations also confirm the h-BaTiO₃ formation.

[1] M. Yashima, T. Hoshina, D. Ishimura et al., *J. Appl. Phys.* 98, 014313 (2005)

[2] S. Förster and W. Widdra, *Surf. Sci.* 604, 2163 (2010)

S12-04

Composition-dependent structural transformations in layered oxides of Rh and Li

D. Mikhailova¹, S. Maletti¹, S. Oswald¹

¹IFW Dresden, Dresden, Germany

Layered oxides with Li based on the α -NaFeO₂ structure represent the most promising positive electrode materials for Li-ion batteries [1]. Isostructural Li-rich materials of the formula Li₂MO₃, or Li(Li_{0.33}M_{0.67})O₂, with M = 3d and 4d elements can demonstrate anomalously high electrochemical capacities up to 300 mAh/g during charging (Li removal), which is attributed to combined cationic and anionic redox reactions including partial oxygen oxidation [2]. The oxygen redox activity is generally associated with a strong covalence of the M – O bonding and significant contribution of O2p states to the bands near the Fermi level. That leads to the formation of so-called "peroxo"-like groups with shortened O-O distances of ~2.3 – 2.4 Å and a cooperative deformation of the oxygen lattice, distorting the MO₆ octahedra into trigonal prisms. The layered character of the lattice remains mostly unchanged. In our previous work, we reported the unique behavior of layered LiRhO₂ upon delithiation [3]. When charged above 4.0 V in Li-ion batteries, it exhibits massive and concerted migration of Rh cations towards empty octahedral positions in the Li-layers resulting in the Li_yRh₃O₆ tunnel-like phase with a rutile-ramsdellite intergrowth structure (γ -MnO₂ type). The Rh migration is accompanied by shortening of O-O distances up to 2.26 Å.

Now, we studied structural changes in layered Li(Li_{0.2}Rh_{0.8})O₂ upon Li removal and insertion, using *operando* powder synchrotron diffraction and X-ray absorption spectroscopy. Despite the pronounced two-step character of Li extraction at high oxidation potentials, no transformation into the γ -MnO₂-type structure was observed (Fig. 1). Monitoring of O-O distances during whole charging process delivered "conventional" values of about 2.8 Å. Therefore, random distribution of Li and Rh on the Li,Rh-layers prevents possibility for accommodation of charge and strains, hence impeding a long-range structural reorganization.

Figure 1. Voltage profile of electrochemical cells with Li(Li_{0.2}Rh_{0.8})O₂ cathode (left) and evolution of the lattice parameters of Li(Li_{0.2}Rh_{0.8})O₂ (right) vs. total Li content during electrochemical Li removal and insertion.

[1] Lithium Batteries: Science and Technology, Springer Science + Business Media, 2009, 708.

[2] M. Oishi et al., *J. Power Sources* 2015, 276, 89-94.

[3] D. Mikhailova et al., *Inorg. Chem.* 2016, 55, 7079–7089.

Figure 1

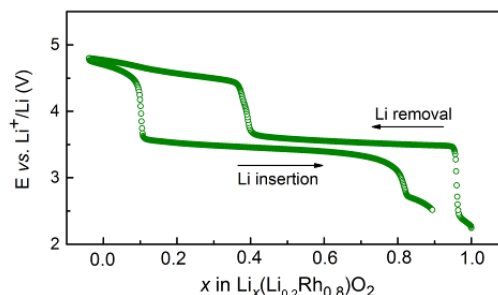
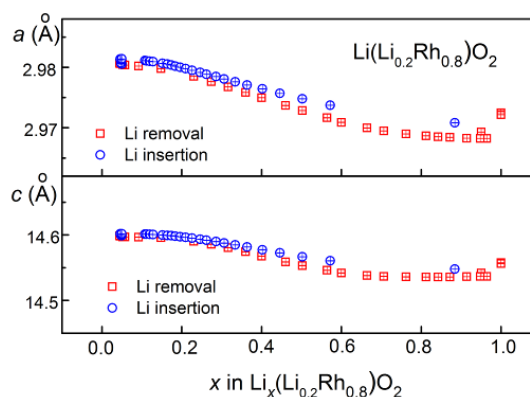


Figure 2



S12-05

Data Mining Force Field: Crystal Properties Estimation and Screening for Polymorphs, Cocrystals and Salts

L. Kuleshova¹, D. W. M. Hofmann^{1,2}

¹FlexCryst, Uttenreuth, Germany

²CRS4, Bioscience, Pula, Italy

Force fields (FF) have a long history of development, and at present a great variety of them exist, addressing a wide range of properties of solids. One can distinguish two main approaches to the matter: FF fitted to high accuracy DFT calculations, and FF, which systematically determine all parameters based on big experimental data sets (Data Mining Force Field)¹. Even if crystal structure prediction becomes reliable, a lot of challenging problems have to be solved: the impact of external conditions, calculations of the salts and so on. Earlier the FF was reported, which allows to predict structural temperature effects in crystals².

Here we show a modernized Data Mining approach, concentrating on energy and structural aspects. It includes the improvement of the energy function, and allows for screening of big data sets for the possible formation of polymorphs, cocrystals, and salts, which play an important role in the pharmaceutical industry. Cocrystallization is a promising approach to generate novel crystal forms of known APIs with improved physico-chemical and pharmacokinetic properties. The actual accuracy of the energy function allows to estimate the solubility, which is one of the most important properties of drugs. The results of experimental vs. virtual screening will be presented for a variety of chemical classes of molecular cocrystals and salts, including carboxylic and amino-acids, which very often cause problems in correct energy estimations and as a consequence - failure in crystal structure prediction. Also for them, the perfect correlation of experimental and predicted energy was found, Fig. 1, and more than 58% of structures have been predicted in ranks 1-20, Fig. 2 (prediction of crystal structure of proline).

The further achievements of Force Field development are awaited via introducing of big varieties of atom types (all-atoms force field).

- [1] Hofmann D., Kuleshova L. Int. Tables (C) 2019
 [2] Hofmann D., Kuleshova L. Chem. Phys. Letters, 699, 115, 2018

Figure 1

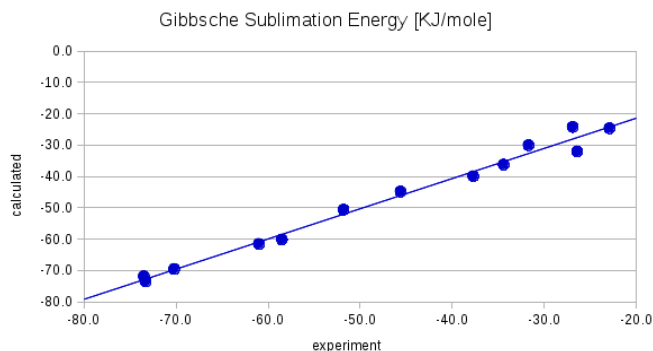
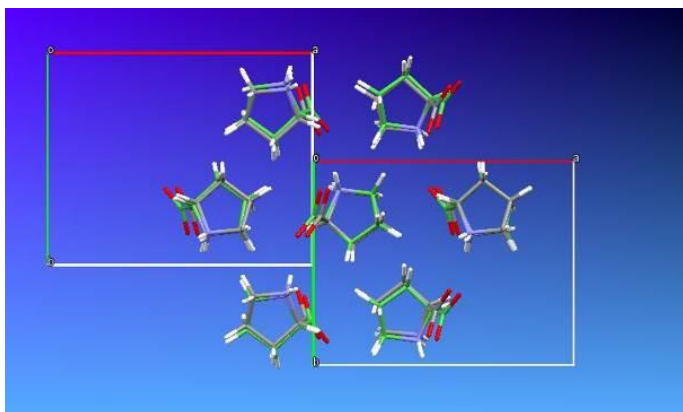


Figure 2



S12-06

Hydrothermal Structure Degradation Mechanisms of porous Materials DAY, AIPO-5, SAPO-34 and Silica Gel
Investigations on long-term stability of porous materials under hydrothermal stress and discussion of the different decomposition mechanisms

T. Herzog¹, J. C. Buhl², W. Lutz³, W. Wieprecht³
¹TH Wildau, INW, Berlin, Germany
²Universität Leipzig, Institut für Mineralogie, Hannover, Germany
³BTU Cottbus-Senftenberg, Institut für Luftchemie, Berlin, Germany

Introduction

This report is a discussion on the 4 different mechanisms of sample decomposition of zeolite DAY, AIPO-5, SAPO-34 and silica gel used in heat pump application, under hydrothermal stress.

Objectives

The structural decomposition of porous materials is studied through a rigorous hydrothermal stress treatment in liquid water using Teflon-coated autoclaves. The modifications were characterized by XRD and SEM.

Results

DAY and AIPO-5 zeolites are hydrothermally stable over a wide temperature range. DAY becomes amorphous with increasing temperature whereas AIPO-5 forms over an immediate state at 140°C a tridymite analogous crystalline phase. SAPO-34 adsorbs water in the same level as DAY. Its hydrothermal stability distinguishes, however, significantly from that of DAY. At a mild temperature of 80°C, a structural degradation of SAPO-34 starts and H₂O sorption values shifts to same values as AIPO-5. At 200°C the not absorbing tridymite analogous phase is formed too.

Conclusions

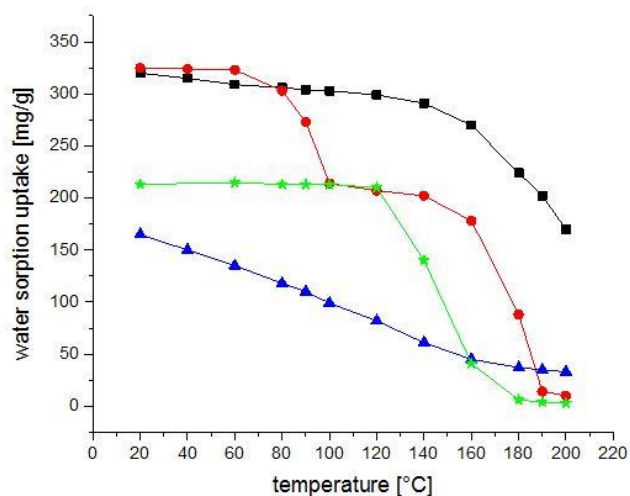
The transition of AIPO-5 and SAPO-34 into this tridymite-type AIPO₄ is a remarkable finding because up to now its synthesis was only performed in dry condition at higher temperature of 950°C and prolonged times of heating (20d), as first described by Flörke[1]. The use of harsh hydrothermal conditions on the adsorbents investigated was helpful for estimation of the long-term behaviour of porous materials, in heat pumps. DAY seems to be useful for applications this type.

Reference

- [1] O. W. Flörke, Z. Kristallogr. 1967, 125, 134-146.

Fig.1: Sorption capacity of zeolites DAY(■), AIPO-5(stars), SAPO-34(●) and silica gel (▲) after a hydrothermal treatment in liquid water of autogenous pressure

Figure 1



Disordered Materials

S13-01

Randomly and domain like occurring planar defects in layered honeycomb materialsS. Bette¹, F. Pielhofer², L. Diehl^{1,3}, B. V. Lotsch¹, T. Takayama³, H. Takagi³, R. E. Dinnebier³¹Max Planck Institute for Solid State Research, Scientific Facility X-ray diffraction, Stuttgart, Germany²University of Regensburg, Regensburg, Germany³LMU München, Munich, Germany**Introduction**

Layered honeycomb materials are currently attracting broad scientific interest due to their chemical (PH-sensing), magnetic (Kitaev magnetism) and electrical (spin orbit coupling) properties. The occurrence of planar defects, i.e. stacking faults, however, impedes the structural characterization and affects the materials properties.

Objectives

The ideal (faultless) and real (degree of faulting) crystal structures of the layered honeycomb materials Na_2RuO_3 , SnTiO_3 , ScSiTe_3 and BiSiTe_3 were investigated by X-ray powder diffraction (XRPD) using Rietveld compatible supercell approaches. The obtained microstructure models were supported by *DIFFaX* simulations, HR-STEM investigations, PDF-analyses and total energy calculations.

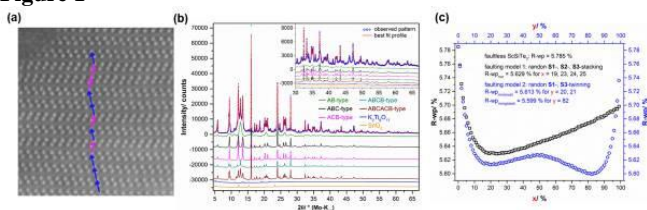
Results

The interlayer Na^+ cations of Na_2RuO_3 and the electron lone pair of Sn^{2+} in SnTiO_3 strictly direct the honeycomb layers of these materials into a staggered conformation, whereas total energy calculations show only a slight preference of this conformation for ScSiTe_3 and BiSiTe_3 . Na_2RuO_3 , ScSiTe_3 and BiSiTe_3 exhibit mainly random distributions of faults, whereas the degree of faulting is significantly higher in BiSiTe_3 than in ScSiTe_3 . In contrast, SnTiO_3 exhibits coherently scattering domains that show different stacking orders.

Conclusions

Investigation on the microstructure of different layered honeycomb material point to the fact that stacking fault disorder is an intrinsic substance property. Hence, understanding and quantification of structural disorder is necessary for a complete characterization of this class of materials.

Fig. 1 (a) TEM-image of SnTiO_3 , indicated by arrows, (b) Rietveld refinement of the measured XRPD pattern of SnTiO_3 using a multiphase approach including five polytypes of SnTiO_3 representing different stacking types and twinning domains, (c) plots of the R-wp vs. the transition probability from a Rietveld refinement of disordered ScSiTe_3 by using a statistical supercell approach.

Figure 1

S13-02

Cu/Zn disorder in $\text{Cu}_2\text{ZnSn}(\text{S}_{1-x}\text{Se}_x)_4$: the off-stoichiometry influenceG. Gurieva¹, A. Franz¹, S. Schorr^{1,2}¹Helmholtz-Zentrum Berlin, EM-ASD, Berlin, Germany²Freie Universität Berlin, Institut für Geologische Wissenschaften, Berlin, Germany

Recently $\text{Cu}_2\text{ZnSn}(\text{S}_{1-x}\text{Se}_x)_4$ quaternary chalcogenides have gained a lot of attention. These kesterite-type compounds, which consist mostly of earth abundant and non-toxic elements, are promising low cost alternative absorber materials for thin film solar. The best photovoltaic performance of kesterite-based thin film solar cells were obtained with Se- rich, off-stoichiometric CZTSSe. The absorber band tailing caused by the exceptionally high density of Cu/Zn disorder is believed to be one of the reasons for the limited open-circuit voltage in CZTSSe devices. A differentiation between the isoelectronic cations Cu^+ and Zn^{2+} and consequently quantification of Cu/Zn disorder within the kesterite type structure is not possible using X-rays diffraction due to their similar scattering factors. But neutrons diffraction can solve this problem; the coherent scattering lengths are sufficiently different for these cations [1]. It was shown by this method that both $\text{Cu}_2\text{ZnSnS}_4$ and $\text{Cu}_2\text{ZnSnSe}_4$ occur in the kesterite structure.[2]

A detailed structural analysis of off-stoichiometric $\text{Cu}_2\text{ZnSn}(\text{S}_{1-x}\text{Se}_x)_4$, grown by solid state reaction, was performed by neutron diffraction at the fine resolution neutron powder diffractometer E9 at BER II ($\lambda=1.7986\text{\AA}$, RT). Rietveld refinement of diffraction data using the FullProf suite software [3] lead to accurate values of lattice constants, and site occupancy factors. The latter have given insights into the cation distribution within the crystal structure of $\text{Cu}_2\text{ZnSn}(\text{S}_{1-x}\text{Se}_x)_4$ solid solutions with different x values. And the most important valued for the Q – disorder parameter, which is a quantitative measure of Cu/Zn disorder in these materials. The correlated information about changes in lattice parameters and cation site occupancies, details on the existing intrinsic point defects and their amounts as well as a comparison of these parameters to the ones from stoichiometric CZTSSe with the same S/S+Se ratio will be presented.

The research leading to the presented results has been partially supported by the STARCELL project as well as INFINITE-CELL project. These projects have received funding from the European Union's Horizon 2020 research and innovation programme under the Marie Skłodowska-Curie grant agreements No 720907 and 777968 respectively.

[1] V.F. Sears, Neutron News 3(1992)26.

[2] S.Schorr, Sol. Mat. Sol. Cells, 95 (2011)1482.

[3] Juan Rodriguez-Carvajal and Thierry Roisnel, www.ill.eu/sites/fullprof

S13-03

Combining experimental and computational techniques to understand phase transitions of the nucleobase adenineD. Sisak Jung¹, I. Halasz², D. McDonagh³, G. Day³¹DECTRIS Ltd., Baden-Dättwil, Switzerland²Institute Ruder Boskovic, Division for Physical Chemistry, Zagreb, Croatia³University of Southampton, Southampton, United Kingdom

Monitoring phase transitions in-situ becomes increasingly difficult if the transitions feature a series of similar structures, and if the occurring phases cannot be isolated from the mixture. In these cases, complete powder X-ray powder diffraction (PXRD) need to be collected in a minimal number of steps and exhibit

statistics and resolution that can allow for the structure determination and refinement. While these problems are successfully addressed at synchrotron beamlines, the laboratory diffractometers are rarely fit for the task. One of the challenging samples is adenine, a small and rigid molecule that exhibits two polymorphs: a monoclinic (**I**) [1] and an orthorhombic (**II**) [2]. Both polymorphs feature a layered structure, what makes their PXRD patterns similar and difficult to resolve when in a mixture. Although both phases are bench-stable at the room temperature, at higher temperatures phase (**I**) transforms into (**II**) [2].

In this work, adenine phase transition is monitored in-situ using a laboratory diffractometer in the Debye-Scherrer geometry. It was equipped with a Mo- source, a specially developed oven and two simultaneously operating detectors. In this way, 74° in 2θ of high-resolution data could be collected in only two shots. The resulting PXRD patterns revealed two additional adenine phases: **III** and **X**. The phase **III** was characterized as a disordered layered structure using the DISCUS program [3]. The phase **X** was indicated by several low intensity peaks. Although these peak positions could be indexed with a triclinic cell of a favorable volume, the data did not allow for cell validation or refinement. To complement the diffraction study, crystal structure prediction was carried out for adenine using quasi-random sampling in a large number of space groups [4, 5]. This has generated a set of structures energetically close to the two known polymorphs. A few of these computer-generated structures could correspond to the phase (**X**) observed in the PXRD patterns. Calculations are ongoing.

[1] Mahapatra, S.; Nayak, S. K.; Prathapa, S. J.; Guru Row, T. N. *Cryst. Growth Des.* 2008, 8, 1223.

[2] Stolar T. et al. *Cryst. Growth Des.* 2016, 16, 3262.

[3] Proffen, T.; Neder, R.B. *J. Appl. Cryst.* 1997, 30, 171-175.

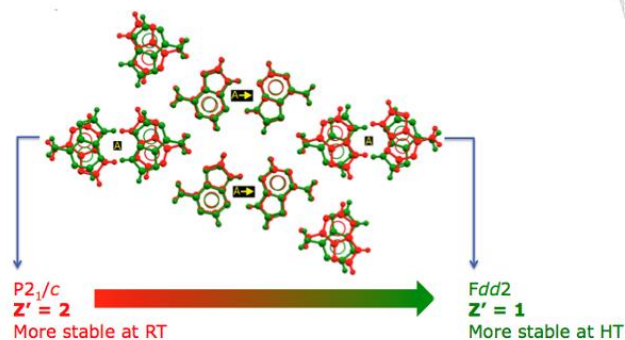
[4] Case, D. H. et al. *J. Chem. Theory Comput.* 2016, 12, 910-924.

[5] Price, S. L. et al. *Phys. Chem. Chem. Phys.* 2010, 12, 8478-8490.

Figure 1



Figure 2



S13-04

A disorder model for the 1-Bromoadamantane Thiourea host guest inclusion compound

E. Schmidt¹, A. Simonov², R. Neder¹

¹Friedrich-Alexander-Universität Erlangen-Nürnberg, Institute for Crystallography and Structural Physics, Erlangen, Germany

²Albert-Ludwigs-Universität Freiburg, Crystallography and Material Sciences, Freiburg i. Br., Germany

1-Bromoadamantane and Thiourea form a disordered host guest inclusion compound [1]. Single crystal diffuse scattering measurements were performed at ID28 at ESRF. With the diffuse scattering data a disorder model is established.

Thiourea molecules form a host channel structure in the space group $R\bar{3}c$ [2] (channel along c , $a=16.23\text{\AA}$, $c=12.45\text{\AA}$, see Fig. 1). The 1-Bromoadamantane guests occupy those channels. The guests

are disordered over various positions within the host framework, giving rise to a distortion of the channel structure. Both, the short range order of the guests and the distortion of the host, result in diffuse scattering.

Fig. 2(a) shows the measured $h0l$ section of the diffuse scattering data. Diffuse layers are visible at $l=1.5n$ with integer n . These layers correspond to the ordering of the guest molecules, which are $2/3c$ apart. Additional broad diffuse maxima at Bragg positions are observed which correspond to the host adapting to the presence of the guest.

Fig. 2(b) shows the measured $hk0$, $hk1.5$ and $hk3$ layers. The diffuse scattering in the $hk0$ layer and hkl layers with integer l show host relaxations. The $hk1.5$ layer shows a hexagonal frustration, which can be explained by a height correlation of the guests in neighboring channels. The $hk3$ layer shows both, diffuse maxima underneath the Bragg peaks due to the host relaxation and a broad diffuse circle in the middle due to the poor longer range guest ordering.

We conclude that the guests only order on a local scale and the interaction between the guest and the host is mediated by the host N-H fragments and the Br atoms of the guest. The analysis of single crystal diffuse scattering allows to establish a disorder model including both host and guest ordering.

- [1] Chao, M.-H., *et al.* (2003). *Angew. Chem. Int. Ed.* 42, 2982.
 [2] Gopal, R., *et al.* (1989). *Acta Cryst.* C45, 257.

Fig. 1: Thiourea host viewed along c .
 Fig. 2:

- (a) Diffuse scattering in the $h0l$ layer.
 (b) $hk0$, $hk1.5$ and $hk3$ layers.

Figure 1

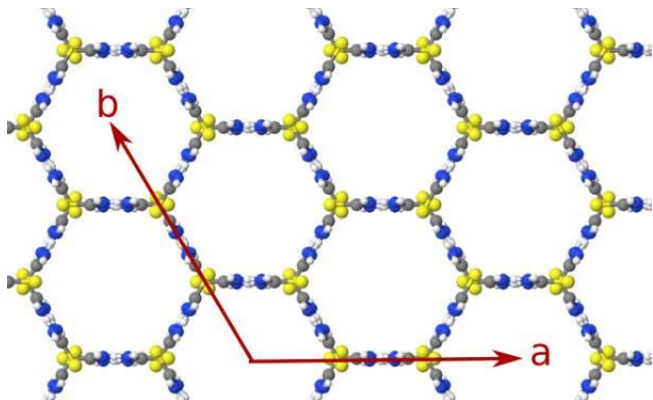
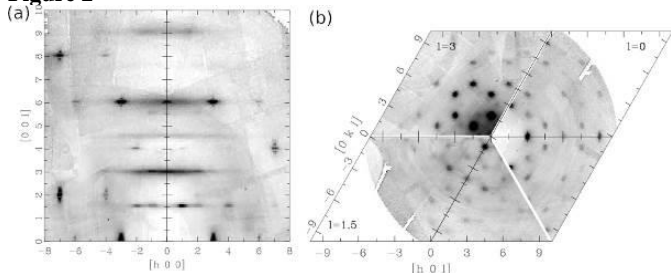


Figure 2



S13-05

Disordered Non-centrosymmetric compound:

$\text{Fe}_{0.43}\text{Mo}_{2.56}\text{SbO}_{9.5}$

S. I. Ali¹, S. Lidin², M. Johnsson³

¹University of Kalyani, Department of Chemistry, KALYANI, India

²Lund University, Department of Chemistry, Lund, Sweden

³Stockholm University, Department of Materials and Environmental Chemistry, Stockholm, Germany

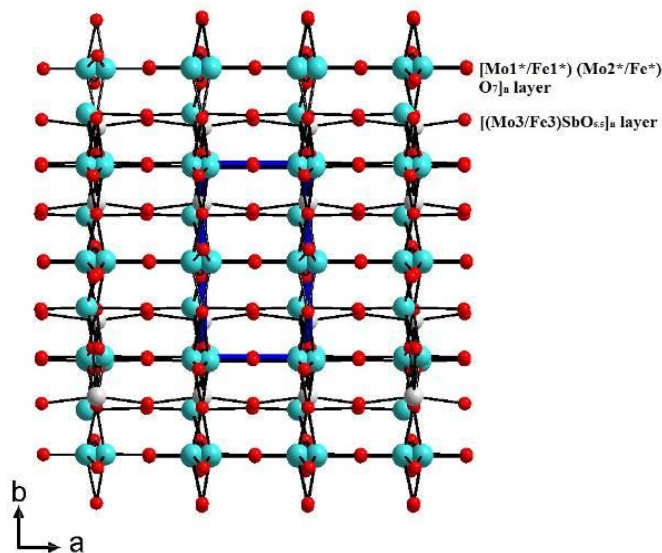
Non-centrosymmetric (NCS) materials is of current interest and of great importance due to that such compounds may show interesting physical properties *e.g.* non-linear second harmonic generation, ferroelectricity etc.[1-2] A large variety of ternary oxides in the M-Sb-O system (M = Mn^{2+} , Fe^{2+} , Co^{2+} , Ni^{2+} , Zn^{2+} , Mg^{2+}) have previously been described in literature.[3-5] However, there are very few quaternary systems have been proposed so far and only one for [M – Fe – Sb – O] system; *e.g.* $\text{FeSb}_{2-x}\text{Pb}_x\text{O}_4$ ($x = 0.2-0.7$) is found.[6]

In our work, Single crystals of $\text{Fe}_{0.43}\text{Mo}_{2.56}\text{SbO}_{9.5}$ were obtained by hydrothermal techniques at 230°C for the first time (Fig. 1). The crystal structure was determined from single crystal X-ray diffraction data. The compound crystallizes in the non-centrosymmetric space group Pc with unit cell parameters $a = 4.0003(2)$ Å, $b = 7.3355(3)$ Å, $c = 12.6985(6)$ Å, $\beta = 90^\circ$. The crystal structure comprises five crystallographically independent M atoms and one Sb^{3+} atom, M atoms are of two kind of partially occupied sites Mo^{6+} and Fe^{3+} . The building blocks consist of $[\text{SbO}_3\text{O}_{0.5}\text{E}]$ octahedra (E = lone electron pair) and $[(\text{Mo}/\text{Fe})\text{O}_6]$ octahedra. The M (Mo, Fe) and O atoms are arranged in a distorted hexagonal 2D-net, not the Sb atoms. The distortion of the net and consequently the symmetry reduction results mainly from the location of the Sb atoms. Disorder manifests itself as a splitting of the metal sites and occurring the short Mo - Fe distances. Six $(\text{Mo}/\text{Fe})\text{O}_6$ octahedra are connected to form a pseudo-hexagonal channel. The Sb^{3+} atom is displaced from the pseudo-six-fold axis.

Ref:

- [1] S. Hu *et al.*, *Chem. Mater.* **2014**, 26, 3631–3636.
 [2] H. Yu *et al.*, *Chem. Mater.* 2017, 29, 1845–1855.
 [3] B. P. de Laune and C. Greaves, *J. Solid State Chem.* **2012**, 187, 225–230.
 [4] H. D. Zhou *et al.*, *J. Solid State Chem.* **2010**, 183, 890–894.
 [5] V. V. Politaev *et al.*, *J. Solid State Chem.* **2010**, 183, 684–691.
 [6] M. J. Whitaker *et al.*, *J. Mater. Chem.*, **2011**, 21, 14523.

Figure 1



S13-06

The concentration quenching of $\text{Ba}_3\text{Bi}_2(\text{BO}_3)_4$ occurs at 50 mol.%. ($\lambda_{\text{ex}} = 393$ nm). The detailed analysis, quantitative characteristics and the role of the Eu^{3+} ions distribution in the crystal strictures $\text{Ba}_3\text{Bi}_2(\text{BO}_3)_4$: Eu^{3+} are given in the presentation.

A. Shablinskii¹, R. Bubnova^{2,1}, S. Filatov², I. Kolesnikov², A. Povolotskiy²

¹Russian Academy of Sciences, Institute of Silicate Chemistry, Saint-Petersburg, Russian Federation

²St. Petersburg State University, Saint-Petersburg, Russian Federation

High Eu^{3+} optimal concentration in a novel $\text{Ba}_3\text{Bi}_2(\text{BO}_3)_4$: Eu^{3+} phosphor

Eu^{3+} phosphors play a key role in red emitting lamps, CTV screen, PDP, mercury vapor lamps, and mercury free fluorescent lamps due to narrow emission in the red region and strong UV absorption. Borates with $A_3\text{REE}_2(\text{BO}_3)_4$ formula ($A = \text{Ca}, \text{Sr}, \text{Ba}$; $\text{REE} = \text{Y}, \text{La}, \text{Yb}$) form the family of luminescent compounds [1]. The crystal structure of $\text{Ba}_3\text{Bi}_2(\text{BO}_3)_4$ ($Pnma$) contains isolated BO_3 triangles and three independent sites for Ba and Bi; which form 8-coordinate, highly distorted polyhedra [2].

The samples of solid solutions, $\text{Ba}_3(\text{Bi}_{2-x})(\text{BO}_3)_4$ ($x = 0, 0.005, 0.1, 0.2, 0.3, 0.4, 0.5, 0.7, 1, 1.3$) were prepared from a melt. The structures of a few Eu-containing single crystals were solved and refined using Jana 2006 software.

The optimal concentration for the similar $\text{Sr}_3\text{Y}_2(\text{BO}_3)_4$ [3] and $\text{Sr}_3\text{Bi}_2(\text{BO}_3)_4$ [4] borates was determined to be 10 and 15 mol.% ($\lambda_{\text{ex}} = 393$ nm). The concentration quenching of $\text{Ba}_3\text{Bi}_2(\text{BO}_3)_4$ occurs at 50 mol.%. ($\lambda_{\text{ex}} = 393$ nm). There are some reasons of $\text{Ba}_3\text{Bi}_2(\text{BO}_3)_4$ high optimal concentration which are provided to the increase of distance between luminescent centers with decreasing of the probability of energy transfer between Eu^{3+} ions. The role of the Eu^{3+} ions distribution in the crystal strictures $\text{Ba}_3\text{Bi}_2(\text{BO}_3)_4$: Eu^{3+} are given in the presentation.

The study was supported by the Russian Foundation of Basic Research No. 18-03-00679. X-ray measurements and photoluminescence were performed in XRD and Optical and Laser Materials Research in St. Petersburg State University.

[1] T.N. Khamaganova, Rus. Chem. Bull. (2017) 187.

[2] S.N. Volkov et al. Z. Krist. 228 (2013) 436.

[3] Y. Zhang, Y. Li, Alloys Compd. 384 (2004) 88.

[4] A.P. Shablinskii et al. J. Sol. St Sci. 70 (2017) 93.

Bio-Crystallography V: Instrumentation and methods

S14-01

Assessing heterogeneity of data compared by correlation coefficients: theory and examples

K. Diederichs¹

¹University of Konstanz, Biology, Konstanz, Germany

Data sets collected from different objects are often affected by systematic differences. In order to understand the changes, these differences need to be detected and analysed. An algorithm recently published [1] uses a multidimensional scaling approach of pairwise correlation coefficients of the individual data sets to separate random and systematic errors. As a result, systematic differences between data sets i, j are revealed by positions of the data sets in a unit sphere, at angles related to the amount of systematic deviation. Application to crystallographic datasets shows the presence of different clusters consisting of isomorphous data sets. Examples from other fields will be presented.

[1] Diederichs, K. (2017) *Acta Cryst. D* 73: 286-293

S14-02

Efficient data collection methods for time-resolved serial synchrotron crystallography enabled the structural analysis of the full turnover of an enzyme

E. C. Schulz¹, P. Mehrabi¹, H. M. Müller-Werkmeister², R. Dousza¹, F. Tellkamp³, E. F. Pai^{4,5,6}, R. J. D. Miller^{1,7,8}

¹Max Planck Institute for the Structure and Dynamics of Matter, Atomically Resolved Dynamics, Hamburg, Germany

²Universität Potsdam, Physical Chemistry, Potsdam-Golm, Germany

³Max Planck Institute for the Structure and Dynamics of Matter, SSU - Machine Physics, Hamburg, Germany

⁴University of Toronto, Department of Biochemistry, Toronto, Canada

⁵University of Toronto, Department of Medical Biophysics, Toronto, Canada

⁶The Campbell Family Cancer Research Institute, Ontario, Cancer Institute, Toronto, Canada

⁷Universität Hamburg, Department of Physics, Centre for Ultrafast Imaging, Hamburg, Germany

⁸University of Toronto, Departments of Chemistry and Physics, Toronto, Canada

Introduction

The functional characterization of **biomolecular catalysis** requires a correlation of the three-dimensional structural ensemble with time-dependent changes. Since the majority of enzymatic reactions occur in the hundreds of milliseconds range, synchrotron light sources are a clear alternative to free electron lasers for these systems due to their wide distribution and their simpler experimental setup.

Objectives

This triggered the development of fixed-target **time-resolved serial synchrotron crystallography** (TR-SSX), which simplifies accessing prevalent biological time-scales ($> ns$)(1–5). Recently, we have developed a novel "**Hit And Return**" (**HARE**)(5) approach for data acquisition. The HARE approach enables efficient data collection at synchrotron microfocus beamlines, collecting ~100k images per hour approximately **equivalent to one time point per hour**. Due to the HARE algorithm time delays from a few milliseconds to several minutes can be acquired with no increase in data collection time. This contrasts conventional methods, which require several hours up to several beamtimes per time-point.

Results

We used the HARE approach to capture **18 time points from 30**

milliseconds to 30 seconds during the non-reversible turnover cycle of fluoroacetate dehalogenase (FACD). These time points include **all key states** involved in enzymatic C-F bond cleavage: **substrate binding** and reorientation, **covalent-intermediate formation**, location of the **water nucleophile and product release**. In total four substrate turnovers can be observed between the two subunits, which are highly coupled but display different conformations. Reactivity is linked to **molecular breathing**, expressed by dynamic changes in lateral FACD dimensions and modulation in water content pointing at an **allosteric communication** pathway between the two subunits.

Conclusions

These results demonstrate the excellent suitability of **TR-SSX** to unravel biomolecular catalysis and provide **key insights into protein dynamics**.

[1] Owen, R. L. *et al. Acta Crystallogr. Sect. D, Struct. Biol.* **73**, 373–378 (2017).

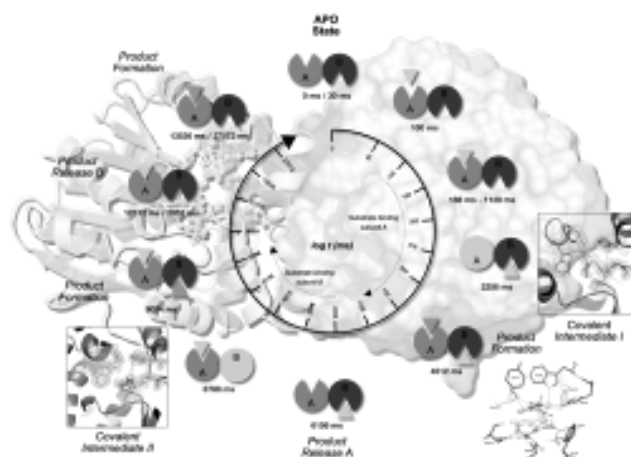
[2] Oghbaey, S. *et al. Acta Crystallogr. Sect. D Struct. Biol.* **72**, 944–955 (2016).

[3] Schulz, E. C. *et al. J. Appl. Crystallogr.* **50**, 1773–1781 (2017).

[4] Mueller, C. *et al. Struct. Dyn.* **2**, (2015).

[5] Schulz, E. C. *et al. Nat. Methods* **15**, 901–904 (2018).

Figure 1



S14-03

Improvements in automated data analysis and processing within autoPROC, combined with advanced characterisation, mitigation and visualisation of the anisotropy of diffraction limits using STARANISO.

C. Vonrhein¹, I. Tickle¹, C. Flensburg¹, P. Keller¹, W. Paciorek¹, A. Sharff¹, G. Bricogne¹

¹Global Phasing Ltd, Cambridge, United Kingdom

The ever higher levels of automation available with modern instrumentations at synchrotron beamlines as well as in-house, require not only efficiency and speed of data processing programs and pipelines, but also new and improved approaches to data analysis itself and to the visual presentation of its results. This is not just a matter of producing "prettier pictures", but of helping ordinary users as well as automated processes to use the most appropriate quality metrics in evaluating experimental protocols and in designing optimal experiments for given instrument capabilities and crystal characteristics.

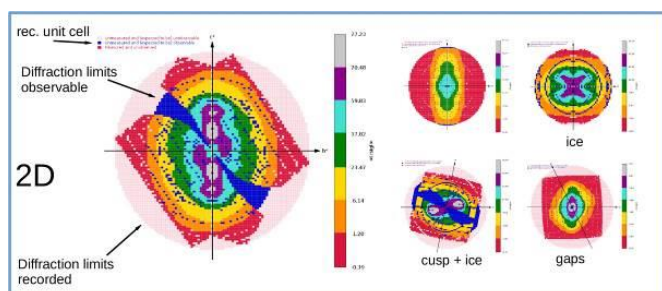
The rapid assessment of the characteristics and quality of conventional (single crystal/sweep) datasets - as well as of

combinations of partial datasets originating from multi-sweep and/or multi-crystal datasets and/or serial experiments – requires well designed visualisation tools to capture all aspects of data characteristics. The proper perception of the relationships between partial datasets can only be achieved through a full 3D visualisation of local geometric properties such as redundancy and of statistical properties such as local averages of $1/\sigma(I)$. To that end we have developed the STARANISO program [1] for analysing and mitigating anisotropy in diffraction data. This capability is available both via autoPROC [2] (our package for automated data processing and analysis of X-ray diffraction data) and the public STARANISO webserver [3] (processing, analysis and visualisation of user-provided datasets, either as merged or unmerged intensity data). A recent additional capability has been provided by the "PDBpeep" server, allowing the analysis and 3D visual examination of diffraction datasets already deposited with PDB entries [4].

- [1] Tickle, I.J. et al (2016). STARANISO. Global Phasing Ltd., Cambridge, UK.
 [2] Vonrhein, C. et al (2011). Data processing and analysis with the autoPROC toolbox. *Acta Cryst. D* **67**, 293-302.
 [3] <http://staraniso.globalphasing.org/>
 [4] <http://staraniso.globalphasing.org/cgi-bin/PDBpeep.cgi>

Figure 1: 2D representation of STARANISO anisotropy analysis as implemented in autoPROC.

Figure 1



S14-04

Facilities for Macromolecular Crystallography at the HZB

M. Gerlach¹, C. Feiler¹, R. Förster¹, C. Gless¹, T. Hauß¹, H. He¹, M. Hellmig¹, A. Kastner¹, M. Rutkiewicz¹, L. Schmuckermaier¹, M. Steffien¹, H. Taberman¹, P. Wilk¹, J. Wollenhaupt¹, M. S. Weiss¹

¹Helmholtz-Zentrum Berlin, Macromolecular Crystallography, Berlin, Germany

The Helmholtz-Zentrum Berlin (HZB) operates three beamlines for macromolecular crystallography (MX) at the electron storage ring BESSY II [1,2,3]. BL14.1 and BL14.2 are tunable in the photon energy range from 5 to 16 keV, while BL14.3 is a fixed-energy side station (13.8 keV). They feature state-of-the-art experimental stations and ancillary facilities, serving more than 100 research groups across Europe. Almost 3000 protein structures measured at BESSY II have resulted in protein data base (PDB) depositions so far, and with nearly 300 PDB depositions in 2017, BL14.1 is among the five most productive MX-beamlines in the world.

The experimental endstation of BL14.1 provides high degree of automation and is equipped with a PILATUS 6M detector, a CATS sample changer robot and an MD2 multi-axis goniometer. BL14.2 features a PILATUS3 S 2M detector, a G-Rob sample changer and a piezo-controlled nanodiffractometer. Its sample dewar can accommodate up to 294 samples, supporting both, SPINE- and

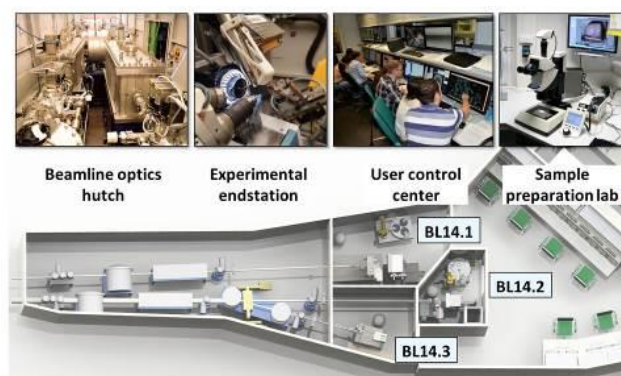
UNIPUCK standards, allowing for high sample-throughput data collection.

Beamline BL14.3 is currently being fully refurbished, and from March 2019 on it will be equipped with a fast MD2-S microdiffractometer, including a mini-kappa axis and a plate manipulator option for *in situ*-crystal screening, supporting several types of 96-well plates. In addition, a new HC-Lab dehydration device has been installed that can be used in combination with a REX rapid nozzle exchanger to freeze samples in a defined hydration state within less than a second [4]. All three beamlines feature MXCuBE version 2 experimental control software, allowing for fast and efficient data collection. Furthermore, the HZB-MX group operates an S1 BioLab which supports the complete workflow from protein purification to crystallization.

Figure 1. Layout of the HZB-MX beamlines BL14.1, BL14.2 and BL14.3 at BESSY II, Berlin

- [1] U. Mueller et al., *J. Synch. Rad.* **19**, (2012), 442
 [2] U. Mueller et al., *Eur. Phys. J. Plus* **130**, (2015), 141
 [3] M. Gerlach et al., *Journal of large-scale research facilities* **2**, (2016), A47
 [4] M. W. Bowler et al., *Cryst. Growth Des.* **15**, (2015), 1043

Figure 1



S14-05

in crystallo optical spectroscopy for Structural Biology at the ESRF: the *icOS* Lab as a tool for time-resolved protein crystallography experiments

A. Royant^{1,2}

¹Institut de Biologie Structurale, Grenoble, France

²ESRF, Grenoble, France

The analysis of structural data obtained by X-ray crystallography on biological macromolecules often benefits from additional information obtained on the crystalline sample by complementary techniques. In particular, various optical spectroscopies (UV-visible light absorption, fluorescence emission, Raman) have been crucial in establishing the nature of the physiological state adopted by certain macromolecules in the crystalline state, or controlling the extent of specific radiation damage to proteins and their active sites. Biological systems of interest are generally coloured via light-absorbing chemical groups (cofactors, metal centres, chromophores). At the European Synchrotron Radiation Facility in Grenoble, the *icOS* Laboratory (formerly named "Cryobench") has been developed since 2000 within the Structural Biology group to provide such complementary techniques either directly on the beamline (for online experiments), or close to the beamline (for offline, preparative experiments). With the EBS upgrade of the ESRF the flux on the Structural Biology beamlines will increase by at least two orders of magnitude, paving the way for time-resolved

protein crystallography experiments. In this context, the *icOS* Lab is currently preparing to be able to perform spectroscopic experiments on protein microcrystals with a 10-microsecond time resolution in order to provide time scales on which diffraction data for example in pump-probe experiments can be collected. Preliminary results will be presented on the photoactivation of a photoreceptor with a 60 ms time resolution.

S14-06

Fixed-target serial crystallography using *in cellulo* grown microcrystals

M. Lahey-Rudolph^{1,2}, R. Schönherr^{1,3}, *L. Redecke^{1,3}

¹University of Lübeck, Institute of Biochemistry, Lübeck, Germany

²Center for Free-Electron Laser Science (CFEL), Coherent Imaging Division, Hamburg, Germany

³DESY, Hamburg, Germany

Due to tremendous improvements in accessible X-ray energy and brilliance within the past decade, *in cellulo* grown protein crystal recently went into the focus of structural biology. High-resolution structural information has already been elucidated several-fold from natively *in cellulo* crystallizing proteins, but also from recombinant proteins that form intracellular crystals [1,2]. Although the underlying cellular processes are poorly understood so far, promising evidence indicates that this phenomenon is not restricted to a limited number of proteins [2,3]. Thus, we established a pipeline that systematically exploits living insect cells as crystallization chambers for recombinant target proteins. Diffraction data collection at an XFEL was usually performed with suspensions of isolated *in cellulo* crystals injected by a liquid jet, but the isolation procedure could affect the diffraction quality of the crystals. Thus, we developed approaches to record serial diffraction data sets of *in cellulo* crystals directly within the living insect cells. Tremendous settling problems of the comparatively large cells in the sample reservoir prevented the use of liquid jets for efficient diffraction data collection using crystal containing insect cells. For determination of protein structures using the SFX approach with conventionally grown crystals, high-speed fixed-target serial crystallography has been successfully established to fully use of the repetition rate of the XFEL LCLS and to overcome low hit rates [4]. We successfully verified the general feasibility of the fixed-target sample delivery approach also for crystal containing insect cells. Using the high-speed Roadrunner II goniometer in combination with a micro-patterned silicon chip (pore size 12 μm) loaded with a monolayer of insect cells that contained *in cellulo* grown crystals of the HEX-1 protein from the fungus *N. crassa* we were able to determine the associated crystal structure at a resolution of 1.75 \AA with a hit rate of more than 60 % and a total data collection time of 12 minutes. Thus, fixed-target serial crystallography appears to be a well-suited approach to efficiently solve structures of *in cellulo* crystallized proteins in very short time.

[1] Redecke, L., Nass, K. et al. *Science* 339, 227-231 (2013).

[2] Schönherr, R. et al. *Biol. Chem.* 399, 751-772 (2018).

[3] Schönherr, R. et al. *Struct Dyn.* 2, 041712 (2015).

[4] Roedig et al. *Nat Methods.* 14, 805-810 (2017).

Extreme/non-ambient conditions

S15-01

A new high-pressure polymorph of ZrSiO₄ revealed by DFT modelling and Raman spectroscopy

B. Mihailova¹, C. Stangarone^{2,3}, N. Waesemann¹, R. Angel², M. Prencepe⁴, M. Alvaro²

¹Universität Hamburg, Earth Sciences, Hamburg, Germany

²University of Pavia, Pavia, Italy

³German Aerospace Centre (DLR), Berlin, Germany

⁴University of Torino, Torino, Italy

Zircon (ZrSiO₄, *I*₄₁/*amd*) and zircon-based ceramics are important technological materials due to their superb mechanical and thermoelastic properties. It is believed that at room temperature a pressure-induced reconstructive phase transition from zircon to reidite (*I*₄₁/*a*) occurs near 20-23 GPa. Our recent Raman scattering analyses of zircon have revealed a gradual softening of the lowest-energy Raman-active phonon mode near 202 cm⁻¹, when pressure increases up to 10 GPa [1]. Structural transformations driven by soft modes are however typical of second-order displacive phase transitions, which has motivated us to further explore the high-pressure state of ZrSiO₄ by DFT calculations [2] and in situ Raman spectroscopy up to 26 GPa.

The DFT simulations reveal (i) a thermodynamic instability of ZrSiO₄ at *p*_r ~9.1 GPa due to the crossing of the Gibbs energies of zircon and reidite, making zircon metastable above *p*_r (ii) a dynamic instability of zircon at *p*_c ~20 GPa, leading to a displacive phase transition to a high-pressure low-symmetry (HPLS) phase (*I*-42*d*); the soft mode that triggers this transition is silent in zircon but becomes Raman-active above *p*_c.

Raman scattering experiments confirm the occurrence of a soft-mode-driven zircon-to-HPLS phase transition at ~21 GPa. The zircon hard mode at ~202 cm⁻¹ couples with the soft mode, leading to a minimum of the hard-mode wavenumber near *p*_c. Further, *dw/dp* of this hard mode abruptly changes at 9.5 GPa, near *p*_r, indicating perturbations in the shape of the corresponding local potential. However, reidite was only detected above ~21 GPa, revealing that at room temperature the potential barrier between zircon and reidite can be overcome only via the formation of the HPLS phase as an intermediate bridging state between zircon and reidite.

Financial support by the European Research Council (Grant 714936) is acknowledged.

[1] Pina Binivignat et al., *Phys. Chem. Mineral.* **45**, 981 (2018).

[2] Stangarone et al., to *Am. Mineral.*

S15-02

Crystalline polymeric carbon dioxide is stable at megabar conditions

R. Miletich¹, K. Dziubek², M. Ende¹, D. Scelta², R. Bini², M. Mezouar³, G. Garbarino³

¹Universität Wien, Institut für Mineralogie und Kristallographie, Wien, Austria

²European Laboratory for Non-linear Spectroscopy, Sesto Fiorentino, Italy

³ESRF, Grenoble, France

Static high-pressure experiments at megabar pressures give evidence for a stable extended form of crystalline carbon dioxide [1]. Synchrotron X-ray diffraction and Raman studies of laser-heated carbon dioxide in a diamond-anvil cell (DAC) suggest the polymeric phase V (space-group symmetry *I*-42*d*) [2] to be the

thermodynamically stable crystalline structure at conditions relevant to the Earth's lowermost mantle.

By using a carbonate crystal as a potential laser absorber, a CO₂ sample compressed to about 120 giga-pascals was successfully heated up to 2700 Kelvin. Contrary to earlier experimental findings, but in agreement with reported theoretical calculations [3-5], neither dissociation into diamond and ϵ -oxygen nor ionization was observed. Even amorphization can be definitely ruled out from the experimental findings.

The observation of β -ReO₂ occurring at the interface to the Re-gasket suggests that earlier findings on the CO₂ breakdown most likely originate from a simple redox reaction between hot CO₂ and the Re gasket used in the DAC [6]. The experimental equation of state and a negative linear compressibility along the tetragonal *c* axis are confirmed. Additional features in the diffraction pattern demonstrate the existence of severe deviatoric stress and lattice deformation along with preferred orientation. Their disappearance on progressive annealing suggest CO₂-V being the stable structure also above one mega-bar.

References

[1] Dziubek et al., *Nat. Comm.* 2018, 9, 3148

[2] Santoro et al., *PNAS* 2012, 109, 5176

[3] Litasov et al., *EPSL* 2011, 309, 318-323

[4] Maeda et al., *Sci Rep.* 2017 7, 40602

[5] Yoo, *PRL* 2013, 83, 5527

[6] Santamaria-Perez et al., *Inorg. Chem.* 2016, 55, 10793

S15-03

Successful quantitative experimental charge density under high pressure - feasibility study

K. Wozniak¹, R. Gajda¹, A. Makal¹, M. Stachowicz¹, S. Sutula¹, P. Fertey²

¹University of Warsaw, Department of Chemistry, Warszawa, Poland

²SOLEIL Synchrotron, Paris, France

We would like to present results of our X-ray measurements conducted on the CRISTAL beamline at the SOLEIL synchrotron (Paris, France). We have studied single crystal of a natural mineral Grossular - Ca₃Al₂(SiO₃)₄, which crystallizes in the space group *I*-3*d* of the cubic crystal system. We wanted to check if it is possible to determine an experimental electron density of a single crystal under pressure. The beamline parameters such as beam wavelength (0.41 Å) and a special type of Diamond Anvil Cell (DAC) with the opening angle 110° let us collect data with the resolution up to 0.35 Å (with 100% completeness up to 0.39 Å). To deal with collected data set of different software was used. CrysAlis(Pro) was used for data reduction. Olex2 for structure solution and refinement. Jana2006 and XD program package for multipole refinement, and WinXPro for visualization of different types of maps. We have compared our results with experimental charge density obtained for Pyrope - Mg₃Al₂(SiO₃)₄ (isostructural with Grossular), measured at low temperature, 30K (Destro *at al.*, 2017) [1]. In case of our measurements for Grossular, the largest features in the residual density ($\Delta\rho$) map are -0.62/+0.52eÅ⁻³ (and they are located near atoms) which is *ca.* five times bigger than for Pyrope at 30K. However, the calculated properties of the charge density at the (3, -1) BCPs as well as the net atomic charges are comparable. We think that thanks to the new type of DACs with the wider opening angle and access to synchrotron radiations for some types of high symmetry crystals, charge density distribution can be determined experimentally. Up to our knowledge, this is the first successful determination of quantitative charge distribution in crystal under high pressure. We will present detailed results of our investigations.

References:

[1] R. Destro, R. Ruffo, P. Roversi, R. Soave, L. Loconte and L. L. Presti, *Acta Cryst. B*, (2017), **73**, 722-736.

S15-04

High pressure suppression of correlation effects in CaMn₇O₁₂

M. Stekiel¹, A. Girard¹, D. Zimmer¹, K. Glazyrin², J. Ruiz-Fuertes³, X. Du⁴, Y. Li^{4,5}, B. Winkler¹

¹Goethe-Universität Frankfurt am Main, Institut für Geowissenschaften, Frankfurt am Main, Germany

²DESY, Photon Sciences, Hamburg, Germany

³Universidad de Calabria, Ciencias de la Tierra y Física de la Materia Condensada, Santander, Spain

⁴Peking University, International Center for Quantum Materials, Beijing, China

⁵Collaborative Innovation Center of Quantum Matter, Beijing, China

CaMn₇O₁₂ has recently attracted great interest as an ideal system for the study of intertwined orbital, magnetic, charge and lattice degrees of freedom [1-4]. These interests were renewed after the report of a huge magnetically-induced ferroelectric polarization (2870 $\mu\text{C m}^{-2}$ for a single crystal) [1]. Upon cooling CaMn₇O₁₂ undergoes a sequence of phase transitions associated with charge, orbital and spin ordering. However, currently nothing is known about its behavior at high pressures. Motivated by its unique properties we wanted to see how pressure affects the correlation effects in CaMn₇O₁₂.

We have performed high-pressure, low-temperature, single-crystal diffraction measurements in order to determine the structural changes in CaMn₇O₁₂. We discovered that at ambient temperature the distortion of the MnO₆ octahedra decreases with increasing pressure and that the octahedra become regular at 29 GPa. Additional resistivity measurements at ambient temperature and high pressure show a decrease in resistivity by three orders of magnitude between 20-30 GPa.

The low temperature measurements were conducted at 200 K and 70 K where CaMn₇O₁₂ exhibits a modulated structural distortion. We observed that the modulation peaks vanish below 7 GPa, with minor impact on the average crystal structure.

These results allow us to determine how pressure affects the correlation effects in CaMn₇O₁₂, and construct its phase diagram. The detailed results of the described measurements will be presented during the conference, together with the possible physical explanation of observed phenomena.

The study is supported by funding from the DFG-ANR project WI1232/41.

[1] D. Johnson et al., *Phys. Rev. Lett.* 108, 067201 (2012).

[2] Sławiński et al., *J. Phys.: Condens. Matter* 20, 104239 (2008).

[3] Perks et al., *Nat. Commun.* 3, 1277 (2012).

[4] S. Souliou et al. *PRB*, 94, 184309 (2016).

S15-05

Structural changes in MgSiO₃ glass up to 138 GPa

C. Prescher^{1,2}, V. Prakapenka³, J. Stefanski²

¹DESY, Hamburg, Germany

²University of Cologne, Institut für Geology and Mineralogy, Köln, Germany

³University of Chicago, Center for Advanced Radiation Source, Chicago, United States

The physical properties of silicate melts at temperature and pressure conditions of the Earth's mantle have a fundamental influence on the chemical and thermal evolution of the Earth. However, direct investigations of melt structures at these conditions are experimentally very difficult or even impossible with current capabilities. In order to still be able to obtain an estimate of the structural behavior of melts at high pressures and temperatures, amorphous materials have been widely used as analogue materials.

Here we report experimental investigations of the structural behavior of MgSiO₃ glass up to 138 GPa using x-ray total scattering and pair distribution function analysis. The very high pressure range for these measurements were enabled by the newly commissioned multichannel collimator setup at GSECARS, APS, which significantly reduces the amount of diamond Compton scattering. This facilitates the collection of total x-ray diffraction patterns up to a maximum Q of 14.5 Å⁻¹ even at very high pressures.

The data clearly shows strong changes in the structure factors and pair distribution functions in the first 50 GPa, corresponding to major changes in Mg-O and Si-O coordination numbers. At higher pressures, the glass structure smoothly changes with pressure and does not show any discontinuities up to the highest pressure reached.

We will present experimental data, discuss densification mechanisms and differences in comparison to literature data and our previous high pressure investigations on the structural changes of SiO₂ and GeO₂ glass at high pressures.

S15-06

Temperature dependence of the crystal structure and magnetic properties of Mn₅Si₃ and MnFe₄Si₃ at high pressures

A. Eich¹, P. Hering², L. Caron^{3,4}, H. Deng^{1,5}, V. Hutanu^{1,5}, M. Meven^{1,5}, K. Friese², A. Grzechnik¹

¹RWTH Aachen University, Institute of Crystallography, Aachen, Germany

²Forschungszentrum Jülich GmbH, Jülich Centre for Neutron Science-2/Peter Grünberg Institut-4 (JCNS-2/PGL-4), Jülich, Germany

³Universität Bielefeld, Faculty of Physics, Bielefeld, Germany

⁴Max Planck Institute for Chemical Physics of Solids, Dresden, Germany

⁵Forschungszentrum Jülich GmbH at Heinz Maier-Leibnitz Zentrum (MLZ), Jülich Centre for Neutron Science (JCNS), Garching, Germany

Refrigeration based on the magnetocaloric effect is a potential alternative to conventional vapor compression refrigeration. One system of particular interest with regard to application is Mn_{5-x}Fe_xSi₃ [1-3]. Pressure affects the interatomic distances in the crystal structure and thus has an influence on the magnetic properties.

The aim of this work is to establish the influence of hydrostatic pressure on the crystal structure of Mn₅Si₃ and MnFe₄Si₃ as well as the pressure dependence of the magnetic transition of MnFe₄Si₃, which at ambient pressure orders ferromagnetically at $T_C \approx 300$ K. Synchrotron X-ray powder diffraction measurements were carried out on Mn₅Si₃ up to 24.2 GPa at room temperature, and on MnFe₄Si₃ up to 12.5 GPa between 100 K and 373 K. Isofield

magnetization measurements and neutron single-crystal diffraction were used to determine the magnetic transition temperature up to pressures of 1 GPa.

For Mn_5Si_3 no pressure-induced phase transition is found; with increasing pressure the lattice parameters and c/a ratio decrease smoothly.

MnFe_4Si_3 shows no clear indication of phase transitions at high temperatures (296 K–373 K) and high pressures. At low temperatures (200 K, 250 K), anomalies in the lattice parameters occur as a function of pressure. They might be related to a transition into a magnetically ordered phase. The trend of decreasing magnetic transition temperature with increasing pressure is also observed in magnetization data and in the intensities of selected magnetic reflections from neutron diffraction experiments at 1 GPa. The pressure-dependent unit cell volume data at 100 K and 150 K exhibit anomalies as two equations of state are necessary to fit each of the data sets, respectively. The bulk moduli determined for both compounds show an increase with amount of incorporated iron.

[1] Bińczycka *et al.* Phys. Stat. Sol. **1973** 19, K13-K17

[2] Hering *et al.* Chem. Mater. **2015** 27, 7218-7136

[3] Song *et al.* J. Alloys Compd. **2002** 334, 249-252

Instrumentation

S16-01

Resolving protein structures with electrons – cryo TEM and micro ED with JEOLE. Katzmann¹¹JEOL (Germany) GmbH, Freising, Germany

It is not just because of the Nobel Prize 2017 in Chemistry that cryo electron microscopy has set new standards in structural biology at a nano scale level. From detailed examination of cellular compartments and their 3-dimensional orientation to protein structure elucidation this technique is now widely applied also outside academia.

JEOL as a leading manufacturer of electron microscopes recently announced its new generation of cryo transmission electron microscopes. This CRYO ARM™ series was developed to enable further exploration in the field of cryo electron microscopy and micro electron diffraction especially in terms of automation for single particle analysis. Unique new features such as a cold field emission source with an unmatched beam quality, the optimized JEOL in-column energy filter and the all new intuitive GUI that comes with a vast bundle of automated routines like parallel illumination set up all qualifies this series as the choice for the challenging cryo applications of the future. Here we present the current line-up of cryo TEMs with selected application examples in order to demonstrate the workflow and solutions JEOL offers to the structural biology community. For the more technically inclined, we also offer some insight to the various parts and the process of constructing this new development.

Figure 1: JEOL cryo TEMs with resolved beta-galactosidase structure in the background

Figure 1



S16-02

Pushing data quality for laboratory Pair Distribution Function experimentsM. Zobel¹, S. Thomä¹, N. Prinz¹¹University of Bayreuth, Chemistry, Bayreuth, Germany

Although the very first laboratory-based X-ray pair distribution function (PDF) analysis was carried out in the 1930s [1], lab PDF studies are rare. Over the last decade, some few studies with lab

PDF data emerged [2,3], but limited Q_{max} or insufficient instrumental resolution impeded a routine use for structural refinements. Based on a STOE STADI P powder diffractometer in Transmission- / Debye-Scherrer geometry, we designed a novel lab PDF diffractometer with monochromatic Ag $K\alpha_1$ radiation covering a Q-range of 0.2 to 21 inverse Angström. High instrumental resolution and low background is provided by a MYTHEN2 4K module, where four MYTHEN2 silicon strip detectors are arranged on one detector arm. It allows rapid in-situ XRD data collection in a heating chamber up to 950 °C over a continuous 2theta range of 72 ° without detector movement in a stationary mode. PDF data is collected for powder samples out to 144 ° 2theta (21 Å⁻¹) in a moving mode within 6 hours. For benchmarking, we measured and refined LaB6 standards with goodness-of-fits $R_w = 0.138$ over 80 Å. To compare with previous lab PDF studies, we refined a powder PDF of ca. 8 nm TiO₂ nanoparticles over 30 Å with $R_w = 0.180$. While all previous lab PDF studies did not show or refine any data for distances > 30 Å – due to a PDF peak overlap beyond ca. 25 Å due to a lack of monochromatization - we can readily refine our TiO₂ PDF data with an R_w as low as 0.222 over 70 Å. Further data on ionic liquids and metal organic frameworks will be presented.

[1] Warren, B. E. & Gingrich, N. S. *Physical Review* **46** (1934) 368[2] Nijenhuis, J. T., Gateshki, M. & Fransen, M. J. *Zeitschrift für Kristallographie Supplements* **2009** (2009) 163[3] Dykhne, T., Taylor, R., Florence, A. & Billinge, S. J. L., *Pharm Res* **28** (2011) 1041[4] Thomä, S. L. J., Zobel, M., *J. Appl. Cryst.*, submitted

S16-03

In-situ and ex-situ magnetic orientation of microcrystals for single crystal X-ray measurementsT. Kimura¹, F. Kimura¹, S. Tsukui¹, C. Tsuboi¹¹Kyoto University, Kyoto, Japan

Introduction

The function of materials and molecules is closely related to their structure. Especially, the function of proteins depends on their tertiary structure and hence the elucidation of their three-dimensional atomic arrangement is of first importance. For this purpose, single crystal X-ray diffraction (SCXRD) is the most reliable and widely used for determination of the protein structure in crystalline phases. However, there are many proteins that do not crystallize to sizes enough for the SCXRD measurement. If a microcrystalline protein sample, or a powder sample in general, is textured, it is expected that we can obtain SCXRD from microcrystalline samples.

Objective

We have developed instruments for *in-situ* and *ex-situ* three-dimensional magnetic alignment of microcrystal suspensions [1]. We have evaluated the performance of these instruments to see that they can provide SCXRD data for the crystal structure determination from powder samples.

Results

Fig. 1 shows an XRD profile from a magnetically aligned and consolidated lysozyme microcrystal suspension from which the crystal structure was determined [2].

Conclusion

Instruments for texturing microcrystalline suspensions were developed, by which crystal structures were determined via SCXRD analysis from microcrystalline powdery samples.

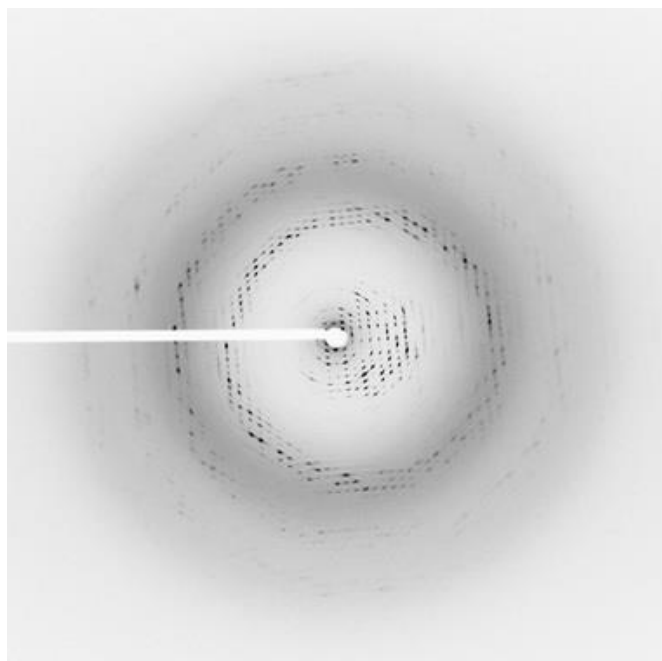
References

- [1] T. Kimura and F. Kimura, *CrystEngComm*, **20**, 861–872 (2018).
 [2] S. Tsukui, F. Kimura, K. Kusaka, S. Baba, N. Mizuno and T. Kimura, *J. Appl. Cryst.*, **49**, 457-461 (2016).

Figure caption

Fig. 1 An XRD profile of a lysozyme microcrystal suspension aligned by magnetic field, followed by consolidation by gelation [2]. XRD measurement was performed at SPring-8.

Figure 1



S16-04

A new single crystal diffractometer at BM20/ESRF

C. Hennig¹, A. Ikeda-Ohno², T. Radoske², A. Scheinost¹
¹Helmholtz-Zentrum Dresden-Rossendorf, Institute of Resource Ecology/
 The Rossendorf Beamline at ESRF / BM20, Grenoble, France
²Helmholtz-Zentrum Dresden-Rossendorf / Institute of Resource Ecology,
 Department of Chemistry of the f-elements, Dresden, Germany

Introduction

The Institute of Resource Ecology / Helmholtz-Zentrum Dresden-Rossendorf operates since 20 years the Rossendorf Beamline (ROBL/BM20) at the European Synchrotron Radiation Facility (ESRF) [1]. The ESRF will interrupt the user operation for a large upgrade between January 2019 and July 2020. This time will be used to refurbish the existing experiments and to extend the experimental capacities including a diffractometer for single crystal diffraction.

Objectives

This diffractometer intends to fill the gap between small molecule and large molecule crystallography. The photon flux of up to 1012 photons/sec allow the structure determination of small single crystals. The analysis of complex intergrown crystals and electron density studies is possible. The energy range of 5-35 keV allows the use of anomalous dispersion. In-situ experiments will be supported.

Results

The objective requires the combination of a large detector, precise

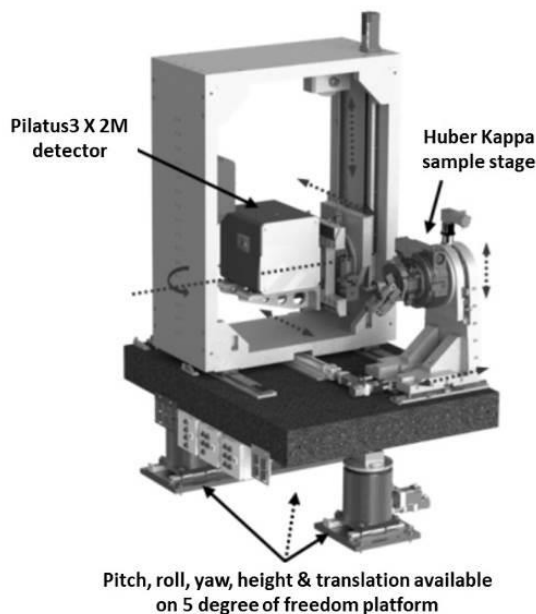
sample position and sufficient space for additional equipment. The diffractometer consists of an adjustable granite table with a metal frame which carry the detector. It follows a design of SNBL/ESRF and is manufactured by Instrument Design Technology Ltd/UK. The Bragg reflexes will be registered with a silicon Pilatus3 X 2M single photon counting detector. Samples will be mounted on a kappa goniometer. A microscope will be placed in a large distance 170 mm from the crystal, which allows to install a cryo cooler (80-400 K), a heater (1200 K), and a Vortex X90 CUBE silicon drift detector with a FalconX1 processor. The data extraction will be performed with CRYSTALIS. Individual components are already tested with X-ray beam.

Conclusion

The new single crystal diffractometer will be accessible starting from August 2020. Crystallographers interested in performing experiments on the new diffractometer are invited to contact C. Hennig (hennig@esrf.fr).

[1] <http://www.esrf.eu/UsersAndScience/Experiments/CRG/BM20>

Figure 1



S16-05

In-situ X-Ray Diffraction Measurements during Low Energy Ion Beam Nitriding and Etching

D. Manova¹, S. Mändl¹
¹Leibniz Institute of Surface Engineering (IOM), Leipzig, Germany

Introduction

In-situ X-ray diffraction measurements (XRD) in high vacuum present an ideal method for directly following diffusion and phase formation processes during ion implantation. However, information depth, ion range, thickness of diffusion layer, incident ion current density and XRD detector have to be in a reasonable relation to

obtain meaningful data. Using broadbeam low energy ion implantation is one option to realize such an experiment. With a 1D linear detector, measurement times of less than 3 minute for a 2 θ range of 20° are possible.

Objectives

As a model system, nitriding of austenitic stainless steel was investigated. Coherent growth of an expanded austenite structure on top of the original grains has been observed. The growth of this layer depends on the nitrogen supply rate with an increasing current density leading to a temperature and time dependent transition from supply-limited to diffusion-limited growth.

Results

However, a detailed analysis of the intensities arising from the substrate and the overlayer shows that the scattering intensity of this overlayer, after correction for its thickness, varies not only with time but also with temperature and processing conditions. This indicates that complex defect formation and annealing mechanisms are active, driven by stress. Using the identical experimental setup with argon instead of nitrogen ions allows direct depth profiling of the materials system at ambient temperatures where all such processes are frozen, indicating a complex distribution of plastic deformation and elastic stress within the modified zone.

Conclusions

The combination of ion etching and in-situ XRD allows determination of gradients for diffusion systems and could be also applied for other materials systems including PVD coatings.

S16-06

Photon counting with mixed mode detection

M. Adam¹, R. Durst², J. Kaercher³, T. Stuerzer², B. Becker²

¹Bruker AXS GmbH, SC-XRD, Karlsruhe, Germany

²Bruker AXS GmbH, Karlsruhe, Germany

³Bruker AXS Inc., Madison WI, United States

Modern single-crystal X-ray diffraction relies entirely on two dimensional pixel array detectors (PAD). Their underlying CMOS technology allows shutterless data collection which has widely eliminated experimental overhead time. Today, two different techniques are competing in the home laboratory market. HPADs, now available for a number of years, count individual X-ray events, based on electron-electron hole pairs and apply an internal threshold to suppress the background noise including the noise originating from the sensor. These detectors produce clear images, which at a first glance are perfectly noise free. However, the need for a threshold introduces a new source of noise for HPADs: charge sharing between pixels resulting in signal loss; Fig1. The limited count-rate capability of HPADs is another source of errors. Signal loss occurs if two individual X-ray photons arrive at the same pixel within a too short time interval as it typically occurs with well diffracting samples (high intensity). In the majority of HPAD detectors ultra-pure silicon (Si) is used as the primary absorber material for the X-ray photons. As Si has rather poor absorption properties for hard radiation, the corresponding detectors have limited sensitivity for Mo- and Ag X-rays. The large pathway of an X-ray photon through the primary absorber layer also leads to unwanted parallax effects. To generate large area HPAD detectors small building blocks are tiled leading to the characteristic blind stripes in the diffraction image.

Mixed-mode detectors offer the advanced technical alternative to HPADs. This rather new technology is now implemented at large research facilities, such as free electron laser sites. For the home market Bruker has developed the PHOTON III series of detectors;

Fig2. Large monolithic sensors without gaps are standard in these detectors. An ultra-low noise floor as well as high read-out speed and frequency of modern CMOS sensors allows the identification of individual X-ray events, very similar to the HPAD detectors. However, mixed-mode detectors first integrate individual X-ray events and then count in a second step. This approach does not require any threshold and truly counts all X-ray events. Thus, mixed-mode detectors do not suffer from charge sharing. Furthermore, mixed mode detectors can cope with higher count rates. X-ray photons are efficiently absorbed within thin high-Z absorber layers minimizing parallax and leading to a smaller signal point spread.

Figure 1

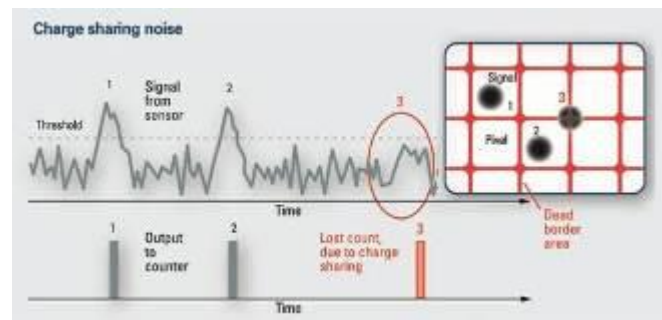


Figure 2



Spectroscopy

S17-01

Changes in the cationic and anionic arrangements in the trilithionite – polyolithionite systemL. Sulcek¹, N. Becker¹, M. Fechtelkord¹¹Ruhr-Universität Bochum, Institut für Geologie, Mineralogie und Geophysik, Bochum, Germany

The cationic and anionic ordering in the octahedral and tetrahedral sheets in the system trilithionite - polyolithionite with composition $K(Li_xAl_{3-x})[Al_{4-2x}Si_{2x}O_{10}](F_{2-y},OH)_y$ ($1.5 \leq x \leq 2.0$; $0.0 \leq y \leq 1.4$) has been investigated using ¹H, ²⁹Si and ¹⁹F solid state NMR spectroscopic and X-ray diffraction experiments. The purpose of this work is, to investigate the cationic and anionic ordering of Si and Al in the tetrahedral sheets and of Al, Li, F and OH in the octahedral sheets. In addition, preferences should be clarified from F to Li-cations or OH to Al-cations. The changes in the tetrahedral and octahedral sheets and the relations to each other is another aspect of this work.

The Si/Al ratio in the tetrahedral sheets can be calculated from the ²⁹Si MAS NMR spectra, which show the nominal oxide composition is the final composition of trilithionite / polyolithionite. Probably signals from different polytypes can be separated in the ¹⁹F MAS NMR spectra. In addition to this the X-ray diffraction experiments confirm the appearance of the polytypes 1M and 2M₁. The percentage of both polytypes can be calculated by using the signal areas of the ¹⁹F MAS NMR spectra. It can be shown, that the ratio of the polytypes is independent of the composition but of the conditions of the synthesis according to Heinrich (1967), Swanson and Bailey (1981) und Chaudry und Howie (1973). Furthermore, the ¹⁹F MAS NMR spectra shows an F preference to Li-rich octahedral clusters and in contrast to this the ¹H MAS NMR spectra reveal the location of OH-groups in the Al-rich octahedral clusters.

[1] Heinrich, E.W. (1967) Micas of the Brown Derby pegmatites, Gunnison County, Colorado. *American Mineralogist*, 52, 1110-1121.

[2] Chaudry, M. N., Howie, R. A. (1973) Lithium-Aluminium Micas from the Meldon Aplite. *Mineralogical Magazine*, 39, 289-296.

[3] Swanson, T.H., Bailey, S.W. (1981) Redetermination of the lepidolite-2M₁ structure. *Clays and Clay Minerals*, 29, 81-90.

S17-02

Fast diffraction and XANES analysis of solid flame reactions at PETRA IIIW. Morgenroth¹, D. Spahr¹, J. Binck¹, J. Song¹, M. Stękiel¹, D. Varentsov², N. Schell³, V. Murzin⁴, B. Winkler¹¹Goethe-Universität Frankfurt am Main, Kristallographie, Frankfurt am Main, Germany²GSI Helmholtzzentrum für Schwerionenforschung GmbH, Darmstadt, Germany³Helmholtz-Zentrum Geesthacht, Geesthacht, Germany⁴Bergische Universität Wuppertal, Wuppertal, Germany

Self-propagating high-temperature synthesis (SHS) allows the synthesis of a very large variety of compounds and new materials in an energy-efficient way [1]. They have therefore been extensively studied and are well characterized with respect to the underlying equilibrium thermodynamics. In contrast, the characterization of the transient processes before, in, and after the reaction fronts have not been characterized yet due to the extreme reaction rates (propagating with 1 – 150 mm/s), temperatures (up to 4 500 K) and heating rates (1 000 - 100 000 K/s).

In a BMBF funded project, our final goal is to contribute to the infrastructure for time resolved diffraction experiments with fs time resolution including an appropriately fast radiometric pyrometry at the HED instrument at European XFEL. For the latter, a pyrometer built by the HED group of GSI has been adopted [2]. First experiments during commissioning of the instrument will include the formation of silicides [3], and will focus on structural changes before, in, and after the reaction front. We have therefore carried out complementary experiments for the reactions $5 Ti + 3 Si \rightarrow Ti_5Si_3$ and $5 Ta + 3 Si \rightarrow Ta_5Si_3$. We performed X-ray powder diffraction at 100 Hz using hard X-rays at the High Energy Materials Science Beamline P07 and QEXAFS up to 30 Hz at the Advanced X-ray Absorption Spectroscopy Beamline P64 at PETRA III. The data analysis is currently in progress and results will be presented at the conference.

The authors gratefully acknowledge financial support by BMBF (SHS@XFEL project 05K16RFB and MatDynamics project 05K16PX1 for the QEXAFS setup). We acknowledge DESY (Hamburg, Germany), a member of the Helmholtz Association HGF, for the provision of experimental facilities.

[1] Merzhanov, A. and Averson, A., Elsevier, 1971, 16, 89-124

[2] Ni, P. et al., *Journal de Physique IV (Proceedings)*, EDP Sciences, 2006, 133, 977-980

[3] Bernert, T., Dissertation, Universität Frankfurt, 2014

S17-03

Element-specific local structure of Cu₂Zn(Sn,Ge)Se₄ kesterite alloysK. Ritter^{1,2}, C. Preiß², G. Gurieva³, R. Gunder³, S. Eckner^{1,2}, R. Chernikov⁴, E. Welter⁴, S. Botti⁵, S. Schorr^{3,6}, C. Schnorr^{1,2}¹Universität Leipzig, Felix Bloch Institute of Solid State Physics, Leipzig, Germany²University of Jena, Institute of Solid State Physics, Jena, Germany³Helmholtz-Zentrum Berlin für Materialien und Energie, Berlin, Germany⁴DESY, Hamburg, Germany⁵University of Jena, Institute of Solid State Theory and Optics, Jena, Germany⁶Freie Universität Berlin, Institut für Geologische Wissenschaften, Berlin, Germany**Introduction**

So-called Kesterites, such as Cu₂ZnSnSe₄, offer a wide range of promising earth-abundant absorber materials for thin film solar cells. Alloying Sn with Ge changes the band gap energy of the material and is proposed as a possible route towards band gap engineering and device optimization. However, alloying typically modifies the local arrangement of the atoms even if the solid solution exhibits the same crystal structure as the parent materials.

Methods

Extended X-ray Absorption Fine Structure Spectroscopy probes the element-specific bond lengths and bond length variations. Measurements were performed at the Cu, Zn, Ge, and Sn K-edge of Cu₂Zn(Sn,Ge)Se₄ powder samples with $0 \leq Ge/(Sn+Ge) \leq 1$ synthesized by solid state reaction. The element-specific bond lengths are used to model the anion position for the different local configurations. Its impact on the band gap energy is estimated by density functional theory based calculations.

Results

The element-specific bond lengths of Cu₂Zn(Sn,Ge)Se₄ alloys are very different from each other and nearly independent of the Ge/(Sn+Ge) ratio despite a significant change of the lattice constants. In particular, the Sn-Se bond length is about 0.15 Å larger than the Ge-Se bond lengths although Sn and Ge share the

same lattice site. As a consequence, the position of the Se anion and the Cu-Se and Zn-Se bond lengths are different for a nearest neighbour configuration containing Sn or containing Ge. Furthermore, the Se position for each configuration shifts with varying Ge/(Sn+Ge) ratio.

Conclusions

The element-specific local structure of $\text{Cu}_2\text{Zn}(\text{Sn},\text{Ge})\text{Se}_4$ kesterite alloys thus deviates from the long-range crystallographic structure featuring different atomic configurations with different bond lengths and anion positions. As demonstrated by ab initio calculations, these structural variations significantly affect the band gap energy, which is a crucial parameter for a solar cell application.

S17-04

Lattice dynamics of the $\text{Sb}_2\text{Te}_{3-x}\text{Se}_x$ solid solution from experiment and theory

M. Herrmann¹, R. Stoffel², M. Küpers², M. Ait Haddouch¹, J. Voigt¹, D. L. Abernathy³, G. Sala³, R. P. Hermann³, R. Dronskowski², K. Friese¹

¹Forschungszentrum Jülich GmbH, JCNS-2/PGL-4, Jülich, Germany

²RWTH Aachen University, Institute of Inorganic Chemistry, Aachen, Germany

³Oak Ridge National Laboratory, Oak Ridge, TN, United States

At ambient conditions Sb_2Te_3 crystallizes in a rhombohedral structure ($R\bar{3}m$), which is formed by repeated $\cdots\text{Te}_2\text{-Sb-Te}_1\text{-Sb-Te}_2\cdots$ layers (Te1/Te2 represent two symmetry-independent Wyckoff positions). Neighboring layers are connected via $\text{Te}_2\cdots\text{Te}_2$ van der Waals interactions [1]. Mixed crystals with $0 < x(\text{Se}) < 2$ [2]. A preferred Se incorporation into the Te1 site of the Sb_2Te_3 structure was suggested previously [2]. The lattice dynamics of Sb_2Te_3 was studied previously by nuclear inelastic and inelastic neutron (INS) scattering experiments [3]. A mode analysis was performed which showed that the different Sb-Te1 and Sb-Te2 bonds result in two separated domains of phonon density [3].

We have synthesized powders and single crystals of $\text{Sb}_2\text{Te}_{3-x}\text{Se}_x$ mixed crystals with representative compositions. Atomic coordinates and site occupancy factors (SOF) were determined from single-crystal data. Mixing enthalpies were predicted from DFT calculations. The lattice dynamics of $x(\text{Se})=0, 0.6, 1.2$ and 1.8 was studied by low-temperature heat capacity [4] and INS measurements on polycrystalline samples. The total PDOS of each sample were determined at temperatures of about 40 K. Theoretical heat-capacity data of the same compounds were obtained from DFT calculations [4].

Our single crystal analysis confirm the preferred Se incorporation into Te1 site of the Sb_2Te_3 structure. The predicted mixing enthalpies show that the preferred Se incorporation results in an energy gain with respect to the formation enthalpy of Sb_2Te_3 . From our heat-capacity data, we have determined the Debye temperatures of all compounds. The Debye temperature increases with an elevated Se content. In our INS data we observed a hardening of all modes with increasing Se content.

[1] Mansour et al. (2014), J. Appl. Phys., 116:083513

[2] Molodkin et al. (1979), Russ. J. Inorg. Chem., 24:176-182

[3] Bessas et al. (2012), Phys. Rev. B, 86:224301

[4] Herrmann et al. (2018), J. Phys., 30:405702

S17-05

A spectroscopic investigation of Eu^{3+} incorporation in LnPO_4 ($\text{Ln} = \text{Tb}, \text{Gd}_{1-x}\text{Lu}_x, x = 0.3, 0.5, 0.7$) ceramics

H. Lösch¹, A. Hirsch², J. Holthausen³, L. Peters⁴, B. Xiao¹, S. Neumeier⁵, M. Schmidt¹, N. Huittinen¹

¹Helmholtz-Zentrum Dresden-Rossendorf, Dresden, Germany

²Fraunhofer Technology Centre Semiconductor Materials, Freiberg, Germany

³ASK Chemicals, Hilden, Germany

⁴RWTH Aachen University, Aachen, Germany

⁵Forschungszentrum Jülich GmbH, Jülich, Germany

In recent years, rare-earth orthophosphates LnPO_4 have attracted attention as potential hosts for the immobilization of specific radioactive waste streams.

In the present work, the incorporation of Eu^{3+} in LnPO_4 host materials predominantly having the xenotime structure has been investigated on the molecular level. As host cations we used Tb and Lu as well as a solid solution series of $\text{Gd}_{1-x}\text{Lu}_x\text{PO}_4$ ($x = 0.3, 0.5, 0.7$). The site selective laser luminescence spectroscopy (TRLFS) technique was applied to study the distribution of Eu^{3+} in the synthetic xenotime phases, while PXRD and Raman spectroscopy were used for bulk structural investigations direct after synthesis and after one year of storage at ambient conditions.

The PXRD patterns of the solid solution series show the formation of a single xenotime phase up to a substitution of $x = 0.5$ both before and after aging. The TRLFS emission spectra also show that Eu^{3+} is substituted for the host cation site in the xenotime hosts. After one year, the emission spectra show a broad dominant signal between the transitions regions of the ${}^7\text{F}_1\text{-}$ and ${}^7\text{F}_2\text{-}$ bands, and the luminescence signal no longer corresponds to Eu^{3+} -incorporation in a xenotime environment, only. These changes indicate a time-dependent change in the local structure of the europium dopant. Based on these observations we suggest an exclusion of Eu^{3+} from the crystal structure and subsequent migration of the cation to the grain boundaries during aging. The migration of Eu^{3+} in void spaces through the crystal structure could be responsible for the additional signals in the emission spectra, while the narrow void space forces an overlap between Eu^{3+} and oxygen atomic orbitals, resulting in the broad signal between the ${}^7\text{F}_1\text{-}$ and ${}^7\text{F}_2\text{-}$ bands.

The segregation of Eu^{3+} to grain boundaries after a relatively short aging in the xenotime materials, indicates that xenotime ceramics will not serve as a suitable waste form for trivalent actinides from high-level nuclear waste.

S17-06

IR-spectroscopic investigation of kieserite-cobaltkieserite solid solutions, $\text{Mg}_{1-x}\text{Co}_x\text{SO}_4 \cdot \text{H}_2\text{O}$, under ambient and low temperature conditions with relevance to Mars and icy moons

D. Talla¹, M. Wildner¹

¹Universität Wien, Institut für Mineralogie und Kristallographie, Wien, Austria

We present results of IR and Raman measurements on synthetic kieserite samples with variable Mg/Co ratio at temperatures T between 313–78K, aiming (i) to assist astronomers in a refined interpretation of spectral data from orbiter and rover missions investigating abundant sulfates on Mars and icy Jovian moons, and (ii) to complement respective structural data [1] showing expected Vegard-type behaviour but an inverted $M_2\text{-}$ size to cell-volume ratio.

At ambient T the IR spectra generally reveal linear positional changes of prominent bands with increasing Co content, in

accordance with cell parameter and structural changes along the solid solution [1]. The stretching modes of the H₂O molecule barely change in position regardless of Co content, whereas the H₂O bending and the symmetric stretching of the SO₄ group at ~1050 cm⁻¹ seem to be promising candidates to infer on the Mg/Co ratio in kieserite. The positions of H₂O stretching bands decrease significantly at low *T*. Conversely, an absorption at ~880 cm⁻¹ increases in wavenumber. The sulfate-related bands remain nearly constant throughout the entire *T* range. Comparable changes with varying Mg/Co ratio and temperature can be observed in the Raman spectra, where better band resolution allows to evaluate the SO₄ bands with higher accuracy. *T*-induced changes in band shift are indeed limited, hardly exceeding 5 cm⁻¹ throughout the entire 313–78K range. This provides a good measure to infer on the sample's composition regardless of *T*, e.g. by using the most prominent Raman band – the ν₁(SO₄) symmetric stretching mode at ~1050 cm⁻¹.

To our belief, the exact knowledge of spectral changes with uptake of cosmochemically relevant cations (Fe, Co, Ni) in the kieserite structure [2] can significantly assist astronomers in a deeper refinement of future orbiter and lander data.

[1] A. Bechtold and M. Wildner, Eur. J. Mineral. **28**, 43 (2016)

[2] J.J. Papike, P.V. Burger, J.M. Karner, C.K. Shearer, 7th Int. Conf. Mars, 3004.pdf (2008)

Complex and aperiodic structures

S18-01

Complex crystal structures of efflorescence phases grown on historic objects

S. Bette¹, G. Eggert², R. E. Dinnebier²¹Max Planck Institute for Solid State Research, Scientific Facility X-ray diffraction, Stuttgart, Germany²State Academy of Art and Design, Stuttgart, Germany

Introduction

During the storage of historic objects over long times corrosion processes may lead to severe damage. The corrosion is often accompanied by the occurrence of efflorescence crystals. Some of these corrosion phenomena have been known for more than 100 years but most of the efflorescence phases, however, are still unknown or only poorly characterized.

Objectives

Profound chemical and structural knowledge of the efflorescence phases is essential for the understanding of the corrosion processes. Both, samples from collections and synthesized samples from model experiments were used for the investigations. All crystal structures were solved *ab-initio* from X-ray powder diffraction (XRPD) data while employing vibrational spectroscopy, thermal and EDX analyses as complementary tools.

Results

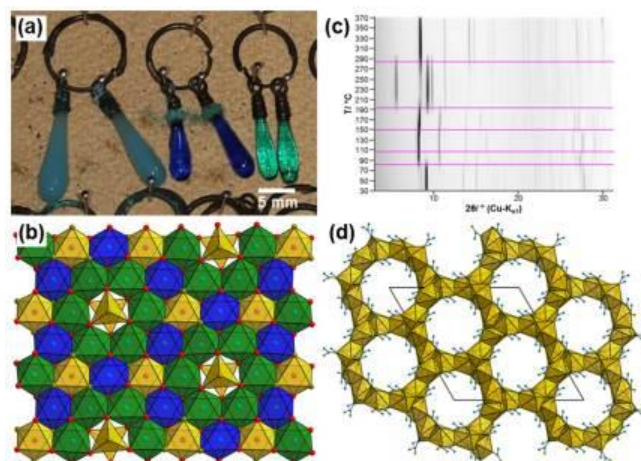
$\text{Zn}_4\text{Cu}_3(\text{Zn}_{1-x}\text{Cu}_x)_6(\text{HCOO})_8(\text{OH})_{18}\cdot 6(\text{H}_2\text{O})$ was identified as an efflorescence phase found on various historic brass objects in contact to glass, e.g. on glass ear rings. White effloresces crystals grown on eggs were found to contain both acetate and formate ions and finally the phase composition was determined as $\text{Ca}(\text{CH}_3\text{COO})(\text{HCOO})\cdot\text{H}_2\text{O}$. By investigation of the dehydration behaviour of the efflorescence salt $\text{Ca}(\text{CH}_3\text{COO})_2\cdot\text{H}_2\text{O}$, two previously unknown subhydrates, $\text{Ca}(\text{CH}_3\text{COO})_2\cdot\frac{1}{2}\text{H}_2\text{O}$ and $\text{Ca}(\text{CH}_3\text{COO})_2\cdot\frac{1}{4}\text{H}_2\text{O}$, were characterized. Anhydrous calcium acetate was found to exhibit three distinct polymorphs, α -, β - and γ - $\text{Ca}(\text{CH}_3\text{COO})_2$, the latter showing a high and low temperature form.

Conclusions

The investigation of efflorescence phases reveals a great variety of complex structures and extends the basis for the identification and the quantitative analysis of the corrosion products in museums and art collections worldwide.

Fig. 1 (a) Ear rings from the Hamburg Museum showing corrosion. (b) $\text{Zn}_4\text{Cu}_3(\text{Zn}_{1-x}\text{Cu}_x)_6(\text{HCOO})_8(\text{OH})_{18}\cdot 6(\text{H}_2\text{O})$ the efflorescence phase. (c) Temperature dependent in-situ XRPD data of $\text{Ca}(\text{CH}_3\text{COO})_2\cdot\text{H}_2\text{O}$ indicating 5 phase transitions, (d) crystal structure of γ - $\text{Ca}(\text{CH}_3\text{COO})_2$.

Figure 1



S18-02

Direct observation of polar nanodomains and nucleation processes in the incommensurate Phase using piezo force microscopy

C. Kofahl¹, G. Eckold¹, F. Güthoff¹¹Georg-August Universität Göttingen, Institute of Physical Chemistry, Göttingen, Germany

Introduction

Incommensurate (INC) phases close to the lock-in transition are predicted to consist of an ordered sequence of commensurate (C) nanodomains separated by discommensurations [1,2]. The existence of these domains and the corresponding multisoliton lattice is usually inferred from diffraction experiments. In ferroelectric systems, surface charges of the polar domains are expected which should be detectable using piezo force microscopy (PFM). In this contribution, we demonstrate that the nanoscaled surface modulation can indeed be visualized in Rb-doped K_2ZnCl_4 crystals as a model system. It is also shown that any variation of the modulation wavelength is associated with the nucleation of topological defects called *stripples* and *anti-stripples*.

Objectives

Using PFM that is sensitive to the polarization of the sample the polar antiparallel nanodomains at the surface can be visualized. If a constant force is applied to the cantilever in contact mode, the application of AC-voltages of 10 V amplitudes leads to deformation at the crystal surface that can be detected with sufficient accuracy even if the piezoelectric coefficient is small. Nanodomains with different polarization can thus be distinguished even at ambient temperature in the metastable state of doped K_2ZnCl_4 .

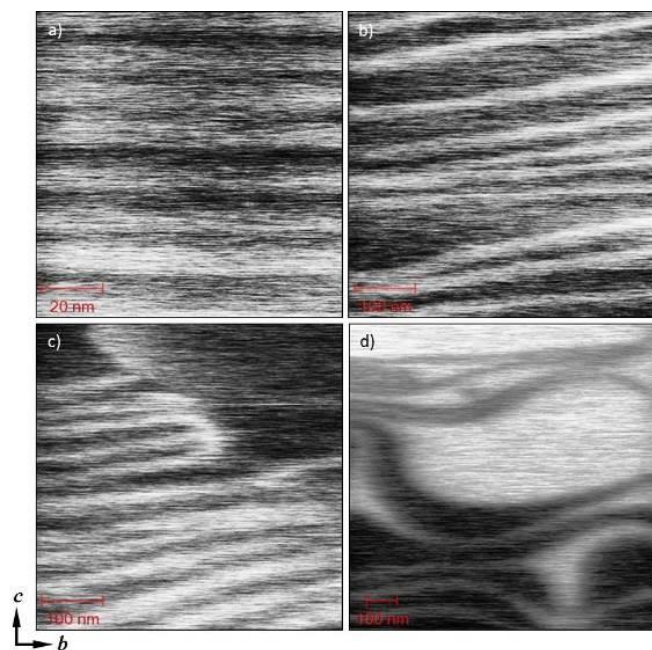
Results

In Fig. 1a, PFM scans are shown which were obtained from a (100)-surface of a K_2ZnCl_4 -crystal doped with Rb. The individual domains of 7 nm width along the modulation direction c are clearly. This is consistent with the bulk periodicity obtained from diffraction data. On ageing, the nucleation of topological defects as theoretically predicted by Parlinski (1987) is shown in Fig. 1b-d.

Conclusion

A direct visualization of polar surface structures in incommensurately modulated systems could be achieved for the first time. The observed pattern reflects the nanoscaled profile of the surface charge in the INC-phase and its variation during coarsening and nucleation processes.

Figure 1



S18-03

Phase transitions of the 3-dimensional charge-density-wave compound CuV_2S_4

S. Ramakrishnan¹, A. Schonleber¹, C. Huebschle¹, N. Hai An Bui¹, F. Feulner¹, M. Anurova¹, D. Chernyshov², N. van Well¹, A. M. Schaller¹, T. Rekiş¹, C. Eisele¹, M. Tolkişn³, S. Ramakrishnan⁴, S. van Smaalen¹

¹University of Bayreuth, Laboratory of Crystallography, Bayreuth, Germany

²SNBL ESRF, Grenoble, France

³DESY, PETRA III, Hamburg, Germany

⁴Tata Institute of Fundamental Research, Department of Condensed Matter Physics and Materials Science, Mumbai, India

The symmetry of the spinel compound CuV_2S_4 at room temperature is described by the space group $\text{Fd}3\text{m}$ [1]. The compound undergoes two phase transitions one at 90 K where the direction pattern shows a charge-density wave (CDW) transition with a modulation wave vector $q = (3/4 + \delta, 3/4 + \delta, 0)$ and the other at 50 K where the wave vector $q = (1/3 + \delta, 1/3 + \delta, 0)$ [2]. The X-ray powder diffraction shows a lowering of the symmetry of the lattice from cubic to tetragonal at temperatures below 90 K [1, 3]. The temperature dependence of the magnetization data report results of the decrease in magnetic susceptibility (χ) at 90 K followed by an upward jump at 54 K [4]. We have studied CuV_2S_4 by single-crystal X-ray diffraction pattern at temperatures down to 5 K. Here we report the modulated crystal structures at phase transitions close to 90 K and 50 K.

References

- [1] S. Kawaguchi, H. Ishibashi, N. Tsuji, J. Kim, K. Kato, M. Takata, and Y. Kubota, *J. Phys. Soc. Jpn.* 82 (2013) 064603.
- [2] R. M. Fleming, F. J. DiSalvo, R. J. Cava, and J. V. Waszczak, *Phys. Rev. B* 24 (1981) 2850.
- [3] H. Okada, K. Koyama and K. Watanabe, *J. Phys. Soc. Jpn.* 73 (2004) 3227.
- [4] I. Naik, C. S. Yadav, and A. K. Rastogi, *Phys. Rev. B* 75 (2007) 115122.

S18-05

The Sc-Pd system: a new 1/1 Mackay type approximant and alloying of aluminum

T. Leisegang^{1,2}, P. Solokha³, T. G. Akhmetshina^{4,2}, R. A. Eremin^{4,2}, A. V. Gurskaya^{4,2}, S. De Negri³, D. M. Proserpio^{2,5}, A. Saccone³

¹Technische Universität Bergakademie Freiberg, Institut für Experimentelle Physik, Freiberg, Germany

²Samara State Technical University, Samara Center for Theoretical Materials Science, Samara, Russian Federation

³Università degli Studi di Genova, Dipartimento di Chimica e Chimica Industriale, Genova, Italy

⁴Samara National Research University, Samara Center for Theoretical Materials Science, Samara, Russian Federation

⁵Università degli Studi di Milano, Dipartimento di Chimica, Milano, Italy

Intermetallic compounds are a wide class of materials exhibiting a large variety of physical properties from low to high temperatures. Among them are construction alloys, magnets, thermoelectrics, superconductors, or hydrogen storage materials. Moreover, those materials have a high potential as electrodes or conversion electrodes for electrochemical energy storage. An example is the (Na-) Sb-Sn system, which is investigated in terms of its use as electrode material for Na-S room temperature batteries. Although intermetallics are of high interest, their chemistry, however, is still a challenging task for solid-state science. These compounds form by two or more metals exhibiting a wide structural diversity—a point of many difficulties in their description and classification. While simple intermetallics with small unit cells are mainly depicted in terms of coordination polyhedra, atomic layers, or polyatomic moieties, for complex structures it is not always the most suitable way of representation. On the early stage, many complex intermetallics were described as a packing of clusters and so called "glue" atoms filling the voids between clusters. Intuitively such a description was made assuming that clusters should be as large as possible without being overlapped. Now another approach where clusters might interpenetrate is becoming popular. The convenience and logic of the cluster representation of complex structures are obvious: intermetallics with more than 1,000 or even 20,000 atoms per unit cell look much simpler when represented as clusters assemblage. In this work, we present a combined study addressing nanoclustering approach as a useful data mining algorithm targeting novel materials designs, synthesis and crystallographic analysis of a new icosahedral Quasicrystal 1/1 approximant in the Sc-Pd system, a combined thermodynamic and DFT modeling of structural peculiarities in the named system as well as the effect of alloying of aluminum and its applicability for novel aluminum-ion battery electrodes.

S18-06

From space group to space groupoid: the local symmetry of low-temperature *E*-vanillyl-oxime

B. Stöger¹

¹TU Wien, X-Ray Centre, Wien, Austria

When describing local symmetry, each operation is associated with a source and a target object (layer, rod, block). The composition of these local operations forms a groupoid [1,2]. Typically, groupoids are used to describe polytypic structures [3].

The room-temperature (RT) crystal structure of *E*-vanillyl-oxime ($P2_1/a$) is well established [4]. On cooling below 190 K, the crystals transform into a low-temperature (LT) phase ($P-1$). The group/subgroup relationship is of index 6 ($Z'=1$ to 6). The six crystallographically unique molecules in the LT phase are pairwise related by local symmetry that is not valid for the overall structure. Thus, the symmetry of this phase is described by a groupoid.

Moreover, each groupoid operation can be identified with an operation of the RT phase. Thus, a finer view of the phase transition is obtained. Usually one distinguishes those operations that are retained and those that are lost. Here, some operations of RT phase are valid for the whole LT phase (the space group operations of P-1). But others remain valid only for parts of the LT phase. By identifying the parts of the LT phase that are equivalent according to local symmetry and the parts for which the local operations apply, a connection between symmetry and topology is established.

[1] H. Brandt. *Math. Ann.* 96, 360–366 (1927)

[2] C. Ehresmann. *Jahresber. DMV* 60, 49–77 (1957)

[3] K. Dornberger-Schiff & K. Fichtner. *Krist. Techn.* 7, 1035–1056 (1972)

[4] B. Jerslev & S. Larsen. *Acta Chem. Scand.* 45, 285–291 (1991)

Young Crystallographers: Lightning talks I

LT1-01

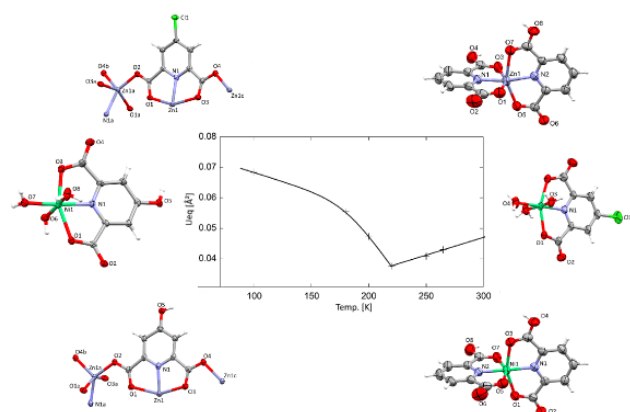
Investigation of a reversible phase transition at low temperatures and the underlying structure property relations for coordination compounds featuring pyridine-2,6-dicarboxylic acid.

M. Kremer¹, U. Englert¹

¹RWTH Aachen University, Institute of Inorganic Chemistry, Aachen, Germany

Single crystal X-ray diffraction measurements can be performed for coordination compounds featuring pyridine-2,6-dicarboxylic acid (PDC) and transition metals cations Zn(II) and Ni(II) at 250K. At lower temperatures, determination of a proper crystal structure becomes nearly impossible. At temperatures below approximately 220K, the previously obtained unit cell can no longer be used, and a much larger unit cell of very bad quality with at least two separate twin domains is calculated by the indexing software. The presumed phase transition was investigated through multiple diffraction experiments at different temperatures. Multiple derivatives of PDC (4-Chloropyridine-2,6-dicarboxylic acid; 4-Hydroxy-pyridine-2,6-dicarboxylic acid), were used to determine a possible relation between the observed phase transition and the used reactants. The results point towards a reversible and reproducible phase transition that can be linked to the structure of the ligand molecules and the strength of the intermolecular bonds formed between the PDC derivatives. During our research, we discovered several new crystal structures, including two previously unreported Metal-Organic Frameworks (MOFs).

Figure 1



LT1-02

Modelling in the 20's – prospects and possibilities

S. Diez¹, R. Neder¹

¹Friedrich-Alexander-Universität Erlangen-Nürnberg, Erlangen, Germany

Based on recent measurements at large synchrotron facilities, we would like to share an overview on the limits of structure refinement of "quasi-amorphous" X-Ray diffractograms. We will shed light on current techniques of high quality data analysis and their immediate results for any experimental work and involved expectations, respectively. In that context it is to elucidate to what detail theoretical model structures are supposed to be consulted.

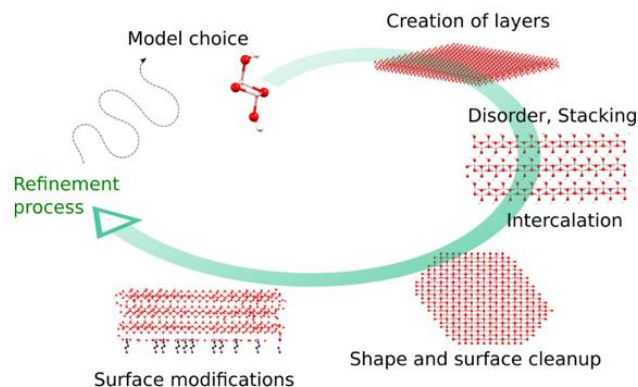
In order to corroborate our statements we investigated an established sol-gel synthesis for AlOOH nanoparticles. In particular the synthesis of Boehmite nanoparticles was utilized since the resulting particles combine several compliant structural

properties. In that regard, it must be noted that a traditional sol-gel synthesis is prone to yield a wide range of particle morphologies and potentially several precursor phases. We tried to fit powder data of a realistic and naturally occurring yield of a synthesis with the demand of reducing the residual factor to the minimum.

Previous studies and data originating from Boehmite particles suggest that the current synthesis does not create other AlOOH polymorphs. Combined with the latest advances and challenges of the new detector 2D generation, we took our liberty to employ a data modelling approach which is by far more detailed as the ones typically considered for nanoparticulate systems. We will present a stepwise creation of the particle structure (Fig. 1) and its successive impact on the theoretically calculated PDF data set.

Based on corrected and refined experimental data sets we'll demonstrate which assumptions may contribute considerably to a more realistic model and are at the same time verifiable in the experimental data set. In contrast to idealised model systems our approach may in particular be of interest and applicability in areas of nanoscience dealing with porous structures, intercalation, disorder or any stabilizing agents on surfaces.

Figure 1



LT1-03

Template effects on the pressure-dependent behaviour of zeolites – A computational case study of chabazite-type fluoroaluminophosphates

M. Fischer^{1,2}

¹Universität Bremen, Fachbereich Geowissenschaften - Kristallographie, Bremen, Germany

²Universität Bremen, MAPEX Center of Materials and Processes, Bremen, Germany

Introduction

There is a continued interest in the pressure-dependent behaviour of zeolites and related framework compounds.¹ It is well known that extra-framework species residing in the voids of these materials have a significant impact on their compressional behaviour, e.g. for isostructural compounds containing different organic template species in the pores. While in-situ diffraction experiments can provide insights into these "template effects", there are often limitations with regard to sample and data quality, rendering a full structural characterisation challenging.

Objectives

The present work employs first-principles calculations in the framework of dispersion-corrected density functional theory (DFT-D) to analyse the pressure-dependent behaviour of four chabazite-type fluoroaluminophosphates containing different organic

template molecules (designated AIPO-CHA_X, where X = template).

Results

DFT-D calculations for AIPO-CHA_morpholinium deliver a bulk modulus that agrees well with the experimental value.² In accordance with experiment, they predict a structural transition at pressures above 3 GPa. The transition is associated with a pronounced elongation of the chabazite cage and a reorientation of the morpholinium molecules. Calculations for three other AIPO-CHA_X systems show a rather drastic influence of the template on the compressibility, with bulk moduli ranging from 19 GPa to 51 GPa. Unlike the morpholinium-containing material, neither of the AIPO-CHA_X systems shows a phase transition below 5 GPa.³

Conclusion

The DFT-D calculations reveal a striking dependence of the compressional behaviour of AIPO-CHA_X materials on the template species. Beyond the rationalisation of experimental findings, predictions can be made for systems that have not (yet) been characterized experimentally.

References

- [1] G. D. Gatta et al., *Phys. Chem. Miner.* **45**, **2018**, 115
 [2] L. Leardini et al., *Z. Kristallogr.* **227**, **2012**, 514
 [3] M. Fischer, *Phys. Chem. Miner.* accepted

LT1-04

Solid state structure of an unusual molecular arene-stabilized bismuth(III)/tungsten(IV) oxidocarboxylate

C. M. Bianga¹, W. Frank¹

¹Heinrich-Heine-Universität Düsseldorf, Institut für Anorganische Chemie und Strukturchemie II, Düsseldorf, Germany

Several heterometallic bismuth-transition metal complexes are described in the literature, most of them with metal–metal bonding and prepared from bismuth(III) halides and metal carbonyls.^[1] Some more examples are characterised by the connection of different metal atoms *via* anionic ligands only.^[2] Studying reaction systems of the type bismuth(II) trifluoroacetate/transition metal compound we obtained some bismuth(III)-transition metal carboxylates of unusual composition.^[3] Here we present a further example from this general class of compounds. The purple oxidocarboxylate **1** results from oxidation of tungsten hexacarbonyl in boiling mesitylene:



For the characterization of such a complex compound the crystal structure determination proves to be essential.

1 crystallises in the monoclinic space group *C2/c* with the unit cell parameters $a = 34.048(7) \text{ \AA}$, $b = 24.175(5) \text{ \AA}$, $c = 17.202(3) \text{ \AA}$, $\beta = 103.39(3)^\circ$ and $Z = 8$. Central unit of the molecular complexes in the solid of **1** are W_3O_4 seco-norcube cages (Figure 1). The bismuth and tungsten atoms are bridged by μ_3 -oxido ligands in an almost planar coordination and additionally by *Z,Z*-type bidentate^[4] trifluoroacetato ligands. The bismuth atoms are also coordinated by one more trifluoroacetato ligand, either unidentate or bidentate chelating^[4]. Finally, the bismuth atoms complete their coordination sphere through coordination of one mesitylene molecule in a nearly ideal η^6 -manner. The solid of **1** might also to be considered as composed of two different types of layers (Figure 2, viewing direction: *b*-axis). One type consists of heterometallic $[\text{Bi}_2\text{W}_3\text{O}_4(\text{O}_2\text{CCF}_3)_{10}]$ units and the other of mesitylene molecules.

- [1] H. Braunschweig, P. Cogswell, K. Schwab, *Coord. Chem. Rev.* **2011**, *255*, 101-117.
 [2] L. Xu, Y. Cui, J. Huang, *Chem. Lett.* **1998**, *27*, 35-36.
 [3] C. M. Bianga, W. Frank, *Z. Kristallogr. Suppl.* **2018**, *38*, 91-92.
 [4] A. Ouchi, Y. Suzuki, Y. Ohki, Y. Koizumi, *Coord. Chem. Rev.* **1988**, *92*, 29-43.

Figure 1

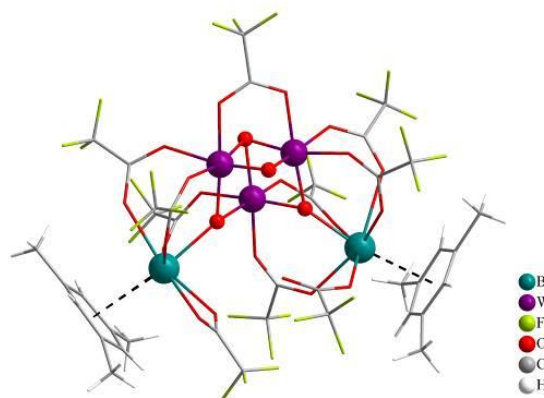
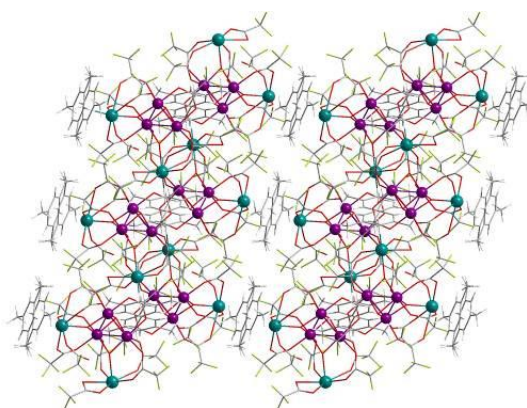


Figure 2



LT1-05

Ion beam assisted thin film growth using mass separated low-energy nitrogen ions

M. Mensing¹, P. Schumacher¹, C. Grüner¹, S. Herath¹, A. Lotnyk¹, J. W. Gerlach¹, B. Rauschenbach¹

¹Leibniz Institute of Surface Engineering (IOM), Leipzig, Germany

Introduction

Ion beam assisted deposition enables the precise engineering of thin film properties by increasing adatom mobility or deliberately generating near surface defects. At hyperthermal ion kinetic energies epitaxial growth can be realized and the impinging particle flux can be used to influence growth mode, crystal orientation or stabilize otherwise metastable crystalline phases.

Objectives

Typical ion or plasma sources generate a blend of multiple ion species. In this study, an energy and mass selected ion beam assisted deposition setup is employed to explore the influence of the predominant ion species (N_2^+ or N^+) during epitaxial nitride thin film growth on the example of GaN on 6H-SiC(0001) without buffer layers or additional dopants. For the selected nitrogen ion species, ion kinetic energies and ion-to-atom arrival ratios are varied.

Results

The deposited thin films are compared concerning their topography, growth mode, crystalline quality and phase composition. Structure analysis revealed the presence of a long-range as well as short-range order in the system. The latter could be attributed to a thin, naturally forming interface layer near the substrate. The higher energy atomic nitrogen ion species was identified to impede the formation of the metastable zinc-blende GaN phase. Molecular nitrogen ions are demonstrated to efficiently dissociate for kinetic energies as low as 20 eV, providing increased growth rates while preserving the crystalline quality.

Conclusion

Energy and mass filtered hyperthermal nitrogen ion species are used to independently investigate their influence during ion beam assisted epitaxy of GaN. The accomplishment of respectable crystal quality during the N_2^+ assisted growth at higher kinetic energies motivates efforts of precisely controlling the involved ion species during thin film growth, as higher ion kinetic energies typically result in higher ion extraction efficiencies and hence larger growth rates.

LT1-06

Crystal growth investigations of lithium iridate, Li_2IrO_3

L. Hollenbeck¹, P. Becker¹

¹University of Cologne, Institute of Geology and Mineralogy, , Cologne, Germany

Recently, the polymorphs of Li_2IrO_3 attracted considerable attention because, through the interplay of electronic correlations, strong spin-orbit coupling and crystal field effects in the d^5 electronic configuration of octahedrally coordinated Ir^{4+} , they form $j=1/2$ Mott insulators with bond-directional magnetic exchange interactions, which are thought to exhibit unconventional magnetism [1,2]. At present, three modifications of Li_2IrO_3 are known: Besides monoclinic α - Li_2IrO_3 with a layer structure of a honeycomb-like arrangement of edge-sharing $[IrO_6]$ octahedra (2D honeycomb) [3], the two orthorhombic modifications with a three-dimensional network of $[IrO_6]$ octahedra, β - Li_2IrO_3 (3D hyper-honeycomb) [4] and γ - Li_2IrO_3 (3D stripy-honeycomb) [5]. The need for high-quality single crystals for the examination of their magnetic properties turns all modifications of Li_2IrO_3 into subjects of crystal growth investigations.

Access to single crystals is possible via growth from the gaseous phase. For this purpose, a modified set up after [6] was realised, in which the educts are separated by rings with spikes forming a "spiral staircase". Depending on the rate of diffusion of the educts, crystallisation takes place on different positions of the "staircase". Furthermore, growth attempts show preferred crystallisation and growth conditions depending on the modification. This also results in different morphologies of the grown crystals. In total, single crystals of α - Li_2IrO_3 of about 1mm and of γ - Li_2IrO_3 of about 0,5mm size are successfully grown. The growth investigations are complemented by DTA and X-ray diffraction.

- [1] Jackeli, G. & Khaliullin, G., *Phys. Rev. Lett.* **102**, 017205 (2009).
- [2] Chaloupka, J. et al., *Phys. Rev. Lett.* **105**, 027204 (2010).
- [3] O'Malley, M.J. et al., *J. Solid State Chem.* **181**, 1803–1809 (2008)
- [4] Biffin, A. et al., *Phys. Rev. B* **90**, 205116 (2014).
- [5] Modic, K.A. et al., *Nat. Commun.* **5**, 4203 (2014).
- [6] Freund, F. et al., *Scientific reports* **6**, 35362 (2016).

LT1-07

Crystallographic Explorations into Uniform Distribution Theory

W. Hornfeck¹

¹Institute of Physics, Prague, Czech Republic

The crystallographic methods applied in structural chemistry for the description of crystal structures focus on a few recurring principles, among them the closest packing of spheres and space group symmetry. While the former concept is locally quantitative, e.g. by giving each atom a coordination number, it rarely offers a similar quantitative global description. The latter concept, however, while being an inherently global descriptor, is purely qualitative. For instance, every so often it happens that crystal structures, e.g. ones related by a phase transition, are very distinct in their symmetry, while being very similar in their local arrangement of atoms at the same time. In other cases, on the contrary, a point can be made for the distinction of structures, although they belong to the same family of structures sharing the same space group symmetry. Moreover, cases exist, in which the arrangement of atoms can be described in ways extending their formal space group symmetry, e.g. by algebraic relations. Thus, it appears to us, that one should search for other concepts, capable of capturing some of these 'hidden symmetries', and in a preferably quantitative and global manner. This is especially true for the description of extended solids, since qualitative and quantitative structural descriptors are well-known for molecules, for which they are successfully used in establishing structure-activity relationships. Here we report about our explorations into the realm of uniform distribution theory, in particular geometric discrepancy theory [1], applying measures for the (ir)regularity of distribution of atoms in space in a crystal chemical context. We highlight examples for the application of the star discrepancy measure in distinguishing variations of a crystal structure belonging to the same general family of structures [2], as well as relations of the diaphony measure to the description of X-ray diffraction by means of the structure factor equation [3].

[1] Matousek, J. (1999). *Geometric Discrepancy*. Berlin, Heidelberg: Springer.

[2] Hornfeck, W. & Kuhn, P. (2014). *Acta Cryst.* A70, 441-447.

[3] Hornfeck, W. & Kuhn, P. (2015). *Acta Cryst.* A71, 382-391.

LT1-08

Visual Diagnostics for Macromolecular X-Ray Diffraction: AUSPEX

A. Thom¹

¹Universität Würzburg, RVZ, Würzburg, Germany

Traditionally, the initial quality of the X-ray data set is evaluated by looking at detector images as they are recorded. An expert user used to be able to recognize problems such as anisotropy, twinning or ice rings from the raw images. After collection, the data would be integrated, scaled and merged with software that required considerable manual intervention and expertise. Data quality indicators were mostly designed so that they could be calculated rapidly with the limited computing power available, and were developed to provide information about the overall data consistency, completeness and resolution [1], often in the form of mean derivatives and R-values. Today, data collection is many orders of magnitude faster, in particular due to the brightness of the X-rays obtained from modern sources such as synchrotron and XFEL beamlines. The high X-ray flux, coupled with fast-readout pixel detectors means that manual inspection of the raw data as it is collected is no longer practical. Unfortunately, there is a severe mismatch between the robustness of our current diagnostic tools and our reliance on automatic processing as many of the quality

indicators in use by the automatic algorithms are not reliable enough for correct decision-making. The lack of visual inspection of detector images by expert users has created a gap in the quality control of experiments. New algorithms which play to the strengths of modern computing power and robust statistical analyses need to be developed and implemented. In addition, much may be gained from taking the whole statistical distribution of the data into account, or even visualising the entirety of the data set instead of mean values. To address this need, we have started a software package for exploratory analyses of crystallographic data. AUSPEX [2] provides a visual and intuitive way of revealing problems in diffraction data that either require a specific processing approach, or indicate that the next crystal of this sample should be treated differently in terms of data collection strategy. The software is available as part of CCP4 and as a web service at auspex.de.

[1] Dauter (2010). *Acta Cryst.* D66, 389.

[2] Thorn et al. (2017). *Acta Cryst.* D73, 729.

LT1-09

In Situ and Nano X-ray Diffraction beamline at PETRA III: research possibilities and first results

A. Khadiev¹, R. Grifone¹, J. Raabe¹, D. Novikov¹

¹DESY, In-situ and nano X-ray diffraction beamline at PETRA III, Hamburg, Germany

In-situ and nano X-ray diffraction beamline at the PETRA III storage ring at DESY went into user operation in September 2018. The scientific case of the beamline concentrates on physics and chemistry of systems dominated by low dimensional and confinement effects, with an emphasis on in situ and operando techniques.

The beamline instrumentation pool is aimed for multiscale analysis of nanostructured materials and processes under ambient and non-ambient conditions. The undulator source and optics are optimized to provide up to 10^{13} photons/sec in the energy range 5-35 keV into variable spot sizes from 1 mm² and down to sub-micrometer values. The beamline currently operates one experimental hut equipped with a heavy-load HUBER diffractometer, which can carry sample cells with up to 150 kg on a hexapod in the 4 circle mode and up to 15 kg on an Eulerian cradle in the 5+2 circle mode. A piezo-driven nanopositioner with a maximum load of 300 g is available for the samples alignment with repeatability < 10 nm and sub-nanometer resolution. X-ray detectors include a state of the art 2D LAMBDA detector with GaAs sensor and time resolution up to 2 kHz. An Andor Shamrock 303i optical spectrograph is available for XEOL measurements combined with XRD and XANES experiments.

In the presentation, we shall show the possibilities provided by the new beamline, present the results of some experimental applications and discuss the plans for future developments.

LT1-10

And yet it moves: Anion Diffusion in the Inverse Perovskites BaLiX₃ (X = H, D, F)

D. Wiedemann¹, E. Heppke¹, A. Franz²

¹Technische Universität Berlin, Institut für Chemie, Berlin, Germany

²Helmholtz-Zentrum Berlin, Structure and Dynamics of Energy Materials, Berlin, Germany

Fluoride and hydride perovskites have sparked interest since the early 2000s in virtue of their possible application in, e.g., semiconductors, optoelectronics, or chemosensors. The compounds BaLiX₃ (X = H, D, F) adopt a cubic perovskite

structure with the positions of high- and low-charge cations swapped with respect to the common arrangement. The hydride–fluoride analogy suggests not only solid-solution behavior but also similar anion-diffusion characteristics.^[1] Our recent study on BaLiF₃ single-crystals indicates immobility of the lithium ions and shows anion diffusion along the LiF₆ edges as the most probable pathway according to topological analyses (see Fig. 1).^[2]

We aim at exploring the pathways and barriers of thermally activated ion migration in perovskites, assessing the tenability of the hydride–fluoride analogy, and testing the suitability of protium instead of deuterium compounds for these investigations. To this end, we have studied powders of BaLiX₃ using neutron diffraction at up to 700 °C. Measurements were carried out at the instrument E9 at Helmholtz-Zentrum Berlin. Atomic models with anion displacement parameters including anharmonic terms were Rietveld-refined against the acquired data. The resulting probability-density functions (PDFs) can be used to visualize the actual pathways of anion diffusion, supported by maps of the scattering-length density reconstructed *via* maximum-entropy methods (MEM). Both approaches enable the calculation of effective one-particle potentials (OPPs) to derive activation barriers and bottleneck positions of migration. For this purpose, the program *CalcOPP* 2.0.0 including guidance and a graphical user interface is introduced.^[3] First results suggest that migration indeed occurs roughly along the LiF₆ edges with activation barriers of *ca.* 0.3 eV (see Fig. 2).

[1] A. J. Maeland, W. D. Lahar, *Z. Phys. Chem.* **1993**, 179, 181–185.

[2] D. Wiedemann, F. Meutzner, O. Fabelo, S. Ganschow, *Acta Crystallogr., Sect. B* **2018**, 74, 643–650.

[3] D. Wiedemann, *CalcOPP 2.0.0 – Calculation of Effective One-Particle Potentials*, Technische Universität Berlin, Berlin (Germany), **2019**.

Fig. 1. Probable anion diffusion pathways in BaLiF₃ as Voronoi–Dirichlet diagram (left) and procrystal-void surface (right) of the [LiBa]³⁺ framework.^[2] Reproduced with permission of the International Union of Crystallography.

Fig. 2. Anion OPP of 0.34 eV in BaLiD₃ at 500 °C derived from PDF including anharmonic terms.

Figure 1

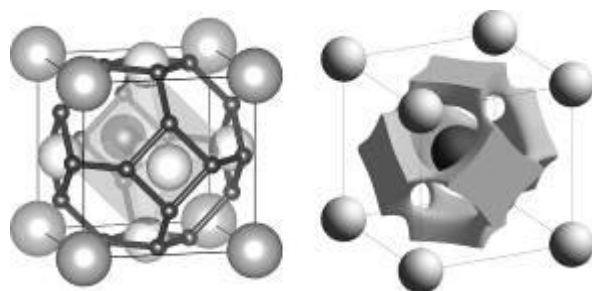
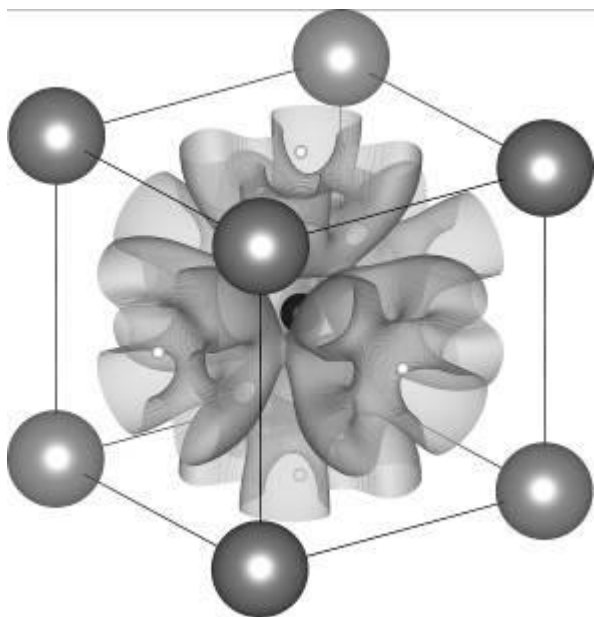
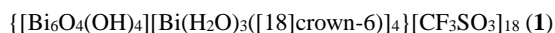


Figure 2


LT1-11
A novel supramolecular bismuth(III) compound derived by hydrolysis of bismuth(III) triflate in acetonitrile

 M. Majewski¹, W. Frank¹
¹Heinrich-Heine-Universität Düsseldorf, Lehrstuhl für Material- und Strukturforchung, Düsseldorf, Germany

The formation of the hexanuclear cation $[\text{Bi}_6\text{O}_4(\text{OH})_4]^{6+}$ upon hydrolysis of bismuth(III) nitrate in acidic solution was proven by Lazarini and Sundvall utilizing single-crystal X-ray diffraction.^[1,2] Further investigations on bismuth oxido salts were realized to examine their potential as new molecular precursors for specialized materials based on bismuth oxide. A promising compound is $[\text{Bi}_6\text{O}_4(\text{OH})_4(\text{OTf})_6(\text{CH}_3\text{CN})_6] \cdot 2\text{CH}_3\text{CN}$.^[3] On the other hand crown ethers have a long history as ligands for bismuth cations like in $[\text{Bi}([12]\text{crown-4})(\text{CH}_3\text{CN})]^{3+}$.^[4] Common aspect of these quite different examples of bismuth complexes is the use of the solvent acetonitrile in synthesis. Therefore, not unexpectedly experiments with the reaction system bismuth(III) trifluoromethanesulfonate/[18]crown-6/acetonitrile led to the isolation of colorless needles of a novel compound with a very unusual composition:



1 crystallises in the monoclinic space group $P2_1/c$ with the unit cell parameters $a = 18.416(4) \text{ \AA}$, $b = 24.970(5) \text{ \AA}$, $c = 36.655(7) \text{ \AA}$, $\beta = 93.19(3)^\circ$ and $Z = 4$. The asymmetric unit contains (i) one $[\text{Bi}_6\text{O}_4(\text{OH})_4]^{6+}$ fragment, in which the bismuth atoms are bridged by both oxido and hydroxido ligands, (ii) four bismuth cations, each enclosed in [18]crown-6 molecules and three H_2O ligands and (iii) 18 trifluoromethanesulfonate anions (Figure 1). The "neutral" H_2O ligands were identified indirectly by calculating the overall neutral charge in the structure instead of localizing the hydrogen atom positions (Figure 2).

In summary we present a novel bismuth oxido and bismuth crown ether complex, which was unambiguously identified by crystal structure analysis.

[1] B. Sundvall, *Acta Chem. Scand.* **1979**, A33, 219–224.

[2] F. Lazarini, *Acta Crystallogr., Sect. B* **1979**, 35, 448–450.

[3] L. Miersch, T. Ruffer, H. Lang, S. Schulze, M. Hietschold, D. Zahn, M. Mehring, *Eur. J. Inorg. Chem.* **2010**, 30, 4763–4769.

[4] R. Garbe, B. Vollmer, B. Neumüller, J. Pebler, K. Dehnicke, *Z. Anorg. Allg. Chem.* **1993**, 619, 271–276.

 Figure 1: Asymmetric unit of **1**.

 Figure 2: On the left the $[\text{Bi}_6\text{O}_4(\text{OH})_4]^{6+}$ cation and on the right one of the $[\text{Bi}(\text{H}_2\text{O})_3([18]\text{crown-6})]^{3+}$ fragment.

Figure 1

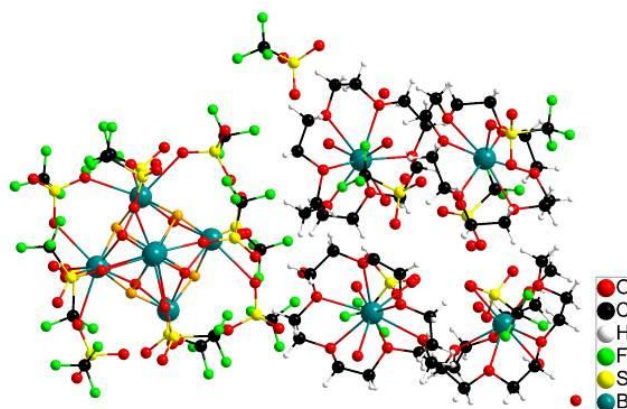
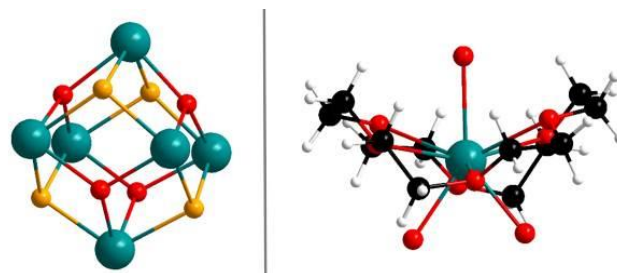


Figure 2


LT1-12
Stabilizing the cubic phase of the triple cation hybrid perovskite $(\text{FA}_{1-x}\text{MA}_x)_{1-y}\text{Cs}_y\text{PbI}_3$

 F. Lehmann^{1,2}, A. Franz¹, S. Schorr^{1,3}
¹Helmholtz-Zentrum Berlin, Berlin, Germany

²Universität Potsdam, Potsdam, Germany

³Freie Universität Berlin, Berlin, Germany

In the last years the research on perovskite based solar cells attracted the research community by its rapid increase in solar conversion efficiencies. Materials as i.e. methyl ammonium lead triiodide (MAPbI_3) and formamidinium lead triiodide (FAPbI_3) are promising candidates for hybrid perovskite absorber layers [1]. A crucial problem hindering the fabrication of these solar cells is the long term stability of hybrid perovskites. Recently, studies about the incorporation of inorganic atoms like Cs^+ or Rb^+ in the crystal structure have shown stabilizing effects on the favorable perovskite phase [2,3].

Hybrid perovskites with the stoichiometry ABX_3 contain an organic unit A [methyl ammonium (MA^+); formamidinium (FA^+), or cesium (Cs^+), B is a metal atom [lead (Pb^{2+})] and X a halide ion [$\text{X} = \text{I}$]. Structural investigations on FAPbI_3 perovskites have shown that it crystallizes either in the cubic space group ($Pm\bar{3}m$), so called α -phase or in the hexagonal space group ($P63mc$), named δ -phase at 293 K [4,5]. Unfortunately, the desired cubic

modification of FAPbI₃ is unstable and transforms to the non-perovskite hexagonal phase, which is not suitable as absorber layer in solar cells.

Our study focuses on stabilizing the high temperature cubic perovskite modification at room temperature by partially substituting FA by MA and Cs. Using X-ray powder diffraction, we systematically studied the triple cation hybrid perovskite (FA_{1-x}MA_x)_{1-y}Cs_yPbI₃ solid solution regarding miscibility and phase stability. We could show that the substitution of $x \geq 0.2$ MA in (FA_{1-x}MA_x)_{1-y}Cs_yPbI₃ hinders the formation of the δ -phase. Furthermore, the maximum solubility of Cs in this solid solution is limited to $x \leq 0.1$.

References

- [1] Saliba et al., *Energy Environ. Sci.* (2016), vol. 9, no. 6, pp. 1989–1997.
- [2] Li et al., *Chem. Mater.* (2016), vol. 28, pp. 284–292.
- [3] Saliba et al., *Science* (2016), vol. 354, pp. 206–209.
- [4] C. Stoumpos, C. D. Malliakas, and M. G. Kanatzidis, *Inorg. Chem.* (2013), vol. 52, no. 15, pp. 9019–9038.
- [5] T. Weller, O. J. Weber, J. M. Frost, and A. Walsh, *J. Phys. Chem. Lett.* (2015), vol. 6, pp. 3209–3212.

LT1-13

Quantitative analysis of electron diffraction patterns from scroll nanotubes

A. Khadiev^{1,2}, Z. Khalitov³

¹DESY, In-situ and nano X-ray diffraction beamline at PETRA III, Hamburg, Germany

²DESY, Hamburg, Germany

³Kazan National Research Technical University named after A.N. Tupolev-KAI, Shared Equipment Center ‘Applied Nanotechnology’, Kazan, Russian Federation

In the past few decades, nanotubes with scroll structure have notably attracted researchers' attention. Interest is mainly driven by their small dimensions, unique topology, represented by a layer rolled into a spiral structure, and other useful and remarkable properties that make them a potential material for future electronic, nanomechanic, nanofluidic and energy-storage devices.

Dimensions and chirality of the nanotubes drastically affect properties of nanotube-based devices and, therefore, the metrology issues play an important role in further development of SNT research and applications. Transmission electron microscopy (TEM) and selected area electron diffraction (SAED) are the most accurate methods for determining basic structural parameters of the single nanotube. Precise analysis of scroll nanotubes (SNT) SAED patterns requires quantitative theory of diffraction which is based on the exact structural models¹ describing arrangement of the atoms in the SNT.

Here we would like to present the quantitative theory of Fraunhofer diffraction based on kinematical approach of cylindrical SNT with Archimedean spiral structure². Analysis of diffraction amplitude allowed us to define diffraction crystallography formulas that govern relations between direct and reciprocal space of SNT. Method based on that formulas can be used for analysis of all basic parameters, as a , b , d , chiral angle (ϵ_c) of SNT from SAED patterns.

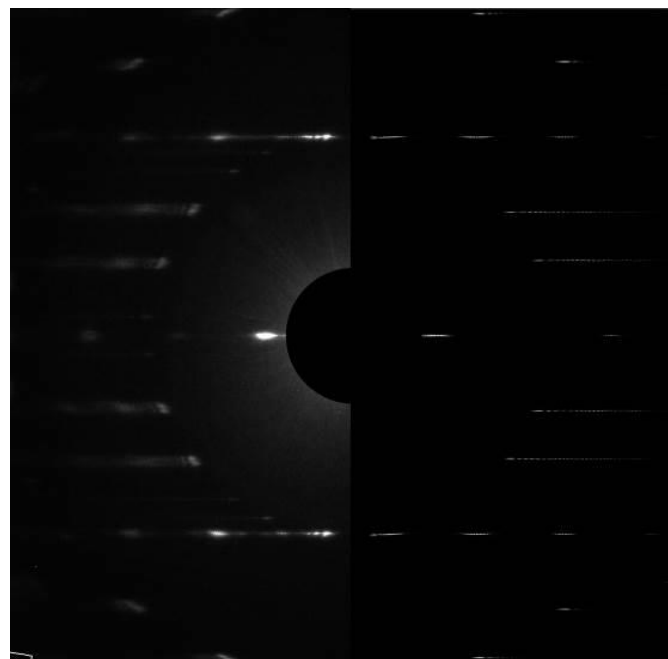
To illustrate proposed method, we perform analysis of SAED patterns and conventional TEM images of WS₂ nanotubes, which were kindly given by Professor R. Tenne's group (Weizmann Institute of Science, Israel). For the case of WS₂ SNT the proposed method reduces the procedural error of a chiral angle determination

by 2 – 2.5 times and cone angle calculation up to 3 times compared to current approaches. Comparative studies of calculated and experimental diffraction patterns showed good agreement between proposed models and real nanotubes (Fig. 1).

Figure 1. The comparison of the experimental (left side of the picture) and calculated (right side of the picture) diffraction patterns of the WS₂ SNT.

- [1] Khalitov, Z., Khadiev, A., Valeeva, D. & Pashin, D. Structure of ordered coaxial and scroll nanotubes: general approach. *Acta Crystallogr. Sect. A Found. Adv.* **72**, 36–49 (2016).
- [2] Khadiev, A. & Khalitov, Z. Quantitative theory of diffraction by cylindrical scroll nanotubes. *Acta Crystallogr. Sect. A Found. Adv.* **74**, 233–244 (2018).

Figure 1



LT1-15

Pressure induced phase transitions of dwornikite

M. Ende¹, T. Kirkkala², M. Lötzenbauer¹, D. Talla¹, R. Miletich¹, M. Wildner¹

¹Universität Wien, Institut für Mineralogie und Kristallographie, Wien, Austria

²University of Jyväskylä, Department of Chemistry, Jyväskylä, Finland

Dwornikite (NiSO₄·H₂O) is an isotypic mineral of kieserite (MgSO₄·H₂O). As sulphates significantly influence melting equilibria on the icy moons of Saturn and Jupiter, possibly leading to subsurface oceans and cryovolcanism [1, 2], their investigation in our solar system receives growing attention [e.g. 3]. For this reason, knowledge of the high-pressure behaviour of respective mineral phases seems to be crucial to consolidate our insight of the internal structure of icy satellites. Although the high-pressure behaviour of sulphate minerals in higher hydration stages have already been subjected to numerous studies, the compression data for the low-hydrogenated phases are still limited.

The objective of this study was to investigate synthetic single crystals by means of in-situ high-pressure X-ray diffraction and Raman spectroscopy at RT using an ETH-type diamond-anvil cell. The investigated hydrostatic pressure reached about 10 GPa.

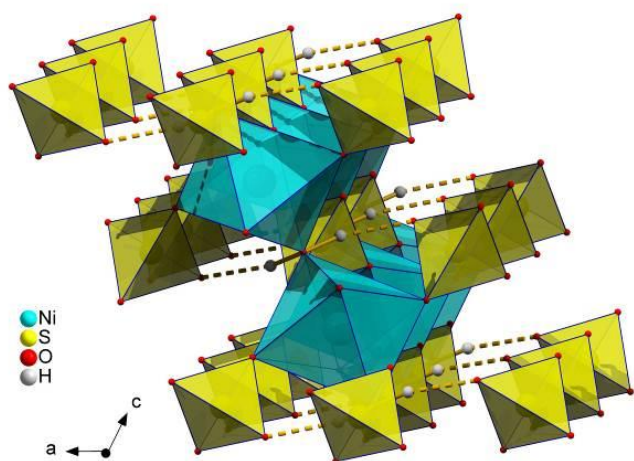
We hereby present first results on structural and lattice parameter changes as well as Raman band shifts revealing two structural phase transitions during the pressure increase. The subsequent crystal-structure investigations at high-pressure conditions revealed that dwornikite undergoes a compression-induced change of symmetry from monoclinic (Fig. 1) to a triclinic high-pressure polymorph, associated with a structural phase transition around 2.3 GPa. The space group seems to change directly from $C2/c$ (No. 15) into $P-1$ (No. 2). For a second discontinuity around 6 GPa it just can be speculated (at the moment) that the H_2O -molecule is breaking the $P-1$ space group symmetry, although the Raman spectra ($100 - 1200\text{ cm}^{-1}$) show no band splitting before the non-hydrostatic pressure region.

Fig. 1: Section of the crystal structure of monoclinic dwornikite ($NiSO_4 \cdot H_2O$).

References

- [1] Kargel, J. S. (1991): *Icarus*, 94, 368-390.
 [2] McCord, T. B., Hansen, G. B., Hibbits, C. A. (2001): *Science*, 292, 1523-1525.
 [3] Wang, A., Freeman, J.J., Jolliff, B.L. (2009): *J. Geophys. Res.*, 114, E04010.

Figure 1



LT1-16

Structure Analyses of Zeolite-Sorbate Systems

V. Stock¹, B. Marler¹

¹Ruhr-Universität Bochum, Geology, Mineralogy and Geophysics, Bochum, Germany

Halogenated hydrocarbons which contaminate water and air are associated with significant environmental problems. Microporous silicates (zeolites) are an effective material to reduce the pollution by selectively adsorbing the organic molecules from various mixtures.

To further investigate the uptake of halogenated hydrocarbons into the pore system of zeolites, the zeolites Silica-ZSM-22 and Silica-ZSM-23 loaded with 1-chlorobutane, 1,4-dichlorbutane or 1-chloropentane were analyzed (the hydrocarbon n-hexane was used for comparison). Both zeolites possess an one-dimensional channel-systems with straight 10-Ring channels. The unit cell dimension along the channel direction is ca. 5.05 \AA . The selected sorbates are unbranched linear molecules with a length of ca. 10 \AA . It was speculated that the sorbed molecules might generate a

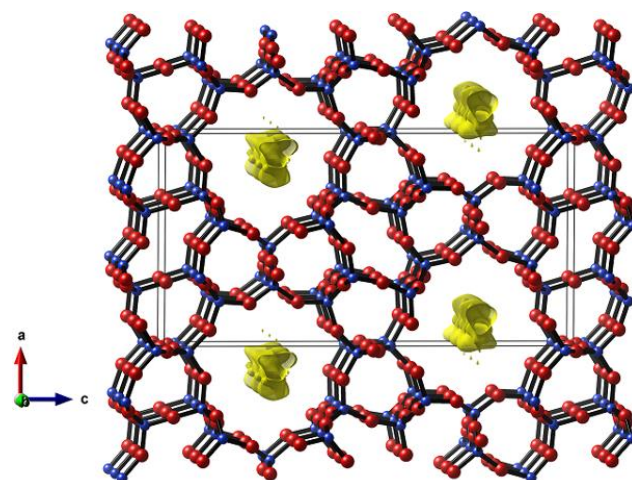
completely ordered (super)structure. The samples were analysed by x-ray powder diffraction (samples kept in sealed glass capillaries), infrared spectroscopy and thermal analysis.

The Rietveld analyses showed that the

- type of zeolite has a substantial effect on the amount of halogenated hydrocarbons being adsorbed. In spite of identical composition (pure SiO_2) and very similar structures, silica-ZSM-23 takes up about twice as much as silica-ZSM-22;
- amount of halogenated hydrocarbons being adsorbed also depends on the polarity of the molecule: the lower the polarity the higher the quantity adsorbed (dichlorbutane => chloropentane/ chlorobutane => n-hexane);
- loading of the zeolites (periodicity along the channel direction: ca. 5.05 \AA) with molecules of a length of ca. 10 \AA did not form a superstructure;
- electron density maxima in the channel-like pores were of similar height, indicating that the chlorine atoms of the molecules did not take up a specific adsorption site (Fig. 1);
- electron density maxima were evenly distributed along the channel without any gap which indicates that the molecules are disordered along the channel extension.

Fig. 1: The structure of ZSM-23 seen along [010] with positive difference electron density representing the disordered molecule (at center of the pore).

Figure 1



LT1-17

Crystal growth, crystal structure, and optical characterization of $CsMTiO_4$ ($M = Al, Fe$ and Ga) crystals with fourfold coordinated titanium Ti^{4+}

J. D. Groeneveld¹, M. Burianek¹, L. Fischer², R. D. Shannon³, R. X. Fischer¹

¹Universität Bremen, Fachbereich Geowissenschaften, Bremen, Germany

²Albert-Ludwigs-Universität Freiburg, Institute of Earth and Environmental Sciences, Geochemistry, Freiburg i.Br, Germany

³University of Colorado, Geological Science/ CIRES, Boulder, United States

Electronic polarizabilities allow the prediction of mean refractive indices of minerals and inorganic compounds using the sum of electronic polarizabilities of ions [1] according to the chemical

composition. In this work the empirical electronic polarizability of tetrahedrally coordinated Ti^{4+} was determined.

Three different crystals containing $^{47}\text{Ti}^{4+}$ were investigated representing three different forms of CsMTiO_4 ($M = \text{Al, Fe, Ga}$) with ABW zeolite structure type. Crystal growth was carried out via a solid-state growth in a sealed platinum tube for CsAlTiO_4 [2] and by growth from the melt for CsFeTiO_4 and CsGaTiO_4 . The refractive indices were measured using the immersion method on a spindle stage with internal refractometer mounted on a petrographic microscope. It was possible to determine the refractive indices for CsAlTiO_4 ($n_X = 1.7160$ (49), $n_Y = 1.724$ (4), $n_Z = 1.7257$ (22)), CsGaTiO_4 ($n_X = 1.7512$ (26), $n_Y = 1.773$ (3), $n_Z = 1.7768$ (23)). Crystal structure and chemical investigations were carried out by single crystal and powder-diffraction methods and electron-microprobe analysis.

From initial measurements we get an electronic polarizability $\alpha = 5.15 \text{ \AA}^3$ for Ti in four-coordination as preliminary result, compared with $\alpha = 5.01 \text{ \AA}^3$ for Ti in six-coordination [1].

We thank the DFG for funding (Fl442/21-2)

References

- [1] Shannon, R. D. and Fischer, R. X., *American Mineralogist* 101, 2016, 2288
- [2] Gatehouse, B. M., *Acta Crystallographica*, C45, 1989, 1674

Young Crystallographers: Lightning talks II

LT2-01

Prediction of Phase Transitions by Data Mining via temperature-dependent Force Fields

 D. W. M. Hofmann^{1,2}
¹CRS4, Modeling & Simulation, Pula, Italy

²FlexCryst, Uttenreuth, Germany

Modern force fields are accurate enough to describe thermal effects in molecular crystals. We applied the recently developed temperature-dependent force field (1) to predict the transition temperature for polymorphs. An estimation of the transition temperature of paracetamol demonstrated the possibility for prediction using the temperature-dependent force-fields.

The earlier approach of force fields for finite temperatures (2) is extended to a force field with a continuous function for the temperature. Each atom pair potential is developed as Taylor series of $1/r^3$. The Pauli repulsion is extended by a temperature dependency: $1/r^{12} \rightarrow (1+\alpha)/r^{12}$. For the parametrization of the force field we used Data Mining on experimental structures (3) with the temperature as an additional descriptor. The parameters of the model have been obtained by training on 21,095 experimental crystal structures for hydrogen bonds in oxygen and nitrogen compounds.

The force field is validated for the prediction of crystal density, temperature density gradients and transition temperature. The crystal density prediction was validated by minimization of all non-ambient crystal structures available in The Cambridge Structure Database. The mean error is halved by taking the temperature into account. We estimated the thermal density gradients of several organic crystals with experimental data of one substance at various temperatures. The error of the predictions varied from 0 to 29 %. Finally, a prediction of the transition temperature of paracetamol demonstrated the prediction of phase transitions.

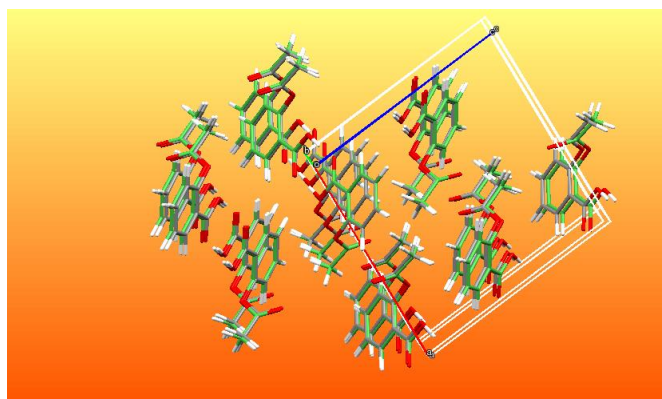
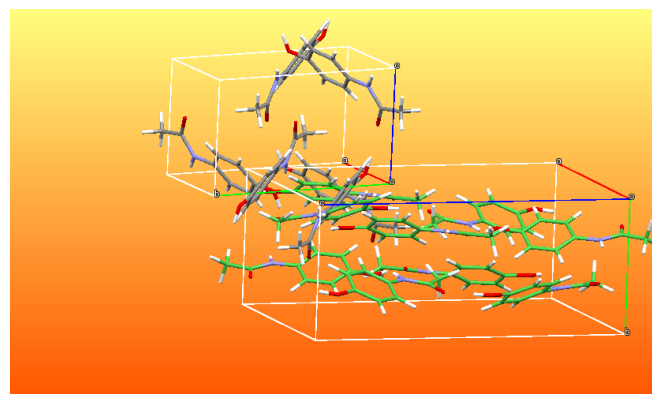
[1] DWM Hofmann, LN Kuleshova, *Chemical Physics Letters* 699, 115-124, 2018.

[2] DWM Hofmann, LN Kuleshova, *Crystal Growth & Design* 14 (8), 3929-3934, 2014

[3] DWM Hofmann, LN Kuleshova, eds. *Data mining in crystallography*. Vol. 134. Springer, 2009.

Figure 1: The expansion of aspirin caused by temperature.

Figure 2: The polymorphism of paracetamol caused by temperature.

Figure 1

Figure 2


LT2-02

Interactions in a two-dimensional Ag^I coordination polymer

 S. van Terwingen¹, U. Englert¹
¹RWTH Aachen University, Institute of Inorganic Chemistry, Aachen, Germany

One of the most important tasks for modern research is to counteract climate change. Global warming is promoted by a variety of greenhouse gases. Therefore, many catalysts have been developed to decompose the latter. Englert and co-workers have reported a highly active Ag/Yb₂O₃ catalyst to decompose nitrous oxide, N₂O.^[1] The catalyst was derived from a bimetallic metal-organic framework (MOF) with the organic linker 3-cyanoacetylacetone. Unfortunately, the costly syntheses towards the MOF drives this system uneconomical.

To prepare similar systems with industrial relevance cheaper ligands have to be investigated. We use 3-(2-(4-pyridyl)ethyl)acetylacetone (HacacPyen) in which the acetylacetone moiety is connected to a pyridyl moiety through an ethyl bridge. Reacting the latter with AgPF₆ leads to a 2D coordination polymer with interesting interactions.

The target compound [Ag(HacacPyen)₂]PF₆ shows considerable intermolecular interactions. Interestingly, two [Ag(HacacPyen)₂]⁺ moieties approach each other and subtend an Ag–Ag distance of 3.2130(6) Å, shorter than the sum of the van der Waals radii of Ag. This contact can be interpreted as an argentophilic interaction.^[2] Furthermore, the acetylacetone moieties of the {[Ag(HacacPyen)₂]PF₆}₂ binuclear species thus formed show a distinct diketo behavior. The two keto groups of one acetylacetone moiety point towards a Ag^I ion of another {[Ag(HacacPyen)₂]PF₆}₂ group. The distances are rather long for Ag–O bonds (2.806(3) Å and 2.915(3) Å).^[3] Nevertheless, they stabilize the packing and connect the binuclear species to form a two-dimensional MOF.

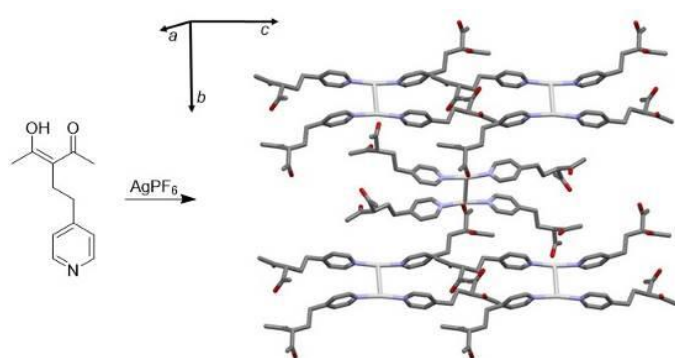
Figure 1: Reaction scheme to form the 2D MOF. PF₆[−] ions are omitted for clarity.

[1] M. Konkol, M. Kondracka, P. Kowalik, W. Próchniak, K. Michalska, A. Schwedt, C. Merckens, U. Englert, *Appl. Catal., B* **2016**, *190*, 85–92.

[2] H. Schmidbaur, A. Schier, *Angew. Chem.* **2015**, *127*, 756–797.

[3] A. D. Burrows, K. Cassar, M. F. Mahon, J. E. Warren, *Dalton. Trans.* **2007**, 2499–2509.

Figure 1



LT2-03

In-situ XRD study on the crystallization of thin HfO₂ films

Z. Balogh-Michels^{1,2}, T. Gischkat¹, I. Stevanovic¹, A. Bächli¹, A. Neels²

¹Rhysearch, Department of Optical Coatings, Buchs SG, Switzerland

²Empa, Department of X-ray Analytics, Dübendorf, Switzerland

Introduction

High end laser optics are often made of ion beam sputtered (IBS) dense, amorphous HfO₂/SiO₂ layers [1]. For high reflection low loss application crystalline layers are advantageous due to reduced Brownian loss [2,3]. Recrystallization of amorphous IBS layers is desirable for industrial scale applications as it is more productive than e.g. molecular beam epitaxy.

Objectives

We present our results on the crystallization of amorphous HfO₂ films on 0001 SiO₂. We deposited 10 and 20 nm thick a-HfO₂ films by a Veeco Spector DIBS instrument. We observed the crystallization in-situ by a Bruker D8 Discover DaVinci XRD machine equipped with an Anton Paar DHS1100 stage. Since we expected polycrystalline films, we used the grazing incidence mode to observe the crystallization.

Results

The 10 nm film underwent two phase transitions. At 700 °C the 111 peak of the cubic HfO₂ appeared. Increasing the temperature to 1000 °C this peak was replaced by the 111 of the monoclinic HfO₂. For the 20 nm film rapid crystallization was observed already at 650 °C and the crystallization was fast at 600 °C. Biswas et al. reported similar thickness dependent crystallization temperature for HfO₂ on Si [4]. At 570 °C the crystallization took 25 minutes and followed parabolic kinetic. This suggests that the long-range atomic transport plays a role on the crystallization.

Conclusions

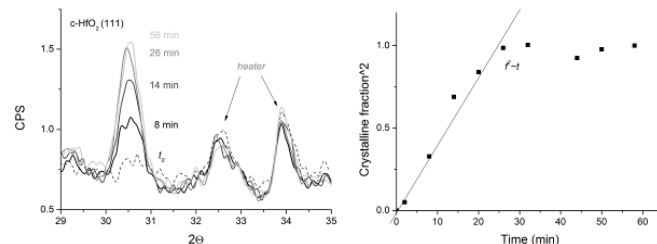
We found that the crystallization temperature depends on the layer thickness. The kinetics of the crystallizations follows a parabolic law, which indicates that long-range atomic transport takes a role in the crystallization.

References

- [1] M. Alvisi et al., *Thin Solid Films*, 358 (2000) 250
- [2] G.D. Cole et al., *Optica*, 3 (2016) 647
- [3] M. Marchio et al., *Opt. Express*, 26 (2018) 6114
- [4] D. Biswas et al., *J. Vacuum Sci. Technol. B*, 34 (2016) 022201

Fig. 1: growth of the HfO₂ peak and the crystalline fraction as a function of the time. The 56 min stage was considered as crystalline.

Figure 1



LT2-04

Site-symmetry method applied for the study of layer and multilayer materials by the Bilbao Crystallographic Server

G. de la Flor¹, D. Orobengoa¹, Y. Kitaev², R. Evarestov³, E. Tasci⁴, M. Aroyo¹

¹University of the Basque Country UPV/EHU, Departamento Física de la Materia Condensada., Bilbao, Spain

²Ioffe Institute, Laboratory of Quantum-size Hierostructures, Saint Petersburg, Russian Federation

³St. Petersburg State University, Institute of Chemistry, Saint Petersburg, Russian Federation

⁴Hacettepe University, Department Physics Engineer, Ankara, Turkey

Introduction

The *Bilbao Crystallographic Server* (www.cryst.ehu.es) [1-2] is a free web server that grants access to crystallographic databases and tools for the resolution of different types of crystallographic, structural chemistry and solid-state physics problems. In the server, there is a section exclusively dedicated to *Subperiodic groups: Layer, Rod and Frieze Groups* which contains the basic crystallographic information and the Brillouin-zone and **k**-vectors tables for the 80 layer groups.

Objectives

The purpose of this contribution is to report on the current state of the tools available on the *Bilbao Crystallographic Server* for the study of materials with layer symmetry, emphasizing on the recently developed program LSITESYM which can be used to describe the electronic structure and surface states of crystals.

Results

The program LSITESYM is based on the *site-symmetry approach* [3] which connects local properties of atoms in crystals with the symmetry of states of the whole crystalline system, *i.e.* it establishes the symmetry relation between the localized states in the crystal (vibrations of atoms and atomic orbitals) and crystal extended states (phonon, electrons, etc.) over the entire Brillouin zone. LSITESYM calculates the site-symmetry induced representations of layer groups which can be applied to analyze the symmetry of the phonon, electron, exciton and biexcitons states in layered and multilayered crystals. Moreover, this procedure also allows the study phase transitions.

Conclusions

The *Bilbao Crystallographic Server* is in constant improvement and development, offering free of charge tools to study an increasingly number of crystallographic systems.

- [1] M. I. Aroyo et al. (2006) *Z. Kristallog.*, **221**, 15-27
- [2] M. I. Aroyo et al. (2011) *Bulgarian Chemical Communications*, 43(2), 183-197
- [3] A. Evarestov and V. P. Smirnov, *Site Symmetry in Crystals. Theory and Applications*, 2nd ed. Springer, 1997.

LT2-05

Crystal structure and de- and rehydration behavior of two new chloride-containing Zeolitic Imidazolate Frameworks

G. Gallo¹, S. Glante², S. Bette¹, M. Hartmann², R. E. Dinnebier¹

¹Max Planck Institut für Festkörperforschung, Stuttgart, Germany

²Friedrich-Alexander-Universität Erlangen-Nürnberg, Erlangen Catalysis Resource Center, Erlangen, Germany

Introduction

Zeolitic imidazolate frameworks (ZIFs) are a large subgroup of metal-organic frameworks (MOFs) whose structures resemble those of the zeolites for the coordination of the central atom (e.g. zinc, cobalt) and for the angle with the imidazolate linkers. In this work, the structure of an unknown hydrated ZIF compound with methylimidazolate and chloride as ligands, $Zn_3(mim)_5ClH_2O \cdot xH_2O$ with $x=0.74$ (**1**), was revealed. The study of its thermal behavior led also to the identification of a new anhydrous structure, $Zn_3(mim)_5Cl$ (**2**). Eventually, the two structures turned out to be interconvertible by hydration/dehydration processes (Fig1,b).

Objectives

Since no single crystals suitable for X-ray structure determination were available, X-ray powder diffraction (XRPD) was used for *ab initio* structure determination of **1** and **2**. The complex dehydration behaviour of **1** was studied by temperature and moisture dependent *in situ* XRPD measurements as well as by TG-DTA analysis.

Results

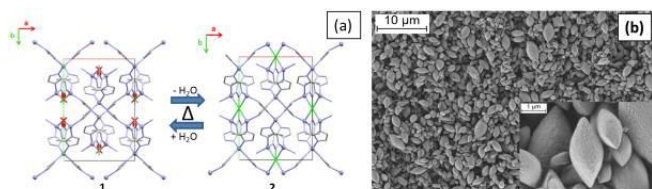
The structure of **1**, with an unusual zeppelin like morphology (Fig1,b), shows two distinct tetrahedrally coordinated zinc sites: one is exclusively coordinated by methylimidazolate ions while the other site exhibits three methylimidazolates and a chloride ion which is occupationally disordered with a water molecule in the coordination sphere. Voids in the zinc methylimidazolate framework are filled by non-coordinated water molecules. Upon heating, at first non-coordinated and subsequently coordinated water molecules are released and the chloride bridges two zinc ions forming the compound **2**.

Conclusions

The use of XRPD revealed the first ZIF compounds where chloride and water act as linkers whereas *in situ* XRPD and TG-DTA analysis allowed to gain an insight of the thermal behavior of **1**. The reversibility of **2** creates perspectives for possible application as sensor or catalysis material.

Fig1.(a) Projections of the crystal structures of **1** and **2** along *c* axis,(b) Zeppelin-like crystallites of **1**.

Figure 1



LT2-06

Automated orientation imaging and phase mapping in the TEM: prospects for reliable detection of martensite in steels

J. Werner¹, T. E. Weirich¹

¹Central Facility for Electron Microscopy, Aachen, Germany

A commercially available system for area recording of spot diffraction patterns (ASTAR, NanoMEGAS SPRL) was employed within a systematic study to analyse the tetragonal lattice distortion of martensite with different amounts of carbon [2, 1].

For testing the sensitivity of the automated indexing software, a series of martensite spot diffraction patterns (SDPs) were simulated for the zone axis $\langle 010 \rangle$, $\langle 011 \rangle$, $\langle 110 \rangle$ and $\langle 111 \rangle$ assuming carbon contents between 0.5 to 2 wt-% C. Subsequent analysis by the ASTAR system provided indexing reliability value RP that can be used to distinguish between the closely related structures of martensite and ferrite. Hence the number of the obtained correct lattice matches and the maximum observable RP value was determined for each SDP orientation using an effective camera length (CL) of 176 mm, whereby the CL corresponds to the actual measurement conditions on the small viewing screen in a FEI Tecnai F20 transmission electron microscope.

The present study shows that the actual measuring conditions in a FEI Tecnai F20 are not sufficient for reliable separation between bcc ferrite and tetragonal martensite since this requires RP values of at least 15 %. However, the performed simulations show that significant improvement of the RP values can be obtained by using larger detector areas and increasing the camera length.

References:

- [1] Roberts C S 1953 in: Journal of Metals, P. 203 – 204
- [2] Moeck et al. 2011 in: Crystal Research and Technology, Volume 46,P. 589 – 606

LT2-07

Defect Characterization of 4H-SiC with Synchrotron White Beam X-ray Topography and High Resolution X-ray Diffractometry

M. Roder¹, P. Wellmann², M. Arzig², J. Steiner², A. Danilewsky¹

¹Albert-Ludwigs-Universität Freiburg, Crystallography, Freiburg, Germany

²Friedrich-Alexander-Universität Erlangen-Nürnberg, Material Department 6 (i-meet), Erlangen, Germany

SiC is a semiconductor which finds its application mainly in power electronics and shows a high variety of different defect types, like Micropipes (MPs), Threading Screw Dislocations (TSDs), Threading Edge Dislocations (TEDs), Basal Plane Dislocations (BPDs) and so on. Over the years, the crystal quality could be improved but still needs optimization. Several SiC wafers grown by Physical Vapor Transport [1] at different conditions were characterized with different X-ray methods. Synchrotron White Beam X-ray Topography (SWXRT) in back-reflection geometry was used to determine defect types. The dominating defect types include TSDs, TEDs and MPs in different defect densities [2]. Additionally full wafer mappings in transmission geometry were recorded to get an impression of the defect densities on different wafer regions. The mappings showed a clear lineation of small-angle grain boundaries in direction of the wafer's misorientation. High Resolution X-ray Diffractometry measurements were performed at positions at which also SWXRT measurements were performed. Rocking curves were recorded in 0004 reflection, which show a difference in their curve shape and full-width at half maximum (FWHM) depending on the crystal quality. Reciprocal Space maps were recorded at the same positions in the same reflection. Depending on the dominant defect type in the measured

area the relation of crystal lattice strain to crystal lattice tilt changes. A higher density of SDs and small-angle grain boundaries induces more tilt. The results of all measurements showed a high defect density in the wafer but inhomogeneously distributed, which points to an unequal temperature distribution vertically and horizontally during growth.

- [1] Wellmann, P., Neubauer, G., Fahlbusch, L., Salamon, M., Uhlmann, N. *Crys. Res. & Technol.*, 50(1):2-9, 2015
 [2] F Dudley, W Huang, S Wang, JA Powell, P Neudeck, and C Fazi., *J. Appl. Phys. D: A. Phys.*, 28(4A):A56, 1995.

LT2-08

Solving structures with native SAD on laboratory X-ray sources

A. Förster¹, C. Schulze-Briese¹, C. Klein²
¹DECTRIS Ltd., Baden-Dättwil, Switzerland
²marXperts, Norderstedt, Germany

Introduction

The solving of macromolecular structures by intrinsic anomalous signal (native SAD) critically depends on the accuracy of the diffraction data. Radiation damage, all but unavoidable at modern synchrotrons, quickly makes the observed anomalous differences unreliable. While ways exist to mitigate damage at synchrotrons, it can also be tackled at the source.

Objectives

We aim to show that laboratory X-ray sources with their limited flux in combination with noise-free photon counting detectors are excellent environments for solving crystal structures by experimental phasing.

Results

In a first set of experiments performed with a microfocus Cu source, we show how accurate anomalous data can be collected from native crystals even at room temperature with doses as low as 30 kGy. Not only does this result in structures of macromolecules as close to their physiological state as crystallography can provide, it also increases throughput in the laboratory by eliminating the time-consuming screening of cryo-conditions.

Next, we show that intrinsic anomalous signal sufficient for structure determination can be detected even in data collected with a Ga source. Thanks to the shorter wavelength of the Ga radiation, datasets complete to 1.2 Å can be collected in a single sweep while accurately measuring the anomalous differences between low-resolution Bijvoet pairs.

Conclusion

A modern laboratory diffractometer with round-the-clock availability powerfully complements synchrotron facilities. After simple upgrades from image plates or CCDs to photon counting detectors, such as PILATUS and EIGER, data of the highest accuracy can be collected, which makes phasing of native macromolecular crystals routinely possible.

LT2-09

Size-dependent structural, spectroscopic and thermoanalytic properties of nano- to poly-crystalline Bi₂Fe₄O₉

A. Kirsch^{1,2}, M. M. Murshed^{1,2}, F. J. Litterst³, T. M. Gesing^{1,2}

¹Universität Bremen, Institut für Anorganische Chemie und Kristallographie, Bremen, Germany

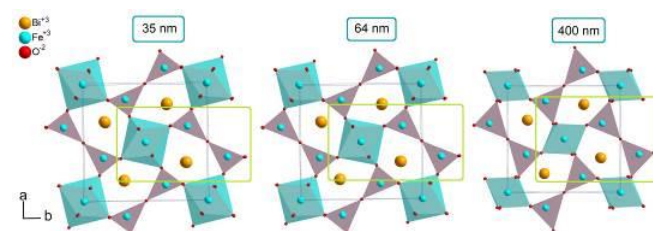
²Universität Bremen, MAPEX Center for Materials and Processes, Bremen, Germany

³Technische Universität Braunschweig, Institute for Condensed Matter Physics, Braunschweig, Germany

The size-dependent physical properties of a given material in the nano-regime are frequently studied. However, simultaneous investigations on the associated structural and spectroscopic features are rare. Using *ex-situ* as well as *in-situ* techniques, we carefully investigated the crystallite size-dependent structural features of mullite-type Bi₂Fe₄O₉ from nano-crystalline (NC) to poly-crystalline (PC, bulk) material. The formation of PC Bi₂Fe₄O₉ from a quantum-crystalline (QC, X-ray amorphous) precursor was monitored by using temperature-dependent X-ray powder diffraction (XRPD). A sol-gel based method was used to produce a QC precursor. Twelve samples with different crystallite sizes from 35.3(4) nm to 401(17) nm were controlled by heating the precursor for 2 h between 900 K and 1073 K. XRPD data Rietveld refinements, UV/Vis, infrared, Raman and ⁵⁷Fe Mössbauer spectroscopies, and differential scanning calorimetry clearly distinguished the crystal-physical properties of Bi₂Fe₄O₉ below and above a critical average crystallite size of 122(2) nm. The significant changes of the lattice parameters below this critical size were explained in terms of strong polyhedral distortions, which played roles in changing the local spin orientations, as evidenced by ⁵⁷Fe Mössbauer spectroscopy. In addition, the change of the antiferromagnetic transition of Bi₂Fe₄O₉ was followed by DSC measurements; a strong decrease in transition enthalpy was observed below the critical average crystallite size.

Figure 1. Visualization of polyhedral distortions in Bi₂Fe₄O₉ with average crystallite sizes of 35 nm and 64 nm compared to 400 nm (bulk).

Figure 1



LT2-10

New concepts for single-crystal sapphire cells to study solid-gas reactions via *in situ* neutron scattering

R. Finger¹, H. Kohlmann¹

¹Universität Leipzig, Inorganic Chemistry, Leipzig, Germany

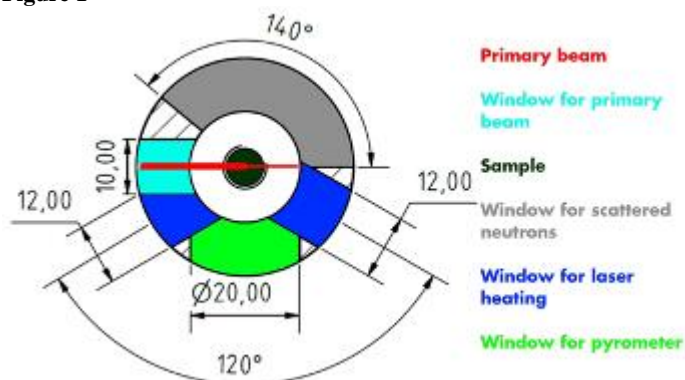
Solid-gas reactions get high attention due to far-reaching applications, e. g. in the synthesis of functional materials or in catalysis. *In situ* investigations offer an insight into the pathways of such reactions. Elevated temperatures and pressures demand a specially designed sample environment, which has to be inert against all reactants and fulfil the requirements of the chosen investigation technique. For neutron powder diffraction a sapphire single crystal cell, based on an idea of Rondinone [1], with a 360° free optical access was developed [2].

Further developments aim at reducing diffraction background and tensions in the sapphire crystal. They led to a holder made of stainless steel with an opening for primary and diffracted beams, for a pyrometer and two for the laser beams used for heating (Fig. 1). To prevent parasitic reflections and the activation of the stainless steel, a neutron absorbing tarnish is used. This cell offers a better mechanic stability and reduces mechanical tension in the sapphire single crystal as compared to a previous design [2] by avoiding double-sided pressing at the flanges. The neutron absorbing tarnish of the cell reduces the background of measurements by absorbing neutrons being scattered outside of the sample volume.

Figure 1: Sectional view of the gas pressure cell in the diffraction plane

- [1] A. J. Rondinone, C. Y. Jones, S. L. Marshall, B. C. Chakoumakos, C. J. Rawn, E. Lara-Curizo, *Can. J. Phys.* **2003**, *81*, 381-385
 [2] A. Götze, H. Auer, R. Finger, T. C. Hansen, H. Kohlmann, *Phys. B (Amsterdam, Neth.)* **2018**, *551*, 395-400

Figure 1



LT2-11

Local magnetic properties and couplings of $\text{Co}_{2-x}\text{Mn}_x\text{B}$: A ^{59}Co and ^{55}Mn zero field NMR study

P. Fritsch¹, F. Hammerath¹, S. Ener², M. Fries², I. Opahle², E. Simon^{2,3}, S. Wurmehl^{1,4}, H. Zhang³, O. Gutfleisch^{3,5}

¹IFW Leibniz Institute for Solid State and Materials Research Dresden, Dresden, Germany

²Budapest University of Technology and Economics, Department of Theoretical Physics, Budapest, Hungary

³Technische Universität Darmstadt, Department of Material Science, Darmstadt, Germany

⁴Technische Universität Dresden, Institute for Solid State Physics, Dresden, Germany

⁵Fraunhofer-Projektgruppe für Wertstoffkreisläufe und Ressourcenstrategie IWKS, Hanau, Germany

Co_2B and its substitution variants show a magnetovolume effect around its Curie Temperature T_c , which is promising for magnetocaloric applications and the generation of thermomagnetic power. The criticality of Co within the EU gives motivation to substitute Co with other, cheaper and less critical elements such as Mn. A series of $\text{Co}_{2-x}\text{Mn}_x\text{B}$ alloys was synthesized. Single phase behaviour with no symmetry change is shown up to $x = 0.8$ by powder. Within the substitution series $0 > x > 0.8$ the macroscopic magnetic properties were investigated. The results expose an anomalous behaviour of spontaneous magnetization and T_c with increasing Mn content as a result of competing exchange interactions. Zero field Nuclear Magnetic Resonance spectroscopy (NMR) was measured for ^{59}Co and ^{55}Mn nuclei to determine the element specific magnetic moments supported by density

functional theory (DFT) calculations. A mutual combination of experimental and theoretical methods reveals that the observed anomaly originates in complex magnetic coupling, as shown by the exchange interactions.

S. Ener et al., Magnetic and magnetocaloric properties of the $\text{Co}_{2-x}\text{Mn}_x\text{B}$ system by experiment and density functional theory, *Acta Materialia* **165**, 2019, 270-277.

LT2-13

Symmetry lowering on heating

M. Krzhizhanovskaya¹, R. Bubnova^{1,2}, S. Filatov¹

¹St. Petersburg State University, Dept. Crystallography, Institute of Earth Sciences, St.Petersburg, Russian Federation

²Russian Academy of Sciences, Institute of Silicate Chemistry, St. Petersburg, Russian Federation

Polymorphism is a common phenomenon for both organic and inorganic compounds. Usually the symmetry of a substance increases on heating. Over the last 20 years we have performed more than a 500 experimental studies of thermal behavior of different compounds by *in-situ* high-temperature powder X-ray diffraction (HTPXRD). Apparently among the oxygen inorganic compounds the cases of symmetry lowering on heating are still very rare. Studying for instance the thermal behavior of about 100 borates, silicates and borosilicates on heating, we found about 30 "usual" cases of symmetry increasing and only three examples of reducing the symmetry.

According to HTPXRD the cubic ANA-type boroleucite, KBSi_2O_6 , undergoes reversible transformations at higher temperatures $I-43d \leftrightarrow$ (at 300 °C) $P2_1/a \leftrightarrow$ (at 550 °C) $\leftrightarrow Ia-3d$ [1].

Crystal structures of γ -, β - and α - $\text{Sr}_2\text{B}_2\text{O}_5$ polymorphs resulting from the $\gamma \leftrightarrow$ (at 292 °C) $\beta \leftrightarrow$ (at 364 °C) $\alpha' \leftrightarrow$ (at 378 °C) α sequence of reversible first-order phase transitions are studied by HT single-crystal X-ray diffraction and HTPXRD [2]. The sequence of phase transitions is associated with an unusual change of symmetry, with triclinic intermediate β - $\text{Sr}_2\text{B}_2\text{O}_5$ phase and monoclinic LT γ - $\text{Sr}_2\text{B}_2\text{O}_5$ as well as HT α - $\text{Sr}_2\text{B}_2\text{O}_5$ phase.

Synthetic okayamalite, $\text{Ca}_2\text{B}_2\text{SiO}_7$, undergoes reversible polymorphic transition at about 550 °C with the decrease in symmetry from tetragonal to orthorhombic [3]. The crystal structure of HT modification was solved from the powder data (900 °C, $P2_12_12$, $R_{\text{Bragg}} = 2.7\%$).

In present study our high-temperature studies and literature data are briefly reviewed from the point of view of phenomenon of symmetry lowering on heating.

The study was supported by the Russian Foundation of Basic Research No. 17-03-00887. XRD measurements were performed in the Research Center for XRD studies of St. Petersburg State University.

[1] M.G. Krzhizhanovskaya et al., *Eur. J. Mineral.* **28** (2016) 15.

[2] S.N. Volkov et al. *Acta Cryst.* **B73** (2017) 1056.

[3] M.G. Krzhizhanovskaya et al. *Phys. Chem. Mineral.* **45** (2018) 463.

LT2-14
Synthesis and crystal structure of new alkali-chalcogenido-manganates/indates A_3MnInQ_4

 M. Langenmaier¹, J. N. Brantl¹, C. Röhr¹
¹Albert-Ludwigs-Universität Freiburg, Institut für Anorganische und Analytische Chemie, Freiburg i. Br., Germany

In the system A -Fe- Q mixed-valent alkali chalcogenido ferrates are well known [1-3], however no analogous manganates were yielded so far [4]. A mixed-valent state was mimicked by a partially replacement of Mn(II) by In(III).

The newly obtained metalates A_3MnInQ_4 (A =Na, K, Rb, Cs; Q =S, Se, Te; for Na only S and Se) are isotypic for the three heavier alkali metals (**4-12**) and crystallize in the $K_3Fe_2S_4$ -type structure [5]. In contrast the Na salts behave differently: Na_3MnInS_4 (**1**) crystallizes in the β - $Ca_3Ga_2N_4$ -type [6] with T_2 supertetrahedra, whereas in $Na_3MnInSe_4$ (**2**) einer-double chains of $[MSe_4]$ tetrahedra are the most prominent feature.

The compounds were obtained by heating stoichiometric mixtures of the elements or binary phases at $T_{max}=1200$ K. The crystals of **4-12** are brittle needles coloured yellow to darkred. In contrast, **1** and **2** form xenomorphic orange crystals. All structures were determined by means of X-ray single crystal diffraction. Mn and In take crystallographically identical positions with a statistically occupation in the ratio 1:1.

The compounds **4-12** crystallize in the space group $Pnma$, with lattice parameters from $a=725.50(2)$, $b=1189.63(3)$ and $c=1148.76(3)$ pm (K_3MnInS_4) to $a=843.79(3)$, $b=1316.35(5)$ and $c=1368.50(5)$ pm ($Cs_3MnInTe_4$). The structure (fig. 1) inhibits ${}^1_{\infty}[MQ_4/2]^{1.5-}$ zig-zag chains running parallel to the b -axis, which consist of edge-sharing tetrahedra (grey fig. 1).

Na_3MnInS_4 crystallizes in $I4_1/acd$ with $a=1324.55(4)$ and $c=1906.94(7)$ pm. The crystal structure shows a three dimensional network of T_2 supertetrahedra ${}^3_{\infty}[M_4S_6S_4/2]^{6-}$ which interpenetrates a second crystallographically identical network of supertetrahedra (grey and golden fig. 2, left)

$Na_3MnInSe_4$ crystallizes in $C2/m$ with $a=1605.50(16)$, $b=415.64(4)$, $c=671.02(7)$ pm and $\beta=90.831(7)^\circ$. Though not isotypic it shows similarities to $Sr_3Sn_2P_4$ [7] with its linear chains of edge- and corner-sharing ${}^1_{\infty}[M_2Se_2Se_4/2]^{3-}$ tetrahedra (fig. 2, right).

[1] P. Stüble, S. Peschke, D. Johrendt, C. Röhr, *J. Solid State Chem.*, **258**, 416, (2018).

[2] P. Stüble, A. Berroth, C. Röhr, *Z. Naturforsch. B*, **71**, 485, (2016).

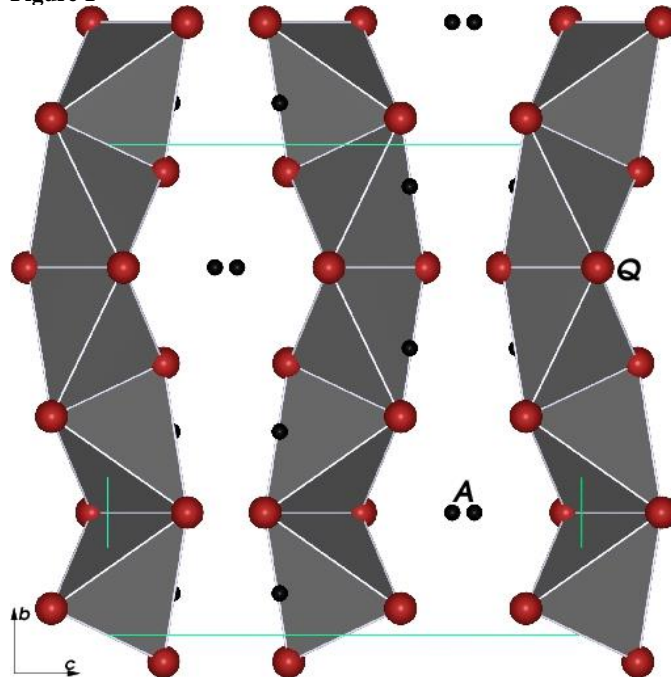
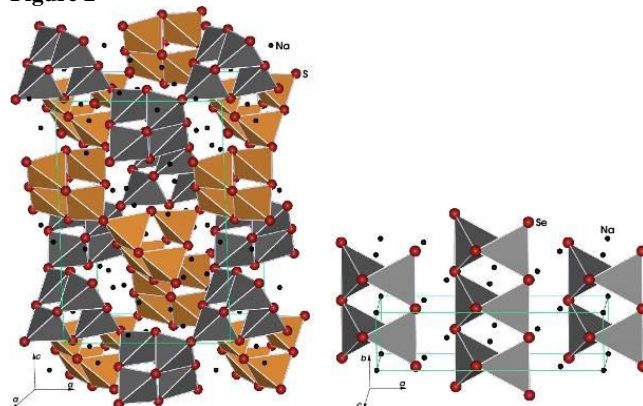
[3] K. O. Klepp, H. Boller, *Monatsh. Chem.*, **112**, 83, (1981).

[4] M. Langenmaier, T. Rackl, D. Johrendt, C. Röhr, *Z. Naturforsch. B*, **73**, 837 (2018).

[5] W. Bronger, U. Ruschewitz, P. Müller, *J. Alloys Compd.*, **218**, 22, (1995).

[6] S. J. Clarke, F. J. DiSalvo, *J. Alloys Compd.*, **274**, 118, (1998).

[7] G. Cordier, H. Schäfer, M. Stelter, *Z. Naturforsch. B*, **41**, 1416, (1986).

Figure 1

Figure 2

LT2-15
Existence or non-existence of iota-alumina?

 S. Lenz¹, H. Schneider¹, R. X. Fischer¹
¹Universität Bremen, Fachbereich Geowissenschaften - Kristallographie, Bremen, Germany

The iota-alumina phase (ι - Al_2O_3) is considered to be the hypothetical end member of the mullite compositional series $Al_2[Al_{2+x}Si_{2-x}]O_{10-x}$ with $x = 1$. This compound has been reported (e.g., [1,2,3]) being synthesized either by quenching a cryolite-alumina melt or by sol-gel routes. The authors identified ι - Al_2O_3 based on a mullite-like diffraction pattern. However, there are no details given on its crystal structure or the lattice parameters of this phase. So the existence of ι - Al_2O_3 is still a matter of debate. For this reason, we reproduced the synthesis method proposed by Ebadzadeh & Sharifi [3] and investigated the synthesized material by X-ray powder diffraction.

The resulting powder pattern closely resembles the pattern shown in [3]. In contrast to that work, Rietveld analysis revealed that the putative iota-phase actually corresponds to a Na-aluminate mullite as it is described by Fischer et al. [4] with lattice parameters: $a = 7.6776(4)$ Å, $b = 7.6762(3)$ Å and $c = 2.9163(1)$ Å. This is supported by EDX analysis, which clearly indicates three single peaks corresponding to O, Na, and Al. This is not surprising since

the applied synthesis route as well as the other synthesis methods described in the mentioned literature have a sodium source in their starting materials as, e.g., cryolite ($\text{Na}_2\text{NaAlF}_6$) or the sodium salt of carboxymethyl cellulose. We assume that the phases designated as $\alpha\text{-Al}_2\text{O}_3$ in the literature are in fact Na-aluminate mullites. Thus, the question about the existence of an Al_2O_3 endmember within the mullite compositional series is still not resolved.

References

- [1] Foster, P.A. *J. Electrochem. Soc.*, 106, 1959, 971-975
- [2] Perrotta, A.J. & Young, J.E. *J. Am. Ceram. Soc.*, 57, 1974, 405-407
- [3] Ebadzadeh, T. & Sharifi, L. *J. Am. Ceram. Soc.*, 91, 2008, 3408-3409
- [4] Fischer, R.X., Schmücker, M., Angerer, P., & Schneider, H. *Am. Min.*, 86, 2001, 1513-1518

We thank the DFG for funding (FI442/24-1).

LT2-16

In-Situ Characterization and Thermal Decomposition Behavior of Ammonium-Exchanged FAU Type Zeolites

A. Gadelmawla¹, I. Spiess¹, J. Birkenstock¹, M. Wendschuh¹, L. Fischer², R. X. Fischer¹

¹Universität Bremen, Fachbereich Geowissenschaften, Bremen, Germany

²Albert-Ludwigs-Universität Freiburg, Institute of Earth and Environmental Sciences, Freiburg, Germany

Ammonium-exchanged zeolites, where the NH_4^+ ion represents the charge-compensating cation, play an important role as precursor materials in the synthesis of H-zeolites. The hydrogen zeolites can be used as catalysts with their protons acting as Brønsted acid sites. Here, we present results on NH_4 -exchanged natural faujasite and synthetic FAU-type zeolites X and Y within the framework of a project studying the mechanisms of deammoniation processes in zeolites by *in situ* methods.

Single crystals of natural faujasite from Limberg Quarries, Sasbach, Kaiserstuhl, Germany, powder samples of zeolite X synthesized according to [1] and powder samples of zeolite Y from Grace GmbHTM were NH_4 exchanged. EDX analysis showed that essentially all extraframework cations were exchanged by NH_4 in the natural single crystal, whereas EDX and FTIR analyses showed partially exchanged in the synthetic powder samples. Powder-diffraction experiments indicate a slight change in the lattice parameters upon ammonium exchange.

TG analyses for NH_4 -Y showed two mass-loss steps accomplished at 450°C and 700°C, which are interpreted as dehydration, deammoniation, and dehydroxylation processes, respectively [2]. NH_4 -X showed only one mass-loss step accomplished at 600°C interpreted as dehydration and deammoniation [3]. The thermal evolution of NH_4 -Y was further assessed by *in situ* high-temperature X-ray diffraction experiments using a Paar HTK1200 heating chamber within a range between 25°C and 750°C.

Single-crystal diffraction data were collected for FAU at 25°C ($a=24.6639(7)$ Å) and for NH_4 -FAU at 25°C ($a=24.733(12)$ Å). The crystal structures were refined in space group *Fd-3m*. *In situ* high-temperature single-crystal X-ray diffraction data were collected for NH_4 -FAU at 200°C, 400°C and 550°C, and are currently under investigation. At 550°C the crystal structure is expected to correspond to a protonated faujasite.

- [1] Charnell, J. F. *J. Cryst. Growth*, 8, 1971, 291-294.
- [2] Chu, P. J. *Catal.*, 43, 1976, 346-352.

- [3] Chu, P., Dwyer, F. G. *J. Catal.*, 61, 1980, 454-460.

LT2-17

Texture formation in obliquely deposited metal thin films

S. Liedtke-Grüner¹, C. Grüner¹, A. Lotnyk¹, M. Mensing¹, J. W. Gerlach¹, P. Schumacher¹, B. Rauschenbach¹

¹Leibniz Institute of Surface Engineering (IOM), Leipzig, Germany

Question

Obliquely deposited metallic thin films consist of three-dimensionally separated, crystalline nano-needles. Such highly porous films are an interesting candidate for plasmonic (bio-)sensing as well as for magnetic applications, for instance. Guided by growth competition and self-shadowing, an evolutionary selection of the crystal orientations takes place. Understanding the selection process of crystal orientations in obliquely deposited metallic thin films is an important issue to optimize such films for specific device applications.

Methods

Titanium, aluminum, chromium, and molybdenum thin films are deposited obliquely under ultra-high vacuum conditions by electron beam evaporation on amorphous substrates at room temperature. The crystal orientations of the entire film are determined by XRD texture goniometry and the time evolution of the surface structure is observed by *ex situ* RHEED.

Results

The incidence angle of the incoming particle flux is found to be one of the main parameters that influences the finally observed texture. A biaxial texture could only be observed at highly oblique incidence conditions, whereas for less oblique deposition geometries a fiber texture is detected. A strong impact of the crystal structure and the growth temperature on the texture formation is found as well. Further, the individual nano-needles are investigated by HR-TEM. Such measurements reveal that these needles are single crystalline if grown at sufficient vacuum levels at room temperature.

Conclusions

In conclusion, the presented results give a first insight into the relevant processes that lead to the formation of biaxially textured metallic thin films composed of individual nano-needles.

Bio-Crystallography I: Signalling, macromolecular interactions and other new structures

P001

Structure-Based Fragment Screening on Dynamin GTPase Domain

H. Taberman^{1,2}, O. Daumke², M. S. Weiss¹

¹Helmholtz-Zentrum Berlin, Macromolecular Crystallography, Berlin, Germany

²Max-Delbrück-Centrum for Molecular Medicine, Berlin, Germany

Dynamin is the founding member of dynamin superfamily of large guanine triphosphatases (GTPase) that are mostly involved in the remodelling of cellular membranes. Dynamin is a multi-domain protein having a critical role in membrane fission events during endocytosis. It forms a helical oligomer around the neck of the invaginating clathrin-coated vesicle, and conformational changes occurring during GTP hydrolysis induce the fission of the tubular membrane [1]. Clathrin-mediated endocytic pathway is the major route of uptake from the plasma membrane, for example, in cell signalling and nutrient intake [2]. Furthermore, it is also exploited by pathogens to enter the cell. The membrane-fission activity of dynamin is entirely dependent on nucleotide binding and hydrolysis by the GTPase domain. This makes it an interesting target for drug development studies aiming to inhibit or increase the GTPase activity, by either competing with GTP or allosteric binding to positively affect the GTPase activity.

The aim of this study is to deploy structure-based fragment screening for finding new small organic molecules that occupy the GTP binding site or bind to allosteric sites of dynamin. The advantage of fragment-based screening is the use of predominantly hydrophilic low molecular weight compounds increasing the probability of finding hits [3]. X-ray crystallography has been shown to be the most reliable and sensitive tool for detecting binders even with very low affinity [4, 5]. The fragment hits can then be used in lead optimisation creating higher affinity compounds that can be used to probe the biology of the target and as a lead in finding novel promising drug candidates specific for dynamin.

References

- [1] Faelber, K. et al. (2012) *Structure*20, 1621.
- [2] Bitsikas, V. et al. (2014) *eLife*3, e03970.
- [3] Murray, C.W. et al. (2012) *Trends Pharmacol. Sci.*33, 224.
- [4] Schiebel, J. et al. (2016) *ACS Chem. Biol.*11, 1693.
- [5] Schiebel, J. et al. (2016) *Structure*24, 1398.

P002

Engineering chimera constructs to crystallize a complex protein structure

R. Amjadi¹, T. Duzendorfer-Matt¹, K. Scheffzek¹

¹Medical university of Innsbruck, biological chemistry division, Innsbruck, Austria

Defining protein domains or segments of a protein that would form diffracting crystals is a major challenge in biomolecular crystallography and may take ages of experimental trial and error odysseys. Especially if the protein domain under study contains inserted domains of much larger size than its own, isolation of such domains may be challenging. Despite substantial efforts, we were unable to obtain diffraction-quality crystals from a purified protein complex of interest, which might be due to conformational flexibility of some regions of participating protein components in this complex. We used sequence and structure comparing approaches to engineer chimera constructs of a two domain signal regulatory module that functions as a membrane recruitment

platform. Our study allows selection of promising constructs although protein expression and crystallization tests are yet to be performed.

- [1] T. Duzendorfer-Matt, E. L. Mercadob, K. Malyc, F. McCormickb, and K. Scheffzek., *PNAS*, (2016), 113:7497-502.
- [2] Daniel M. Rosenbaum, Vadim Cherezov, Michael A. Hanson2, Søren G. F. Rasmussen, , *Science* (2007), 318: 1266-1273.

Bio-Crystallography III: Enzymes

P003

Structural studies on the substrate and cofactor binding modes of FAD-dependent monooxygenases

J. Kratky¹, T. Heine², R. H. Weiße¹, D. Tischler², N. Sträter¹

¹Universität Leipzig, Institute of Bioanalytical Chemistry, Leipzig, Germany

²Technische Universität Bergakademie Freiberg, Environmental Microbiology, Freiberg, Germany

Introduction and Objectives

Styrene monooxygenases (SMOs) catalyse the enantioselective epoxidation of styrene and structurally related compounds. They are of interest for the development of new biocatalytic production processes for pharmaceuticals and fine chemicals. Our aim is to improve the substrate specificity and enantioselectivity of the SMO StyA1 for such applications. Hence, we used protein crystallography to determine the binding modes of substrates and the cofactor FAD. Crystal structures of the SMO StyA1 in the absence and presence of FAD revealed conformational changes involved in cofactor binding. Additionally, we will report on challenges on the road to obtain structural information about the substrate binding mode and our approach to overcome them.

Material and Methods

Diffraction data sets from single crystals of wildtype StyA1 and mutants were collected at the BESSY II beamlines 14.1 and 14.2.

Results

Co-crystallisation of StyA1 with FAD revealed that the highest occupancy reached for this cofactor is 90 % and could only be achieved by using indole as a substrate. Based on our results we propose that a chain flip is related to the cofactor binding. First insights into the substrate binding mechanism of SMOs were achieved by co-crystallisation with different substrates like indole. For the first time the function of the substrate tunnel and a gatekeeper could be demonstrated.

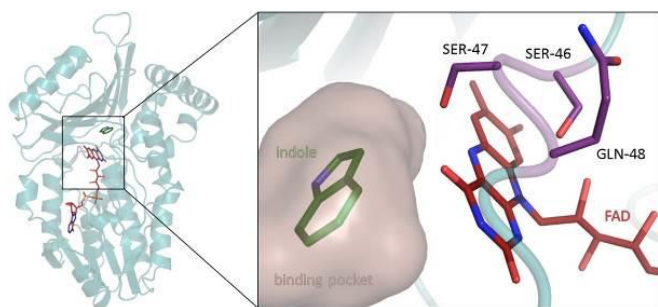
Conclusion

Crystallisation studies under anaerobic conditions with FADH₂ will be performed to hopefully overcome the low cofactor binding affinity in the case of several tested substrates. Furthermore, engineering of the enantiospecificity of StyA1 would be a huge advantage for biocatalytic applications of this protein. Based on our data rational design of StyA1 becomes possible now.

Figure Legends:

Figure 1. Substrate binding mode of indole. Binding mode of indole (green) within the binding pocket (pink) in presence of the cofactor FAD (red, resolution: 1.71 Å).

Figure 1



Bio-Crystallography IV: Structure-based drug design**P004****Substrate specificity determinants of the proprotein convertase furin beyond the S4 pocket.**S. O. Dahms¹, K. Harges², T. Steinmetzer², H. Brandstetter¹, M. E. Than³¹University of Salzburg, Department of Biosciences, Salzburg, Austria²Philipps-Universität Marburg, Department of Pharmaceutical Chemistry, Marburg, Germany³Leibniz Institute on Aging - Fritz Lipmann Institute (FLI), Jena, Germany

The proprotein convertase furin is a highly specific serine protease modifying and thereby activating proteins in the secretory pathway by proteolytic cleavage. Its substrates are involved in many diseases, including cancer and infections caused by bacteria and viruses. Understanding furin's substrate specificity is crucially important for the development of pharmacologically applicable inhibitors. Using protein X-ray crystallography, we investigated the extended substrate binding site of furin in complex with peptide-derived inhibitors at up to 1.9 Å resolution. The structural data revealed molecular details of furin-substrate interactions at the S5 and S6 pockets. The arginine residue at P6 induced an unexpected turnlike conformation of the inhibitor backbone, which is stabilized by intra- and intermolecular H-bonds. In addition, we confirmed the binding of arginine to the previously proposed S5 pocket (S5-1). An alternative S5 site (S5-2) could be utilized by shorter side chains as demonstrated for a 4-aminomethyl-phenylacetyl residue, which shows steric properties similar to those of a lysine side chain. The herein identified molecular interaction sites at P5 and P6 might be useful to improve next-generation furin inhibitors and help to evaluate furin substrates more precisely.

P005**An approach to improve the solubility of poorly water soluble anti-cancer drug - dasatinib**M. S. T. Abdul Azeze¹, P. Palanisamy², V. Thiruvengadam³, C. Ghoroi⁴, S. Meyyanathan¹¹JSS College of Pharmacy-Udhagamandalam, Pharmaceutical Analysis, The Nilgiris, India²Indian Institute of Technology Gandhi Nagar, Biological Engineering, Gandhi Nagar, India³Indian Institute of Technology Gandhi Nagar, Physics and Biological Engineering, Gandhi Nagar, India⁴Indian Institute of Technology Gandhi Nagar, Chemical Engineering, Gandhi Nagar, India

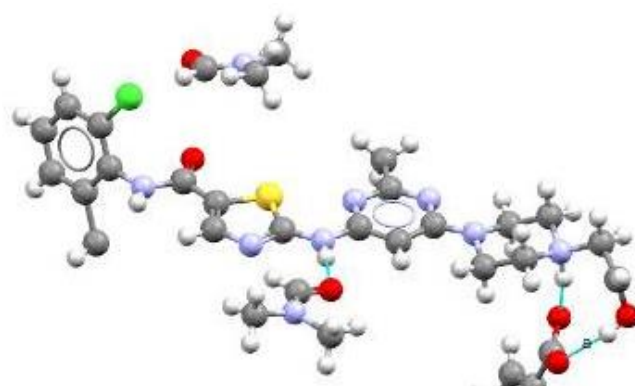
Dasatinib (DAS) is a BCS (Biopharmaceutical Classification System) class II drug used for the treatment of chronic myeloid leukemia. Bioavailability of this drug is limited by its water solubility. There is an urgent desperation, to improve the solubility of the drug by forming new stable co-crystals with enhanced physico-chemical properties. In this present work, 4-chlorobenzoic acid (4-CBA) and 4 hydroxybenzoic acid (4HBA) were selected as cofomers based on their ability to form a supramolecular synthon network with the drug molecule. Co-crystals were prepared at room temperature (25 °C) by the solution crystallization method. Physico-chemical and thermal properties of the grown crystals were analyzed using UV, FT-IR and DSC analyses. The structures of co-crystals were analyzed by SCXRD and the structures were refined using Olex2 software. The asymmetric unit of the DAS-4CBA co-crystal (Fig.1) comprises one DAS, one 4-CBA and two DMF molecules, whereas DAS-4HBA co-crystal contains one DAS, one 4-HBA and one DMF and two water molecules. Molecular packing of DAS-4CBA co-crystal is facilitated through a hydroxyl group of dasatinib and the carbonyl oxygen of 4CBA and DAS-4HBA co-crystal is through carbonyl oxygen of dasatinib and the hydroxyl group of 4HBA. These H-bond networks play an important role in enhancing the water solubility of the drug.

Keywords: Bioavailability, solubility, co-crystallization, H-bonding

Fig.1 Asymmetric unit of dasatinib- 4 -Chlorobenzoic acid co-crystal

References:

- [1] Dolomanov O.V, Bourhis L.J, Gildea R.J, Howard J.A.K, and Puschmann H. (2009). OLEX.J. Appl Cryst. 42: 229–341.
- [2] <http://www.olexsys.org/>
- [3] Food and Drug Administration, Washington (USA): Dasatinib (Sprycel), Application number: 21-986 & 22-072, Clinical Pharmacology and Biopharmaceutics Review(s).
- [4] Desiraju, G. R.: "Crystal Engineering. The Design of Organic Solids", Elsevier, 1989.
- [5] Desiraju, G. R. and Steiner, T.: "The Weak Hydrogen Bond in Structural Chemistry and Biology", Oxford University Press, 1999

Figure 1**P006****Structural studies on inhibitor binding to human kallikrein 7**S. Hanke¹, J. Pippel¹, C. A. Tindall², D. Ulbricht², J. T. Heiker², N. Sträter¹¹Universität Leipzig, Institute of Bioanalytical Chemistry, Leipzig, Germany²Universität Leipzig, Institute of Biochemistry, Leipzig, Germany

The serine protease kallikrein7 is a member of the human tissue kallikreins. Its dysregulation leads to pathophysiological inflammation processes in the skin, which causes diseases such as psoriasis. Small molecule inhibitors, which inhibit the active site of the human kallikrein 7 (hK7), are being developed for the treatment of kallikrein7 associated diseases. We aim to understand the mode of inhibition of these compounds by X-ray crystallography.

We could obtain crystals by co-crystallization that diffract to 1.9 Å. However, structure analysis showed only very weak and uninterpretable electron density in the active center of hK7. After optimizing the purification strategy with an affinity chromatography column that contains an immobilized binding partner of hK7, which binds to the active site of hK7, we could separate active from inactive species after refolding the protease from inclusion bodies. These experiments indicated that the previously obtained preparations were largely inactive, although crystallization and melting point determination indicated correctly folded protein. Crystal structure analysis of the inactive protein part indicates a modification of an active site asparagine. Mass spectrometry analyses for identification of the covalent modification showed that the asparagine was deamidated to an aspartate. Based on the electron density map the modification could be identified as an L-Iso-Aspartate leading to the inactive species of hK7. This indicates that the location and orientation of the

peptide backbone near the catalytic triad of the protease plays an essential role for the activity of this protease. Further on we focused on characterizing inhibitor binding to the fully active hK7 preparation. After optimizing the crystallization conditions, we obtained co-crystals diffracting to 1.89 Å. These crystals show clear electron density of the covalent inhibitor attached to an active site histidine residue. It is the first crystal structure of a kallikrein protease with this class of suicide inhibitors. Based on these studies the structural basis of hK7 inactivation by covalent modification could be demonstrated. Further work focuses on the characterization of the initial non-covalent complex important for inhibitor specificity.

Bio-Crystallography V: Instrumentation and methods

P008

P11 at PETRA III: A Versatile Beamline for Serial and High-Throughput Crystallography

A. Burkhardt¹, E. Crosas¹, O. Lorbeer¹, S. Guenther¹, T. Pakendorf¹, B. Reime¹, J. Meyer¹, P. Fischer¹, N. Stübe¹, M. Warmer¹, A. Meents¹
¹DESY, Hamburg, Germany

Beamline P11 is located at PETRA III, the high brilliance 3rd generation synchrotron radiation source at the Deutsches-Elektronen Synchrotron DESY in Hamburg, Germany. P11 is dedicated to imaging and diffraction experiments of biological samples, with a special focus on protein crystallography [1,2]. The installation of a third experimental endstation for serial synchrotron crystallography is planned. The high photon flux (1.3×10^{13} ph/s at 12 keV) provided at the sample position allows for structure determination from weakly diffracting microcrystals and serial crystallography experiments [3-7]. The X-ray beam size at the sample position can be freely chosen between $4 \times 9 \mu\text{m}^2$ and $200 \mu\text{m}^2$ ($v \times h$). The P11 crystallography endstation can be operated between 5.5 and 25 keV and provides full SAD/MAD capability. Energy and beam size changes can be easily realized within a few minutes. The crystallography endstation is equipped with a high-precision single axis goniostat, a rapid automatic sample changer, a large capacity storage Dewar and a fast Pilatus 6M detector, which allows to collect a data set within 2 – 3 min. P11 provides a very stable setup for high-throughput crystallography, which makes the beamline ideally suited for industrial applications like e.g. pharmaceutical drug design and fragment screening.

- [1] A. Burkhardt *et al.*, EPJ Plus 131:56 (2016)
- [2] A. Meents *et al.*, Proc. SPIE 8851, 88510K (2014)
- [3] F. Stellato *et al.*, IUCrJ 1, 204 (2014)
- [4] K. R. Beyerlein *et al.*, IUCrJ 4, 769 (2017)
- [5] P. Roedig *et al.*, Sci. Rep. 5, 10451 (2015)
- [6] P. Roedig *et al.*, J. Appl. Cryst. 49, 968 (2016)
- [7] A. Meents *et al.*, Nat. Commun. 8, 1281 (2017)

P009

Investigation of protein crystals within living insect cells using small-angle X-ray scattering

R. Schönherr¹, C. Jeffries², M. Lahey-Rudolph¹, C. E. Blanchet², D. I. Svergun², L. Redecke¹

¹University of Lübeck, Biochemistry, Lübeck, Germany

²EMBL, Hamburg, Germany

Question

In cellulo protein crystallization within living insect cells enables the easy growth of a huge number of high-quality microcrystals, providing enormous potential for structural biology. However, a disadvantage of this method is that the small size of the crystals may prevent the timely detection of crystals within cell cultures. If the crystal size is in the low μm -regime, time consuming electron microscopy is essentially the only method available to identify crystal-positive cultures. At synchrotrons, powder diffraction beamlines have, at present, also been not very effective as a high-throughput technique for *in cellulo* crystal detection, especially in cases where ratios of crystals to cells are low in the cultures. Considering this, our goal is to establish high-throughput *in cellulo* crystal detection and analysis on a low background SAXS beamline.

Methods

Semi-adherent High Five insect cells were infected with different recombinant baculoviruses to efficiently transfer the respective target gene into the whole cell culture. 48 to 96 hours after

infection, a highly dense culture of living insect cells was injected into the EMBL P12 bioSAXS beamline using an automated liquid handling sample changer. The P12 beamline at the storage ring PETRA III (DESY, Hamburg) combines high-brilliance with engineering design principles to keep background scattering contributions from the instrument to a minimum.

Results

The use of high brilliance SAXS at P12 has eliminated the methodological bottle neck of detection. It is possible to assess within seconds whether an infected cell culture contains microcrystalline material based on the presence of defined peaks in the SAXS profile, even under conditions of high cell culture dilution. The detection limit can be as low as 0.2 % of crystal containing cells. Using the highly sensitive SAXS setup it is possible to investigate protein crystal growth directly within the living cells.

Conclusions

The investigation of *in cellulo* microcrystals using SAXS is uniquely informative for down-stream X-ray crystallography applications at synchrotron or free-electron laser sources, but also opens opportunities to understand the mechanisms underpinning biological crystallization processes. Such experiments will shine a light on how growth conditions, stress, temperature, starvation, cellular compartmentalization, and the choice of cell lines, affect the size, scattering capabilities and formation of *in cellulo* crystals.

P010

EMBL Beamlines for Macromolecular Crystallography at PETRA III

T. Schneider¹, G. Bourenkov¹, G. Pompidor¹, I. Bento¹, J. Hakanpää¹, S. Panneerselvam¹, D. von Stetten¹

¹EMBL, c/o DESY, Hamburg, Germany

EMBL-Hamburg operates two MX beamlines, P13 and P14, at PETRA III (DESY, Hamburg). For both beamlines, remote access is available.

P13 delivers high photon fluxes at energies down to 4 keV. Combining X-rays in the 4-6 keV energy range with beam sizes down to $15 \mu\text{m}$ diameter while maintaining high photon flux allows to perform full data collections with optimized anomalous signal in less than 5 minutes. S-SAD phasing is achieved routinely; the feasibility of MAD-phasing at the Ca K-edge (4.05 keV, 3.1 \AA) has been demonstrated. Diffraction measurements at low energies on P13 do not require any special preparation of the sample, i.e. a crystal attached to a standard SPINE-pin can be automatically mounted onto the goniostat.

P14 can be run in two modes, one providing a collimated homogeneous beam that can be shaped to any size between 10 and $200 \mu\text{m}$ (crystal life-time ~ 2 minutes at 100 K), the second mode producing micro-focus conditions with a beam size on the $5 \mu\text{m}$ scale (crystal life-time ~ 500 ms at 100 K). The collimated beam can be used to illuminate large (50 - $200 \mu\text{m}$) and small crystals homogeneously and/or to resolve diffraction from large ($>1000 \text{ \AA}$) unit cells. Prominent recent applications of the collimated beam have been the determination of a set of structures of the human 20S proteasome in complex with different ligands [1] and the phasing of the crystal structure of the mediator complex consisting of 15 proteins [2]. The micro-focus beam can be used conveniently for serial data collections both on cryogenically cooled crystalline suspensions [3] and *in situ* on crystals as grown in CrystalDirect™ crystallization plates. *In situ* structure determinations have been successfully performed from crystals in

crystallization drops, in lipidic cubic phase, or as grown in living cells [4].

In 2018, a second endstation has been added to P14 providing an environment optimized for pump-probe experiments. Data storage and processing facilities have been significantly upgraded to 1 PetaByte and 1000 Cores, respectively.

The beamlines are embedded in the Integrated Facility for Structural Biology offering access to up-stream service such as characterization of samples prior to crystallization, high throughput crystallization, and automatic crystal harvesting with a CrystalDirect™ Harvester.

References:

- [1] Schrader ... Chari (2016) *Science* 353:594-598.
- [2] Nozawa, Schneider, Cramer (2017) *Nature* 545:248-251.
- [3] Gati ... Redecke (2014), IUCrJ
- [4] Collab. projects

P011

Better data from laser-shaped crystals

T. Barthel^{1,2}, N. Matsugaki³, M. Hikita³, M. S. Weiss¹, T. Senda³

¹Helmholtz-Zentrum Berlin, Macromolecular Crystallography, Berlin, Germany

²Freie Universität Berlin, Berlin, Germany

³Institute of Materials Structure Science, High Energy Accelerator Research Organization, the Structural Biology Research Center, Photon Factory, Tsukuba, Japan

Even though most protein structures so far have been solved with X-ray crystallography, collecting high quality diffraction data still remains challenging for a lot of proteins. Especially when using low energy X-rays for novel structure determination the signal-to-noise ratio is still one of the limiting factors, despite significant advancement of the beamline set-ups in the last years. Deep UV lasers are able to shape samples in a way to remove residual solvent around the crystal to minimize absorption effects. Also, the shape and size of the crystals can be altered. Consequently, it is expected that diffraction data collected from laser-shaped crystals can be better in terms of overall data quality as well as in terms of signal-to-noise ratio, especially for long wavelength experiments. As SAD phasing is one most common method for *de novo* structure determination, our project investigates possible improvements made by laser-shaping protein crystals with a focus on low energy SAD X-ray experiments and resulting anomalous data quality. On the poster, a few pilot experiments will be described with different crystal sizes and different low energy wavelengths.

P012

An all-in-one sample holder for macromolecular X-ray crystallography

C. Feiler¹, D. Wallacher², M. S. Weiss¹

¹Helmholtz-Zentrum Berlin, Macromolecular Crystallography, Berlin, Germany

²Helmholtz-Zentrum Berlin, Sample Environment, Berlin, Germany

Structure determination of protein macromolecules requires the growth of high quality crystalline material.

Various types of sample holders have been developed and are widely used in protein X-ray crystallography.

Collection of diffraction data from a single protein crystal involves a number of manual handling step, including crystal fishing, cryo protection and mounting onto an individual sample

holder. Numerous enhancements have been done in order to improve many handling steps, including *in-situ screening* to characterize well-diffracting crystals [1, 2].

We have developed a novel type of sample holder, which acts as an all-in-one platform. As a replacement of commonly used cover slips, it supports all steps in the workflow from crystal setup to data collection without any direct crystal handling. Further, crystal manipulation is realized in-place and does not require any handling steps of individual crystals.

Diffraction data collection can be carried out at both, ambient and cryogenic temperature. Additionally, the sample holder is compatible with the SPINE standard format and can therefore be used with automatic sample mounting robots. Finally, with using the new type of sample holder, the number of crystals/dewar can be drastically increased.

The patent protected sample holder can be used on both, 22- and 18-millimeter standard 24-well plates [3–7]. Auxiliary tools support a straightforward workflow, using the novel sample holder with a minimized chance of damaging sensitive crystalline material.

References:

- [1] le Maire, A. *et al.* In-plate protein crystallization, in situ ligand soaking and X-ray diffraction. *Acta Crystallographica Section D: Biological Crystallography*. **67**(9), 747–755, (2011).
- [2] Soliman, A.S.M., Warkentin, M., Apker, B., Thorne, R.E. Development of high-performance X-ray transparent crystallization plates for in situ protein crystal screening and analysis. *Acta Crystallographica Section D: Biological Crystallography*. **67**(7), 646–656, (2011).
- [3] Feiler, C. Wallacher, D. Weiss, MS. - Sample holder, patent-registered: DE 10 2017 129 761.8, WO application under preparation.
- [4] Feiler, C. Wallacher, D. Weiss, MS. - Soaking stand: Patent pending: DE 10 2018 123 090.7
- [5] Feiler, C. Wallacher, D. Weiss, MS. - XtalToolHT: patent pending: DE 10 2018 125 129.7
- [6] Feiler, C. Wallacher, D. Weiss, MS. - protection of utility patents: DE 20 2018 106 955.1
- [7] Feiler, C. Wallacher, D. Weiss, MS. - Design registration: DE 40 2018 100 962.8

Complex and aperiodic structures

P013

Ir₃Sn₈O₄: A cluster compound with incommensurately modulated crystal structureM. Lüdicke¹, T. Söhnel², K. Finzel¹, T. Doert¹¹Technische Universität Dresden, Department of Inorganic Chemistry, Dresden, Germany²The University of Auckland, School of Chemistry, Auckland, New Zealand

Tin – transition metal (TM) – oxide compounds are flexible towards substitution and mixing of TMs including Ru, Os, Fe, Ti and Ir^[1-4]. The crystal structures feature main group polyhedra which are centered by transition metals and linked via oxygen atoms. Here we present the structure of an iridium tin oxide with an exceptional metal-oxygen ratio of 11:4, namely Ir₃Sn₈O₄.

Ir₃Sn₈O₄ powder was prepared by a solid state reaction from a stoichiometric mixture of IrSn₂ and SnO₂ in evacuated and sealed quartz tubes. Micrometre-sized, black single crystals can be obtained from Ir and IrO₂ in a tin flux under inert conditions. The crystals can be extracted with dilute HCl. Ir₃Sn₈O₄ forms a (3+1)-dimensional structure which can be described in the orthorhombic superspace group $Pnnn(\frac{1}{2}\beta\frac{1}{2}q)0q$ with $a = 684.70(2)$ pm, $b = 899.29(3)$ pm, $c = 919.90(3)$ pm, and $\mathbf{q} = (0.5\ 0.239\ 0.5)$. The structure is related to the rutile type and consists of IrSn₆-octahedra sharing corners along the **b** and **c** directions and edges along **a**. The Ir–Ir distances vary from 319.7 pm to 407.4 pm along **a** due to a strong positional modulation. Most strikingly, the modulation describes Ir–Ir-pairs with short interatomic distances of 319.7–321.2 pm which shift through the structure. Despite the large positional modulation function for Ir, initial ELI-D calculations do not support significant Ir–Ir interactions.

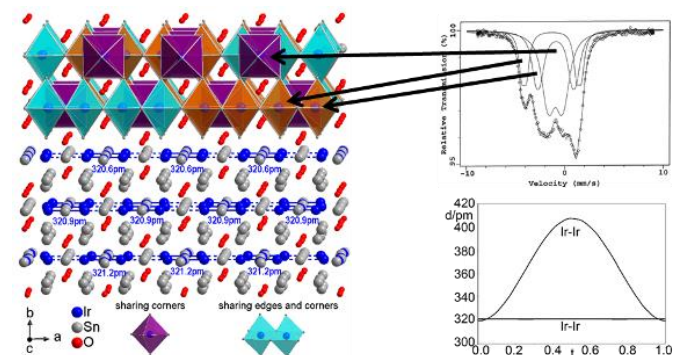
Ir₃Sn₈O₄ exhibits an electronic band gap of 0.07 eV and is diamagnetic. ¹³⁹Ir-Mössbauer spectroscopy revealed three different contributions. One Mössbauer signal can be assigned to the IrSn₆-octahedra which only shares corners, the other two can be correlated with the IrSn₆-polyhedra sharing edges and corners.

Figure

Section of the incommensurately modulated structure of Ir₃Sn₈O₄ in the **a,b**-plane showing IrSn₆-octahedra sharing corners and edges (left). Assignment of the ¹³⁹Ir-Mössbauer signals (top right). Variation of Ir–Ir-distances for one modulation period (bottom right).

References

- [1] A. Simon, J. Köhler, H. Mattausch, W. Reichelt, T. Söhnel, O. Rademacher, H. Oppermann, *Angew. Chem.* **1995**, 632, 2307–2309.
- [2] T. Söhnel, W. Reichelt, *Acta Cryst. C* **1997**, 53, 9–11.
- [3] T. Söhnel, P. Böttcher, W. Reichelt, F. E. Wagner, *Z. Anorg. Allg. Chem.* **1998**, 624, 708–714.
- [4] H. Hillebrecht, M. Ade, *Z. Anorg. Allg. Chem.* **1999**, 625, 572–576.

Figure 1

P014

Magneto-elastic phase transitions of the unconventional spin-Peierls compound TiOCl at high pressures and low temperaturesA. M. Schaller¹, M. Bykov², E. Bykova^{2,3}, K. Glazyrin³, S. van Smaalen¹¹University of Bayreuth, Laboratory of Crystallography, Bayreuth, Germany²University of Bayreuth, Bayerisches Geoinstitut (BGI), Bayreuth, Germany³DESY, Photon Sciences, Hamburg, Germany

The transition-metal oxychloride TiOCl belongs to a class of low-dimensional magnetic materials MOCl (M = Ti, V, Cr, Fe) whose unique magnetic behavior depends on the orbital order of the 3d electrons of M³⁺. Orbital order of the single 3d electron of Ti³⁺ makes TiOCl a quasi-1D magnetic system that develops a spin-Peierls pairing of magnetic moments at low temperatures [1]. The spin-Peierls state, characterized by a dimerization of the lattice, is reached via an intermediate incommensurate phase [2]. Pressurizing MOCl at ambient temperatures leads to a normal-to-incommensurate structural transition at ≈ 15 GPa, which is not related to electronic effects or magnetic order [3,4]. The combination of high pressures (HP) and low temperatures (LT) allows to access physics that is not yet understood: the effect of the structural phase transition on the magnetic order of TiOCl. Single crystal HP-LT X-ray diffraction has been carried out at P02.2/PETRA III in order to resolve this fundamental question as well as to determine the pressure dependence of the spin-Peierls phase, the pressure dependence of the structural distortions within the magnetically ordered phase and to investigate a possible spin-Peierls state of the high-pressure phase. The results show that there is a distinctively different behavior of the modulation wave vector components within the incommensurate phase (antiferromagnetic state at ambient pressure) at high and low temperatures. This suggests a strong interference of structurally and magnetically driven phase transitions that is further elucidated with structure model refinements. A detailed understanding of the mechanisms in MOCl with varying external parameters will boost and facilitate the understanding of strongly correlated electron systems with different interfering degrees of freedom (lattice, orbital and spin) in general.

- [1] Seidel et al., *Phys. Rev. B* 67, 020405(R) (2003).
- [2] Schönleber et al., *Phys. Rev. B* 77, 094117 (2008).
- [3] Bykov et al., *Phys. Rev. B* 88, 014110 (2013).
- [4] Bykov et al., *Sci. Rep.* 5, 9647 (2015).

P015

LaTe_{1.8} - A new incommensurately modulated structure in the series REX_{2-δ}H. Poddig¹, T. Doert¹¹Technische Universität Dresden, Inorganic Chemistry II, Dresden, Germany

The structures of the rare earth metal polychalcogenides REX_{2-δ} (X = S, Se, Te; 0 ≤ δ ≤ 0.2) share a common motive of puckered [REX] double layers and planar [X] layers and are structurally related to the ZrSSi type. This class of compounds adopts different (super)structures, according to chalcogen defects in their planar layers. The deficient sulfides and selenides form X²⁻ and X₂²⁻-anions, whereas larger entities were observed for the tellurides.^[1,2]

Crystals of LaTe_{1.8} were grown in an alkali halide flux in a glassy carbon crucible inside a quartz ampule. Main reflections of the diffraction image indicate a tetragonal unit cell with $a = 450.00(5)$ pm and $c = 918.1(1)$ pm. Satellite reflections were observed and indexed with two modulation wave vectors $q_1 = (0.275, 0.310, 0.500)$ and $q_2 = (-0.275, 0.310, 0.500)$. These wave vectors are incompatible with a fourfold rotational symmetry. The modulated structure was thus solved and refined in the orthorhombic superspace group $Pmmm(\beta, \gamma, \frac{1}{2})000(-\beta, \gamma, \frac{1}{2})000$ and revealed an occupancy modulation of the Te atoms, coupled to a displacive modulation. A variety of tellurium entities, like Te²⁻ and Te₂²⁻ anions similar to the anions commonly observed in rare earth metal polysulfides and polyselenides,^[1] but also Te₃²⁻ and Te₃⁴⁻ anions and [Te₄]-squares are found in the modulated telluride layers, the latter being a prominent structural feature in CeTe₂^[2] and PrTe₂^[3], (figure 1). The distances of the different anions, e.g. about 280 pm for Te₂²⁻ or 283 pm for Te₃²⁻, are well in accordance with literature data.

LaTe_{1.8} differs from the respective deficient sulfides and selenides LaX_{2-δ} in its lower chalcogen content. However, the structure of LaSe_{1.85} shows a very similar incommensurate site occupancy and displacive modulation.^[4]

[1] T. Doert, C. J. Müller, *Reference Module in Chemistry, Molecular Sciences and Chemical Engineering*, Elsevier, 2016.

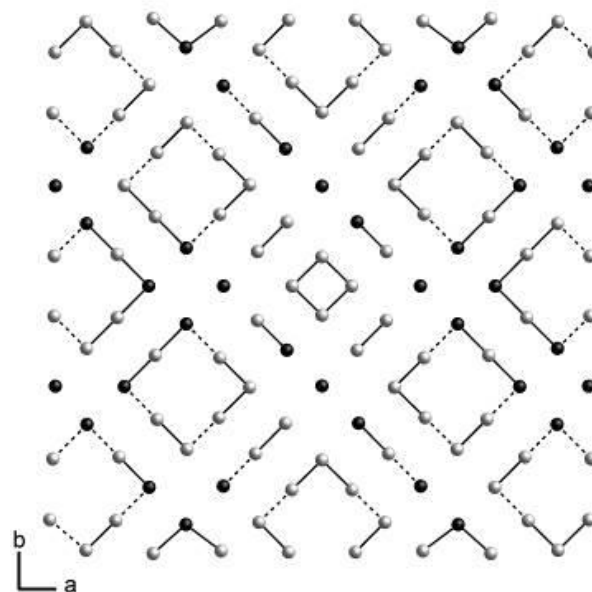
[2] K. Stöwe, *J. Alloys Compd.* **2000**, 307, 101–110.

[3] K. Stöwe, *Z. Anorg. Allg. Chem.* **2000**, 626, 803–811.

[4] C. Graf, T. Doert, *Z. Kristallogr. - Cryst. Mater.* **2009**, 224, 12, 568–579.

Figure 1. Section of the modulated Te-layer in LaTe_{1.8} with short distances marked by bold lines, long distances marked by dashed lines; the occupancy modulation is visualized by using black color for fully occupied positions and grey for partially occupied Te sites.

Figure 1



P016

The Superspace Piano - A comprehensive introduction to the fundamental concepts of higher-dimensional superspace crystallography based on the simple one-dimensional pattern of black and white keys of a common musical instrumentP. B. Klar¹¹Czech Academy of Sciences, Institute of Physics, Prague, Czech Republic

The first contact with (3+n)d superspace is often rather abstract, especially if the mind gets twisted by the additional spatial dimensions. Nevertheless, its fundamental concepts are essential to understand the crystallography of modulated structures and quasicrystals. To facilitate the first contact, here a comprehensive and self-explanatory route is suggested starting with the simplified, one-dimensional pattern of black and white keys of a piano.

The embedding of the commensurate, repeating unit of seven white and five black keys in a (1+1)d superspace description illustrates the lattice periodicity, atomic domains and occupational modulation functions (Fig. 1). Changing some parameters of the Superspace Piano model provides a straight forward introduction to concepts like displacive modulation functions by depicting a 1-dimensional section through superspace (Fig. 2).

The framework of the Superspace Piano allows to communicate the essential aspects of superspace crystallography in a short time and thus is a useful tool for presentations of any kind that require a basic understanding of the superspace formalism. Animations were generated to exemplify relevant parameters of modulated structures.

Figure 1: Two-dimensional superspace description of the one-dimensional pattern of black and white keys. α is a parameter of the modulation wave vector and t is the one-dimensional section through superspace that represents the key pattern at the bottom. Black vertical bars describe the occupancy of the black keys, that is either 0 or 1.

Figure 2: The same model as in Figure 1, but with an additional displacive modulation function with amplitude $A = 0.15$. Note the different spacing between white and black keys with respect to Figure 1.

Figure 1

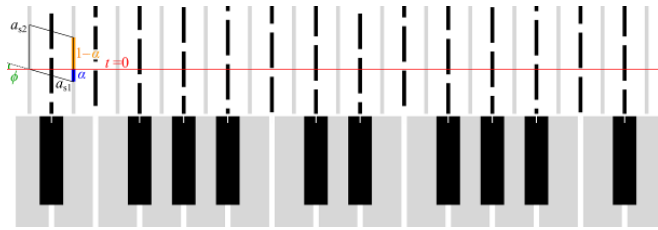
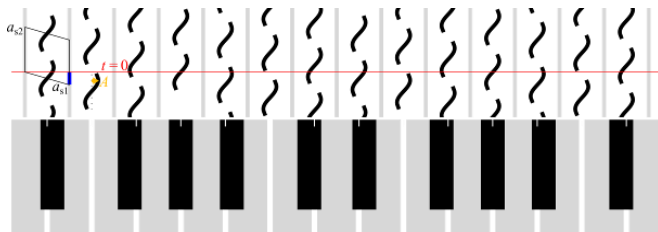


Figure 2



Disordered Materials

P017

Orientationally disorder in monomethyl-quinacridone investigated by Rietveld refinement, pair distribution function analysis and lattice-energy minimizationsC. Schlesinger¹, S. Hammer¹, M. Schmidt¹¹Goethe-Universität Frankfurt am Main, Institut für analytische und anorganische Chemie, Frankfurt am Main, Germany

The crystal structure of the poorly crystalline, reddish organic pigment 2-monomethyl-quinacridone (C₂₁H₁₄N₂O₂, Figure 1) was solved successfully from X-ray powder diffraction data. The structure solution leading to a crystal structure in P-1 with Z = 1, therefore with a molecule on the inversion centre. However, the molecule which itself is not inversion-symmetric, needs to be orientationally disordered with a disorder of CH₃ versus H. The disorder and the local structure was investigated using various ordered structural models in P 1 and P-1, Z = 1, 2, and 4. All models were analysed by three approaches: Rietveld refinement, pair distribution function (PDF) analysis and lattice-energy minimization.

All Rietveld refinements with TOPAS V4 [1] converged with acceptable R-values. All lattice-energy minimizations using the DREIDING [2] force field within the MATERIALS studio software [3] were within a range of 6 kJ mol⁻¹. In addition all fits to the PDF using TOPAS V6 [4] were quite reasonable. However, all methods favour a statistical orientational disorder with a preferred antiparallel orientation of neighboring molecules.

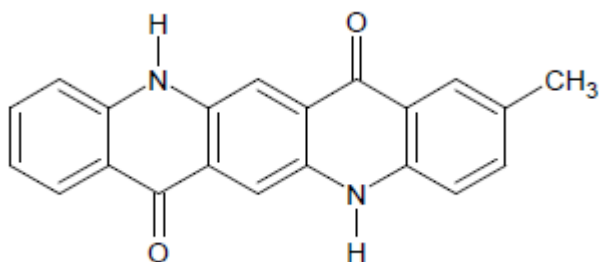
[1] Coelho A. A., TOPAS-Academic 4.1, Coelho Software, 2007, Brisbane, Australia.

[2] Mayo S. L., Olafson B. D., Goddard III W. A., J. Phys. Chem., 1990, 94, 8897.

[3] BIOVIA Dassault Systèmes, Materials Studio, 4.4, 2008, San Diego.

[4] Coelho A. A. J. Appl. Cryst. 2018, 51, 210-218.

Figure 1



P018

A practical approach to generating models for disordered polymers using the x-ray pair distribution function*M. Terban¹, S. Machlus², B. Hinrichsen³, R. E. Dinnebier¹¹Max Planck Institute for Solid State Research, Scientific Facility X-ray diffraction, Stuttgart, Germany²Florida State University, Tallahassee, United States³BASF, Ludwigshafen, Germany

Molecular polymers are a class of materials which typically exist in a weakly crystalline or completely amorphous state. They are critical to a wide variety of technologies, yet detailed structure characteristics are still poorly understood, and structure characterization from X-ray diffraction is typically qualitative.

Even in the best cases, samples often require rigorous sample treatments such as extrusion and annealing in order to generate structural states amenable to powder or fiber diffraction. Better characterization methods are needed to quantitatively explore the local structuring of polymers in their as-used state.

The pair distribution function (PDF) method allows for accessing local structure information such as bonding environment, molecular conformation, polymer chain packing, and overall domain structure. Unfortunately, this information can still be quite difficult to access without prior knowledge about the structure, whether underlying molecular motifs or average crystal structure. Here, we show how to access useful qualitative and quantitative information about the structure of amorphous and disordered polymers for a variety of examples. Furthermore, a practical methodology will be shown for using this information, coupled with monomer structure and connectivity, to both develop and verify candidate models for the local structure by refinement against the information contained in the PDF. This method should provide a useful approach to obtaining starting models for better understanding structure in amorphous materials or for more rigorous energetic calculations and property prediction.

Extreme/non-ambient conditions

P019

A novel stability field of a high pressure high temperature polymorph of dolomite

J. Binck¹, S. Chariton², L. Bayarjargal¹, L. Dubrovinsky², B. Winkler¹
¹Goethe-Universität Frankfurt am Main, Institut für Geowissenschaften, Frankfurt am Main, Germany
²University of Bayreuth, Bayerisches Geoinstitut (BGI), Bayreuth, Germany

During the subduction of oceanic crust significant amounts of carbon bearing sediments may be transported into the Earth's mantle [1]. However, the solubility of carbon into major mantle minerals was shown to be very low [2]. Hence, carbonates are believed to be likely hosts for carbon in the mantle. Dolomite, CaMg(CO₃)₂, is thought to constitute up to 50 % of the world's surface carbonate reservoirs [3]. Also, diamond inclusions show evidence for the presence of dolomite in the mantle [4]. Experimental studies have provided indication for the existence of high pressure high temperature polymorphs of dolomite [5,6].

Here, we have studied the phase stability of dolomite at high pressures and temperatures, employing a combination of Raman-spectroscopy and synchrotron single-crystal X-ray diffraction using laser-heated diamond anvil cells. We observed the formation of a new dolomite polymorph at 50 GPa and after annealing at 2300 K, which persisted upon pressure release to 27 GPa. A preliminary data analysis indicated that this compound has the structure of a polymorph recently predicted by DFT based calculations [7]. Since this new structure is stable at pressure and temperature conditions found along the Earth's geotherm, we conclude that significant amounts of the phase may be present in the mantle.

Financial support by the DFG (FOR2125/CarboPaT, BA4020 and WI1232) is gratefully acknowledged.

- [1] Litasov and Ohtani, Phys. Earth Planet. Interiors 177, 46 (2009).
- [2] Keppler et al., Nature 424, 414 (2003).
- [3] Zenger et al., SEPM Spec. Publ. 28, (1980).
- [4] Brenker et al., Earth Planet. Sci. Lett. 260, 1 (2007).
- [5] Mao et al., Geophys. Res. Lett. 38 (2011).
- [6] Merlini et al., Am. Min. Lett. 102, 1763 (2017).
- [7] Solomatova and Asimow, Am. Min. 102, 210 (2017).

P020

High temperature X-ray diffraction studies of oxygen-deficient Ca(Mn,Ti)O_{3-δ} perovskites

S. Stöber¹, H. Pöllmann¹
¹Martin-Luther-Universität, Institut für Geowissenschaften und Geographie Mineralogie/Geochemie, Halle (Saale), Germany

The aim of this study was to investigate the temperature driven structural changes in oxygen-deficient Ca(Mn,Ti)O_{3-δ} perovskites.

The phases were synthesized by the Pechini methods, varying the substitution Mn⁴⁺ <=> Ti⁴⁺ in the range 0 ≤ x ≤ 1. The investigated phases were all single phased, which has been proven by ICP/OES and microprobe analysis. X-ray diffraction (HT-XRD) data were collected at room and non ambient temperatures between 298 to 1273 K (Mo radiation) applying a PANalytical Empyrean diffractometer equipped with an Anton Paar HTK 1200N oven chamber with capillary extension and a GaliPIX^{3D} detector. For the evaluation of the X-ray data TOPAS-Academic (version 6) was used.

Different modifications with space groups *Pbnm*^{1/1}, *Cmcm*, *I4/mcm* and *Pm-3m* were detected. The stability fields and transformation temperatures were determined. The refinement of structure data yielded temperature dependent alterations in tilting and distortion of B - site octahedra^{2/2} and differentially coordinated A - site polyhedra. Symmetry-mode Rietveld refinement (Isodistort Version 6.5.0)^{3/3} was applied and the results are compared with the traditional refinement of atomic xyz coordinates.

- [1] Ross, N. L., J. Zhao, et al. (2004): "High-pressure structural behavior of GdAlO₃ and GdFeO₃ perovskites." Journal of Solid State Chemistry 177(10): 3768-3775.
- [2] Glazer, A. (1972): "The classification of tilted octahedra in perovskites." Acta Crystallographica Section B 28(11): 3384-3392.
- [3] B. J. Campbell, H. T. Stokes, D. E. Tanner, and D. M. Hatch, "ISODISPLACE: An Internet Tool for Exploring Structural Distortions. J. Appl. Cryst. 39, 607-614 (2006).

P021

Temperature-dependent structural investigation of [Na₈(ReO₄)₂][AlSiO₄]₆ sodalite: Phase transitions and thermal stability

H. Petersen¹, L. Robben¹, T. M. Gesing¹
¹Universität Bremen, Institut für Anorganische Chemie und Kristallographie, Bremen, Germany

The title compound attracted some interest, because of the template anion's (ReO₄⁻) chemical analogy to the radioactive ⁹⁹TcO₄⁻, whose properties lead to concerns regarding storage and processing. Studies of synthesis conditions for incorporation of ReO₄⁻ in the SOD structure [1,2] show the suitability of SOD framework as a solid matrix material for ⁹⁹TcO₄⁻ [3], now the prediction of the thermal behavior and stability of a ⁹⁹TcO₄-SOD by analyzing the ReO₄-SOD is required.

The presented study analyses the thermal behavior via temperature-dependent (TD) PXRD, TD Raman and heat-capacity measurements. Two phase transition are observed. A template driven order-disorder transition in the SOD structure (statically disordered <218.6(1) K vs. dynamically stabilized >218.6(1) K), observable in a disorder-increase on the template-position. A second phase transition from the partially collapsed (P-43n) to fully expanded SOD (Pm-3n) occurs at 442(1) K. The comparison of the transition temperatures *T_C* of SODs (MnO₄⁻: *T_C* = 597(1) K [4], NO₃⁻: *T_C* = 935 K [5]) with similar anion sizes reveals a decrease of *T_C* with increasing anion size (ReO₄⁻ > MnO₄⁻ > NO₃⁻). The ReO₄-SOD shows the lowest *T_C* for this phase transition. An extraordinary high thermal stability (decomposition temperatures *T_d* = 1320 K) of the ReO₄-SOD was observed (SODs with *T_d* above 1123 K are defined as thermally very stable [6]). Most SODs with tetrahedral template anions decompose below 1100 K (e.g. MnO₄⁻ 1060 K [4]; ClO₄⁻ 893 K [7]).

- [1] J.O. Dickson et al., Chem. Geol. 395 (2015) 138–143.
- [2] J.O. Dickson et al., Microporous Mesoporous Mater. 214 (2015) 115–120.
- [3] E.M. Pierce et al., Environ. Sci. Technol. 51 (2017) 997–1006.
- [4] H. Petersen et al., Microporous Mesoporous Mater. 242 (2017) 144–151.
- [5] C. Rüscher et al., Zeitschrift fuer Krist. 218 (2003) 332–344.
- [6] R.M. Barrer, J.F. Cole, J. Chem. Soc. (1970) 1516–1523.
- [7] M.T. Weller, K.E. Haworth, J. Chem. Soc., Chem. Commun. (1991) 734–735.

P022

Crystal chemistry at multimegabar pressures

N. Dubrovinskaia¹, L. Dubrovinsky¹

¹University of Bayreuth, Bayreuth, Germany

Modern science and technology rely on the fundamental knowledge of matter that is provided by crystallographic studies. The most reliable information about crystal structures and their response to changes in pressure and temperature is obtained from single-crystal diffraction experiments. Advances in diamond anvil cell (DAC) techniques and double-stage DACs, as well as in modern X-ray facilities have increased the accessible pressure range for structural research up to multimegabar range. We have developed a methodology to perform single-crystal X-ray diffraction experiments in double-side laser-heated DACs. Our results demonstrated that the solution of crystal structures, their refinement, and accurate determination of thermal equations of state of elemental materials, oxides, carbides, borides, carbonates, and silicates from single-crystal diffraction data are possible above 200 GPa at temperatures of thousands of degrees. These resulted in findings of novel compounds with unusual compositions, crystal chemistry, and physical properties. We illustrate application of new methodology for simultaneous high-pressure and high-temperature single crystal diffraction studies using examples of investigations of chemical and phase relations in the Fe-O system, transition metals carbonates, silicates, and nitrides.

P023

Is GeI₄'s liquid-liquid transition identifiable as a percolation transition of 'bonds'?

K. Fuchizaki¹, H. Naruta¹, T. Sakagami²

¹Ehime University, Physics, Matsuyama, Japan

²AGC Techno Glass Co., Ltd., Material Group Technology Center, Shizuoka, Japan

In 1980, Stanley and Teixeira argued that the thermodynamic anomalies in water are ascribable to the phenomena associated with a percolation transition of hydrogen bonds [1]. To our knowledge, there has been no quantitative discussion regarding a relation between a liquid-liquid transition and a percolation transition after this pioneering work.

Recently, we have shown that liquid GeI₄ undergoes a pressure-induced crossover from the low-pressure to high-pressure liquid state [2]. Here, we examine a possible microscopic pathway of the crossover by conducting an isothermal-isobaric molecular dynamics simulation. We prepared three sizes of a system consisting of 216, 1000, and 2744 molecules to allow a finite-size scaling analysis. The model employed was composed of rigid tetrahedral molecules interacting via iodine centers connected by Lennard-Jones (LJ) interaction. The LJ parameters were adjusted to reproduce the density at ambient conditions and the melting curve [3]. The deviation of the model's melting curve from the actual one amounts to 40% at 1 GPa [3].

We define a *physical* bond between the nearest intermolecular iodine sites satisfying the conditions of forming the metallic I₂ bond. We then focus on the formation of molecular clusters in *dynamic* networks of the bonds. The clusters, which are mainly formed by molecules whose nearest pairs are in edge-to-edge, face-to-edge, and vertex-to-edge orientations, grow as pressure increases, and the onset of percolation is observed below 1 GPa. The finite-size scaling analysis for the percolation probability (the strength of an infinite network) and the mean cluster size (which correspond to order parameter and susceptibility, respectively, in thermal critical phenomena) identifies that the threshold pressure is 0.85 ± 0.01 GPa for the present model, which is near the extension

of the boundary between the two liquid phases [4]. We thus speculate that the liquid-liquid crossover of GeI₄ is brought about by percolation of molecular networks.

[1] H. E. Stanley and J. Teixeira, *J. Chem. Phys.* 73, 3404 (1980).

[2] K. Fuchizaki *et al.*, *J. Phys.: Condens. Matter* 30, 045401 (2018).

[3] K. Fuchizaki and Y. Asano, *J. Phys. Soc. Jpn.* 84, 064601 (2015).

[4] K. Fuchizaki, H. Naruta, and T. Sakagami, submitted to *J. Phys.: Condens. Matter*.

P025

The Limitations on Quasi-harmonic Thermal-Pressure Equations of State from Anisotropic Thermal Pressure

R. Angel¹, G. Zaffiro¹, C. Stangarone^{1,2}, B. Mihailova³, M. Murri¹, M. Alvaro¹

¹University of Pavia, Earth and Environmental Sciences, Pavia, Italy

²German Aerospace Centre (DLR), Institute for Planetary Research, Berlin, Germany

³Universität Hamburg, Dept. Earth Sciences, Hamburg, Germany

Thermal-pressure Equations of State (EoS) describe how the volume or density of a material changes with both pressure and temperature. Several EoS, including the Mie-Grüneisen-Debye (MGD), are based on the Quasi-Harmonic Approximation (QHA). This says that the frequencies of the vibrational modes of the material are solely dependent upon the volume. Thus, under QHA, it is assumed that vibrational frequencies do not change along isochors. This is true for cubic crystals and elastically isotropic materials, but QHA-based EoS are frequently used for non-cubic crystalline materials.

The thermal pressure in any direction in a crystal is the ratio of the thermal expansion to the compressibility [1]. It defines how the unit-cell parameters change with P and T, and it therefore controls how the cell parameters change along isochors. The changes in the unit-cell parameters are strains, and the frequencies of phonon modes change under strain by an amount defined by their phonon-mode Grüneisen tensors [2]. When the thermal pressure is anisotropic, the unit-cell parameters change along isochors, even while the volume remains constant. Therefore the frequencies of vibrational modes change along the isochors and the QHA is invalid. This is confirmed by experimental measurements of the elastic properties of rutile, which cannot be fit with a MGD or other QHA-based EoS. It also means that the components of the phonon-mode Grüneisen tensors have different values for temperature- and pressure-induced strains; this provides a simple way to detect from Raman spectra whether anisotropic thermal pressure is significant in a crystal.

[1] Nye (1957) *Physical Properties of Crystals*

[2] Angel et al. (2018) *Zeit. Krist.*, in press, DOI: 10.1515/zkri-2018-2112

This work was supported by ERC starting grant 714936 "True Depths" to Matteo Alvaro.

in situ/in operando studies

P026

The thermal behavior of the zincophosphate hydrosodalite between 13 K and 300 K

L. Robben^{1,2}

¹Universität Bremen, Institut für Anorganische Chemie und Kristallographie, Bremen, Germany

²Universität Bremen, MAPEX Center for Materials and Processes, Bremen, Germany

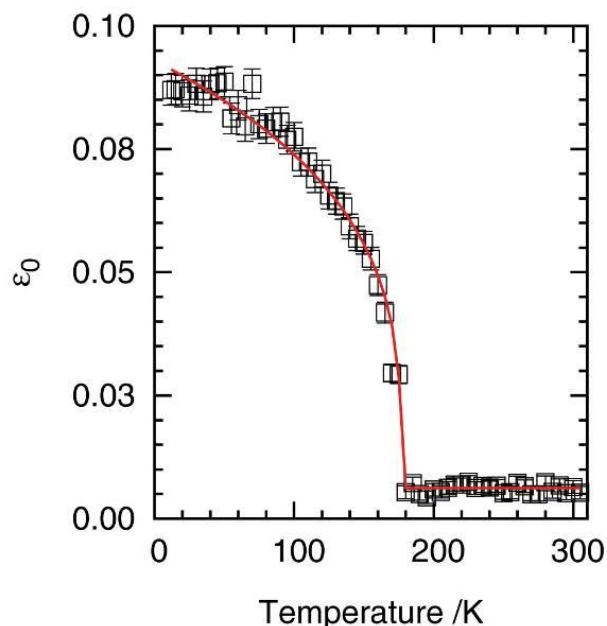
Structural studies of sodalites at temperatures well below ambient conditions are rare. Only the pure silica sodalites with their organic templates have gained some interest in this respect. In that case, the reports indicate a close correlation between template molecule and the occurrence of phase transitions at low temperatures. A first study on the $[\text{Na}_6(\text{H}_2\text{O})_8][\text{ZnPO}_4]_6$ sodalite showed a reversible phase transition around 180 K in heat capacity measurements and temperature-dependent Raman spectroscopy [1]. The objective of this study is to evaluate the nature of the phase transition by X-ray diffraction.

Powder diffraction pattern of $[\text{Na}_6(\text{H}_2\text{O})_8][\text{ZnPO}_4]_6$ were collected between 13 K and 300 K. At 300 K the structure is described in space-group with a lattice parameter $a = 882.689(5)$ pm. Upon cooling the data reveal a distinct change of symmetry at 177(5) K. The data collected at 13 K were used for structure solution and refinement. The structure solution was carried out by indexing of the reflections and comparison with possible space-groups which are sub-groups of , leading to space-group with lattice parameters $a = 1239.88(9)$ pm and $c = 882.9(1)$ pm.

A displazive phase transition at 177(5) K of $[\text{Na}_6(\text{H}_2\text{O})_8][\text{ZnPO}_4]_6$ was found and the low-temperature structure was respectively solved. This displazive phase transition occurs with a doubling of the unit cell volume and a highly increased strain, which is the order parameter (see figure). The strain arises from severe tetrahedra distortion in the low-temperature phase.

[1] L. Robben, T.M. Gelsing, Z. Krist. Supp. 36 (2016) p. 126

Figure 1



P027

In situ phase transformation study of calcium sulfates

L. Ritterbach¹, P. Becker¹

¹University of Cologne, Institute of Geology and Mineralogy, , Cologne, Germany

The Atacama desert in northern Chile is one of the driest places on earth and therefore of great interest for interdisciplinary research on the evolution of earth surface and life under extreme conditions. One major aspect to scrutinize is the so-called gypsum crust, as large parts of the desert are covered with calcium sulfates originating from volcanic and oceanic sources. It has been proven by [1] that all three natural phases of the $\text{CaSO}_4 - \text{H}_2\text{O}$ system (gypsum $\text{CaSO}_4 \cdot 2\text{H}_2\text{O}$, bassanite $\text{CaSO}_4 \cdot 0.5\text{H}_2\text{O}$, anhydrite CaSO_4) are abundant, leading to the assumption that the $\text{CaSO}_4 \cdot n\text{H}_2\text{O}$ ($n = 0-2$) system exhibits phase transformations under temperature and humidity conditions as present in the Atacama.

By in situ powder XRD measurement using an Anton-Paar climate chamber mounted on a Bruker X-ray diffractometer with Bragg-Brentano geometry these transformations were investigated under application of controlled temperature and humidity. The time-, temperature- and humidity- dependent measurements also showed, besides the mentioned natural three phases, during bassanite rehydration the occurrence of subhydrates ($\text{CaSO}_4 \cdot x\text{H}_2\text{O}$, $0.5 < x < 2$). The refinements rather hint to gradual than stepwise uptake of water molecules in the crystal structure. The system's transition kinetics follows the nucleation and crystal growth based Johnson-Mehl-Avrami-Kolmogorow (JMAK) equation but reacts sensitively to small changes in sample environment and properties such as preparation techniques, grain size and shape and pore volume and density.

To enhance the reliability of the quantitative description of the system $\text{CaSO}_4 \cdot n\text{H}_2\text{O}$ concerning subhydrate evolution and parametrization of phase transition kinetics, the XRD investigations are complemented by time-, temperature- and humidity- dependant DSC/TGA.

[1] Flahaut et al., Icarus, Volume 282, 2017, Pages 152-173.

P028

Mechanism of the decomposition of thermoelectric Cu_2Se : in situ X-ray diffraction tomography and ex situ analyses

M. Jakob¹, G. Vaughan², O. Oeckler¹

¹Universität Leipzig, IMKM, Leipzig, Germany

²ESRF, ID15a, Grenoble, France

During the last few years, mixed ionic and electronic conductors (MIECs) have attracted much interest in the field of thermoelectric research due to their seemingly outstanding thermoelectric performance. Well-known examples comprise Cu_{2-x}Se , [1] or Zn_4Sb_3 . [2] However, decomposition under working conditions (electrical current, thermal gradient) is a problem due to electromigration. This has been reported in a qualitative way: for instance, copper is deposited at the electrical negative pole which corresponds to the hot side of a p-type semiconductor. [3] In order to obtain insight into these processes, we constructed an apparatus which enables applying currents up to 10 A and, simultaneously, a temperature gradient between ambient temperature and 450 °C on bar-shaped samples while performing diffraction experiments at high-energy synchrotron beamlines. With this setup, stress tests at different temperature gradients and different currents were performed on Cu_2Se samples while investigating the whole sample in situ. 3D X-ray diffraction tomography (3D-XRDCT) at beamline ID15a, ESRF Grenoble yields detailed spatial information on the

phases present. This method delivers a powder diffraction pattern for each micron-sized volume increment of the sample investigated. Such measurements can be complemented by ex situ SEM and EDX measurements.

Cu_{2-x}Se undergoes an order-disorder phase transition at ~150 °C. With x > 0, the transition temperature decreases down to ~110 °C for x = 0.2. The presence of deposited copper at the hot side and the migration of the phase boundary between the high-temperature and low-temperature phases present in sample under a temperature gradient can be observed as a function of time in reconstructed maps from 3D-XRDCT data. The phase boundary moves towards regions of lower temperatures when Cu₂Se decomposes into Cu_{2-x}Se + Cu, which leads to lower performance under working conditions.^[4] This study presents a new access to the investigation of thermoelectric materials in situ by 3D-PXRCT and gives a detailed insights into the processes in the MIEC material Cu₂Se.

[1] H. Liu, X. Shi, F. Xu, L. Zhang, L. Chen, Q. Li, C. Uher, T. Day, G. J. Snyder, *Nat. Mater.* **2012**, *11*, 422.

[2] G. J. Snyder, M. Christensen, E. Nishibori, T. Caillat, B. B. Iversen, *Nat. Mater.* **2004**, *3*, 458.

[3] D. R. Brown, T. Day, T. Caillat, G. J. Snyder, *J. Electron. Mater.* **2013**, *42*, 2014.

[4] J. Yu, K. Zhao, P. Qui, X. Shi, L. Chen, *Ceram. Int.* **2017**, *43*, 11142.

P029

In situ XRD of multi-cation doped Mn-spinel, LiNi_{0.3}Cu_{0.1}Fe_{0.2}Mn_{1.4}O₄, as 5V cathode material for Li-ion batteries using Ag laboratory source.

M. Knapp¹, P. Sharma¹, S. Darma¹, H. Ehrenberg¹

¹Karlsruhe Institute of Technology (KIT), IAM-ESS, Karlsruhe, Germany

Development of high-voltage cathode materials for electric vehicle applications has gained significant scientific attention in the recent years. LiNi_{0.5}Mn_{1.5}O₄ (LNMO) spinels are considered as promising candidates due to their high operating potential, environmental friendliness, low cost and good thermal stability. However, their electrochemical properties are greatly affected by the crystal structure and it is known that LNMO with a disordered structure shows superior electrochemical performance. The suitability of multi-cation substitution to stabilize the structure is investigated in LiNi_{0.3}Cu_{0.1}Fe_{0.2}Mn_{1.4}O₄ synthesized via a modified sol-gel route at a calcination temperature of 850 °C. The structural characterization by X-ray diffraction (XRD) and Raman spectroscopy confirmed the formation of a disordered spinel along with the presence of Li₂MnO₃ impurity phase. Truncated octahedral, crystalline microparticles were obtained which not only suppressed side reactions but also enhanced cycling performance in a voltage window of 3.5-5.3 V. Laboratory *in situ* XRD using a STOE diffractometer with Ag target and an in-house designed sample holder in transmission geometry was utilized to investigate the Li⁺ ion (de-)insertion mechanism into the spinel system. Charging rates of C/10 and exposure times of 20 min resulted in diffraction patterns of sufficient quality. The charging occurred by a solid solution mechanism whereas a secondary spinel was observed during discharging which can be attributed to the inhomogeneous distribution of particle size.

P030

Li/O incorporation-induced structural evolution during synthesis of Li-Mn-rich oxides

W. Hua¹, B. Schwarz¹, M. Knapp¹, M. Etter², A. Schökel², J. R. Binder¹, S. Indris¹, H. Ehrenberg¹

¹Karlsruhe Institute of Technology (KIT), Institute for Applied Materials - Energy Storage Systems (IAM-ESS), Eggenstein-Leopoldshafen, Germany
²DESY, Hamburg, Germany

As promising candidate for advanced cathode materials, the lithium-rich 3d-transition-metal (TM) layered oxides (LLOs) could exhibit much higher discharge specific capacities (> 250 mAh g⁻¹) than the current traditional layered cathode materials (~ 180 mAh g⁻¹) used in lithium ion batteries (LIBs). Unfortunately, the original formation mechanism of these layered oxides during synthesis has not been completely understood, i.e. how is lithium and oxygen inserted into the matrix structure of the precursor during high-temperature lithiation reaction? In order to trace the structural evolution of the precursor without lithium source and the mixture of the precursor together with lithium source during heating, *in situ* high-temperature synchrotron radiation diffraction experiments were performed at P02.1 beamline, Deutschen Elektronen-Synchrotron DESY in Hamburg. The *in situ* high-temperature diffraction results show that the precursor consisted of layered TMOOH (C2/m) and tetragonal TM₃O₄ (I4₁/amd) becomes a single cubic spinel TM₃O₄ phase (Fd-3m) as a consequence of oxygen loss during thermal treatment. In contrast, oxygen would be incorporated into the host architecture during preparation of LLOs starting from a mixture of the precursor together with lithium carbonate. The uncovered lithiation mechanism shows the original formation of LLOs, which not only offers valuable information for industrial operation, but also contributes to a comprehensive understanding of the relationship between the preparation, structure and electrochemical properties in these materials.

P031

Crystallization studies with in-situ analytical methods

T. Y. Nguyen¹, J. Stroh¹, F. Emmerling¹

¹BAM Federal Institute for Materials Research and Testing, 1.3 Structural Analysis, Berlin, Germany

Introduction

In pharmacy and materials technology, the synthesis and purification of compounds based on crystallization are essential steps for the effectiveness of the drug and the material quality. Different theories including classical and non-classical pathways are developed to describe the mechanism of crystallization. Nevertheless, early stages at atomic and mesoscale of crystallization are still insufficiently understood.¹

Objectives

Crystallization processes of different materials were studied in-situ using levitated droplets in combination with synchrotron X-ray methods and Raman spectroscopy. An ultrasonic levitator as a contact-free sample holder avoids any influences of container surfaces. The climate unit allows controlling the temperature and humidity of the sample environment.²⁻³

Results

The in-situ combination of XRD and Raman spectroscopy proves to be a powerful technique for the screening of crystallization from solution to study amorphous and crystalline phases.⁴ The application of the pair distribution function analysis from the total X-ray scattering data indicates the presence of polyamorphism in paracetamol.⁵ The different amorphous states are crucial intermediates, whose properties are determined by the used solvents. The choice of the solvent and the supersaturation degree

triggers and controls certain crystallization pathways and allows obtaining the desired crystalline modification.

Conclusion

Crystallization from solutions follows specific pathways different from those predicted by the classical nucleation theory. To study these pathways, it is of utmost importance to eliminate any possible influencing factors, so that the system is stabilized in an undisturbed levitated environment. Under acoustic levitation it is possible to study homogeneous crystallization processes using different analytical techniques.

[1] C. Sun, D. Xu, and D. Xue, *Crystengcomm*, 15(38):7783–7791, 2013.

[2] S. E. Wolf, J. Leiterer, M. Kappl, F. Emmerling, W. Tremel, *JACS*, 130: 12342-12347, 2008.

[3] M. Schlegel, A. Sarfraz, B. Müller, U. Panne, F. Emmerling, *Angew. Chem. Int. Ed.*, 51:4993-4996, 2012.

[4] Y. Nguyen Thi, K. Rademann, and F. Emmerling, *CrystEngComm*, 17:9029-9036, 2015.

[5] T. Y. Nguyen, E. A. Roessler, K. Rademann, and F. Emmerling, *Zeitschrift für Kristallographie-Crystalline Materials*, 232(1-3):15-24, 2017.

Inorganic crystal structures

P032

Effect of amino acids on CaCO₃ precipitation

L. AMER¹

¹Laboratoire de physique des matériaux et catalyse. Université de Bejaia, physics, Bejaia, Algeria

Introduction

The biomineralisation of CaCO₃ is both a scientific and economical promising approach for the synthesis of this mineral, which is in great demand in several fields. Indeed, the living organisms adopt an effective strategy to elaborate this mineral with remarkable properties using soft chemistry condition. This is done by secreting organic matter, rich in amino acids, which directs mineralisation and the growth of its polymorphs. Recently, this biogenic process has experienced a rapid growth with the development of refinement methods that allow a quantitative analysis essential for understanding this process.

Objectives

In this work, we studied the precipitation of CaCO₃ particles in aqueous solution in the presence of three amino acids (aspartic, glutamic and glycine acids). The effect of the amino acids on the crystal's mean sizes and polymorph volume content at ambient temperature are examined using X-rays and Rietveld method.

Results

It was found that the different acids had a different behaviour towards the polymorphs of CaCO₃. In fact, the aspartic acid promotes the precipitation of calcite; this was reflected by increasing of its volume fraction from 84(1)% to 97(6)% , and its average crystallites size from 1628(64) Å to 1745(24) Å. The same effect was obtained by incorporating glycine acid with an increase in the average crystallites size of calcite to 2200(44) Å. In contrast, the glutamic acid has a stabilising effect on the vaterite phase with an increase in its volume fraction from 16(1) to 77(5) % in disfavour of calcite phase which decreases from 84 to 23%. The mean crystallites size of vaterite increased from 180(14) (Å) to 508(10) (Å).

Conclusion

The results confirm that organic matter influences the precipitation of the mineral phase by a stabilising or inhibiting effect in a selective way according to the structure of the polymorph and the additive.

Keywords: Biomineralisation, CaCO₃, Quantitative analysis, Rietveld method.

P033

Heteroepitaxial growth of α -, β -, γ - and κ -Ga₂O₃ phases by metal-organic vapor phase epitaxy

S. Merker¹, V. Gottschalch¹, H. Krautscheid¹

¹Universität Leipzig, Inorganic Chemistry, Leipzig, Germany

The wide-bandgap semiconductor Ga₂O₃ is a promising candidate for ultrahigh-voltage devices, photo catalyst, gas sensors, transparent conductive devices, spintronic applications, photoelectric water splitting and many more. The five known phases (α -, β -, γ -, δ - and κ -Ga₂O₃) have direct bandgaps E_g in the range of 4.9 to 5.3 eV.

Although there are many reports on β -Ga₂O₃ and few about epitaxy of α -, γ - and κ -Ga₂O₃^[1], but systematic studies are still lacking. Therefore, we are interested in improved metal-organic vapor

phase epitaxy (MOVPE) growth conditions for the different Ga₂O₃ phases and their epitaxial relationship to different substrates.

Trimethylgallium (TMG) and N₂O were used as common precursors for gallium and oxygen, respectively. Through variation of growth temperature, pressure, gas phase composition and substrate selection we were able to selectively grow α -, β -, γ - and κ -Ga₂O₃ on *c*-, *a*- and *r*-plane Al₂O₃, (001) and (111) MgO, (001) and (111) MgAl₂O₄ and on a (0001) Al₂O₃ | (0001) GaN heterostructure. X-ray diffraction (θ -2 θ - and ϕ -Scans) was used to identify the various Ga₂O₃ phases and the epitaxial relationship for all obtained heterostructures.

We were able to confirm and find new epitaxial relationships for already known systems. Furthermore, we will present the results on the growth of new combinations, e.g., pseudo hexagonal κ -Ga₂O₃ on *a*- and *r*-plane Al₂O₃ and (111) MgAl₂O₄ or defect spinel structured γ -Ga₂O₃ on *c*-Al₂O₃, (100) and (111) MgAl₂O₄, (100) MgO and (0001) Al₂O₃/GaN.

[1] H. von Wenckstern, Adv. Electron. Mater. (2017) 1600350.

P034

Investigation into Crystal Structure and Hydrogen-Bond Network of Sr[MnO₄]₂ · 3 H₂O at Low Temperature

M. Conrad¹, T. Schleid¹

¹University of Stuttgart, Institute for Inorganic Chemistry, Stuttgart, Germany

The synthesis and crystal structure of strontium permanganate trihydrate (Sr[MnO₄]₂ · 3 H₂O) at room temperature [1] has recently been reexamined in literature [2]. However, as the hydrogen positions could not be refined by now, investigations of the hydrogen-bond network within the structure was yet to be done.

A phase-pure sample of the title compound was synthesized by means of cation exchange [2]. A column filled with the activated ion-exchange resin Amberlite IR-120 was loaded with an aqueous SrCl₂ solution. Subsequently, an aqueous solution of K[MnO₄] was passed through leading to the exchange of these cations. Afterwards, the solvent was slowly removed until about 10 mL of water were remaining. Finally, the solution was dried in a desiccator yielding dark purple crystals of Sr[MnO₄]₂ · 3 H₂O.

The crystal structure of Sr[MnO₄]₂ · 3 H₂O has been determined at 100 K from single-crystal X-ray diffraction data collected using a κ -CCD diffractometer with a molybdenum source ($\lambda = 71.07$ pm).

Sr[MnO₄]₂ · 3 H₂O crystallizes in the cubic space group $P2_13$ with the lattice parameter $a = 960.56(4)$ pm for $Z = 4$ (CSD-433349). There are two crystallographically different Mn⁷⁺ cations each surrounded by four oxygen atoms forming virtually ideal tetrahedra ($d(\text{Mn}-\text{O}) = 160 - 163$ pm, $\angle(\text{O}-\text{Mn}-\text{O}) = 108.9 - 110.0^\circ$). Furthermore, the structure contains a single crystallographically unique Sr²⁺ cation, which is surrounded by ten oxygen atoms ($d(\text{Sr}-\text{O}) = 260 - 274$ pm) as tetracapped trigonal prism. Seven of these oxygen atoms belong to [MnO₄]⁻ tetrahedra, whereas the remaining three are part of water molecules H₂O_{3w} forming a triangular face of the [SrO₁₀] polyhedron. The structure is further stabilized by strong O_{3w}-H \cdots O hydrogen bonds ($d(\text{H}\cdots\text{O}) = 232 - 270$ pm) connecting the permanganate anions with each triangular face formed by the water of hydration at the Sr²⁺ cations, without breaking the cubic symmetry of the room-temperature structure with $a = 964.19(7)$ pm [2].

References

- [1] A. Ferrari, A. Braibanti, G. Bigliardi, A. M. Lanfredi: *Acta Crystallogr.* **1966**, 21, 681.
 [2] H. Henning, J. M. Bauchert, M. Conrad, Th. Schleid: *Z. Naturforsch.* **2017**, 72 b, 555.

Figure 1

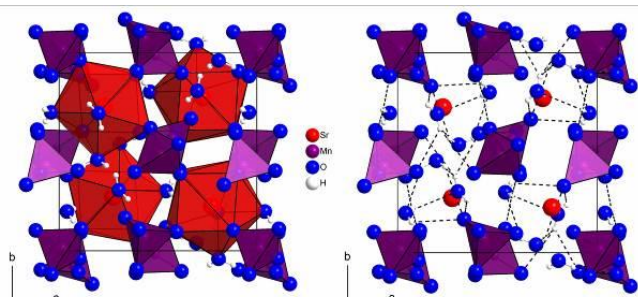


Figure 1. View at the extended unit cell of strontium permanganate trihydrate (left) and its hydrogen-bond system (right).

P035

New Ca/Mg/Zn intermetallics of the intergrowth family of $Ba_2Li_{4.2}Al_{4.8}$ (1a)/ Th_6Mn_{23} (1b)/ $EuMg_{5+x}$ (1c)-type structures.K. Köhler¹, C. Röhr¹¹Albert-Ludwigs-Universität Freiburg, Institut für Anorganische und Analytische Chemie, Freiburg i. Br., Germany

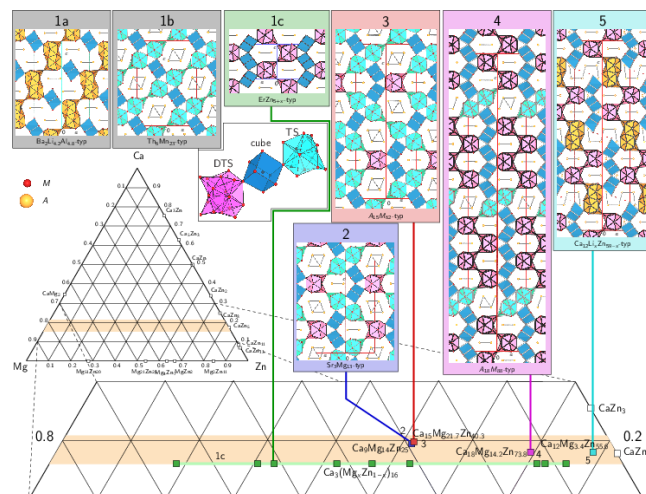
The complex structures of intermetallics $A^II_xM_y$ such as e.g. alkaline-earth zincides ($M=Zn$) are usually described using the connection of A or M centered polyhedra. However, the results of bandstructure calculations (e.g. charge distributions, b.c.p.s) show, that the division into A cations and M polyanion are more appropriate [1-3]. The resulting polyanion contains $[M_4]$ tetrahedra, which are fused to form larger units such as e.g. tetrahedra stars (TS in fig. 1) and double TS (DTS) [2]. In some cases M centered cubes occur as additional structure elements within the M anion. Finally the large AM_x cation coordination polyhedra and the fused M polyhedra tile the space.

Ternary intermetallic compounds $A_mM_nM'_o$ of the title family formed between one of the heavier alkaline-earth metals Ca, Sr, or Ba (A) and Li/Zn and Li/Al respectively (M/M') show a remarkable series of related structures at an A/M ratio between 3.8 and 5.3 (fig. 1) [2,3]. They can be arranged into an intergrowth series deduced from the three structure types $Ba_2Li_{4.2}Al_{4.8}$ (1a) [2], Th_6Mn_{23} (1b) and $EuMg_{5+x}$ (1c). Five further structures can be derived from these: the hexagonal structures of $Sr_9Li_{17.5}Al_{25.5}$ [2], $Ca_{15}Li_xZn_{75-x}$ [3] and Sr_3Mg_{13} (2) [4], the rhombohedral structure of $Ca_{12}Li_xZn_{59-x}$ (5) [3] and $Ca_6Li_xAl_{23-x}$ [2], the latter as a representative for the cubic Th_6Mn_{23} basis type.

In the system Ca/Mg/Zn (cf. also [5]) two new ternary phases were obtained. The structures of $Ca_{15}Mg_{21.7}Zn_{40.3}$ ($A_{15}M_{62}$, 3) and $Ca_{18}(Mg,Zn)_{88}$ ($A_{18}M_{88}$, 4) are closely related to the Th_6Mn_{23} - and the $EuMg_{5+x}$ -type. The structure of 3 ($P6_3/mmc$, $a=938.67(5)$, $c=4062.6(3)$ pm) contains one $EuMg_{5+x}$ and two Th_6Mn_{23} building units with an almost complete Mg/Zn order within the M positions. The structure of 4 ($R-3m$, $a=915.71(5)$, $c=8021.9(6)$ pm) can similarly be described as an arrangement of four $EuMg_{5+x}$ and one Th_6Mn_{23} motives. Different from 3, most of the M positions herein are statistically occupied by Mg and Zn. Unfortunately, disorder remains along the $0,0,z$ line intersecting the centers and common corners of the linked cubes; for fully centered cubes, the ideal composition of 4 is $A_{18}M_{87}$.

- [1] M. Schwarz, M. Wendorff, C. Röhr, *Z. Kristallogr.* **232**, 515 (2017).
 [2] U. Häussermann, M. Wörle, R. Nesper, *J. Alloy. Comp.* **446**, 173 (2007).
 [3] Q. Lin, R. Zhu, G. J. Miller, *Inorg. Chem.* **55**, 5041 (2016).
 [4] J. Erassme, H. Lueken, *Acta Crystallogr.* **43B**, 244 (1987).
 [5] K. Köhler, C. Röhr, *Z. Anorg. Allg. Chem.*, accepted.

Figure 1



P036

The impact of replacements in anion and cation sublattices on optical properties of calcium orthovanadate single crystal

E. Dunaeva¹, L. Ivleva¹, I. Voronina¹, M. Doroshenko¹, A. Papashvili¹¹Russian Academy of Sciences, Prokhorov General Physics Institute of, Moscow, Russian Federation

Introduction.

At the current stage of information technologies development of new systems for controlling laser radiation and information flows is in interest. Particularly, great attention is attracted to compact, chemically and thermally stable solid-state nonlinear optical materials. Among them calcium orthovanadate is a very promising material as multifunctional laser-host, nonlinear-optical and ferroelectric medium. Its partially disordered structure gives wide possibilities to alter its characteristics by substitution of the host ions by the ions of rare-earth or transition metals.

Objectives

In the paper we investigate the influence of Tm^{3+} , Ho^{3+} and Mn^{2+} - $5+$ doping on spectroscopic and laser properties of $Ca_3(VO_4)_2$ and consider the possibilities of creation of effective laser-nonlinear medium.

Results

Calcium orthovanadate crystals doped with Tm^{3+} , Ho^{3+} , Mn^{2+} - $5+$ ions of high chemical homogeneity and optical quality were successfully grown by Czochralski method. The general formula of rare-earth-doped calcium vanadate can be written as $Ca_{3-x}R_x(VO_4)_2$, where R is (Tm+ Ho) element. Divalent calcium is replaced by trivalent rare earth ions. Compensation of electroneutrality can be carried out either by vacancies in Ca positions, or by a partial decrease in the formal charge of V^{5+} ions occupying tetrahedral positions.

At Mn doping, the transition-metal ion can take different charges states and introduces into cationic (Ca^{2+}) or anionic (VO_4^{3-}) sublattices: $Ca_{3-y}Mn_{2+y}(V_{1-x}Mn_{5+x}O_4)_2$. Annealing in the air

atmosphere can strongly influence the Mn²⁺/Mn⁵⁺ ratio and, hence, optical properties.

Results of investigations of the optical quality, domain structure, spectroscopic and laser properties of the doped crystals are presented.

Conclusion

The formation conditions of phases of different compositions and properties depending on the doping ions positions in crystal structure are given. The laser action in near and mid-IR ranges was demonstrated.

P037

New transition metal phosphonates obtained by mechanochemistry

I. Akhmetova¹, M. Wilke², F. Emmerling¹

¹Bundesanstalt für Materialforschung und -prüfung, Berlin, Germany

²Paul Scherrer Institute, Villigen, Switzerland

Metal phosphonates are metal-organic compounds consisting of a metal core and a phosphonate ligand. Depending on the nature of the ligand, metal phosphonates appear in different structures covering the range from molecular compounds to three-dimensional networks. Due to their structural diversity, the chemistry of metal phosphonates has gained great interest during the last decades. Metal phosphonates can be used for various applications as gas storage and separation, magnetism, and energy conversion. Especially transition metal phosphonates are promising candidates as electrocatalysts. Mechanochemistry is a versatile approach for green and fast synthesis of pure substances. By milling the reactants, various organic, inorganic, and metal-organic compounds can be obtained in high yields. Here, we present the synthesis of different new metal phosphonates obtained by grinding of metal acetates with respective phosphonic acids. By varying the ratio of the reactants, we are able to determine the composition of the final products. The addition of small amounts of liquid to the grinding process tends to increase the product's crystallinity. The crystal structures of the new compounds were determined from powder X-ray data.

[1] H. Kulla, S. Haferkamp, I. Akhmetova, M. Rollig, C. Maierhofer, K. Rademann, F. Emmerling, *Angew. Chem. Int. Edit.* **2018**, *57*, 5930.

[2] M. Wilke, I. Akhmetova, K. Rademann, F. Emmerling, *J. Mater. Sci.* **2018**, *53*, 13733-13741.

[3] I. Akhmetova, K. Schütjajew, M. Wilke, A. Buzanich, K. Rademann, C. Roth, F. Emmerling, *J. Mater. Sci.* **2018**, *53*, 13390-13399.

P038

Hexaaquacopper(II) Decachloro-*closo*-decaborate Tetrahydrate: *Jahn-Teller* Distorted Octahedra in $\text{Cu}(\text{H}_2\text{O})_6[\text{B}_{10}\text{Cl}_{10}] \cdot 4 \text{H}_2\text{O}$

K. Bareiß¹, T. Schleid¹

¹University of Stuttgart, Institute for Inorganic Chemistry, Stuttgart, Germany

The previously reported crystal structures of $\text{Mg}(\text{H}_2\text{O})_6[\text{B}_{10}\text{H}_{10}] \cdot 4 \text{H}_2\text{O}$ by *Yisgedu et al.* [1] and $\text{M}(\text{H}_2\text{O})_6[\text{B}_{10}\text{H}_{10}] \cdot 2 \text{H}_2\text{O}$ ($M = \text{Mn}, \text{Fe}, \text{Co}, \text{Ni}, \text{Zn}$) by *Zimmermann* and *Schleid* [2] led to the preparation of perchlorinated analogues, such as the green copper(II) salt $\text{Cu}(\text{H}_2\text{O})_4[\text{B}_{10}\text{Cl}_{10}] \cdot 5 \text{H}_2\text{O}$ by *Kleeberg* and *Schleid* [3]. We now present the synthesis and structural characterization of the blue copper(II) salt $\text{Cu}(\text{H}_2\text{O})_6[\text{B}_{10}\text{Cl}_{10}] \cdot 4 \text{H}_2\text{O}$ crystallizing in the monoclinic space group $P2_1/m$ with $a = 854.89(5)$ pm,

$b = 1711.74(9)$ pm, $c = 927.38(5)$ pm and $\beta = 106.617(3)^\circ$ for $Z = 2$. The crystal structure contains $[\text{Cu}(\text{H}_2\text{O})_6]^{2+}$ octahedra that are connected by extra crystal-water molecules to form chains along the a -axis (Figure 1). The charge balance is fulfilled by $[\text{B}_{10}\text{Cl}_{10}]^{2-}$ cluster anions featuring typical B–B bond lengths of 167 – 168 pm to the lids and 179 – 181 pm inside the square antiprism as well as B–Cl distances of 179 – 181 pm, which perfectly fit the values of triclinic $\text{Cu}(\text{H}_2\text{O})_4[\text{B}_{10}\text{Cl}_{10}] \cdot 5 \text{H}_2\text{O}$ [3]. Regarding the hexaaquacopper(II) octahedron, Cu^{2+} is coordinated by three crystallographically different oxygen atoms from water molecules at distances of 195 pm (2x), 205 pm (2x) and 228 pm (2x). This leads to a noticeable *Jahn-Teller* elongation of more than 20 pm, which shows that the *Jahn-Teller* distortion of the $[\text{Cu}(\text{H}_2\text{O})_6]^{2+}$ octahedron in the green $\text{Cu}(\text{H}_2\text{O})_4[\text{B}_{10}\text{Cl}_{10}] \cdot 5 \text{H}_2\text{O}$ is not only caused by the bigger size of the chlorine as compared to the oxygen atoms and can be reproduced by a pure water-coordination sphere leading to the blue copper(II) salt with a higher amount of crystal water and symmetry.

Experimental

In order to prepare decachloro-*closo*-decaborate hydrates of divalent copper, basic copper(II) carbonate was neutralized using an aqueous solution of the acid $(\text{H}_3\text{O})_2[\text{B}_{10}\text{Cl}_{10}]$. The reaction mixture was filtrated and slowly evaporated isothermally in order to obtain the blue copper(II) salt $\text{Cu}(\text{H}_2\text{O})_6[\text{B}_{10}\text{Cl}_{10}] \cdot 4 \text{H}_2\text{O}$ or the green $\text{Cu}(\text{H}_2\text{O})_4[\text{B}_{10}\text{Cl}_{10}] \cdot 5 \text{H}_2\text{O}$ representative.

References:

[1] T. B. Yisgedu, X. Chen, H. K. Lingam, Z. Huang, A. Highley, S. Maharrey, R. Behrens, S. G. Shore, J.-C. Zhao, *J. Phys. Chem.* **2011**, *C 115*, 11793.

[2] L. W. Zimmermann, Th. Schleid, *Z. Kristallogr.* **2013**, *228*, 558.

[3] F. M. Kleeberg, Th. Schleid, *Z. Kristallogr.* **2017**, *Suppl. 37*, 107.

Figure 1

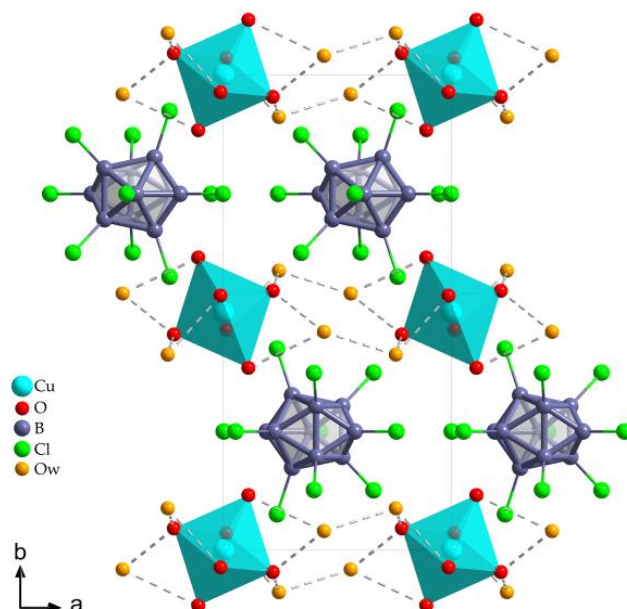


Figure 1: Extended unit cell of $\text{Cu}(\text{H}_2\text{O})_6[\text{B}_{10}\text{Cl}_{10}] \cdot 4 \text{H}_2\text{O}$ showing isolated $[\text{B}_{10}\text{Cl}_{10}]^{2-}$ anions as bicapped square antiprisms and chains $1\text{D}-[\text{Cu}(\text{H}_2\text{O})_6](\text{H}_2\text{O})_{4/2}^{2+}$ along $[100]$ consisting of hexaaquacopper(II) octahedra and additional crystal-water molecules.

P039

Structural Diversity of Hybrid Lead Bromide Perovskites with Pyridine and Diazines

M. Krummer¹, M. Daub¹, B. Zimmermann¹, H. Hillebrecht¹¹Albert-Ludwigs-Universität Freiburg, Institut für Anorganische und Analytische Chemie, Freiburg i. Br., Germany

Organic-inorganic hybrid lead perovskites possess properties which are promising for applications in the field of optoelectronics.^[1] A variety of structures emerge depending on the implemented cations.^[2] The aim of this investigation was the synthesis and characterization of lead bromide perovskites with regard to possible applications in optoelectronic devices, whereby pyridinium (*Py*), pyridazinium (*Pyrd*), pyrimidinium (*Pyrm*) and pyrazinium (*Pyrz*) were used as cations.

PyPbBr₃ (*Pnma*, $a = 7.755(6)\text{\AA}$, $b = 9.564(5)\text{\AA}$, $c = 28.670(47)\text{\AA}$) is composed of 1D chains of face-sharing octahedra oriented alongside the [010]-axis. The *APbBr₃* analogues of pyrazinium (*P2_{1/n}*, $a = 16.167(3)\text{\AA}$, $b = 7.968(0)\text{\AA}$, $c = 16.199(4)\text{\AA}$, $\beta = 113.21(5)^\circ$) and pyridazinium (*P2_{1/n}*, $a = 16.517(4)\text{\AA}$, $b = 7.884(3)\text{\AA}$, $c = 16.565(9)\text{\AA}$, $\beta = 121.2440(10)^\circ$) are isostructural to each other. The structure contains distorted face-sharing *PbBr_{6/2}*-octahedron chains along the [010]-axis, similar to *BaNiO₃*.

PyrmPbBr₃ (*P-1*, $a = 4.3790(5)\text{\AA}$, $b = 10.3158(12)\text{\AA}$, $c = 11.7185(13)\text{\AA}$, $\alpha = 107.515(9)^\circ$, $\beta = 96.786(9)^\circ$, $\gamma = 90.832(9)^\circ$) on the other hand crystallizes as a distorted variant of the *NH₄CdCl₃*-type in which the featured motif is chains of edge-sharing double octahedra.

The structure of *Pyrm₄Pb₃Br₁₀* (*C2/c*, $a = 23.4621(6)\text{\AA}$, $b = 8.3293(2)\text{\AA}$, $c = 21.8599(8)\text{\AA}$, $\beta = 121.2440(10)^\circ$) contains, analogous to *BaRuO₃*, chains of three face-sharing octahedra, which are connected over four edges forming layers in the (001)-plane.

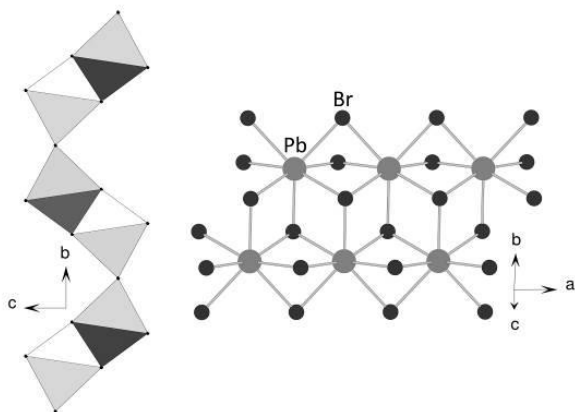
PyPb₂Br₅ (*P2_{1/m}*, $a = 4.1019(8)\text{\AA}$, $b = 15.263(3)\text{\AA}$, $c = 10.554(2)\text{\AA}$, $\beta = 93.29(3)^\circ$) by comparison shows a unique behavior by building 2D zigzag layers along the (001)-plane, in which lead is seven-fold coordinated by bromide.

Figure 1: Polyhedra in *PyPb₂Br₅* viewed along the [100]-axis (left) and the coordination of *Pb²⁺* in *PyPb₂Br₅* (right).

[1] J. S. Manser, J. A. Christians, P. V. Kamat, *Chem. Rev.* **2016**, *116*, 12956

[2] L. Mao, C. C. Stoumpos, M. G. Kanatzidis, *J. Am. Chem. Soc.* **2018**. DOI:10.1021/jacs.8b10851

Figure 1



P040

Synthesis and characterization of self-supported SOD-LTN layers for membrane applications

I. Peschke¹, J. C. Buhl¹¹Leibniz Universität Hannover, Institut für Mineralogie, Hannover, Germany

Introduction

Besides their applications as sorbents, ion exchange materials, catalysts or molecular sieves, recent developments in zeolite research focus on membrane technologies (e.g. [1, 2]). Zeolite-type materials like sodalite (SOD) or Linde-type N (LTN) with their 3-dimensional framework structures providing uniform pore systems at molecular scale allow for technical use as desiccants or in gas separation techniques. LTN adsorbs H₂O preferentially over N₂ or O₂, and was proposed as desiccant for such gas streams [3]. SOD membranes were e.g. successfully used to desalinate aqueous solutions [4].

Usually, syntheses of zeolite membranes require several steps and utilization of support materials. Here, a simple synthesis technique of SOD-LTN membranes without necessity of support materials is presented.

Objectives

The study aims at the clarification of LTN-SOD phase relationships to obtain single phase self-supported zeolite layers for membrane applications by recycling of Si-rich waste material under isostatic-isothermic conditions.

Results

The Si-rich waste material, a filter residue, consists of nm-sized (~350 nm) amorphous powder with > 90 wt.-% SiO₂, confirmed by DLS, XRD and XRF. Syntheses with Si:Al ≈ 1 under open alkaline (7 M NaOH) hydrothermal conditions ($T = 373\text{ K}$, $4 \leq t \leq 72\text{ h}$) result in two phase products of SOD + LTN, confirmed by FTIR and XRD (Fig. 1). Elongation of *t* promotes SOD crystallization. LTN phase fractions increase with shorter *t*, although physically stable layers only form at $t \geq 8\text{ h}$. A pure $[\text{Na}_8(\text{H}_2\text{O})_2(\text{OH})_2][\text{AlSiO}_4]_6$ SOD layer was obtained at $t = 144\text{ h}$ ($P4\bar{3}n$, $a = 890.84(3)\text{ pm}$). The layer thickness is ~250 μm as determined by SEM. SOD crystallizes with spherulitic morphology and can clearly be distinguished from the angular to cubic shaped LTN crystals.

Conclusion

Self-supported SOD-layers can be obtained by simple experimental design. At 373 K SOD is thermodynamically more stable, additionally growing from LTN crystals by recrystallization.

[1] J. Caro, M. Noack, *Micropor. Mesopor. Mat.* **15** (2008) 215-233.

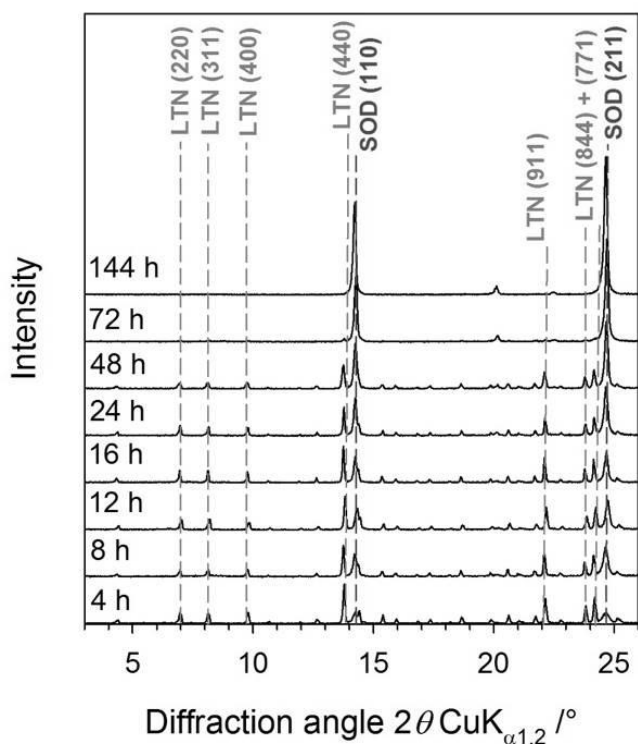
[2] N. Kosinov, J. Gascon, F. Kapteijn, E.J.M. Hensen, *J. Membrane Sci.* **499** (2016) 65-79.

[3] N. Acara, US Patent Office 3,414,602 (1968).

[4] S. Khajavi, J.C. Jansen, F. Kapteijn, *J. Membrane Sci.* **326** (2010) 52-57.

Figure 1: Low diffraction angle area of SOD-LTN XRD patterns with different synthesis times together with Miller indices of selected reflections.

Figure 1



P041 Optical properties of SnS2 synthesized by a facile chemical route

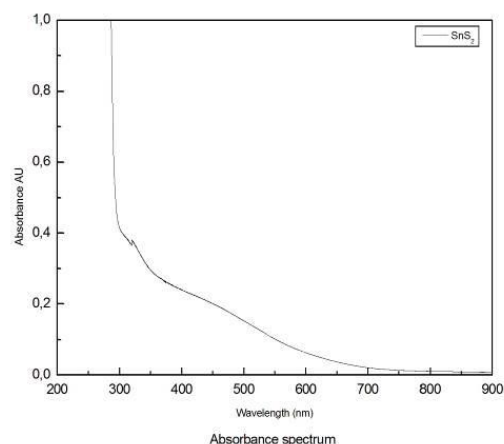
K. Ihadjaren^{1,2}, A. Souici^{1,2}

¹Abderrahmane Mira-Bejaia, Physics, Bejaia, Algeria

²University of Abderrahmane Mira, Physics, Bejaia, Algeria

In recent decades, the nanomaterial science has made surprising progress. Owing to their new physicochemical properties, induced by the effect of size, various fields of applications are today possible particularly in medicine, optoelectronic, photovoltaic...etc. specifically tin disulfide (SnS₂) has a great potential for use in a several range of applications then attracted much attention. The aim of this work is the synthesis as well as the investigation of optical and structural properties of SnS₂ nanoparticles. Great effort has been devoted to the facile synthesis and characterization of nanomaterials due to their properties and for synthesis method, chemical route is used in presence of CTAB molecule as stabilizing agent. The quantum size effect on optical properties of these nanoparticles is followed during their growth by UV-visible spectrophotometry. The crystalline structures were analyzed by XRD diffraction characterization of SnS₂ nanoparticles in presence of CTAB and the size is around of 9 nm. These results show that the organic molecules play a crucial effect on the optical properties and morphology of nanoparticles.

Figure 2



P042 Synthesis and Characterization of the Hydroxoferrates(III) A₂Fe₂O₃(OH)₂ (A = K, Rb, Cs)

R. Albrecht¹, J. Hunger¹, T. Doert¹, M. Ruck¹

¹Technische Universität Dresden, Dresden, Germany

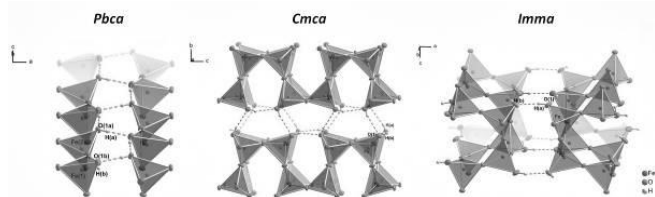
Hydroxoferrates with elements of the first two main groups of the periodic table represent a scarcely explored branch of the otherwise so manifold iron chemistry. Na₅Fe^{II}O₃OH^[1], synthesized in a sodium hydroxide flux e.g., is the only known quaternary hydroxoferrate of an alkaline metal. Implying the recently developed hydroflux method^[2] which uses almost equimolar amounts of alkaline metal hydroxides and water, we were able to synthesize the three new alkali metal hydroxoferrates A₂Fe₂O₃(OH)₂ (A = K, Rb, Cs) as yellowish green plates or rods.

The hydroxoferrates crystallize in orthorhombic space groups: K₂Fe₂O₃(OH)₂ adopts a structure in space group *Pbca* with lattice parameters of $a = 831.8(1)$ pm, $b = 1732.8(1)$ pm, $c = 843.6(1)$ pm, whereas Rb₂Fe₂O₃(OH)₂ and Cs₂Fe₂O₃(OH)₂ are dimorphic. Plate-like crystals of Rb₂Fe₂O₃(OH)₂ and Cs₂Fe₂O₃(OH)₂ crystallizes in *Cmca* (lattice parameters $a = 912.7(1)$ pm, $b = 1697.9(1)$ pm, $c = 850.0(1)$ pm for A = Rb and $a = 945.2(1)$ pm, $b = 1716.5(1)$ pm, $c = 871.0(1)$ pm for Cs), for rod-like crystals space group *Imma* (lattice parameters $a = 1701.2(1)$ pm, $b = 836.3(1)$ pm, $c = 918.6(1)$ pm for A = Rb and $a = 1742.9(1)$ pm, $b = 845.8(1)$ pm, $c = 953.3(1)$ pm for Cs) is found. All three structures consist of alternating layers of alkali metal ions and hydroxoferrate anions, the latter built up by one-dimensional (1D) chains of corner sharing [FeO₃OH]⁴⁻ tetrahedra. These tetrahedra are connected to adjacent 1D chain via hydrogen bonds forming a 2D network. The hydroxide groups are located in cavities, which are formed due to lateral shifts of the 1D chains. K₂Fe₂O₃(OH)₂ forms hydrogen bonds along these cavity, whereas the hydrogen bonds in the *Cmca* modification of A₂Fe₂O₃(OH)₂ (A = Rb, Cs) extend between the hydroxoferrate layers. In the *Imma* modification hydrogen bonds are also found between the hydroxoferrate layers. Thermal analysis revealed K₂Fe₂O₃(OH)₂ to decomposes at 260 °C, whereas the decomposition of the rubidium and cesium hydroxoferrates starts around 350 °C. The higher thermal stability of the latter is probably due to additional H-bond connecting the hydroxoferrate layers.

Figure: Crystal structure of the alkali metal hydroxoferrates in their modifications (alkali metal atoms not shown) indicating the [FeO₃OH]⁴⁻ tetrahedra connected by hydrogen bonds.

Literature:

- [1] D. E. Gheorghie, et al., *Z. anorg. allg. Chem.* **2012**, 638, 2087–2092.
 [2] W. M. Chance, et al., *Inorg. Chem.* **2013**, 52, 11723–11733.

Figure 1**P043****Crystal structure of 2-Ethylanilinium Dihydrogenophosphite**
C₈H₁₂NH₂PO₃A. Kheireddine¹, M. Belhabra², H. Hamdi Ben Yahia¹, S. Belaouad²¹QEERI-HBKU-QF, Energy Storage, DOHA, Qatar²Hassan II University of Casablanca, Laboratory of chemistry and physics of materials, Departement of Chemistry, Casablanca, Morocco

The 2-Ethylanilinium Dihydrogenophosphite was prepared by the action of Phosphorous acid H₃PO₃ on an aqueous solution of 2-Ethylaniline C₈H₁₁N. C₈H₁₂N.H₂PO₃ crystallizes in the triclinic system with centric space group P-1. Its unit-cell dimensions are a = 4.6042 (2) Å, b = 10.3863 (4) Å, c = 10.7848 (5) Å, α = 90.115 (3)°, β = 97.878 (3)°, γ = 98.462 (3)°, Z = 2 and V = 505.18 (4) Å³. The crystal structure was refined down to R = 0.0362, wR = 0.1007 for 1989 reflections satisfying criterion I ≥ 2σ (I).

P044**Low temperature properties of lead stannate, Pb₂SnO₄**W. Morgenroth¹, D. Spahr¹, M. Avalos-Borja², M. Tolkiehn³, C. Paulmann⁴, B. Winkler¹¹Goethe-Universität Frankfurt am Main, Frankfurt am Main, Germany²Instituto Potosino de Investigacion Cientifica y Tecnologica, Division de Materiales Avanzados, San Luis Potosí, Mexico³DESY, Hamburg, Germany⁴Universität Hamburg, Mineralogisch-Petrographisches Institut, Hamburg, Germany

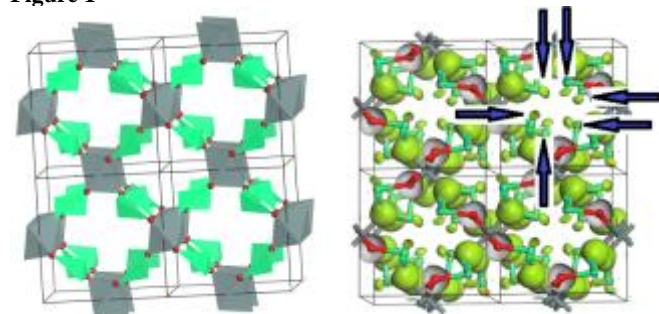
In contrast to other ortho-stannates, such as Ca₂SnO₄, Ba₂SnO₄ or Sr₂SnO₄, the structure of lead stannate, Pb₂SnO₄ (Fig. 1, [1]) is characterized by channels aligned parallel to the c-axis. Crystal chemical considerations and DFT-based calculations point toward the presence of a stereochemically active lone electron pair localized on the lead atom.

In order to benchmark electron density distributions obtained from DFT calculations, we carried out temperature dependent single crystal X-ray diffraction experiments at the recently commissioned Chemical Crystallography Beamline P24 at PETRA III. The data analysis is currently in progress and results will be presented at the conference.

The authors gratefully acknowledge financial support by BMBF (project 05K16RFB), DFG (Wi1232) and Conacyt (grant FC-2015-2-947). We acknowledge DESY (Hamburg, Germany), a member of the Helmholtz Association HGF, for the provision of experimental facilities. Parts of this research were carried out at PETRA III.

- [1] Gavarrri et al., *J. Solid State Chem.*, 36:81-90, 1981.

Fig. 1 Structure of Pb₂SnO₄, in which edge-sharing SnO₆ octahedra form chains. The open voids in the structure are occupied by stereochemically active lone electron pairs (arrows), visualised in an electron density difference map obtained from DFT calculations.

Figure 1**P045****Two New Strontium Nitridogermanates: Sr₄[GeN₄] and Sr₁₇Ge₆N₁₄**L. Link¹, Y. Lin¹, R. Niewa¹¹University of Stuttgart, Institute for Inorganic Chemistry, Stuttgart, Germany

Binary nitrides of main group elements have industrial applications as semiconductors and hard materials, while structures and properties of ternary compounds are currently explored [1]. In nitrogen-rich systems containing germanium, nitridogermanates with tetrahedral [Ge^{IV}N₄]⁸⁻ or trigonal planar [Ge^{IV}N₃]⁵⁻ units such as Ca₄[GeN₄] [2] and Ba₉[GeN₃]₃N [3] tend to form. Known nitridogermanate germanides, such as Sr₁₁Ge₄N₆ [4] or Sr₃Ge₂N₂ [5] contain kinked [Ge^{IV}N₂]⁴⁻ units next to isolated Ge⁴⁻ anions or infinite Ge²⁻ chains, respectively.

Synthesis was carried out in sealed niobium ampoules using alkali metals as flux. Sodium was then removed by dissolution in liquid ammonia. Using this method, single crystals of two new strontium nitridogermanates were grown from strontium nitride, germanium and sodium azide in liquid sodium.

Sr₄[GeN₄] is isostructural to Ca₄[GeN₄], but appears black, while Ca₄[GeN₄] is reported to be orange and transparent. Germanium is coordinated by only slightly distorted nitrogen tetrahedra, whereas the environment of strontium is more irregular.

Black Sr₁₇Ge₆N₁₄, more precisely written as Sr₁₇[GeN₄]₂[GeN₃]₂[Ge]₂, contains isolated, slightly distorted tetrahedral [Ge^{IV}N₄]⁸⁻ and trigonal planar [Ge^{IV}N₃]⁵⁻ units, as well as isolated Ge⁴⁻ ions. Strontium is coordinated by mixed, irregular polyhedra of germanide and nitride ions. The structure is unique in containing germanium in oxidation states 4 as well as -4. It is also the only compound known as of yet to feature both [Ge^{IV}N₄]⁸⁻ and [Ge^{IV}N₃]⁵⁻ units.

In both compounds, strontium atoms have coordination numbers 5–6 and are coordinated by both vertices and edges of nitridogermanate units.

References:

- [1] J. Häusler, W. Schnick; *Chem. Eur. J.*; 2018; 24; 11864-11879.
 [2] S. J. Clarke, F. J. DiSalvo; *Inorg. Chem.*; 2000; 39; 2631-2634.
 [3] P. D. Gon, F. J. DiSalvo; *Bull. Korean Chem. Soc.*; 2008; 29; 2413-2418.

- [4] Z. A. Gal, J. Clarke; Chem. Commun.; 2005; 2005; 728-730.
 [5] S. J. Clarke, G. R. Kowach, F. J. DiSalvo; Inorg. Chem.; 1996; 35; 7009-7012.

P046

New Solvate Complexes $[\text{Be}(\text{Sol}v)_4]\text{I}_2$ of Beryllium Iodide with Polar Aprotic Solvents

C. Hoch¹, T. Hohl¹, T. Sinn¹

¹LMU München, Department Chemie, München, Germany

Introduction

In the last years, amalgams of less noble metals have been prepared by electrocrystallization [1]. For this, the iodides of the metals are dissolved in an aprotic, polar solvent, e.g. N,N-dimethylformamide (DMF). DMF complex solutions normally are readily reduced at a mercury cathode to form the respective amalgams. Only $[\text{Be}(\text{DMF})_4]^{2+}$ shows such a high stability/inertness that its electrochemical decomposition affords an overvoltage high enough to decompose the solvent rather than the complex.

Objectives

Several candidate solvents for $[\text{Be}(\text{Sol}v)_4]\text{I}_2$ complex salts were tested for stability. From their crystal structures and Raman spectra the strength of the Be–D bonding (D = donor atom) can be estimated.

Results

The complex salts $[\text{Be}(\text{DMF})_4]\text{I}_2$, $[\text{Be}(\text{NMP})_4]\text{I}_2$ and $[\text{Be}(\text{Pyr})_4]\text{I}_2$ (NMP = N-methylpyrrolidone, Pyr = pyridine) crystallize with isolated tetrahedral $[\text{Be}(\text{Sol}v)_4]^{2+}$ complex units ($[\text{Be}(\text{DMF})_4]\text{I}_2$: space group $P2_1/c$ (no. 14), $a = 12.700(4)$ Å, $b = 11.6893(17)$ Å, $c = 15.475(3)$ Å, $\beta = 94.64(3)^\circ$, $Z = 4$; $[\text{Be}(\text{NMP})_4]\text{I}_2$: space group $Pbca$ (no. 61), $a = 13.941(5)$ Å, $b = 15.754(3)$ Å, $c = 24.634(7)$ Å, $Z = 1$; $[\text{Be}(\text{Pyr})_4]\text{I}_2$: space group $C2/c$ (no. 15), $a = 17.8799(13)$ Å, $b = 7.6174(5)$ Å, $c = 18.2611(14)$ Å, $\beta = 113.508(4)^\circ$, $Z = 4$). Their point symmetry is low in all cases, however, the complexes show only small deviation from T_d symmetry broken only by rotation of the four complexing solvent molecules towards each other. The Be–O/Be–N contacts are 161.3(3)–162.3(3) pm (DMF), 159.9(10)–161.4(11) pm (NMP) and 173.2(3)–173.6(3) pm (Pyr).

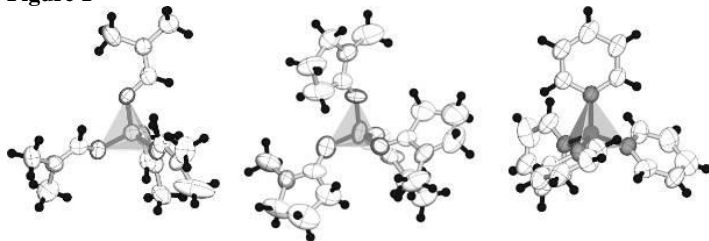
Conclusion

By analyzing the crystal structures of new solvent complexes $[\text{Be}(\text{Sol}v)_4]\text{I}_2$ parameters can be identified in order to choose a polar solvent suitable for electrocrystallization reactions towards a beryllium amalgam.

- [1] F. Tambornino, J. Sappl, F. Pultar, T. M. Cong, S. Hübner, T. Gifftthaler, C. Hoch, *Inorg. Chem.* **55** (2016), 11551-11559.

Figure 1: Complex cations $[\text{Be}(\text{DMF})_4]^{2+}$ (left), $[\text{Be}(\text{NMP})_4]^{2+}$ (center) and $[\text{Be}(\text{Pyr})_4]^{2+}$ (right).

Figure 1



P047

Synthesis and Crystal Structure of Three New Lithium Gallides

J. Sappl¹, C. Hoch¹

¹LMU München, Department Chemie, München, Germany

Introduction

In search of new, highly polar intermetallic phases we have focused on the binary system Lithium - Gallium.

Objectives

By combining thermoanalytical and synthetic studies, we have established three new binary Li-Ga phases on the Gallium-rich side of the Li-Ga phase diagram. Their crystal structures were characterized based on single crystal and powder diffraction data.

Results

The Ga-richest phase is LiGa 6 . It crystallizes in a new structure type with space group R3c (no. 167, $a = 6.1851(8)$ Å, $c = 23.467(4)$ Å, $Z = 6$). Peritectic decomposition occurs at ca. 80 °C, in accordance with previous studies predicting the existence of this phase on the basis of thermoanalytical measurements [1]. Its crystal structure contains Li-centered [Ga 18] polyhedra (Fig. 1, left). The second new phase is LiGa 2 , crystallizing in a new structure type with space group Cmce (no. 64, $a = 8.51953(4)$ Å, $b = 14.44163(7)$ Å, $c = 15.29226(7)$ Å, $Z = 36$). Its crystal structure contains Li-centered [Ga 12] icosahedra (Fig. 1, center), interconnected by tetravalent Ga atoms. The peritectic decomposition temperature here is at ca. 332 °C, close to the decomposition temperature of the third new phase, Li 43 Ga 76-x , at 366 °C. It crystallizes with space group P6 3 mc (no. 186, $a = 13.7700(19)$ Å, $c = 23.250(5)$ Å). Its crystal structure is built from groups of three [Ga 10] icosahedra with two cut corners and linked by a [Ga 2] unit. Further Ga atoms form Li-centered [Ga 16] Frank-Kasper polyhedra (Fig.1, right).

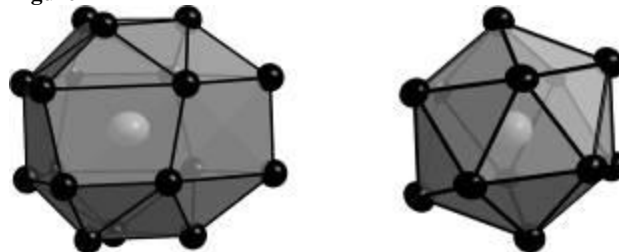
Conclusion

Three new lithium gallides could be prepared and their crystal structures elucidated. Their calculated electronic structures show typical features of polar intermetallics.

- [1] M. Tillard-Charbonnel, C. Belin. C. R. Acad. Sci. Paris., 306 (1988), 1161-1164.

Figure 1: left:[Ga 18] polyhedron occurring in the crystal structure of LiGa 6 , center: [Ga 12] icosahedron from LiGa 2 , right: [Ga 16] polyhedron from Li 43 Ga 76-x . All polyhedra are centered by Li atoms (light gray).

Figure 1



P048

Crystal Structures of Cs_3VO_4 and $\text{Cs}_3\text{VO}_4 \cdot 2\text{H}_2\text{O}$ C. Hoch¹, C. A. Zegarra Solano¹¹LMU München, Department Chemie, München, Germany

Introduction

A series of subvalent oxometalates with composition Cs_9MO_4 , M being a trivalent metal, has been described [1]. Not all trivalent metals, however, form the respective suboxometalates. It is still unclear which crucial points are decisive for phase formation in these systems.

Objectives

Cesium suboxovanadate(III) might be a candidate for a new member of the suboxometalate family. Its synthesis may be realized following the reaction $8 \text{Cs} + 5 \text{Cs}_2\text{O} + \text{V}_2\text{O}_3 \rightarrow 2 \text{Cs}_9\text{VO}_4$.

Results

Cs_3VO_4 , cesium-orthovanadate(V), was prepared from mixtures of cesium, Cs_2O and V_2O_3 or V_2O_5 . Crystals formed within a liquid mixture of cesium suboxides (with V_2O_3) or as a phase-pure powder (with V_2O_5 , space group $Pnma$ (no. 62), $a = 12.5140(3) \text{ \AA}$, $b = 9.0292(2) \text{ \AA}$, $c = 6.66601(2) \text{ \AA}$, $Z = 4$, Rietveld refinement). The dihydrate recrystallized from Cs_3VO_4 powder samples stored under dried paraffin oil as a consequence slow diffusion of humidity into the sample (space group $Cmc2_1$ (no. 36), $a = 14.321(3) \text{ \AA}$, $b = 8.4280(17) \text{ \AA}$, $c = 9.2632 \text{ \AA}$, $Z = 4$, single crystal refinement). Cs_3VO_4 adopts the Cs_3AsO_4 structure type [2], the dihydrate adopts a new acentric structure type. Formation of a vanadate(V) starting from V_2O_3 can only be understood by taking into account that Cs_2O may act as an oxidizing agent. This is due to its thermal decomposition into cesium and cesium hyperoxide which can act as a powerful oxidizing agent: $2 \text{Cs}_2\text{O} \rightarrow 3 \text{Cs} + \text{CsO}_2$; and $2 \text{O}_2^- \rightarrow \text{O}_2 + \text{O}_2^{2-}$ and following reactions.

Conclusion

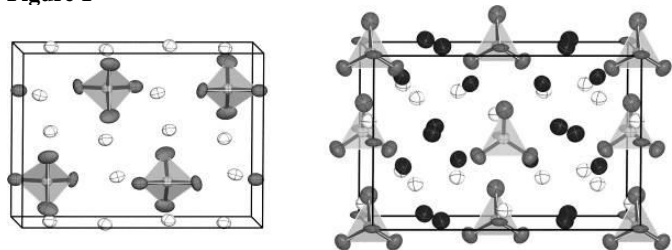
Suboxometalates are thermodynamically instable towards internal redox reactions and towards thermal decomposition. Only when the thermal activation energy necessary for a reaction to suboxometalates is lower than the activation energy of one of the two decomposition pathways, a suboxometalate can be obtained. In the other cases, 'normal' ionic metalates with high metal content are formed. In the utmost cases, the lattice energy of a highly charged orthometalate from soft cations like cesium is very low, and hygroscopic behavior is found.

[1] C. Hoch, J. Bender, A. Wohlfarth, A. Simon, *Z. Anorg. Allg. Chem.* **635** (2009), 1777-1782.

[2] F. Emmerling, M. Idilbi, C. Röhr, *Z. Naturforsch.* **B57** (2002), 599-604.

Figure 1: Projections on the unit cells of Cs_3VO_4 (left, along (001)) and its dihydrate, $\text{Cs}_3\text{VO}_4 \cdot 2\text{H}_2\text{O}$ (right, along (010)), H atoms could not be localized, water-O atoms in dark grey). The orthovanadate(V) anions are drawn as transparent tetrahedra.

Figure 1



P049

Synthesis and characterization of $\text{Pt}_3\text{Cu}_2\text{Sn}$ S. Schellhase¹, W. Morgenroth¹, E. A. Juárez-Arellano², J. Binck¹, N.Tamura³, C. Stan³, A. Barkov⁴, B. Winkler¹¹Goethe-Universität Frankfurt am Main, Institut für Geowissenschaften, Frankfurt am Main, Germany²Universidad del Papalopan, Tuxtepec, Oaxaca, Mexico³ALS, Lawrence Berkeley National Laboratory, Berkeley, CA, United States⁴Research Laboratory for Industrial and Ore Mineralogy, Cherepovets State University, Cherepovets, Russian Federation

Recently, a single mineral grain with composition close to $\text{Pt}_3\text{Cu}_2\text{Sn}$ was found in a placer deposit at the River Bolshoy Khailk deposit in the western Sayans, Russia. After an initial characterization by microdiffraction at the ALS (beam line 12.3.2) we have submitted a request to register this new phase as a new mineral species to Commission on New Minerals and Mineral Names. As this mineral is exceedingly rare, we have begun to synthesize samples in order to enable more detailed studies of the structure and the properties of this first ternary Pt-Cu-Sn compound.

Synthesis were carried out by heating stoichiometric mixtures of the elements either in a furnace or in an electric arc melter. Samples were characterized by powder diffraction, differential scanning calorimetry and SEM/EDX studies. Density functional theory-based model calculations complemented the experimental studies. Currently, we are able to synthesize nearly phase pure samples of $\text{Pt}_3\text{Cu}_2\text{Sn}$ accompanied by a minor impurity phase (Cu_5Sn_4 [1]). Rietveld refinement of $\text{Pt}_3\text{Cu}_2\text{Sn}$ in space group $P4/mmm$, with Pt on 0,0,0 and disordered Cu and Sn on $1/2, 1/2, 1/2$, was successful. The lattice parameters obtained here are $a = 2.8221(1) \text{ \AA}$, $c = 3.6364(1) \text{ \AA}$ and $V = 28.96(1) \text{ \AA}^3$, in good agreement with values on the natural sample and the results of the DFT calculations. Further properties are currently being determined and will be presented at the conference.

Financial support from the German BMBF (project 05K16RFB) and the German Science Foundation (WI1232) is gratefully acknowledged.

[1] Lindin, S.; Larsson, A.K.; *Journal of Solid State Chemistry* **118**, 313-322 (1995).

P050

An unusual interaction revisited: Slipped $\text{Sn}^{\text{II}}-\pi$ -arene bonding in isodurene solvated $[\text{SnCl}][\text{MCl}_4]$ ($M = \text{Al}, \text{Ga}$)J. Merkelbach¹, W. Frank¹¹Heinrich-Heine-Universität Düsseldorf, Institut für Anorganische Chemie und Strukturchemie, Düsseldorf, Germany

The electrostatic character of π -arene interactions with main group metal cations is well known and was shown within a broad variety of complexes throughout the years. In recent times these interactions gained importance in understanding biochemical systems and processes like ion channels^[1] and protein folding^[2]. A deeper look into the specifics of these systems could be crucial to modify and utilize cation- π interactions. By adding two new compounds to the already known class of arene solvated $[\text{SnCl}][\text{MCl}_4]$ salts (with $M = \text{Al}, \text{Ga}$) we aim to further proof the previously claimed strong correlation between arene basicity and Sn-arene bond valence as well as the intrinsic nature of slipped π -bonding.^[3]

Colourless crystals of the isotopic compounds (space group type $P-1$) $[\text{1,2,3,5}-(\text{CH}_3)_4\text{C}_6\text{H}_2\text{SnCl}][\text{MCl}_4]$ ($\mathbf{1}$: $M = \text{Al}$ with

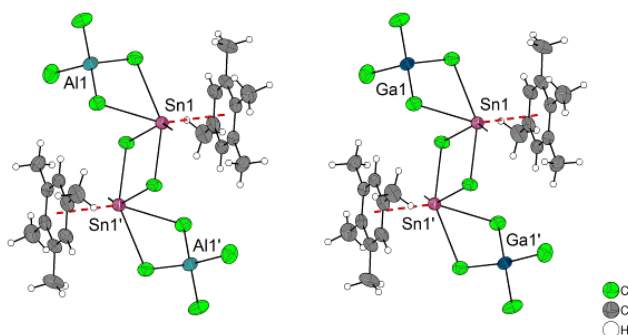
$a = 8.4548(3) \text{ \AA}$, $b = 9.2618(3) \text{ \AA}$, $c = 11.2611(4) \text{ \AA}$,
 $\alpha = 84.858(3)^\circ$, $\beta = 72.413(3)^\circ$, $\gamma = 90.306(3)^\circ$, $Z = 2$;
 $R_1 = 0.0236$, $wR_2 = 0.0949$, 4504 reflection and 159 parameters;
2: $M = \text{Ga}$ with $a = 8.4443(4) \text{ \AA}$, $b = 9.2521(5) \text{ \AA}$,
 $c = 11.2835(6) \text{ \AA}$, $\alpha = 84.548(4)^\circ$, $\beta = 72.700(4)^\circ$, $\gamma = 90.159(4)^\circ$,
 $Z = 2$; $R_1 = 0.0315$, $wR_2 = 0.0680$, 3836 reflection and 158
 parameters) were obtained from solutions of isodurene and
 $[\text{SnCl}][\text{MCl}_4]$ in chlorobenzene. The unit cells contain dimers of
1/2 with a central planar $\text{Sn}_2\text{Cl}_2^{2+}$ -fragment. Three additional Sn–
 Cl-contacts are present to neighbouring tetrachloridometallate
 anions. An isodurene molecule in a π -coordinated mode with a
 pronounced ring slippage completes the Sn^{II} coordination sphere.
 The strength of the Sn^{II} –arene interaction is between that of the
 corresponding mesitylene and durene derivatives.

Figure 1. Dimers of **1** (left) and **2** (right) (50 % probability ellipsoids).

References:

- [1] M. E. Weber, E. K. Elliott, G. W. Gokel, *Org. Biomol. Chem* **2006**, *4*, 83.
 [2] M. M. Gromiha, M. Suwa, *Int. J. Biol. Macromol.* **2005**, *35*, 55.
 [3] W. Frank, *Z. Anorg. Allg. Chem.* **1990**, 585, 121.

Figure 1



P051

Serendipitous Formation of Single-Crystalline $\text{Mg}_2[\text{SiS}_4]$

P. Djendjur¹, T. Schleid¹

¹University of Stuttgart, Institute for Inorganic Chemistry, Stuttgart, Germany

Ternary alkaline-earth metal chalcogenides with elements from the fourth group of the periodic table have the general formula AE_2MCh_4 ($AE = \text{Mg, Ca}$; $M = \text{Si, Ge, Sn}$; $Ch = \text{O, S, Se}$) and are already known since 1960 [1, 2]. The oxides of this series were even described at the beginning of the last century [3, 4]. With few exceptions, they build structures that are isotypic to the classical mineral *olivine*, containing isolated $[MCh_4]^{4-}$ tetrahedra ($M = \text{Si, Ge, Sn}$; $Ch = \text{O, S, Se}$). However, most of the characterization for these compounds never got beyond the point of determining the unit-cell parameters by X-ray powder diffraction methods.

The oxidation of magnesium metal with sulfur and potassium azide in the presence of elemental iodine and caesium iodide as fluxing agent (molar ratio: 10:6:4:3) in evacuated silica ampoules at 900 °C for 10 days lead to the formation of pale pink, plate-like single crystals of $\text{Mg}_2[\text{SiS}_4]$ as a by-product after reaction with the container material SiO_2 . The corresponding diffraction data of this substance could be obtained and refined successfully for an up-to-date crystal-structure analysis.

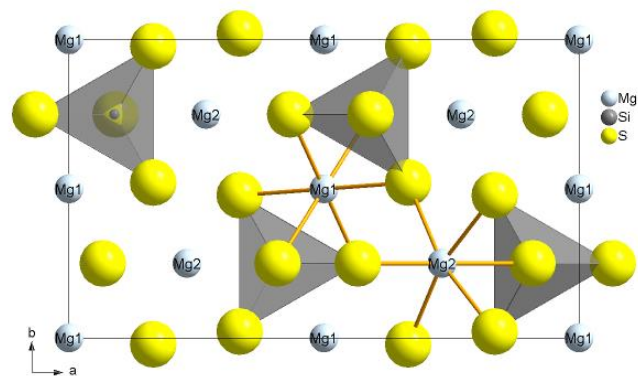
This magnesium thiosilicate crystallizes in the orthorhombic space group $Pnma$ with the lattice parameters $a = 1266.21(8) \text{ pm}$, $b = 738.96(5) \text{ pm}$, $c = 591.15(4) \text{ pm}$ and $Z = 4$. In its crystal structure, the sulfide anions form a hexagonally closest packed lattice with the silicon atoms occupying one eighth of the tetrahedral holes as Si^{4+} cations ($d(\text{Si}-\text{S}) = 211.2 - 215.6 \text{ pm}$, $\angle(\text{S}-\text{Si}-\text{S}) = 103.6 - 115.1^\circ$), while the Mg^{2+} cations fill half of the octahedral voids ($d(\text{Mg1}-\text{S}) = 253.3 - 258.7 \text{ pm}$, $d(\text{Mg2}-\text{S}) = 256.1 - 263.1 \text{ pm}$). According to this structure description, *olivine* represents the hexagonal counterpart of the cubic *spinel* MgAl_2O_4 according to $\text{Al}_2[\text{MgO}_4]$.

Figure 1: Extended unit cell of *olivine*-type $\text{Mg}_2[\text{SiS}_4]$ as viewed along [001].

References:

- [1] A. Weiss, G. Rocktäschel: *Z. Anorg. Allg. Chem.* **1960**, *307*, 1.
 [2] A. Weiss, G. Rocktäschel, W. Ritter: *Z. Naturforsch.* **1964**, *19 b*, 958.
 [3] W. L. Bragg, G. B. Brown: *Z. Kristallogr.* **1926**, *63*, 538.
 [4] H. O'Daniel, L. Tscheischwili: *Z. Kristallogr.* **1942**, *124*, 104.

Figure 1



P052

$\text{Nd}_7[\text{SbO}_6]_3$: A New Ternary Rare-Earth Metal(III) Oxoantimonate(V)

F. C. Goerigk¹, T. Schleid¹

¹University of Stuttgart, Institute for Inorganic Chemistry, Stuttgart, Germany

With $\text{Nd}_7[\text{SbO}_6]_3$, a new rare-earth metal(III) oxoantimonate(V) was synthesized. In hitherto research, two different ternary neodymium(III) oxoantimonates(V) were already prepared and described with the compositions NdSbO_4 and Nd_3SbO_7 [1, 2]. Compared to these compounds, where the present $[\text{SbO}_6]^{7-}$ octahedra are connected via edges or corners, in $\text{Nd}_7[\text{SbO}_6]_3$ only isolated octahedra without any Sb–O–Sb connection appear. The structure is highly related to the one of $\text{La}_7[\text{RuO}_6]_3$ [3]. Lilac water- and air-stable single crystals of $\text{Nd}_7[\text{SbO}_6]_3$ were synthesized through the reaction of neodymium sesquioxide (Nd_2O_3) and antimony sesquioxide (Sb_2O_3) using an excess of caesium fluoride (CsF) as fluxing agent in a lid-covered corundum crucible. The reaction was carried out with access to air in a muffle furnace at 800 °C for four days, subsequent slow cooling to 600 °C over six days and final quenching to room temperature within one day. The composition of the single crystals was confirmed by X-ray spectroscopy performed on a *Cameca SX-100* electron microprobe. The crystal structure of $\text{Nd}_7\text{Sb}_3\text{O}_{18}$ ($\equiv \text{Nd}_7[\text{SbO}_6]_3$) was examined by single-crystal X-ray diffraction on a *Bruker κ-CCD* diffractometer with $\text{Mo-K}\alpha$ radiation ($\lambda = 71.07 \text{ pm}$). $\text{Nd}_7[\text{SbO}_6]_3$ crystallizes in the trigonal space group $R\bar{3}c$ with $a = 978.07(2) \text{ pm}$

and $c = 5574.4(2)$ pm for $Z = 12$. The structure exhibits three crystallographically different positions for Nd^{3+} . Nd1 is coordinated eightfold by oxygen atoms in the shape of a distorted bicapped trigonal prism with Nd–O distances of 238.7 – 277.8 pm. Nd2 also shows an eightfold coordination sphere as bicapped trigonal prism of oxygen atoms with Nd–O distances of 242.5 – 253.2 pm, while Nd3 is coordinated by nine oxygen atoms arranged as tricapped trigonal prism with distances of 241.5 – 262.6 pm. All antimony atoms are surrounded as Sb^{5+} cations by six oxygen atoms building up $[\text{SbO}_6]^{7-}$ octahedra with Sb–O distances of 194.1 – 203.1 pm. Single-crystal Raman measurements confirm the presence of $[\text{SbO}_6]^{7-}$ octahedra through the appearance of the corresponding vibration signals in the Raman spectrum.

References

- [1] S. Gerlach, R. Cardoso-Gil, E. Milke, M. Schmidt: *Z. Allg. Anorg. Chem.* **2007**, 633, 83.
- [2] K. P. F. Siqueira, R. M. Borges, E. Granado, L. M. Malard, A. M. De Paula, R. L. Moreira, E. M. Bittar, A. Dias: *J. Solid State Chem.* **2013**, 203, 326.
- [3] P. Khalifah, Q. Huang, D. M. Ho, H. W. Zandbergen, R. J. Cava: *J. Solid State Chem.* **2000**, 155, 189.

Figure 1

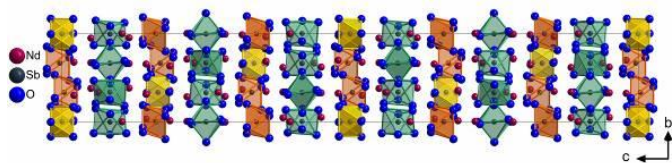


Figure 1. Extended unit cell of $\text{Nd}_7[\text{SbO}_6]_3$ as viewed along a -axis emphasizing $[\text{SbO}_6]^{7-}$ octahedra with Sb^{5+} central cations.

P053

CsBaInClBr[SeO₃]₂: A New Halide Oxoselenate(IV) Containing Three Different Cations

S. Greiner¹, T. Schleid¹

¹University of Stuttgart, Institute for Inorganic Chemistry, Stuttgart, Germany

Through solid-state reactions it was possible to synthesize the caesium barium indium(III) chloride bromide oxoselenate(IV) $\text{CsBaInClBr}[\text{SeO}_3]_2$ (CSD-434220) from a mixture of barium dichloride (BaCl_2), indium sesquioxide (In_2O_3) and selenium dioxide (SeO_2) in a molar ratio of 1:1:4 with additional caesium bromide (CsBr ; all chemicals: ChemPur, 99.9 %) as flux and reactant in fused silica glass ampoules within 9 hours at 900 °C. Afterwards the mixture was tempered for 5 days, before the furnace was cooled down within 99 hours to 500 °C and then just switched off. The new compound crystallizes in the orthorhombic space group *Imma* with $a = 558.17(4)$ pm, $b = 1343.29(10)$ pm, $c = 1456.82(11)$ pm and $Z = 2$. The halide site is mixed occupied by chloride and bromide in a ratio of 50.5(6)% to 49.5(6)%, in the following description labelled as X. In the crystal structure one distinct In^{3+} cation exists, which is sixfold coordinated by two X^- anions and four oxygen atoms from four terminally attached ψ^1 -tetrahedral $[\text{SeO}_3]^{2-}$ units as *trans*- $[\text{InO}_4\text{X}_2]^{7-}$ octahedron ($d(\text{In}-\text{O}) = 216$ pm, $d(\text{In}-\text{X}) = 260$ pm). The Cs^+ and Ba^{2+} cations both reside in pentagonal prismatic coordination polyhedra. In the case of Cs^+ these prisms are built by six X^- anions and four oxygen atoms from two bidentate $[\text{SeO}_3]^{2-}$ groups ($d(\text{Cs}-\text{O}) = 334$ pm, $d(\text{Cs}-\text{X}) = 355 - 398$ pm). In contrast, the Ba^{2+} -centered polyhedra exclusively consist of ten oxygen atoms from terminal and edge-grafting $[\text{SeO}_3]^{2-}$ anions ($d(\text{Ba}-\text{O}) = 263 - 319$ pm). These pentagonal prisms are connected via common edges to form one-

dimensional strands along [100] and their further edge sharing^(e) results in double strands with the formula $1\text{D}-\{[\text{Cs}(\text{O}^e)_{4/1}(\text{X}^e)_{6/3}]^{10-}\}$ and $1\text{D}-\{[\text{Ba}(\text{O}^e)_{4/1}(\text{O}^e)_{6/3}]^{10-}\}$, respectively. Both types of double strands join together via their still terminal oxygen atoms (O^e) to $2\text{D}-\{[\text{CsBaO}_4\text{X}_2]^{7-}\}$ layers spreading out parallel to the (010) plane. Each of these layers is connected by the *trans*- $[\text{InO}_4\text{X}_2]^{7-}$ octahedra via $X\cdots\text{O}$ edges erecting the three-dimensional network with a sequence of octahedron / space for two lone pairs / octahedron along [001] (Figure 1). The Se^{4+} cations themselves form ψ^1 -tetrahedral $[\text{SeO}_3]^{2-}$ anions ($d(\text{Se}-\text{O}) = 163 - 172$ pm, $(\text{O}-\text{Se}-\text{O}) = 98 - 101^\circ$) with their lone pairs and three oxygen atoms each.

Figure 1

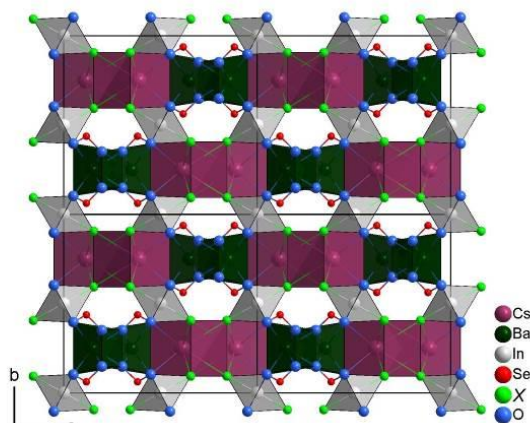


Figure 1. Three-dimensional network of the $\text{CsBaInClBr}[\text{SeO}_3]_2$ structure resulting from the intersection of $2\text{D}-\{[\text{CsBaO}_4\text{X}_2]^{7-}\}$ layers through *trans*- $[\text{InO}_4\text{X}_2]^{7-}$ octahedra via common $X-\text{O}$ edges and Se^{4+} cations within ψ^1 -tetrahedral $[\text{SeO}_3]^{2-}$ anions.

P055

Crystal engineering of inorganic-organic hybrid materials: layered double salts derived from sodium ethanesulfonate and "simple" halides

F. Thoelen¹, W. Frank¹

¹Heinrich-Heine-Universität Düsseldorf, Lehrstuhl für Material- und Strukturforschung, Düsseldorf, Germany

Short-chained alkanesulfonates and metal acids were shown to generate novel layered inorganic-organic hybrid materials containing distinct layers of halogenometallate complexes.^[1] In addition to former experiments with sodium methanesulfonate^[2], we here present two new compounds $\text{Na}_5(\text{H}_2\text{O})(\text{C}_2\text{H}_5\text{SO}_3)_4\text{X}$ (**1**: $\text{X} = \text{Cl}$, **2**: $\text{X} = \text{Br}$), which were simply synthesised by mixing an aqueous solution of sodium ethanesulfonate and the corresponding hydrohalogenic acid, followed by the evaporation of the solvent.

1 and **2** are isotypic, both crystallizing in the monoclinic space group type *Ia*. (**1**: $a = 18.446(4)$ Å, $b = 5.4081(11)$ Å, $c = 22.891(5)$ Å, $\beta = 104.215(3)^\circ$, $Z = 4$, $R_1 = 0.0348$, $wR_2 = 0.1030$, 4968 reflections, 303 parameters; **2**: $a = 23.0349(9)$ Å, $b = 5.444(9)$ Å, $c = 18.5390(8)$ Å, $\beta = 103.707(3)^\circ$, $Z = 4$, $R_1 = 0.0444$, $wR_2 = 0.1019$, 5105 reflections, 293 parameters).

In the solids of **1** and **2**, halide anions and inverse tenside-like bilayered cationic arrays $\{[\text{Na}_5(\text{C}_2\text{H}_5\text{SO}_3)_4]_2\}^{2+,x,y}$ are present in an arrangement that reminds on the structure of the short-chained sodium alkanesulfonates.^[3] The bilayered arrays feature hydrophilic and hydrophobic regions, the latter formed by ethane groups of the ethanesulfonate. The hydrophobic layers are disrupted by an alternating sequence of water molecules and halide

ions, each coordinating to a single sodium cation of the cationic bilayers in a noncentrosymmetric arrangement of X- and H₂O. With values of 2.805(4) Å (1) and 2.962(5) Å (2), Na–X (X = Cl, Br) distances are close to the corresponding distances in the NaX type structures. Therefore, both compounds might formally be described as double salts Na₄(C₂H₅SO₃)₄ · NaX · H₂O (X = Cl, Br) of sodium ethanesulfonate with the respective sodium halide. Between the halide anions and water molecules of neighbouring bilayered arrays, chains of weak hydrogen bonds are formed in **1** (O–H···Cl, D···A 3.305(2) Å - 3.309(4) Å) and **2** (O–H···Br, D···A 3.398(4) Å - 3.429(5) Å).

- [1] V. Verheyen, W. Frank, *Z. Kristallogr. Suppl.* **2009**, 29, 41.
 [2] F. Thoelen, W. Frank, *Z. Kristallogr. Suppl.* **2018**, 38, 90.
 [3] C. H. Wei, B. E. Hingerty, *Acta Cryst.* **1981**, B37, 1992.

Figure 1

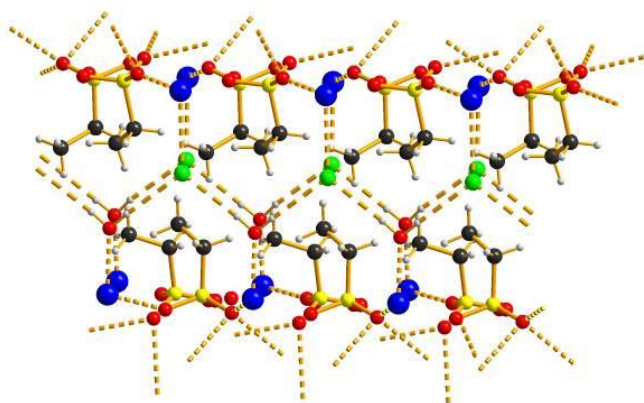
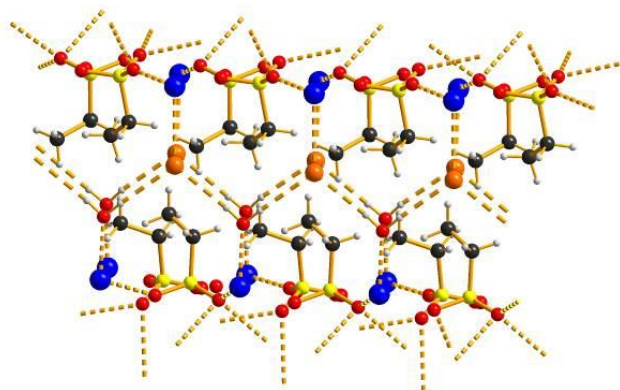


Figure 2



P056

Crystal structures of $M^{2+}Zr(SO_4)_3$ with $M = Mg, Mn, Co, Ni, Zn$ and Cd , and their relationship with $Fe_2(SO_4)_3$

G. Gerald¹, T. Dominik¹, W. Manfred¹

¹Universität Wien, Institut für Mineralogie und Kristallographie, Wien, Austria

We recently initiated a study on the crystal chemistry of zirconium oxysalts synthesized at low-hydrothermal conditions [1,2]. Here we present a new group of isotopic or closely related sulfates of the general formula $M^{2+}Zr(SO_4)_3$ with $M = Mg, Mn, Co, Ni, Zn$ and Cd , as well as a mixed-valent $(Fe^{3+,2+}Zr)_2(SO_4)_3$, and elucidate their structural relationships with the monoclinic modification of $Fe_2(SO_4)_3$.

Except for the Mg-representative, all $MZr(SO_4)_3$ compounds crystallize in the structure type of monoclinic anhydrous ferric sulfate $Fe_2(SO_4)_3$ with space group $P21/n$ and $Z=4$, comprising two different octahedral Fe^{3+} sites. In the isotopic $MZr(SO_4)_3$ structures Zr^{4+} occupies the marginally smaller and slightly less distorted Fe1 site ($\langle Fe1-O \rangle = 1.978$ Å), the M^{2+} cations are located in the Fe2 site ($\langle Fe2-O \rangle = 1.993$ Å). The resulting mean $Zr-O$ bond lengths hardly scatter between 2.057 and 2.060 Å, while average $M^{2+}-O$ distances range from 2.060 Å ($M=Ni$) up to 2.256 Å ($M=Cd$) depending on the M^{2+} cation size. This demonstrates the flexibility of the $Fe_2(SO_4)_3$ structure type, which is also known for $In_2(SO_4)_3$, $Sc_2(SeO_4)_3$, $Yb_2(SeO_4)_3$, $Fe_2(SeO_4)_3$, $Al_2(WO_4)_3$, $Sb_2(PO_4)_3$ and $V_2(PO_4)_3$.

On the other hand, in spite of the fact that the Mg^{2+} cation size lies between Ni^{2+} and Zn^{2+} , $MgZr(SO_4)_3$ crystallizes in a different but related structure with a larger unit cell, space group Pc , $Z=8$. This phase may be derived from the $AlFe(MoO_4)_3$ structure type (space group $P21/a$, $Z=8$), but with reduced symmetry.

Both the strict differentiation of Zr vs. the M^{2+} cations on the two available octahedral sites as well as the incompatibility of the Mg^{2+} cation lacking d -orbitals may be related to different electron deformation densities found for the two Fe sites in $Fe_2(SeO_4)_3$ [3].

- [1] G. Giester and M. Wildner, *Monatsh. Chem.* **149**, 1321 (2018)
 [2] M. Wildner and G. Giester, *Monatsh. Chem.*, in press. (2019)
 [3] P.C. Christidis, P.J. Rentzeperis, A. Kirfel, G. Will, *Z. Kristallogr.* **164**, 219 (1983)

P057

$NaCe_{18}O_9F_{19}Se_9$: A Sodium-Containing Compound in the $Ce_2OF_2Se-Ce_6O_2F_8Se_3$ System

C. Buyer¹, S. Wolf¹, T. Schleid¹

¹University of Stuttgart, Institute for Inorganic Chemistry, Stuttgart, Germany

The crystal structures of the hexagonal RE_2OF_2Se ($RE = Nd, Sm, Gd - Ho$) and $RE_6O_2F_8Se_3$ series ($RE = La - Nd$) [1] are nearly the same. Both crystallize in the space group $P6_3/m$ and offer empty channels parallel to the c -axes. In $NaCe_{18}O_9F_{19}Se_9$ (CSD-1886571), these channels contain Na^+ cations at the $2b$ position and in additional channels analogously F^- anions reside at the $2c$ position. For the $RE_6O_2F_8Se_3$ series these channels (F^- at $2c$ position) are fully occupied, whereas they remain completely empty in the RE_2OF_2Se series. So $NaCe_{18}O_9F_{19}Se_9$ corresponds to the formula $Ce_2OF_2Se \cdot \frac{1}{9} NaF$ and the crystals are yellow needles with the lattice parameters $a = 1384.27(8)$ and $c = 396.42(3)$ pm for $\frac{2}{3}$ formula units per unit cell. They were obtained by the reaction of Ce, CeO_2 and CeF_3 with Se (5:3:4:6) in a melt of $NaCl$ as fluxing agent for 7 days at 850 °C in sealed niobium ampoules. $Ce_6O_2F_8Se_3$ [1] without any sodium has cell parameters such as $a = 1385.63(9)$ and $c = 398.39(3)$ pm and the aforementioned F^- channels are fully occupied. This is possible cause of a mixed $6h$ position with 67 % O^{2-} and 33 % F^- anions for $Ce_6O_2F_8Se_3$, which exclusively contains O^{2-} in the case of $NaCe_{18}O_9F_{19}Se_9$. Just like for $Ce_6O_2F_8Se_3$ the crystal structure exhibits a framework of $(Ce^{3+})_4$ tetrahedra with O^{2-} and F^- anions in their centers, which share *cis*-oriented edges (Figure 1). The first Ce^{3+} cation is surrounded by a capped square antiprism according to $[(Ce1)O_3F_2Se_4]^{13-}$, pretty much like Ce^{3+} in $PbFCl$ -type $CeFS$ [2], but the capping anion is $(F_3)^-$, which is occupied only by about $\frac{1}{3}$. The second Ce^{3+} cation centers a tricapped trigonal prism $[(Ce2)OF_6Se_2]^{9-}$. The Na^+ cations are octahedrally surrounded by F^- anions ($d(Na^+-F^-) = 247$ pm) and can be maximally occupied by a factor of $\frac{1}{2}$ owing to too short distances ($d(Na^+ \cdots Na^+) = 198$ pm) along the c -axis.

[1] D. D. Zimmermann, H. Grossholz, S. Wolf, O. Janka, A. C. Müller, Th. Schleid: *Z. Anorg. Allg. Chem.* **2015**, 641, 1926–1933.
 [2] Th. Schleid, H. Grossholz: *Z. Anorg. Allg. Chem.* **2001**, 627, 2693–2699.

Figure 1

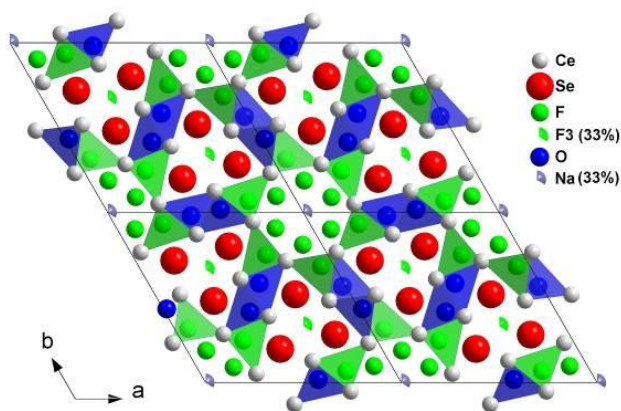


Figure 1. Framework of edge-sharing tetrahedra in the crystal structure of $\text{NaCe}_3\text{O}_4\text{F}_{15}\text{Se}_6$ with channels along $[001]$, partly filled with Na⁺ cations (33%), and channels along $[\frac{1}{2}, \frac{1}{2}, 1]$ and $[\frac{1}{2}, \frac{1}{2}, \frac{1}{2}]$ partly filled with F⁻ anions (33%).

P058

A new ternary structure among alkali metal trielides - Structural relations between long-known and new cluster compounds

M. Falk¹, C. Röhr¹

¹Albert-Ludwigs-Universität Freiburg, Institut für Anorganische und Analytische Chemie, Freiburg i. Br., Germany

Alkali metal trielides show a complex structure diversity in between simple intermetallics, Zintl phases, cluster compounds and boron-analogous phases.

The newly discovered mixed phase Cs_7M_{15} ($M = \text{Ga}, \text{In}$) was obtained in the course of a systematic study of Ga/In alkali compounds. The study's aim is the exploration of the 'coloring' within complex polyanions of the binary compounds with the two triels In and Ga differing both in size (covalent radii: Ga: 126 pm, In: 144 pm) and electronegativity (Ga: 1.82, In: 1.49) and to explore additional new polyanion topologies [1].

The structure of Cs_7M_{15} ($P-4m2$, $a = 649.5$, $c = 1599.7$ pm for Ga:In = 11:4) can be seen as cluster compound "link" in between Cs_2M_3 [2] ($I4/mmm$, mono-layers of exo-bonded $[M_6]$ octahedra) and AM_3 [3, 4] ($I-4m2$, 3D network of $[M_8]$ trigondodecahedra), built up from distorted pentagonal $[M_7]$ bipyramids connected via a four-bonding M atom to form double-layers (fig. 1). The structure consists of five Cs and M positions whereby In occupies the $M(4)$ position preferably, followed by $M(1)$ and $M(5)$. This element distribution can be explained by both larger calculated Bader volumes and the less negative charges. According to Wade's electron counting rules, the *closo* $[M_7]$ clusters carry a charge of 3- and the DOS shows a minimum at E_F , similar to the DOS of Cs_2M_3 and CsM_3 .

Additionally, superstructures with different stacking of the double-layers or with both octahedra and pentagonal bipyramids have been observed. Some of them exhibit a strong disorder within the Cs layers and an ambiguous Cs/In distribution. The Cs_7M_{15} structure and related superstructures start to appear at a percentage of ~35% Ga where no more Ga can be incorporated into the Cs_2M_3 structure. Their existence range reaches up to ~75% Ga. In contrast, the phase width of CsM_3 extends throughout the whole

range between CsIn_3 and CsGa_3 (fig. 2). Formation and structures of corresponding Rb compounds are also currently being investigated.

 Fig. 1: Crystal structures of Cs_2In_3 (left), Cs_7M_{15} (middle) and CsM_3 (right).

Fig. 2: Obtained single crystals in the system Cs-In-Ga (excerpt).

References:

- [1] M. Falk, C. Röhr, *Z. Anorg. Allg. Chem.* **643**, 2070 (2017).
- [2] S. P. Yatsenko, K. A. Chuntunov, A. N. Orlov, Ya. P. Yarmolyuk, Yu. Grin, *J. Less-Common Met.* **108**, 339 (1985).
- [3] K. A. Chuntunov, S. P. Yatsenko, Yu. Grin, Ya. P. Yarmolyuk, A. N. Orlov, *J. Less-Common Met.* **99**, 15 (1984).
- [4] J. H. N. v. Vucht, *J. Less-Common Met.* **108**, 163 (1985).

Figure 1

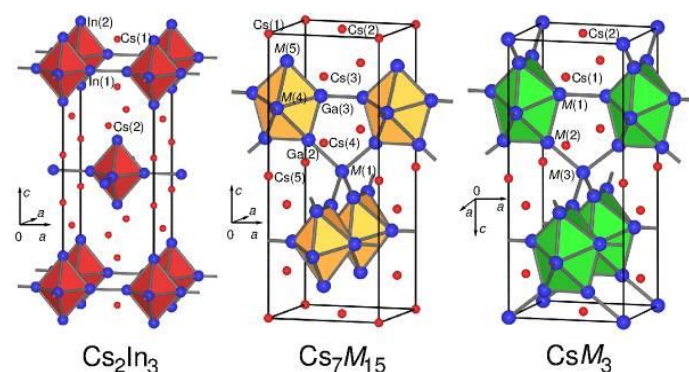
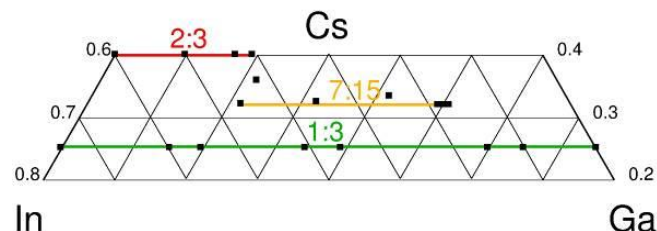


Figure 2



P059

Investigation of F⁻-containing phases in fluoro-calcium aluminate cements and F-loss during sintering

S. Galluccio¹, H. Pöllmann¹

¹Martin-Luther-Universität, Mineralogy/ Geochemistry, Halle (Saale), Germany

Fluorspar (CaF_2) reacts as a mineralizer in clinker production. Fluorine is the earliest known mineralizer [1] and reduces the temperature of initial melt formation and the formation temperature of intermediate phases. Several studies showed, that thereby the sintering temperature can be reduced without decreasing the clinker quality [2-4]. Fluorine acts also as a flux as the viscosity and surface tension of the melt is reduced [5]. Also in the production of the commonly used OPC, fluorides can be used as they support the formation of the main clinker phase alite.

Fluoro-calcium aluminate cements were produced using CaCO_3 , $\gamma\text{-Al}_2\text{O}_3$ and 0.5%, 1%, 1.5%, 2% resp. 2.5% fluorspar as mineralizer. The homogenized raw meals were sintered at 1300°C for 2h. The formed clinker phases were analyzed by X-ray powder diffraction and quantified by the Rietveld method. During

sintering, fluorine can volatilize and thus damage the furnace and cause pollution of the environment. The fluoride concentration was measured with a Combination Fluoride Electrode by dissolving the clinker in 19% HCl. For the measurement, the pH value had to be increased by adding sodium acetate. The determined fluoride values could then be compared with the amount of fluorine in the raw meal to calculate the volatile fluorine content.

P060

Sr₂H₃Br: An Unexpected Phase in the SrH₂–SrBr₂ System

D. Rudolph¹, J. L. Hoslauer¹, T. Schleid¹

¹University of Stuttgart, Institute for Inorganic Chemistry, Stuttgart, Germany

When Hagemann *et al.* investigated the ternary systems $M-X-Z$ ($M = \text{Ca, Sr, Ba, Pb}$; $X = \text{H, F}$; $Z = \text{Cl, Br}$), they found out that besides the simple PbFCl-type structure for the composition MHZ , which is realized for all combinations of the given cations and anions, a mutual exclusion for the two other known phases and structures, namely M_2X_3Z and $M_7X_{12}Z_2$, should exist. In their publication, they concluded that for each combination of M , X and Z , either M_2X_3Z or $M_7X_{12}Z_2$ is found, but never both of them [1]. While for the system Sr–H–Br the phases SrHBr [2] and Sr₇H₁₂Br₂ [3] were already known, we were recently able to obtain the unexpected third phase Sr₂H₃Br (CSD-433586), disproving Hagemann's exclusion idea. Yellow crystals of Sr₂H₃Br were prepared using strontium metal, Na[NH₂], NaBr and metallic sodium as fluxes at 900 °C for 4.5 days in cleaned niobium capsules and by using strontium metal and [NH₄]Br (4:1) under the same conditions [3]. The crystal structure was determined using single-crystal X-ray diffraction. Sr₂H₃Br crystallizes with an *anti*-CdI₂-type structure for its Sr₂Br part in the trigonal space group $P\bar{3}m1$ ($a = 418.95(4)$ pm, $c = 734.23(7)$ pm), where the H[–] anions occupy half of the octahedral and half of the tetrahedral interstices between the hexagonally closest packed Sr²⁺ layers. In this stuffed layer structure, the Sr²⁺ cations are coordinated by ten anions in the shape of a tetracapped trigonal prism [SrH₇Br₃]^{8–}. Since they are hexagonally closest packed, the H[–] anions occupy all octahedral and all tetrahedral voids in every second layer, while the Br[–] anions reside in the remaining octahedral interstices (Figure 1). Bond lengths of 240(4) pm and 247(1) pm for the Sr–H_{tet} and 282(1) pm for Sr–H_{oct} contacts were found. The three Sr²⁺–Br[–] distances were determined to be 328.9(1) pm. These values are in good agreement with these (Sr²⁺–H[–], Sr²⁺–Br[–]) for SrHBr (241 pm, 324 – 346 pm) [2], Sr₇H₁₂Br₂ (241 – 286 pm, 317 – 322 pm) [3], SrH₂ (235 – 276 pm) [4] and SrBr₂ (311 – 359 pm) [5].

References

- [1] H. Hagemann, V. D'Anna, M. Lawson Daku, F. Kubel: *Cryst. Growth Des.* **2012**, *12*, 1124.
- [2] P. Ehrlich, H. Görtz: *Z. Anorg. Allg. Chem.* **1956**, *288*, 148.
- [3] O. Reckeweg, J. C. Molstad, S. Levy, C. Hoch, F. J. DiSalvo: *Z. Naturforsch.* **2008**, *63 b*, 513.
- [4] D. Colognesi, G. Barrera, A. J. Ramirez-Cuesta, M. Zoppi: *J. Alloys Compd.* **2007**, *427*, 18.
- [5] J. G. Smeggil, H. A. Eick: *Inorg. Chem.* **1971**, *10*, 1458.

Figure 1

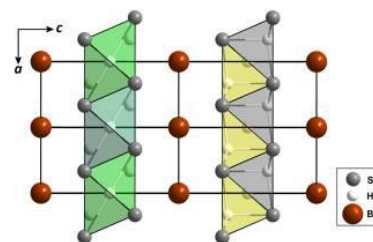


Figure 1. Crystal structure of Sr₂H₃Br with highlighted [HSr₄]⁷⁺ tetrahedra and [HSr₆]¹¹⁺ octahedra.

P061

KSm[P₂Se₆]: The Structural Missing Link within the KRE[P₂Se₆] Series

B. Schulz¹, T. Schleid¹

¹University of Stuttgart, Institute for Inorganic Chemistry, Stuttgart, Germany

New potassium lanthanoid(III) selenidophosphates(IV) $KLn[P_2Se_6]$ ($Ln = \text{Ce} - \text{Nd, Sm, Gd} - \text{Dy}$) have been synthesized. It was observed that the structure of the $KLn[P_2Se_6]$ series varies with the size of the Ln^{3+} cation. $KSm[P_2Se_6]$ with mid-size Sm^{3+} crystallizes in the monoclinic space group $P2_1$ with the lattice parameters $a = 679.87(3)$ pm, $b = 762.36(3)$ pm, $c = 1027.43(5)$ pm and $\beta = 91.652(3)^\circ$ for $Z = 2$. The representatives with the earlier lanthanoids (Ce – Nd) adopt the $KLa[P_2Se_6]$ -type structure [1] (monoclinic, $P2_1/c$) whereas for the smaller ones (Gd – Dy) the orthorhombic $KY[P_2Se_6]$ -type structure (space group: $P2_12_12_1$) is found [2].

In the crystal structure of $KSm[P_2Se_6]$ there is only one unique Sm^{3+} cation coordinated by eight selenium atoms forming a bicapped trigonal prism [SmSe₈]. These polyhedra are connected via common edges (Figure 1, left). The earlier Ln^{3+} cations ($Ln = \text{La} - \text{Nd}$) are surrounded by nine selenium atoms [1], while $Gd^{3+} - Dy^{3+}$ also have eight selenium atoms in their first coordination sphere [2]. The main building block of all compounds is a trigonal selenium antiprism [P₂Se₆]^{4–} (Figure 1, right) with $d(\text{P} - \text{Se}) = 213 - 222$ pm, which exhibits two central phosphorus atoms connected by a direct P–P bond ($d = 221$ pm). The K⁺ cations are eight- to ninefold coordinated by selenium and the isotypic structure of $KSm[P_2S_6]$ is already known [3].

For the synthesis of $KSm[P_2Se_6]$, samarium powder was mixed with red phosphorus, selenium and potassium chloride in a molar ratio of 1:1:4:1. The reactants were tempered at 950 °C for 4 days in evacuated glassy silica ampoules. After the furnace was cooled down to 200 °C within 37.5 hours and then switched off, amber-colored, plate-shaped single crystals of $KSm[P_2Se_6]$ were obtained suitable for a structure determination by X-ray diffraction.

- [1] J. H. Chen, P. K. Dorhout, *Inorg. Chem.* **1996**, *35*, 5627–5633.
- [2] J. H. Chen, P. K. Dorhout, *Inorg. Chem.* **1995**, *34*, 5705–5706.
- [3] L. M. Schoop, R. Eger, R. K. Kremer, A. Kuhn, J. Nuss, B. V. Lotsch, *Inorg. Chem.* **2017**, *56*, 1121–1131.

Figure 1

Figure 1. Bicapped trigonal prisms [SmSe₂] connected via edges (left) and the staggered conformation of the ethane-like [P₂Se₄]⁴⁻ anion as Newman projection along the P–P bond (right).

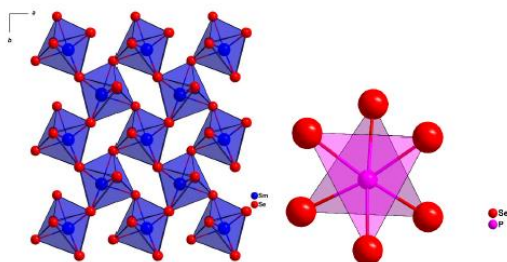
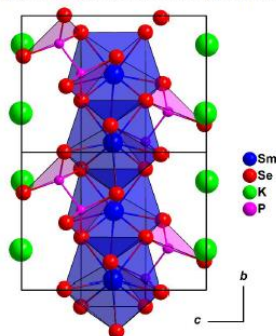


Figure 2. Crystal structure of KSm[P₂Se₄] as viewed along [100].



P062

Eu₂ScTaO₆: The Last Member of the Eu₂RETaO₆ Series

C. Funk¹, E. Brücher², J. Köhler², T. Schleid¹

¹University of Stuttgart, Institute for Inorganic Chemistry, Stuttgart, Germany

²Max-Planck Institute for Solid-State Research, Stuttgart, Germany

Sato *et al.* synthesized oxidic double *perovskites* A₂BB'O₆ with divalent europium (A), trivalent lanthanides (B) and pentavalent tantalum (B') already in 1976 [1]. Now Eu₂ScTaO₆ originated from appropriate mixtures of Eu₂O₃, Ta₂O₅, Ta and Sc₂O₃ with a 0.1 molar excess of tantalum powder. This mixture was pelletized (5000 kg·cm⁻²) and heated in a high-temperature furnace under an argon stream on a tantalum foil for 12 h at 1300 °C. This procedure got repeated eight times, after the pellet was ground, ball-milled again, repelletized, and put in the high-temperature furnace for 12 h at finally 1450 °C. Eu₂ScTaO₆ was obtained phase-pure as red brown compound, confirmed by EDX measurements.

The crystal structure could be determined by powder X-ray diffraction on a *STOE STADI P* with CuK_α radiation. Eu₂ScTaO₆ crystallizes in the cubic *elpasolite*-type structure (Eu on 8c (1/4, 1/4, 1/4), Sc on 4a (0, 0, 0), Ta on 4b (1/2, 1/2, 1/2), O on 24e (0.26417(14), 0, 0)) with the space group *Fm-3m* and *a* = 800.17(3) pm for *Z* = 4 (Figure 1, top left). Six oxide anions surround both the Sc³⁺ and Ta⁵⁺ cations as octahedra (*d*(Sc–O) = 211 pm, *d*(Ta–O) = 189 pm), which are alternately sharing common corners. The Eu²⁺ cations reside in twelfold coordination of cuboctahedrally arranged oxide anions (*d*(Eu–O) = 283 pm).

By heating Eu₂ScTaO₆ in air it oxidizes to Eu₂ScTaO₇ with *pyrochlore*-type structure (Figure 1, bottom left) [1]. The magnetic susceptibility shows *Curie-Weiss* behavior (Figure 1, top right) with ferromagnetic interactions, despite in literature antiferromagnetic ordering is described for the rest of the Eu₂RETaO₆ series [1, 2]. The intersection of the *Curie-Weiss* fit with the *x*-axis occurs at 1.3 K. This must be a result of the runty

unit cell of Eu₂ScTaO₆, which is way smaller than the published one for Eu₂LuTaO₆ [2]. The Eu²⁺···Eu²⁺ distances of 400 pm are still longer than in *perovskite*-type EuTiO₃ with *d*(Eu···Eu) = 390 pm and thus should be not close enough for ferromagnetic interactions as mentioned by Greedan *et al.* according to ferromagnetic *halite*-type EuO with *d*(Eu···Eu) = 363 pm [3]. The optical band gap of Eu₂ScTaO₆ was determined to 2.1 eV with the *Kubelka-Munk* function (Figure 1, bottom right).

[1] K. Sato, G.-Y. Adachi, J. Shiokawa: *J. Inorg. Nucl. Chem.* **1976**, 38, 1287–1289.

[2] Y. Misawa, Y. Doi, Y. Hinatsu: *J. Solid State Chem.* **2011**, 184, 1478–1483.

[3] J. E. Greedan, G. J. McCarthy: *Mater. Res. Bull.* **1972**, 7, 531–541.

Figure 1

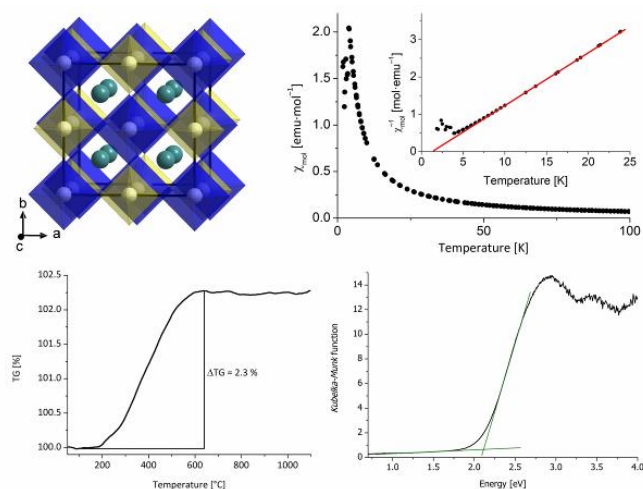


Figure 1. Crystal structure of Eu₂ScTaO₆ (top left), its magnetic susceptibility at 10 kOe (top right), its mass increase under static air atmosphere up to 1100 °C (bottom left) and its optical band gap (bottom right).

P063

CsTb₃STe₄: The First Quaternary Lanthanoid Chalcogenide with Ordered S²⁻ and Te²⁻ Anions

T. Schleid¹, S. P. Meyer¹, F. Lissner¹

¹University of Stuttgart, Institute for Inorganic Chemistry, Stuttgart, Germany

Oxide chalcogenides of the trivalent lanthanoids are well prospected, but attempts to substitute O²⁻ by the heavy chalcogenides (S²⁻, Se²⁻ or Te²⁻) often yield in compounds M₂(Ch₁)_{3-x}(Ch₂)_x (Ch = S – Te) with either mixed occupation or the formation of the pure sesquisulfides M₂Ch₃ is preferred. Only for the example of Nd₂S₂Te [1] an ordering of the S²⁻ and Te²⁻ anions according to the Ce₂O₂S-type structure [2] happens.

By the oxidation of terbium metal with sulfur and tellurium in the presence of cesium bromide as flux at 850 °C for 10 days, the first quaternary chalcogenide with ordered anions could be obtained as main product. The new compound CsTb₃STe₄ occurs as black rods and crystallizes orthorhombically in the space group *Pnma* with *a* = 1924.1(2) pm, *b* = 433.61(3) pm and *c* = 1493.5(1) pm for *Z* = 4. The unit cell is filled with one crystallographically unique Cs⁺, but three independent Tb³⁺ cations as well as one S²⁻ and four Te²⁻ anions, all occupying 4c *Wyckoff* positions.

In the crystal structure (CSD-425435) all three different Tb³⁺ cations are sixfold coordinated in the manner of distorted

octahedra. Tb1 is surrounded by two S^{2-} and four Te^{2-} anions, while Tb2 and Tb3 carry only one S^{2-} but five Te^{2-} anions as ligands. With distances like $d(Tb-S) = 271 - 278$ pm and $d(Tb-Te) = 297 - 320$ pm there is high resemblance to Tb_2S_3 and Tb_2Te_3 . The main structural feature (Figure 1, left) is dominated by two types of strands. Bicapped trigonal prisms $[CsTe_8]^{15-}$ with Cs-Te distances ranging from 370 to 456 pm are first connected via their inner caps to dimers $[Cs_2Te_{14}]^{26-}$ and these finally share faces to form anionic double chains $1D-\{[CsTe_4]^{7-}\}$ (mid). Their cationic counterpart is built up by vertex-connected $[STb_4]^{10+}$ tetrahedra resulting in chains $1D-\{[STb_3]^{7+}\}$ (right).

References

- [1] Th. Schleid, E. K. Klein: *Z. Anorg. Allg. Chem.* **2001**, 627, 807.
 [2] W. H. Zachariasen: *Acta Crystallogr.* **1949**, 2, 62.

Figure 1

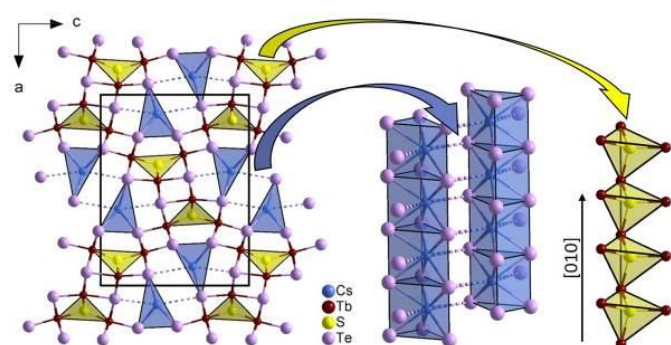


Figure 1. View at the complete crystal structure of $CsTb_3STe_4$ along $[010]$ (left), which contains two types of strands: Anionic double chains $1D-\{[CsTe_4]^{7-}\}$ (mid) and cationic single chains $1D-\{[STb_3]^{7+}\}$ (right) of vertex-shared $[STb_4]^{10+}$ tetrahedra.

P064

Structural characterization of barium (imido)-nitridophosphate networks

D. Günther¹, S. Wendl², L. Eisenburger², W. Schnick², O. Oeckler¹

¹Universität Leipzig, IMKM, Leipzig, Germany

²LMU München, Department Chemie, München, Germany

As the element combinations P/N and Si/O are isoelectronic, (imido)-nitridophosphates can be expected to show similar structural and physical properties as oxosilicates. As N atoms can occur as triply-bridging vertices in such tetrahedra-based networks, e.g. in $\alpha-P_3N_5$,^[1] (imido)-nitridophosphates possibly offer an even greater structural diversity. The new highly condensed compounds $BaHP_6N_{11}$ and BaP_8N_{14} were synthesized by high-temperature high-pressure reactions following equations (1) and (2), respectively.

For both microcrystalline compounds, structure determination was based on single-crystal data collected with microfocused synchrotron radiation. Suitable crystallites were identified by electron diffraction and EDX in the TEM and transferred to the synchrotron beamline (ID11, ESRF).^[2] The crystal structures of the title compounds are built up from all-side vertex-sharing PN_4 tetrahedra, forming P_3N_{10} entities (Figure, center). In $BaHP_6N_{11}$, one of these is connected to six further units, leading to two types of layered substructures with triangular voids (Figure, left). Alternating stacking of the layers leads to a framework structure that hosts the Ba atoms (black, Fig. 1, left). BaP_8N_{14} , in contrast, is a layered compound built up from slabs that consist of PN_4 tetrahedra and are separated by Ba atoms (Figure, right). Each slab is composed by four single layers consisting of *sechser* rings. Comparable motifs have been observed, e.g., in SrP_8N_{14} . This gives interesting insights into size effects in nitridophosphates.^[3]

Acknowledgements: We thank the Deutsche Forschungsgemeinschaft (grants OE530/6-1 and SCHN 377/18-1) for funding and the ESRF, Grenoble (project CH-4318) for granting beamtime.

Literature

- [1] S. Horstmann, E. Irran, W. Schnick, *Z. Anorg. Allg. Chem.* **1998**, 624, 620-628.
 [2] F. Fahrnbauer, T. Rosenthal, T. Schmutzler, G. Wagner, G. B. M. Vaughan, J. P. Wright, O. Oeckler, *Angew. Chem. Int. Ed.* **2015**, 54, 10020-10023.
 [3] S. Wendl, W. Schnick, *Chem. Eur. J* **2018**, 24, 15889.

Figure 1

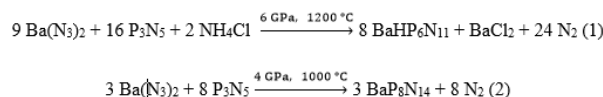
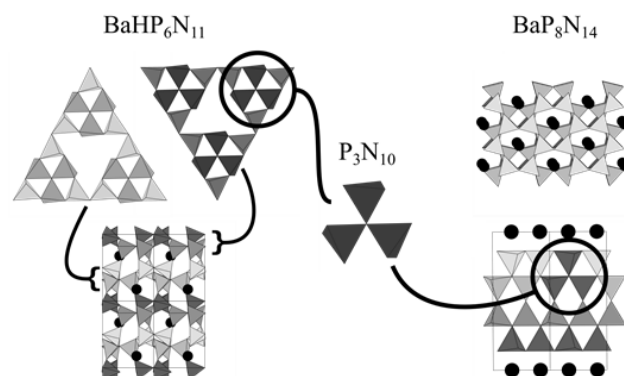


Figure 2



P065

The crystal structure of $CaSiH_{\approx 4/3}$ revisited

H. Auer¹, H. Kohlmann¹

¹Universität Leipzig, Institut für Anorganische Chemie, Leipzig, Germany

$CaSiH_{\approx 4/3}$ was the first Zintl phase hydride showing a polyanionic backbone of group 14 elements with an element-hydrogen contact. After its discovery and the initial claim of a covalent silicon-hydrogen interaction by DFT calculations [1], the bonding character was questioned again based on neutron diffraction and neutron vibrational spectroscopy data [2]. Until now, the bonding situation was not clear for this fundamental compound.

$CaSiH_{\approx 4/3}$ is a Zintl phase hydride. One hydrogen atom per formula unit is located in tetrahedral Ca_4 -voids. The remaining hydrogen atoms coordinate silicon atoms leading to an idealised formula $CaHSi_{2/3}(SiH)_{1/3}$. The silicon binding hydrogen site is always underoccupied ($\approx 50\%$) leading to an actual composition of $CaSiH_{1.2}$.

We did a thorough reinvestigation of $CaSiH_{\approx 4/3}$ using laboratory X-ray and neutron diffraction of the corresponding deuteride. We used 2H -NMR to determine the quadrupolar coupling (CQ) of the silicon coordinating deuterium site and interpreted these data under the aid of density functional theory calculations. Finally, we collected neutron total scattering data to directly measure the deuterium-silicon distance.

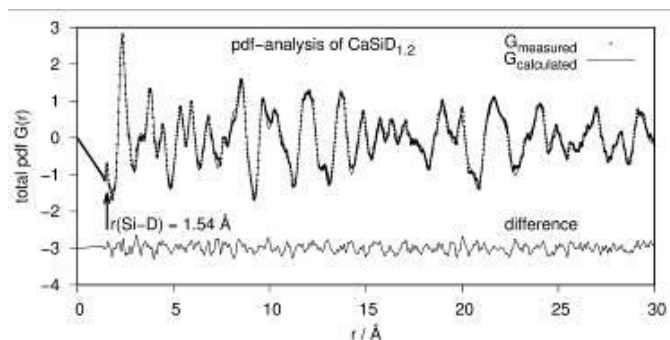
Powder diffraction patterns of $\text{CaSiD}_{2/3}$ show anisotropically broadened reflections. Depending on the parametrisation, the Si-D bond lengths strongly change. Therefore, we chose a local approach using $^2\text{H-NMR}$ and total scattering. The silicon bound deuterium site shows a quadrupole interaction of $\text{CQ} = 58(2)$ kHz corresponding to a structural model with a bond length of $1.56(1)$ Å [3]. We can now substantiate this result by a pdf-analysis (see figure). The first peak corresponds to the Si-D distance and is located at 1.54 Å.

Therefore, our data allow a conclusive interpretation of the bonding situation as a covalent interaction with a Si-D bond length of 1.54 Å.

- [1] N. Ohba, M. Aoki, T. Noritake, K. Miwa, S. Towata, *Phys. Rev. B* **2005**, *72*, 75104.
 [2] H. Wu, W. Zhou, T. J. Udovic, J. J. Rush, T. Yildirim, *Phys. Rev. B* **2006**, *74*, 224101.
 [3] H. Auer, R. Guehne, M. Bertmer, J. Haase, H. Kohlmann, *Z Kristallogr. Suppl.* **2018**, *38*, 11.

Fig. 1 Pair distribution function (pdf)-analysis of $\text{CaSiD}_{1.2}$ based on neutron total scattering data.

Figure 1



P066

Crystal chemistry of alkali nona-stannid cluster compounds: Novelties from binary and novel ternary Ga-containing phases

C. Röhr¹, B. Lehmann¹

¹Institut für Anorganische und Analytische Chemie, Freiburg, Germany

Nido-clusters Sn_9^{4-} are found in the series of binary alkali stannides A_4Sn_9 and - together with twice as much Sn_4^{4-} tetrahedra - in the compounds $\text{A}_{12}\text{Sn}_{17}$ [1-3]. Although these type of clusters are known since E. Zintl himself [4], the structural characterization of their pure alkali salts is still a difficult challenge, mainly due to the massive disorder of the anions. Thus, for many compounds, only the overall hierarchical arrangement of the anions could be determined to date (Fig. 1a). The diffraction images of the new Cs stannide Cs_4Sn_9 , which was obtained from the ternary sample CsZn_2Sn_2 at $T_{\text{max}} = 1280$ K, exhibit only few reflections, which strongly decrease at higher Θ angles; this and the cubic Laue symmetry as well as the lattice parameter of $a=1655$ pm indicate a plastic-crystalline phase with a Cr_3Si arrangement of the fully disordered Sn_9^{4-} anions (cf. the triclinic structure of Rb_4Sn_9 [5]). In the same system, the likewise missing phase $\text{Cs}_{12}\text{Sn}_{17}$ (*Pbca*, $a=2559.25(6)$, $b=3088.29(8)$, $c=8087.9(2)$ pm, $R1=0.128$ %) crystallizes with a huge unit cell (Fig. 1c: gold). Herein, the Sn_9 clusters and Sn_4 tetrahedra anions take the positions of Mg and Zn atoms in MgZn_2 . Some clusters and tetrahedra are again disordered, but the correct orientation and geometry of the individual moieties could be treated/refined reliably (Fig. 2).

Ternary Ga-containing samples $\text{A}_3\text{Ga}_2.5\text{Sn}_{2.5}$ yielded the new isotopic compounds $(\text{K/Rb})_{13}\text{GaSn}_{16}$ ($P2_1/n$, $a=2427.94(6)/2504.88(13)$, $b=2582.46(7)/2659.03(2)$, $c=2963.56(7)/3045.9(2)$ pm, $\beta=90.400(2)/90.444(5)^\circ$, $R1=0.1025/0.1185$), which again exhibit a MgZn_2 topology, in this case of Sn_4^{4-} and $[\text{GaSn}_8]^{5-}$ clusters. Although the Ga positions in the nona-clusters are not explicitly resolved due to the disorder, the increased amount of A cations, which fits the number of nona-clusters and a - compared to the pure binaries $\text{A}_{12}\text{Sn}_{17}$ - considerably increased molar volume (Fig. 1b) are indications for the distinct Ga content of the nona-clusters in these compounds.

- [1] Th. F. Fässler, *Coord. Chem. Rev.*, **215**, 347 (2001).
 [2] C. Hoch, M. Wendorff, C. Röhr, *J. Alloys Compd.* **361**, 206-221 (2003).
 [3] C. Hoch, C. Röhr, M. Wendorff, *Acta Crystallogr.* **C58**, 45 (2002).
 [4] E. Zintl, J. Goubeau, W. Dullenkopf, *Z. Phys. Chem. A* **154**, 1-46 (1931).
 [5] M. Baitinger, ThD thesis, TU Darmstadt, 2000.

Fig. 1: Structure chemistry of the compounds A_4M_9 , $\text{A}_{12}\text{M}_{17}$ and $\text{A}_{13}\text{GaSn}_{16}$.

Fig. 2: Example of the disorder of one of six different Sn_9^{4-} clusters in $\text{Cs}_{12}\text{Sn}_{17}$.

Figure 1

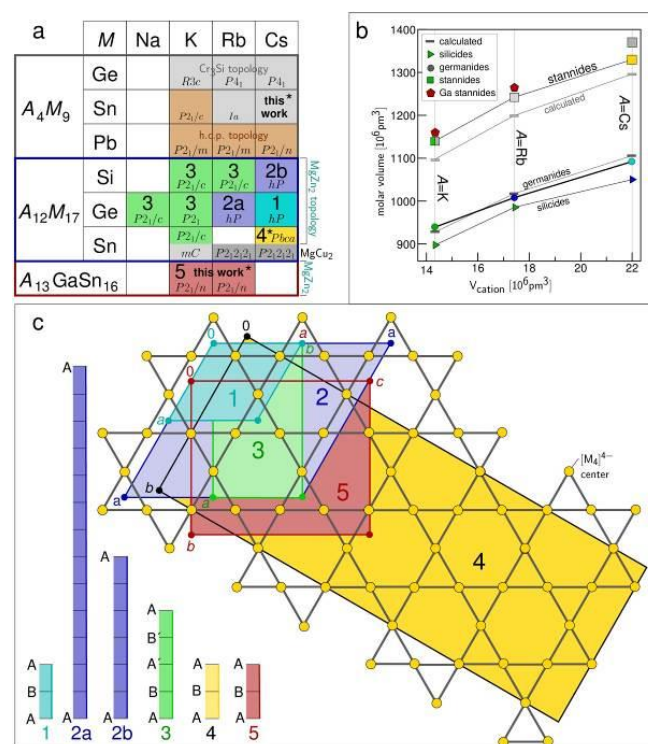
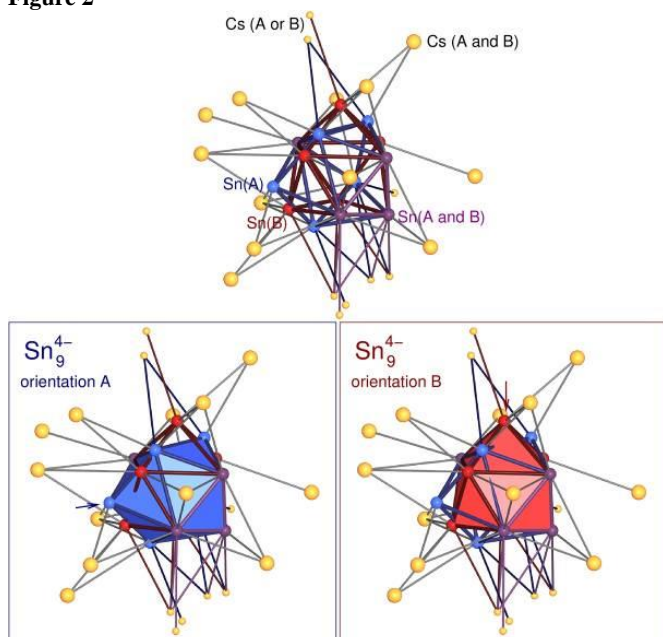


Figure 2



P067

Experimental Characterisation of Chemical Bonding in Elemental Boron Phases

C. Eisele¹, S. Dey², S. Mondal³, C. Paulmann^{4,5}, S. van Smaalen¹¹University of Bayreuth, Laboratory of Crystallography, Bayreuth, Germany²Indian Institute of Science, Education, and Research, Kolkata, Department of Chemical Sciences, Kolkata, India³CSIR-Central Glass & Ceramic Research Institute, Functional Materials & Devices Division, Kolkata, India⁴DESY, PETRA III, P24, Hamburg, Germany⁵Universität Hamburg, Mineralogisch-Petrographisches Institut, Hamburg, Germany

In contrast to all other stable elements in the periodic table, crystalline boron is still lacking of an indisputable phase diagram [1]. In recent times, previously established crystal structures of several boron phases and even their existence have been very questioned. Currently, there are three boron phases undoubtedly confirmed, namely α -, β -, and γ -boron [1].

Both α -boron and γ -boron feature a framework of interconnected icosahedra [2], whereby the γ -boron framework is supplemented by B₂ dumbbells [2].

The crystal structure of β -boron is much more complex. Its most widely accepted structure model was published by Slack *et al.* in 1988 [3]. Its framework consists of icosahedra and B₂₈-B-B₂₈ clusters. Furthermore, five so-called partially occupied sites, that are located in between the framework, were introduced by Slack [3]. According to Slack's model β -boron crystallises in space group *R*-3*m* and comprises 320.6 atoms per hexagonal unit cell.

Contrary to α -boron and the high-pressure phase γ -boron [4], the nature of the chemical bonding in β -boron has still not unambiguously clarified.

We have reinvestigated the crystal structure of β -boron with reduced symmetry based on high-resolution X-ray diffraction at 100 K. The aim is to get a more detailed structure model of β -boron along with a topological analysis of its chemical bonds via multipole refinements. By enlightening the bonding situation we

are also striving to get a deeper understanding of the peculiar physicochemical properties of β -boron, for example its striking thermodynamic stability at ambient pressure in all temperatures areas below the melting.

References

- [1] Shirai, *Jpn. J. Appl. Phys.* **56**, 05FA06 (2017).
- [2] Albert and H. Hillebrecht, *Angew. Chem. Int. Ed.* **48**, 8640 (2009).
- [3] A. Slack *et al.*, *J. Solid State Chem.* **76**, 52 (1988).
- [4] Mondal *et al.*, *Phys. Rev. B* **88**, 024118 (2013).

P068

A₃PCr₄O₁₆ (A = K, Cs) with supertetrahedral [PCr₄O₁₆]³⁻ units – rather orthophosphates with [PO₄]³⁻ tetrahedra and CrO₃ adducts than quaternary phosphatesH. Hillebrecht¹, M. Daub¹¹Albert-Ludwigs-Universität Freiburg, Institut für Anorganische Chemie, Freiburg, Germany

Chromate(VI)-phosphates with a composition A₃PCr₄O₁₆ (A = alkali metal) are known since a very long time. They contain supertetrahedral units [P(CrO₄)₄]³⁻ with a PO₄-tetrahedron in the centre. These quaternary phosphates are very unusual units. Recently it was shown by Wickleder *et al.*, that oligosulphates [SO₃]_nSO₄²⁻ (n = 4, 6) should be described not as polysulphates but as SO₃-adducts to SO₄²⁻ with increasing n [1]. So the [P(CrO₄)₄]³⁻ can alternatively be described as CrO₃ adduct to a PO₄ tetrahedron: [PO₄(CrO₃)₄]³⁻. Therefore we investigated A₃PCr₄O₁₆ (A = K, Cs) by means of single crystal XRD and ³¹P-NMR spectroscopy.

Room temperature measurement for K₃PCr₄O₁₆ confirms the data published previously [2], resulting in isolated [PCr₄O₁₆]³⁻ units]. The most significant feature are the high displacement parameters of the terminal O-atoms of the CrO₄ tetrahedra. At 150 K [*Pc*, Z = 8, a = 14.9964(5), b = 23.6262(7), c = 18.4679(6) Å, β = 106.602(2)°] there is a 4-fold super structure (b" = 2b; c" = 2c) caused by rotation of the [PCr₄O₁₆]³⁻ anions. P–O distances are typically for phosphates with isolated PO₄ tetrahedra (1.50 Å). Terminal Cr–O distances are close to 1.60 Å while the bridging ones are around 1.85 Å.

³¹P-MAS-NMR experiments revealed a chemical shift around 0 ppm. This is typical for Q0, i. e. isolated PO₄ tetrahedra. This confirms the interpretation from XRD results that K₃PCr₄O₁₆ should be seen as an orthophosphate and not as a quaternary phosphate, where negative shifts below –20 ppm are expected.

The new compound Cs₃PCr₄O₁₆ [*R*3*m*, Z = 3, a = 12.434(2), c = 10.383(2) Å] is at room temperature isotypically to the rhombohedral NH₄-compound [3]. The O-atoms of the CrO₃ unit show severe disorder, that hinders a discussion of the structural features in detail.

Figure 1: Structure of the [PCr₄O₁₆]³⁻ anion in K₃PCr₄O₁₆ at room temperature (left) and 150 K (right); ellipsoids with 50% probability.

- [1] M. Wickleder *et al.* *Angew. Chem. Int. Ed.* **2012**, *51*, 4997; **2016**, *53*, 16165.
- [2] M. T. Averbuch-Pouchot *et al.* *J. Solid State Chem.* **1981**, *38*, 253.
- [3] M. T. Averbuch-Pouchot *et al.* *J. Solid State Chem.* **1981**, *36*, 381.

Figure 1

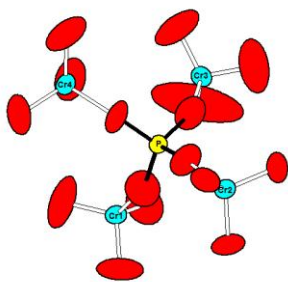
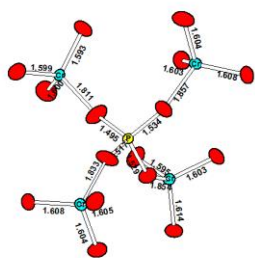


Figure 2


P070
Two Novel Mixed Alkali Praseodymium Orthoborates: $K_{1.319(8)}Li_{1.681(8)}Pr_2(BO_3)_3$ and $K_2LiPr(BO_3)_2$.

 P. Chen¹, M. Gogolin¹, M. M. Murshed^{1,2}, T. Gesing^{1,2}
¹Universität Bremen, Chemische Kristallographie fester Stoffe, Institut für Anorganische Chemie und Kristallographie, Bremen, Germany

²Universität Bremen, MAPEX Center for Materials and Processes, Bremen, Germany

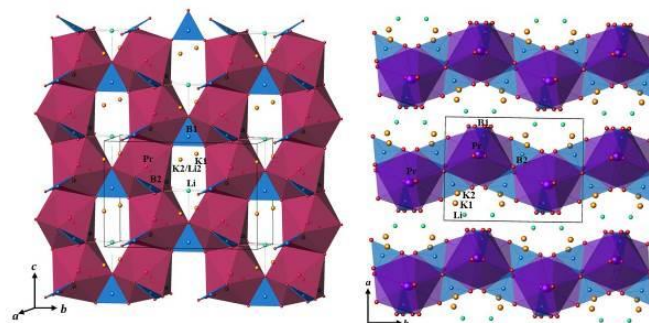
Crystals of two mixed alkali praseodymium orthoborates, $K_{1.319(8)}Li_{1.681(8)}Pr_2(BO_3)_3$ and $K_2LiPr(BO_3)_2$ were obtained by spontaneous crystallization. $K_{1.319(8)}Li_{1.681(8)}Pr_2(BO_3)_3$ was found to adopt the polar $Amm2$ space group with lattice parameters $a = 502.87(10)$ pm, $b = 1101.4(2)$ pm, $c = 731.41(15)$ pm. The structure is built by face-sharing PrO_9 chains sharing corners with planar BO_3 groups in the bc plane. These chains are further corner-shared and bridged by additional planar BO_3 groups along the a axis to build a three dimensional network $3_{\infty}[Pr_4B_6O_{18}]^{6-}$ with K and Li ions populating cavities in the structure. $K_2LiPr(BO_3)_2$ crystallizes in the monoclinic space group $P2_1/c$, with cell parameters $a = 712.27(5)$ pm, $b = 950.24(6)$ pm and $c = 999.26(6)$ pm, $\beta = 90.993(3)^\circ$. In this structure, corner-sharing PrO_8 polyhedra, interlinked by BO_3 groups form $2_{\infty}[Pr_4B_8O_{24}]^{12-}$ sheets in the bc plane. These $2_{\infty}[Pr_4B_8O_{24}]^{12-}$ sheets stack along a axis, in a layered manner with K and Li ions occupying the interlayer space. We found both two novel compounds offering infinite channels for lithium ions, which might be suitable for lithium-ion mobility.

Figure 1: Crystal structures of $K_{1.319(8)}Li_{1.681(8)}Pr_2(BO_3)_3$ (left) and $K_2LiPr(BO_3)_2$ (right).

References:

- [1] P. Chen *et al.*, *Z. Anorg. Allg. Chem.* **642** (2016), 424–430.
- [2] S. Bräuchle *et al.*, *J. Solid State Chem.* **253** (2017), 242–248
- [3] L. Zhao *et al.*, *Res. Bull.* **48** (2013) 277–280.
- [4] J. Zhao *et al.*, *Inorg Chem.* **53** (2014) 2501–2505.

Figure 1


P071
Structural diversity of 5-ammonium valeric acid lead iodides through incorporation of methylammonium or solvent

 M. Daub¹, H. Hillebrecht¹
¹Albert-Ludwigs-Universität Freiburg, Institut für Anorganische und Analytische Chemie, Freiburg i. Br., Germany

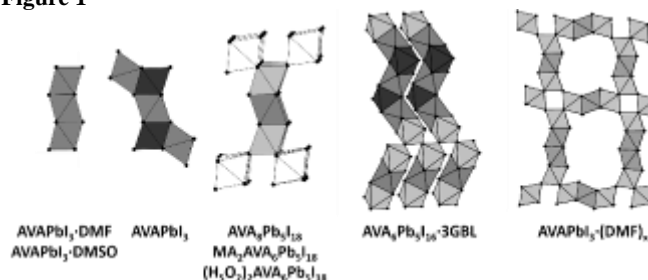
Lead halide perovskites $APbX_3$, $MAPbI_3$ (MA = methylammonium, CH_3NH_3) in particular, are from great interest because of the usage as efficient absorber layer in the so called perovskite solar cell's (PSC). [1] 5-ammonium valeric acid iodide ((AVAI, $HO_2C(CH_2)_4NH_3I$), is a widely used additive that shows promising improvements in terms of the stability of such PSC devices. [2] For a better understanding, which crystalline phases could be involved, we investigated the system PbI_2 -AVAI-(MAI)-(solvent) by using SC-XRD. As shown in fig 1 we found a great structural diversity. $AVAPbI_3 \cdot Lm$; (Lm = DMF, DMSO) consist of PbI_6 octahedra forming 1D chains by sharing common faces. In $AVAPbI_3$ also 1D chains of octahedra sharing common faces are found, but now with $Pb_{1/2}I_{4/2}$ and $Pb_{1/1}I_{4/2}I_{1/3}$ octahedral units. This is achieved through sharing opposed and adjacent faces alternatingly. In $A_2(AVA)Pb_5I_{18}$ (A = AVA, MA, H_5O_2) the topology of the Pb-I network can be described as a 2D $hcch$ perovskite. For $AVA_6Pb_5I_{16}$ (GBL)₃ a complex 2D structure with structural elements of the previous described topologies is found. In $AVAPbI_3 \cdot (DMF)_x$ a complex 3D framework structure with two different channels is build up by PbI_6 octahedra sharing common faces and corners.

Fig. 1 crystalline phases within PbI_2 -AVAI-(MAI)-(solvent). Gray octahedra share two opposite faces, dark gray ones share two adjacent faces, light gray ones are linked through corner and face sharing and white octahedra are exclusively connected by sharing common corners.

[1] M. M. Lee, J. Teuscher, T. Miyasaka, T. N. Murakami, H. J. Snaith, *Science* **2012**, *338*, 643–647.

[2] G. Grancini, C. Roldan-Carmona, I. Zimmermann, E. Mosconi, X. Lee, D. Martineau, S. Narbey, F. Oswald, F. De Angelis, M. Grätzel, M. K. Nazeeruddin. *Nature Communications*. **2017**, *8*, 15684.

Figure 1



P072

Observation of a polymorph of trisodium hexachlororhodate on dehydration

M. Etter¹¹DESY, FS-PE, Hamburg, Germany

Several trisodium hexachlorometalates (Na₃MCl₆ with e.g. M = Ir, Rh) are highly hygroscopic and often exhibit simultaneously multiple hydrated phases at ambient conditions. In order to determine the different crystal structures of these hydrated compounds, *in situ* powder X-ray diffraction experiments are performed, where the temperature is slowly increased and the evaporation of water leads to less hydrated compounds with lower water content until finally the anhydrous phase is formed. Usually, during this process the different hydrated phases become separated, which makes it easier to distinguish them and to start crystal structure solution attempts.

However, after performing a couple of *in situ* powder X-ray diffraction measurements on Na₃RhCl₆ and Na₃IrCl₆ it became clear, that also at elevated temperatures mixtures of hydrated phases are always present until the anhydrous compound is formed. Therefore, only the crystal structures of the anhydrous phases of Na₃RhCl₆ and Na₃IrCl₆ have been determined so far [1, 2].

Intriguingly, in some of the heating experiments on Na₃RhCl₆ a second phase coexisted at elevated temperatures together with the anhydrous phase until it was transformed fully into the known anhydrous Na₃RhCl₆ compound. This phase was determined to be a polymorph of Na₃RhCl₆ which surprisingly possesses the same space group as the stable anhydrous Na₃RhCl₆ phase, although lattice parameters and motif are different.

In this presentation structural details of the dehydrated Na₃RhCl₆ polymorph will be given as well as an overview to the so far performed *in situ* powder X-ray diffraction experiments on the hydrated phases.

[1] M. Etter, "The crystal structure of trisodium hexachlororhodate (Na₃RhCl₆)", Powder Diffraction 33 (2018), Issue 1, pp. 62-65, DOI: 10.1017/S0885715618000155

[2] M. Etter, Sebastian Bette and Melanie Müller, "The crystal structure of trisodium hexachloroiridate (Na₃IrCl₆)", submitted to Acta Cryst. E

P073

Rationalisation of the chemical composition and crystal structure in zinc germanium oxide nitrides

Z. Wang^{1,2}, J. Breternitz¹, S. Schorr^{1,2}¹Helmholtz-Zentrum Berlin, Structure and Dynamics of Energy Materials, Berlin, Germany²Freie Universität Berlin, Institut für Geologische Wissenschaften, Berlin, Germany

Zinc-group IV-nitrides are being considered as promising candidates for photovoltaic absorber materials, containing uniquely elements of low toxicity and low resource criticality.¹ Further to band gap tuning by alloying group IV elements, it has been postulated based on DFT calculations that these compounds possess a second mechanism for bandgap tuning through cation disorder.²

Herein, we study the effect of oxygen inclusion into the model system zinc germanium oxide nitride (ZGON) and its structural consequences. While pure zinc germanium nitride crystallises in the orthorhombic β-NaFeO₂-type structure with two defined cation

sites, more oxygen rich ZGON crystallises in the parent wurtzite-type structure with disordered cations on only one crystallographic site (Figure 1, left). This order-disorder transition can, therefore, effectively mimic the effects of cation disorder in the pure nitrides.

Using a two-reaction model for the ammonolysis of Zn₂GeO₄ introduced by Bacher *et al.*,³ (Figure 1, right) it is not evident that O-substitution and Zn-displacement occur simultaneously, and it is hence more complicated to determine the overall composition. Nonetheless, we have found a relationship between the Zn/Ge elemental ratio, easily accessible from XRF spectroscopy, and the O-substitution for the later reaction stages, which allows a convenient estimation of the overall composition (Figure 1, right). We assess this model with published data of the system⁴ as well as our own results⁵ to prove its reliability.

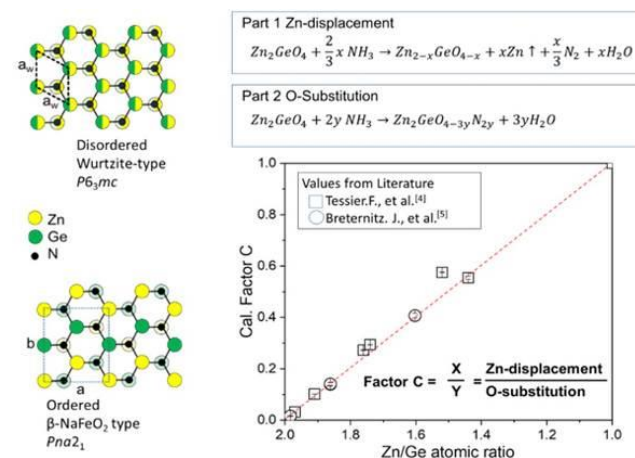
References

- [1] P. Narang, S. Chen, N. C. Coronel, S. Gul, J. Yano, L.-W. Wang, N. S. Lewis, H. A. Atwater, *Adv. Mater.* **2014**, *26*, 1235-1241
- [2] D. Skachov, P. C. Quayle, K. K. Kash, W. R. L. Lamprecht, *Phys. Rev. B* **2016**, *94*, 205201.
- [3] P. Bacher, G. Rault, M. Ghers, O. Merdrignac, J. Guyader, Y. Laurent, *Mater. Chem. Phys.* **1989**, *21*, 223-235.
- [4] F. Tessier, P. Maillard, Y. Lee, C. Bleugat, K. Domen, *J. Phys. Chem. C* **2009**, *113*, 8526-8531.
- [5] J. Breternitz, Z. Wang, A. Glibo, A. Franz, M. Tovar, S. Berendts, M. Lerch, S. Schorr, *submitted*.

Figure legends

Figure 1 Crystal structures of disordered (top left) and cation ordered (bottom left) ZGON; Two part reaction mechanism (top right)³ and factor C model assessment (bottom right).

Figure 1



P074

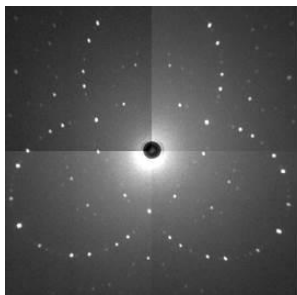
Neutron laue diffractometer für ambient and non-ambient single crystal analysis

M. Tovar¹, D. Wallacher¹, N. Grimm¹, A. Hoser¹, A. Budzianowski², D.Rusinek², D. Paliwoda³, S. Schorr^{1,4}¹Helmholtz-Zentrum Berlin, Berlin, Germany²National Centre for Nuclear Research, Otwock, Poland³Institute of Physics, Warsaw, Poland⁴Freie Universität Berlin, Berlin, Germany

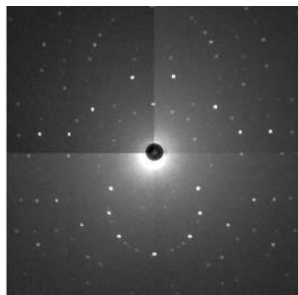
The FALCON Laue diffractometer at the Berlin neutron source BERII was developed in collaboration with the ILL, Grenoble. It is designed for fast neutron scattering data acquisition of single crystals and makes use of a white ("pink") neutron beam with

wavelength band of 0.8-3.2 Å. Pattern acquisition is performed by means of a backscattering and a transmission detector consisting of four iCDD cameras each. The detectors cover a read active area of 400x400 mm² and can be moved to optimize sample-detector distance. A chamber for non-ambient measuring conditions was developed. It opens up Laue data acquisition in temperature range of 80-450K. Examples for single crystal orientation, single crystal quality analysis, as well as non-ambient Laue diffraction will be presented.

Figure 1



Transmission Laue image, $\Omega=0^\circ$



Transmission Laue image, $\Omega=90^\circ$

Instrumentation

P075

Shine Bright Like a Diamond: Microfocus X-ray Sealed Tube Sources with Diamond Hybrid Anode Technology

J. Graf¹, T. Stürzer², H. Ott², M. Benning³, D. Roger^{2,4}, P. Radcliffe⁴, J. Schmidt-May⁴, C. Michaelsen⁴

¹Incoatec GmbH, Application, Geesthacht, Germany

²Bruker AXS GmbH, Karlsruhe, Germany

³Bruker AXS Inc., Madison, United States

⁴Incoatec GmbH, Geesthacht, Germany

Diamond exhibits several unique properties, such as high thermal conductivity, low thermal expansion, extreme hardness, chemical inertness and a fairly high transmission coefficient for X-ray radiation. The thermal conductivity of diamond is about 5 times higher than that of copper and the highest known conductivity of all bulk materials. Therefore, diamond is increasingly replacing traditional materials for the thermal management in challenging applications where a high local heat load needs to be dissipated, such as in heat sinks for high-power microelectronic devices. In X-ray sources, diamond can be used as a transparent heat sink directly coupled to the anode material. This improves the heat dissipation considerably and allows for an increase in tube brilliance by applying a higher power load on the anode.

The I μ S DIAMOND is a new type of microfocus sealed tubes using a unique anode technology, the diamond hybrid anode. It takes advantage of the exceptional high thermal conductivity of diamond by using a bulk industrial diamond as a heat sink, which is coated with a thin layer of the target material, such as Cu, Mo or Ag, making the heat dissipation in a diamond hybrid anode more efficient. Consequently, the I μ S DIAMOND can accept a higher power density in the focal spot on the anode. The intensity loss over time for the I μ S DIAMOND is only a few percent over 10,000 h of full power operation, which is significantly lower than the intensity degradation observed for microfocus rotating anodes. Therefore, the intensity of the I μ S DIAMOND is about 20% higher than the average intensity output of a modern microfocus rotating anode.

The I μ S DIAMOND establishes a new class of X-ray sources, combining an intensity output that exceeds the average intensity of a microfocus rotating anode with all the comfort and lifetime of a standard microfocus sealed tube with a bulk anode. In this presentation, we will be discussing the main features of the I μ S DIAMOND.

P076

Method for Determination of the Anisotropic Rotational Diffusion Constant of Microcrystals Dispersed in Viscous Liquid Medium

F. Kimura¹, S. Horii¹, I. Arimoto¹, T. Doi¹, M. Yoshimura², M. Wada^{1,3}, T. Kimura¹

¹Kyoto University, Kyoto, Japan

²National Synchrotron Radiation Research Center, Hsinchu, Taiwan

³Kyung Hee University, Yongin-si, South Korea

Introduction

Determination of the anisotropic rotational diffusion constants of microcrystals in suspension is difficult because the control of their initial orientation is difficult. Triaxial orientation of microcrystals can be realized by using modulated magnetic fields, which will serve as an initial orientation of microcrystals. In this study, we determined the anisotropic rotational diffusion constants D_{rot} of ErBa₂Cu₄O₈ (Er124) microcrystals in a suspension by *in-situ* monitoring of the temporal change of the broadening of X-ray diffraction (XRD) spots.

Objectives

Determine anisotropic D_{rot} of microcrystals in suspensions.

Results

We define $\langle\theta^2\rangle$, $\langle\psi^2\rangle$, and $\langle\phi^2\rangle$ as the mean square rotational fluctuations about the a , b , and c axes, respectively, of an Er124 microcrystal as shown in Fig. 1. The fluctuations $\langle\theta^2\rangle$ and $\langle\psi^2\rangle$ are approximately equal to the variances $\sigma^2(t)$'s of the $\{0k0\}$ and $\{h00\}$ XRD azimuthal peaks, respectively, where t is the elapsed time of rotational relaxation. Upon turning off the magnetic field, the variance starts to increase due to rotational diffusion, which is expressed by $\sigma^2(t) = \sigma^2(0) + 2D_{rot}t$, where D_{rot} is the rotational diffusion constant. $\sigma^2(t)$ was obtained as a function of time, from which D_{θ} , D_{ψ} and D_{ϕ} were determined. We obtained $D_{\theta} = 2.1 \times 10^{-6}$, $D_{\psi} = 0.9 \times 10^{-6}$, and $D_{\phi} = 1.1 \times 10^{-6}$ rad²/s.

Conclusion

By combination of the triaxial initial orientation of microcrystals in suspension with subsequent temporal XRD monitoring, we successfully determined the rotational diffusion constants about the different crystallographic axes of the microcrystals of ErBa₂Cu₄O₈⁽¹⁾.

Acknowledgements

This work was partly supported by A-STEP, JST.

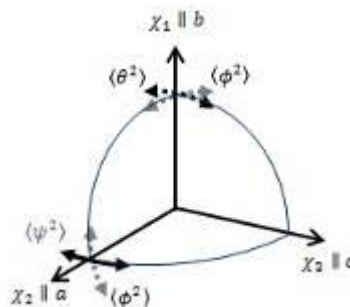
Reference

[1] F. Kimura, S. Horii, I. Arimoto, T. Doi, M. Yoshimura, M. Wada, and T. Kimura, *J. Phys. Chem. A*, 2018, **122** (46), pp 9123–9127.

Figure legend

Figure 1. Definition of the mean square fluctuations $\langle\psi^2\rangle$, $\langle\theta^2\rangle$, and $\langle\phi^2\rangle$ about the b , a , and c axes, respectively.

Figure 1



P077

Advanced anomalous diffraction capabilities at KMC-2 (BESSY II)

D. M. Többens¹, I. Zizak¹, S. Schorr¹

¹Helmholtz-Zentrum Berlin, Structure and Dynamics of Energy Materials, Berlin, Germany

The monochromator of KMC-2 beamline [1] at synchrotron BESSY II, Berlin can now be controlled directly from the diffraction endstation. This allows for seamless usage of photon energy as an adjustable parameter, extending the range of possible techniques employing anomalous diffraction. In particular, Multi Energy Diffraction Analysis (MEAD) is feasible now. In this technique individual Bragg peaks are tracked over an elemental X-ray absorption edge. The intensity changes depending on the structure factor can be highly characteristic for Miller indices selected for a specific structural problem. This method is suitable

for thin-films, where Rietveld-based approaches are problematic. KMC-2 allows active stabilization of the monochromator intensity to 0.3% standard deviation and complementary collection of the fluorescence spectrum and is thus well suited for this experimental technique.

We demonstrate feasibility and exigencies for the determination of copper-zinc ordering in crystal structures. Cu^{+1} and Zn^{2+} are isoelectronic and assume very similar coordination geometry, are thus undistinguishable by normal X-ray diffraction. A well-characterized [1] sample of CZTSe ($\text{Cu}_2\text{ZnSnSe}_4$), with Kesterite structure and carefully tempered for maximum Cu/Zn order, has been analyzed for procedure development. Results of 110 Bragg peak analysis clearly proves Kesterite over Stannite structure, while Bragg peak 011 (figure) reveals strong ordering within the Kesterite structure. The quality of the results is comparable to previous anomalous Rietveld analysis [1,2] or MEAD [3] analyses, but required only comparatively short measuring times.

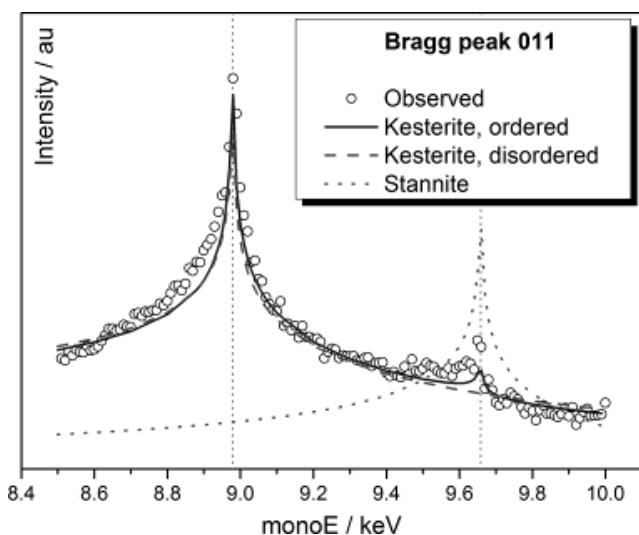
[1] Helmholtz-Zentrum Berlin für Materialien und Energie: *J large-scale research facilities*, **2**, A49 (2016)

[2] D. M. Töbrens et al.: *Phys Status Solidi (b)* **253**(10), 1890 (2016)

[3] D. M. Töbrens et al.: *Powder Diffr.* **31**(03), 168 (2016)

[4] H. Nozaki et al.: *J Alloys Compd.* **524**, 22 (2012)

Figure 1



P078

Sample environment chamber for the manipulation of temperature and electric field for synchrotron measurements

M. Nentwich¹, T. Weigel¹, M. Zschornak^{1,2}, C. Richter³, E. Mehner¹, H. Stöcker¹, D. C. Meyer¹

¹Technische Universität Bergakademie Freiberg, Institut für Experimentelle Physik, Freiberg, Germany

²Helmholtz-Zentrum Dresden-Rossendorf, Institute of Ion Beam Physics and Materials Research, Dresden, Germany

³ESRF, ID01, Grenoble, France

During the design and construction phase of the *Chemical Crystallography Beamline P24*, our group designed a sample environment chambers for (resonant) *X-Ray Diffraction (XRD)* experiments within one hemisphere of solid angle. The main applications targeted are the *in-situ* and *in-operando* research of materials for energy conversion and storage. Here, we will present the possibilities of the complex *Nordseekammer* and some

preliminary results gained during the previously started commissioning phase of beamline P24.

The *Nordseekammer* consists of a standard vacuum cross, a heater, a cooling system, electrical feedthroughs, and radiolucent domes. This equipment allows a nominal temperature range of -196 °C (liquid nitrogen) up to +1200 °C. We already successfully tested the chamber in the range of -177 °C and +400 °C. The electrical contacts allow the application and measurement of voltages in the range of 10 μV up to 5 kV. We already performed electro-forming experiments applying 500 V to a SrTiO₃ bulk sample over more than 20 hours while measuring currents in the magnitude of nA and μA. At the moment, the chamber possesses three different dome materials: PC, PS, and PEEK. Previous experiments show satisfactory results using the optically transparent PC domes with tolerable radiation damage at the dome itself.

We aim to extend the possibilities of the chamber by establishing automated control and measurement of temperature, voltage, and current. On the one hand, this enables the characterization of the pyroelectric coefficient of energy conversion materials. On the other hand, the cycle stability of energy storage materials can be evaluated. Both characterizations could be performed while X-Ray Diffraction experiments are conducted thus allowing simultaneous structure characterization, even under resonant conditions.

P079

Extreme Condition Single Crystal Diffraction with Hot Neutrons on HEiDi at MLZ

M. Meven¹, A. Grzechnik², H. Deng¹, R. Dutta¹, K. Friese³

¹RWTH Aachen University, Institute of Crystallography, Outstation@MLZ, Aachen, Germany

²RWTH Aachen University, Institute of Crystallography, Garching, Germany

³Forschungszentrum Jülich GmbH, JCNS 2 / PGI 4, Jülich, Germany

Single crystal diffraction is one of the most versatile tools for detailed structure analysis. Due to their specific peculiarities neutrons are a very useful probe for structural studies on various hot topics related to physics, chemistry and mineralogy. The single crystal diffractometer HEiDi at the research neutron source at the Heinz Maier-Leibnitz Zentrum (MLZ) offers high flux, high resolution and large q range, low absorption and high sensitivity for light elements.

In order to adapt this instrument to the most recent scientific topics its sample environment is continuously extended and improved. For instance, at low temperatures various multiferroic compounds from the melilite family were studied not only in order to reveal their orthorhombic antiferromagnetic structures but also the risks of misinterpretation of structural data due to multiple scattering [1].

At very high temperatures studies on Nd₂NiO_{4+δ} and Pr₂NiO_{4+δ} brownmillerites concerning their oxygen diffusion pathways reveal anharmonic displacements of the apical oxygens pointing towards the interstitial vacancy sites which create a quasicontinuous shallow energy diffusion pathway between apical and interstitial oxygen sites [2]. Recent studies use a special mirror furnace developed at MLZ which allows not only temperatures > 1300 K but also atmospheres with various oxygen content and pressure around the sample to study their influence to the evolution of the occupation of the interstitial sites.

Last but not least recently a BMBF funded project was launched in order to develop new pressure cells for HEiDi which can be combined with its existing low temperature equipment in order to study structural properties down to temperatures below 10 K, e.g.

MgFe₄Si₃ compounds and their magnetic features ([3] and A. Eichs contribution to this annual meeting).

Aside from some scientific examples this contribution focuses on the overview of the most recent instrumental developments at HEiDi.

- [1] A. Sazonov et al.; Origin of forbidden reflections in multiferroic Ba₂CoGe₂O₇ by neutron diffraction: Symmetry lowering or Renninger effect?; *J. App. Cryst.* 49(2) (2016).
 [2] M. Ceretti et al.; Low temperature oxygen diffusion mechanisms in Nd₂NiO_{4+δ} and Pr₂NiO_{4+δ} via large anharmonic displacements, explored by single crystal neutron diffraction; *J. Mater. Chem. A* 3 (2015).
 [3] A. Grzechnik et al.; Single-Crystal Neutron Diffraction in Diamond Anvil Cells with Hot Neutrons; *J. Appl. Cryst.* 51 (2018).

P080

First single crystal diffraction experiments on the Ga- and In-MetalJet

N. Nöthling¹, C. W. Lehmann¹

¹Max-Planck-Institut für Kohlenforschung, Chemical Crystallography and Electron Microscopy, Mülheim an der Ruhr, Germany

Herein we report the first single crystal diffraction experiments using the In-rich ExAlloy I2 in our MetalJetD2+ X-ray source. The synchrotron-like photon flux densities as well as the source spectra have been characterized in our previous work. The experimental base is an optimized and stepper motor driven, HUBER Diffraktionstechnik phi-axis goniometer. It is mounted on top of a self-constructed x-, y-, z-stage which allows three additional translational motions. Data acquisition was realized by using a Dectris Pilatus 300k CdTe hybrid pixel detector for high quantum yields at fixed theta positions. Initial results of indexing, data integration, structure solution and refinement are shown. Data of both radiation types (Ga and In K-alpha) will be compared to conventional x-ray sources. We plan to expand the single axis to a four circle goniometer equipped with a low temperature cryo stream.

P081

Prediction of possible uranium compounds in drinking waters

N. Tegshbayar^{1,2}, O. Bolormaa², K. Tsookhuu¹

¹National University of Mongolia, Department of Physics, Ulaanbaatar, Mongolia

²National University of Mongolia, Chemistry, Ulaanbaatar, Mongolia

Uranium content in drinking water is very low and it" concentration is not easy to determine. This work introduces a hypothetical method of estimating the chemical composition of uranium in water in Piper's and Forbaux's diagram based on the results of the uranium content, physical-chemical properties and major ions in water. The Piper diagram describes the dominated major ions in the water, or the chemical composition of the water and the geochemical evolution of the water, whereas the Whitney diagram or the E-diagram diagram defines the thermodynamic conditions of the constituent properties of the chemical in a variety of solutions. In figure 1 shows Piper diagram of the hydro-chemical analysis of UB in the groundwater samples and in Figure 2 shows Forbaux diagram in which the black spot on the middle of the diagram shows the range of the selected samples.

For selected samples calculated correlation between major elements which is shown in Table 1.

Table 1. Correlation analysis UB drinking water for uranium-major ions

	Ca ²⁺	Mg ²⁺	Cl ⁻	CO ₃ ²⁻	HCO ₃ ⁻	SO ₄ ²⁻	U
Ca ²⁺	1						
Mg ²⁺	0.668	1					
Cl ⁻	0.807	0.4911	1				
CO ₃ ²⁻	0.252	0.3740	0.2831	1			
HCO ₃ ⁻	0.337	0.5120	0.4260	0.731	1		
SO ₄ ²⁻	-0.1120	0.4320	0.0270	0.538	0.660	1	
U	-0.0190	0.3620	0.0870	0.804	0.744	0.7411	1

r(x,y,α = 0.05, f = 48) = 0.288

Based on these results, it can be predicted the chemical compounds such as uranium hydrocarbonate UO₂ (HCO₃)₃ and uranium carbonate UO₂ (CO₃)₂ in drinking water.

References

- [1] Tegshbayar. N, Ankhnybayar, B, Batdulam. B , Bolormaa. O, Tsookhuu Kh "Uranium hydrochemical study of ground and drinking waters in Ulaanbaatar city, Mongolia" Int. Cong. On Chemistry and Materials science, Ankara, Turkey, 5-7 October, pp 87, 2017
 [2] Pourbaix, M., Atlas of electrochemical equilibria in aqueous solutions. 2d English ed. 1974, Houston, Tex.: National Association of Corrosion Engineers.
 [3] Piper, A.M. (1953). *A Graphic Procedure in the Geochemical Interpretation of Water Analysis*. Washington D.C.: [United States Geological Survey](#). OCLC 37707555. ASIN B0007HRZ36.
 [4] N.Tegshbayar, K.Tsookhuu, Seasonal Variation of Radon Content in Drinking Water of Ulaanbaatar, Normal University of Inner Mongolia, China J.Science, 2017, No 1, China P 1-7

Figure 1

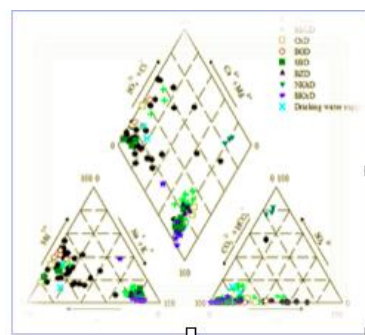


Figure 1. Piper's diagram for drinking water of Ulaanbaatar city

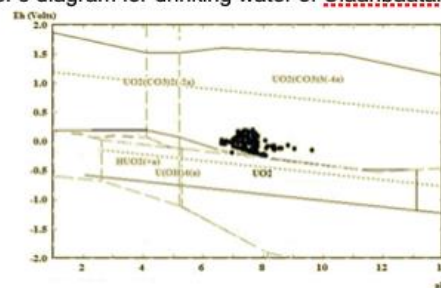


Figure 2. Pourbaix diagram for drinking water of Ulaanbaatar city

P082

Numerical simulation of Coherent Phasing Method for Macromolecular Electron Crystallography

K. Khakurel¹

¹ELI beamlines, Prague, Czech Republic

Ultrafast electrons sources are constantly evolving in the past decade. The short probe-pulse from such sources enables to follow the events in physical and biological sciences at unprecedented time scale. The only competent technique that allows following the changes in molecules at the length scales comparable to their atomic dimensions, is crystallography. In crystallography, an array of molecule interacts with electrons and the corresponding diffraction

photographs are recorded. Such diffraction photographs contains the information on themagnitude of scattered wave but the phase information is entirely lost. In this project, we propose to develop a novel phasing method for crystalline object, based on iterative phasing algorithm. The iterative phasing method we propose to use is called Ptychography. Use of Ptychographic phasing can relax the stringent requirement posed in existing phasing methods used in crystallography. Here, we present a comprehensive numerical study on the use of Ptychographic phaing of electron crystallography. The poster will present the current computational and instrumental needs to develop such phaing method for macromolecular elctron crystallography.

Micro- and nanocrystalline materials (powder diffraction, EM, ...)

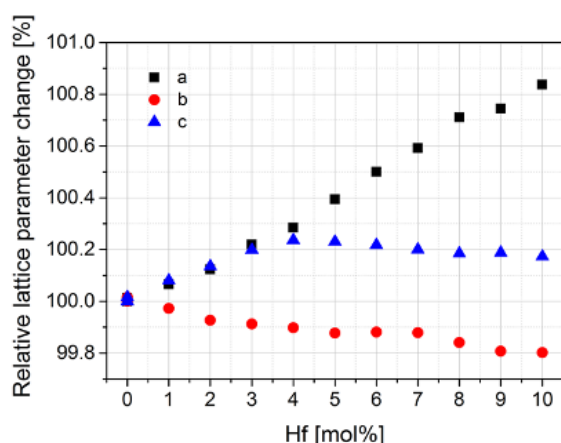
P084

Combinatorial search for new alternative fuel cell electro-catalyst support materials

K. Stöwe¹, A. Clausing¹, D. Reichert¹, T. Schwarz¹, M. Weber²¹Chemnitz University of Technology, Chemical Technology, Chemnitz, Germany²Saarland University, Saarbrücken, Germany

The competitive capability and economic efficiency of electro-catalytic devices as for instance the proton exchange membrane fuel cell (PEMFC) are directly related to electro-catalyst performance and costs. FC electro-catalysts are typically supported by carbon blacks (CB), although these materials undergo severe degradation and corrosion under the operation conditions of low pH, high humidity and electrode potential as well as oxidative environment on the cathode side of the fuel cell. Therefore, there is a growing demand for alternative catalyst support materials. There is only a small number of conducting inorganic oxides qualifying them as electro-catalyst support materials as iridium and ruthenium dioxide. The usage of precious metal elements is limited by their low abundance and high cost. Thus, we performed a combinatorial screening of potential metal oxides on stability in acidic media revealing stable binary oxides. For oxides with insufficient conductivity mutual doping was tested as method to improve their properties. Powder XRD data as function of dopant grade revealed structural parameters as lattice parameters and crystallite sizes indicating solid solution formation, electric conductivity measurements displayed electronic changes of the materials prepared. We report here on screening and characterisation results of electrode materials as combination of an acid stable oxide as IrO₂ in dilution of one of the other stable binary oxides as TiO₂ or SnO₂ as well as other solid solution systems. These were prepared by different synthesis methods as precursor-based sol-gel methods, wet impregnation as well as continuous precipitation in an impinging jet microreactor setup. The impact of the synthesis method on the solid solution formation as well as the conductivity mechanism (e.g. percolation theory versus band structure effects in solid solution mixed metal oxides) is elucidated by different physical characterisation methods and discussed.

Figure 1



P085

Cellular automata models for intra-cage reactions in sodalites

L. Robben^{1,2}¹Universität Bremen, Institut für Anorganische Chemie und Kristallographie, Bremen, Germany²Universität Bremen, MAPEX Center for Materials and Processes, Bremen, Germany

The concept of cellular automata (CA) was formulated by John von Neumann and Stanislaw Ulam in 1948 [1,2]. CA are exactly computable models of systems, consisting of a cell grid, several cell states and a set of rules determining cell state changes. Their time-dependent behaviour governed by the rule set can be very complex, even for very simple rule sets. Sodalites are the simplest zeolites, their framework, build by 3-dimensional connected TO₄ tetrahedra, forms only one cage type (*sod*). These cages form a body-centred cubic net. Using this net as a CA grid, the cell states can describe the cage filling ion and the rule set can be understood as a description of chemical reactions or diffusion processes. Thus, CA should be able to describe intra-cage reactions in sodalites.

The aim of the study is to develop CA models for different intra-cage reactions in sodalites and to derive parameters describing structure properties for comparison with experimental data.

Therefore, CA models were developed for 3 reactions in aluminosilicate sodalites (decomposition of MnO₄⁻ [3], reaction of NO₂⁻ in CO₂ atmosphere [4] and in air). In the first two cases the models can reproduce the different template ordering schemes. For the reactions of nitrat-sodalite in different atmospheres the different shapes of the experimentally determined Avrami-plots were reproduced by the CA models, helping to understand the reaction behaviour.

Out of the obtained results we can conclude that CA are a very useful tool to simulate intra-cage reactions in sodalites, they are easy to implement and computationally efficient. If the exact reaction mechanism is unclear, different mechanisms can be implemented in the rule set and their consequences on experimentally determinable parameters can be evaluated.

[1] Vichniac, *Physica*10D (1984) 96[2] J. Kari, *Theo. Comp. Sci.*334 (2005) 3[3] H. Petersen et al., *Micro. Meso. Mater.* 242 (2017) 144[4] M. Šehović et al., *Z. Krist.* 230 (2015) 263–269.

P086

Synthesis and characterisation of ultra-small monometallic and bimetallic noble metal nanoparticles (Ag, Au, Pt, AgPt, AgAu)

O. Wetzel¹, M. Epple¹, K. Loza¹, M. Heggen¹¹University of Duisburg-Essen, Inorganic Chemistry, Essen, Germany

Ultra-small nanoparticles are particles with a size of 1 to 3 nm and define the transition from nanoparticles to single molecules.[1] Due to their small size and the corresponding high specific surface area, the particle properties are different compared to the bigger particles. For instance, the continuous energy band of bulk metals is split into discrete energy values with decreasing particle size (size quantization effect). Hence, the surface plasmon resonance disappears.[2] Furthermore, an autofluorescence was reported for ultra-small gold particles.[3]

These properties make ultra-small particles very interesting for biomedical research. Their extreme small diameter allow them to pass through a cell membrane and even enter in the cell nucleus.[1]

The autofluorescence enables an observation without additional fluorescent ligands.

In order to achieve a controllable synthesis of monodisperse ultra-small particles with uniform diameter, the metal cations were first reacted with thiols like 11-mercaptoundecanoic acid or L-cysteine and then reduced with sodium borohydride. Monometallic (Ag, Au, Pt) and bimetallic particles were prepared (AgPt, AgAu). The particles were characterized by transmission electron microscopy (TEM), differential centrifugal sedimentation (DCS), ultraviolet-visible spectrophotometry (UV-Vis), and nuclear magnetic resonance spectroscopy (NMR).

TEM shows monodisperse particles with a size of about 2 nm, in good agreement with the diameter from DCS in dispersion. The lack of surface plasmon resonance in the UV-Vis confirms the absence of bigger particles.

References:

- [1] Zarschler K, et al, Nanomedicine: NBM 2016, 12, 1663.
- [2] M.M. Alvarez, J. T. Khoury, T. G. Schaaff, M. N. Shafiqullin, I. Vezmar, R. L. Whetten, J. Phys. Chem. B, 1997, 101, 3706.
- [3] S. Ristig, D. Kozlova, W. Meyer-Zaika M. Eppele, J. Mater. Chem. B, 2014, 2, 7887[EMPD1]

P087

XPS investigations on quartzite surfaces of natural rock samples for proof of Al exposure

K. J. Huenger¹, M. Kositz², M. Danneberg², J. Radnik³

¹BTU Cottbus-Senftenberg, Research & Materials Testing Institute, Cottbus, Germany

²BTU Cottbus-Senftenberg, Chair Building Materials&Chemistry, Cottbus, Germany

³BAM Federal Institute for Materials Research and Testing, Department 6.1, Berlin, Germany

Introduction

ASR (alkali silica reaction) is a damaging reaction, which influences the durability of concrete. To inhibit this reaction high aluminum containing additives are added to the concrete mixtures, which are very effectively. The inhibition mechanisms are not completely understood. However one effect is that the dissolution rate of silica from aggregates is strongly reduced by presence of Al. One reason for this could be changes of the surfaces properties. This point of view has been discussed for some years [1,2].

Objective

Solubility experiments of quartzite grains, prepared as thick sections with and without the presence of soluble Al in the alkaline KOH-solution, show a reduction of the silica concentration. First advices for a very thin layer on the surface can be given by light microscope characterizations. Due to the fact, that many methods failed so far, the XPS method was selected to investigate this thin layer.

Results

The effect of Al to reduce the silica releasing rate can be demonstrated. XPS spectra of the quartzite surface confirm an Al exposure there. (Fig. 1). Depth profile measurements were made to determine the layer thickness of this Al containing sheet with 8-10 nm (Fig. 2). The calibration occurs with a quartz crystal. Binding energies could be measured with high-resolution XPS, measured results can be discussed.

Conclusion

It should be possible to characterize surface areas of natural stones prepared and polished in the same way as for light microscopy

investigations by using XPS. The assumed thin layer on the surface of quartzite grains can be confirmed in first steps. The layer thickness is approx. 8-10 nm which is obviously too thin for using other methods. However the composition and structure of such a sheet is not clearly yet. Binding energy results indicate an aluminium structure with an octahedral coordination, an aluminosilicate structure has to be preferred, because of the conditions of the sheet formation.

Figure 1

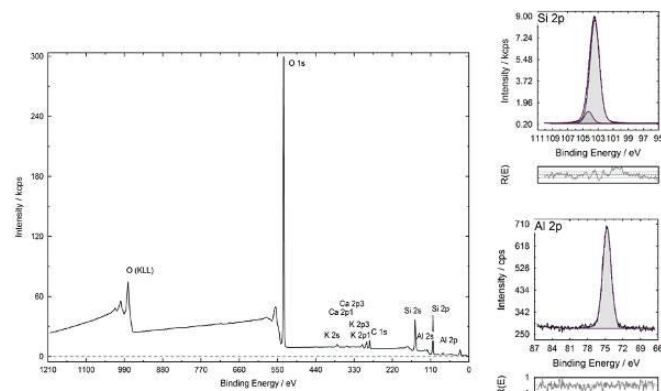


Fig. 2: XPS-results of stored quartzite samples, right: high resolved Si2p and Al2p-spectra

Figure 2

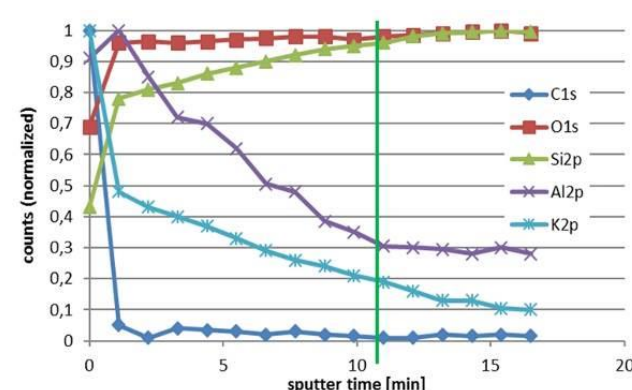


Fig. 2: XPS-results (depth profile) of a quartzite sample, deposited in „Metakaolin-solution“ (1 min = 1 nm)

P088

Crystal structure of kaňkite, FeAsO₄·3.5H₂O, and its dehydration product Fe₂(AsO₄)(HASO₄)(OH)(H₂O)₃

J. Majzlan¹, J. Plášil², L. Palatinus², G. Steciuk²

¹University of Jena, Institute of Geosciences, Jena, Germany

²Czech Academy of Sciences, Institute of Physics, Praha, Czech Republic

Kaňkite is a mineral that commonly occurs at sites where mining waste with arsenopyrite (FeAsS) are weathering in contact with atmospheric oxygen and water. Along with similar minerals, it is responsible for retention and release of arsenic, an element of concern for public health and environment. Characterization of such wastes, including the identification of the phases that control solubility of arsenic and other elements, requires the knowledge of the structures of the participating phases (for powder X-ray diffraction screening) and their spectroscopic signature.

In this work, we have attempted to solve the structure of kaňkite by precession electron diffraction tomography. A structure was solved and refined; initially, we believed that we solved the structure of kaňkite. The powder XRD data, however, could not be indexed

with the unit cell determined by electron diffraction. Variable-temperature powder X-ray diffraction showed that kaňkite dehydrates to another, better crystalline phase with composition $\text{FeAsO}_4 \cdot 2\text{H}_2\text{O}$ at temperatures of 55–65 °C. The structure of this phase was the solved structure. It possesses the space group Cc and the model was refined by the full-matrix least-squares method by Jana2006. The model converged to $R(\text{obs}) = 9.52\%$, $wR(\text{obs}) = 8.91\%$ (with $\text{GOF} = 3.40$) for 2126 observed reflections with $[I_{\text{obs}} > 3\sigma(I)]$. The structural formula of the dehydration product is $\text{Fe}_2(\text{AsO}_4)(\text{HAsO}_4)(\text{OH})(\text{H}_2\text{O})_3 (= \text{FeAsO}_4 \cdot 2\text{H}_2\text{O})$. The structure of the dehydration product of kaňkite consists of corrugated heteropolyhedral sheets. Pairs of $\text{Fe}\Phi_6$ octahedra, flanked by five adjacent arsenate tetrahedra, could be seen as the building units of the corrugated sheets. Based on the similar topology of $\text{FeAsO}_4 \cdot 2\text{H}_2\text{O}$ and the mineral lausenite $[\text{Fe}_2(\text{SO}_4)_3 \cdot 5\text{H}_2\text{O}]$, and the structural relationship between lausenite and kornelite $[\text{Fe}_2(\text{SO}_4)_3 \cdot 7.5\text{H}_2\text{O}]$, we conjecture that the structure of kaňkite could be also built by corrugated sheets. One polyhedral linkage between a $\text{Fe}\Phi_6$ octahedron and an $\text{As}\Phi_4$ tetrahedron in the sheet of the dehydrated kaňkite needs to be broken to allow for stretching of the sheets, the introduction of an additional H_2O molecule into the sheet and perhaps also additional H_2O molecules in between the sheets. Additional work shows that even under cryogenic conditions, kaňkite rapidly converts to its dehydration product. At $T = 120 \text{ K}$, the unit cell is even larger than at room temperature.

P089

Heterocyclic Ligands for Water Sorption in Metal–Organic Frameworks: A Structural Study Using the Rietveld Method

M. Wharmby¹, H. Reinsch², D. Lenzen², M. Wahiduzzaman³, G. Maurin³, N. Stock²

¹DESY, P02.1/FS-PE, Hamburg, Germany

²Christian-Albrechts Universität zu Kiel, Institut für Anorganische Chemie, Kiel, Germany

³Université Montpellier, Institut Charles Gerhardt Montpellier, Montpellier, Germany

The application of metal-organic frameworks (MOFs) as water sorbents for de-/humidification and water production applications has grown in popularity in recent years. MOFs constructed from high-valence metals, such as Zr^{4+} or Cr^{3+} , have demonstrated good stability under operating conditions (i.e. repeated ad-/desorption cycles under hydrothermal conditions), with a number of Al^{3+} -based MOFs showing even better stability and water sorption performances. For instance, aluminium isophthalate $[\text{Al}(\text{OH})(\text{O}_2\text{C}-\text{C}_6\text{H}_4-\text{CO}_2)]$, also known as CAU-10 (CAU = Christian-Albrechts-Universität), [1] has achieved at least 10,000 water sorption cycles. [2] By replacing the isophthalate unit with structurally similar heterocyclic linker molecules (i.e. 2,6- and 3,5-pyridinedicarboxylic acids or furandicarboxylic acid), three new coordination compounds were obtained, the structures of which were refined by the Rietveld method. [3,4] Two of these have extended 3d-networks and demonstrate promising water sorption properties: CAU-10-pydc and MIL-160 (MIL = Matériaux Institut Lavoisier). [5] Interestingly both compounds show a displacive phase transition on ad-/desorption of water, which has also been fully characterised. For MIL-160, DFT calculations have been used to verify the locations of water molecules determined as part of the Rietveld refinement and these have been found to be in excellent agreement.

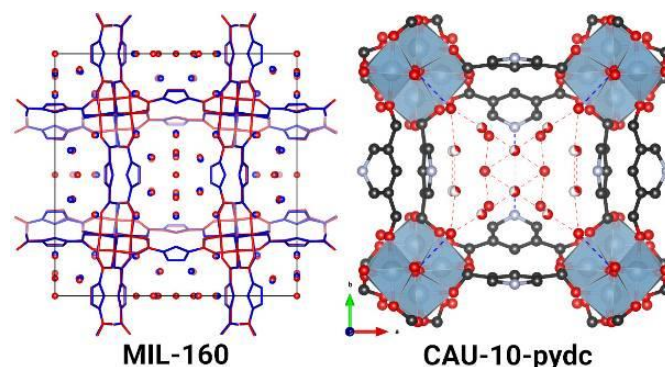
References

- [1] H. Reinsch, et al., *Chem. Mater.* **2012**, 25, 17–26.
- [2] D. Frohlich, et al., *J. Mater. Chem. A* **2016**, 4, 11859–11869.
- [3] M. Wahiduzzaman, et al., *Eur. J. Inorg. Chem.* **2018**, 2018, 3626–3632.
- [4] M. T. Wharmby, N. Stock, *Z. Anorg. Allg. Chem.* **2018**, 644,

1816–1825.

[5] A. Cadiou, et al., *Adv. Mater.* **2015**, 27, 4775–4780.

Figure 1



P090

New tricks for an old dog: The Powder Diffraction and Total Scattering Beamline P02.1 at PETRA III, DESY

M. Wharmby¹, M. Etter¹, A. Schökel¹, J. C. Tseng¹, M. Wendt², S. Wenz²

¹DESY, P02.1/FS-PE, Hamburg, Germany

²DESY, FS-PE, Hamburg, Germany

Powder X-ray diffraction (PXRD) is widely used as an initial characterisation method and to study the bulk behaviour of periodic solids under application of external stimuli. In many cases, the local structural changes which occur are of as much interest as the periodic behaviour; moreover, being able to probe partially or fully amorphous compounds allows the researcher to investigate a wider range of samples. Following a recent upgrade of the Powder Diffraction and Total Scattering Beamline, P02.1, the PETRA III third generation synchrotron light source (DESY, Hamburg), it is now possible to simultaneously collect both PXRD and total-scattering data; processing of the latter yields a Pair Distribution Function (PDF) containing information on the local structure. With a fixed energy of 60 keV, the beamline is able to collect total-scattering data for PDF data with a Q_{Max} of at least 20 \AA^{-1} , whilst PXRD data can be collected with a resolution of 0.005° ($\Delta Q \sim 2.65 \times 10^{-3} \text{ \AA}^{-1}$) over an angular range of $0\text{--}12^\circ 2\theta$ (equivalent to more than $100^\circ 2\theta$ with standard $\text{Cu K}\alpha$ radiation), more than adequate for Rietveld refinement. Moreover, the beamline offers a wide range of non-ambient sample environments, including variable temperatures (hot-air blower – RT–1100 K; cryostream – 90–500 K; cryostat – 10–300 K), gas sorption (up to 1 bar pressure) and electrochemistry, which may be used to understand the behaviour of samples in situ or operando. A robot is also now available for automated beamline.

This poster will offer current and potential future users to find out about the recent developments at P02.1, as well as our future plans for automation. This is also an excellent opportunity to discuss these changes and other user requirements for upcoming beamtime applications with beamline staff.

Figure 1



Organic molecules and coordination compounds

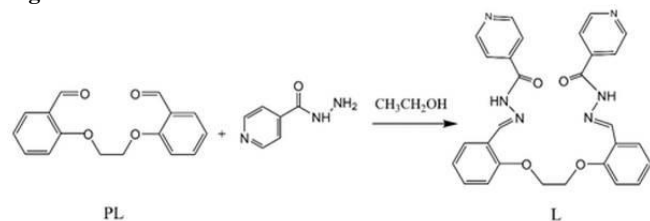
P092

Bulk Crystallized Hydrazone Ligand vs. Its Layered Crystallized Zn(II) ComplexL. Noohinejad¹, S. A. Hosseini-Yazdi¹, N. van Well², S. van Smaalen²¹University of Tabriz, Inorganic Chemistry, Tabriz, Iran²University of Bayreuth, Laboratory of Crystallography, Bayreuth, Germany

The chemistry of transition metal complexes of the hydrazone ligands has attracted extensive attention because of their versatile framework topologies and their biological relevance [1-3]. Hydrazones are compounds, that can coordinate to the metal either as a neutral ligand or as a deprotonated anion and they exist in two tautomeric forms, keto and enol. The delocalization and the configurational flexibility of the molecular chain can give rise to a great variety of coordination modes. Here we present the synthesis, characterization and crystal structures of a hydrazone ligand with N_6O_4 donor sets (**L**) and its Zn(II) complex which is in a neutral and keto form of **L**. **L** was synthesized based on Schiff base condensation of 2-[3-(2-formylphenoxy)-2-hydroxypropoxy]benzaldehyde (**PL**) [4] and 4-Pyridinecarboxylic acid hydrazide. 1:1 molar ratio of $Zn(CH_3COO)_2 \cdot 2H_2O$ and **L** in solvents mixture of methanol and chloroform gave rise to the $[ZnL]$. CH_3OH complex. Spectroscopic methods, e.g. FT-IR and NMR used for characterization of compounds. Single Crystals were grown by slow evaporation in methanol. SCXRD showed that both, **L** and **ZnL** crystallize in a primitive monoclinic lattice, with the space group $P2_1/n$ for **L** and $P2/c$ for the Zn(II) complex. Morphology of crystals has been studied by SEM. Pt-coated samples were prepared for dried crystals and Low-vacuum SEM used for crystals in liquid. Crystals of **L** showed the bulk crystalline forms and **ZnL** showed layered crystalline forms. The Zn(II) complex is a good candidate for studying in biological systems. E.g. enzymes with one zinc binding site in carbonic anhydrase and carboxy peptidase A.

- [1] March, J. (1985), *Advanced Organic Chemistry: Reactions, Mechanisms, and Structure* (3rd ed.), New York: Wiley.
 [2] Wu, A. M.; Senter, P. D. (2005). *Nature Biotechnology*.23(9): 1137–1146.
 [3] Kalia, J.; Raines, R. T. (2008). *Angew. Chem. Int. Ed.*47(39): 7523–7526.
 [4] Khandar, A. A.; Hosseini-Yazdi, S. A. (2003). *Polyhedron*. 22 (11) 1481-1487

Figure 1



P093

Single-source precursors for ternary aluminatesS. Kuesel¹, H. Krautscheid¹¹Universität Leipzig, Inorganic Chemistry, Leipzig, Germany

Ternary oxides, e.g. the group of spinels, show a broad range of interesting properties depending on the nature of the cation. Some of them are semiconductors or exhibit suitable magnetic properties; their applications range from catalysis, electrode materials to pigments.^[1-5]

With the aim to form pure ternary oxide materials by thermal decomposition of single-source precursors we synthesize transition metal containing mixed metal aluminate complexes with alkoxide ligands. These molecular precursors are characterized single-crystal X-ray diffraction, temperature dependent X-ray powder diffraction (TPXRD) and thermal analysis (TG, DTA).

The prepared mixed-metal alkoxides contain transition metal and Al^{3+} in 1:2 molar ratio. By salt metathesis and transesterification, complexes with two different types of ligands are available. Adding a co-ligand improves the formation of crystalline compounds. Their molecular structures and their thermal properties (melting point, thermolysis behavior) are investigated (e.g. $Co[Al(O^iPr)_4]_2(BiPy)$, cp. Fig. 1), the phase composition of the residue after thermal decomposition depends on the gaseous environment during thermolysis.

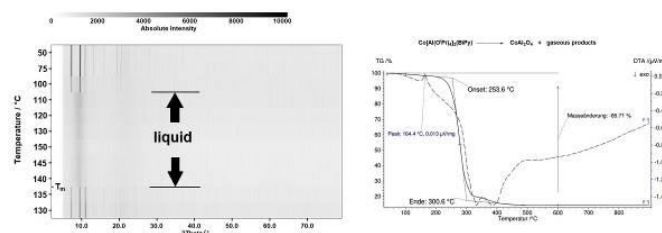
A series of eight new coordination compounds with Al^{3+} and divalent transition metal ions, Fe^{2+} , Co^{2+} , Ni^{2+} or Zn^{2+} , were obtained and characterized. Syntheses, crystal structures and results of thermolysis studies will be presented.

Fig. 1: Temperature dependent XRD pattern (left) and TG/DTA curve (right) of $Co[Al(O^iPr)_4]_2(BiPy)$.

Literature:

- [1] G. T. Anand, L. J. Kennedy, J. J. Vijaya, *J. Alloys Compd.* **2013**, 581, 558.
 [2] T. Suzuki, H. Nagai, M. Nohara, H. Takagi, *J. Phys.: Condens. Matter.* **2007**, 19, 145265.
 [3] A. Arandia, A. Remiro, V. Garcia, P. Castano, J. Bilbao, A. G. Gayubo, *Catalysts* **2018**, 8, 322.
 [4] F. Bai, Q. Li, T. Yang, J. Chen, X. M. Hou, *Ionics* **2018**, 24, 1.
 [5] A. Zhang, B. Mu, A. Hui, A. Wang, *Appl. Clay Sci.* **2018**, 160, 153.

Figure 1



P094

New 2D networks with a direct fluorine-metal bond:**MF(CH₃COO) (M: Sr, Ba, Pb)**S. Breitfeld^{1,2}, G. Scholz², F. Emmerling¹, E. Kemnitz²¹Bundesanstalt für Materialforschung und -prüfung, Berlin, Germany²Humboldt-Universität zu Berlin, Chemie, Berlin, Germany

Fluorinated metal-organic frameworks and coordination polymers have been in the focus of interest since several years. Promising applications are based on their excellent electrical and optical properties, their thermal stability and the presence of hydrophobic channels. In general, two possibilities exist to implement fluorine into such networks: (i) using perfluorinated organic linkers, or (ii) adapting a synthesis strategy for realizing direct metal-fluorine bonds. The mechanochemical synthesis of coordination polymers with alkaline earth metals using fluorinated organic linkers allows an easy access to such fluorinated networks [1]. In addition, recently we published the mechanochemical synthesis of BaF-benzenedicarboxylate, with fluorine directly coordinated to the

metal cation Ba^{2+} [2]. In the present study, new coordination polymers with 2D network structures with fluorine directly coordinated to the metal ion were prepared both via mechanochemical synthesis and fluorolytic sol-gel synthesis. The crystal structures of barium acetate fluoride, strontium acetate fluoride and lead acetate fluoride were solved from X-ray powder diffraction data and confirmed by the ^{19}F MAS NMR spectrum and the FT IR spectrum. Dependent on the synthesis route the samples show different morphologies. The new 2D networks of $\text{BaF}(\text{CH}_3\text{COO})$, $\text{SrF}(\text{CH}_3\text{COO})$ and $\text{PbF}(\text{CH}_3\text{COO})$ were further characterized by thermal analysis and SEM imaging.

[1] A. Al-Terkawi, G. Scholz, F. Emmerling, E. Kemnitz, Dalton Trans. **47** (2018) 5743-5754.

[2] S. Breitfeld, G. Scholz, F. Emmerling, E. Kemnitz, J. Mater. Science **53** (2018) 13682-13689.

P095

Rational Design of Proton-Electron Transfer System Based on Nickel Dithiolene Complexes with Pyrazine Skeletons

Y. Kimura¹, M. Hayashi¹, Y. Yoshida¹, H. Kitagawa¹

¹Kyoto University, Graduate School of Science, Kyoto, Japan

Introduction

π -Conjugated molecular materials with hydrogen-bonded lattice have attracted great interest because they have a potential to exhibit unique physical properties derived from proton-coupled electron transfer in solids. Among such materials, a quinhydrone complex composed of hydroquinone and 1,4-benzoquinone, i.e., proton-electron donor and acceptor, respectively, has proton-electron transfer (PET) state consisting of degenerated neutral radical (DNR) molecules under high pressure. In a PET state, electrical conductivity, magnetism, and dielectricity are expected to coexist. However, there are no materials to show the PET state under ambient conditions due to the instability of DNR state.

Objectives

To understand the effect of chemical modification on the stability and proton-electron coupling in DNR molecules with a PET state and to establish a molecular design principal for the stabilized PET state, we investigated nickel dithiolene complexes with pyrazine skeletons using experimental and theoretical methods.

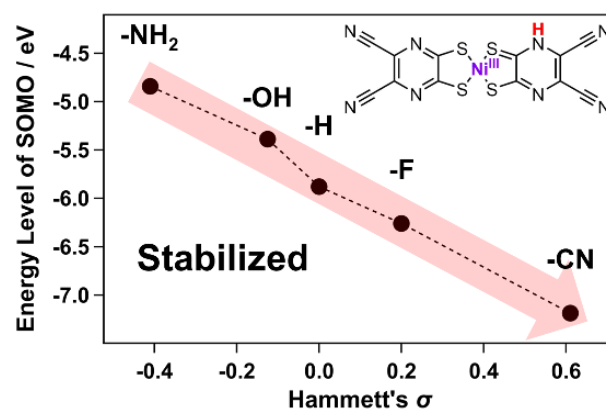
Results

A Pourbaix diagram constructed from absorption spectroscopic and cyclic voltammetric measurements strongly suggests that the PET state of the cyano-substituted complex is significantly more stable compared with that of the non-substituted complex. Crystallographic studies revealed that the degree of the coupling between protons and electrons varies depending on Hammett's σ value of the substituents; the electronic state of the non-substituted complex appears to be most sensitive to the protonated state. These results are supported by theoretical calculations.

Conclusion

Our theoretical and experimental studies revealed that the stability and the proton-electron coupling of the PET state of the nickel dithiolene complexes with pyrazine skeletons can be readily controlled by the introduction of substituents.

Figure 1



P096

An experimental and theoretical approach to control salt vs. co-crystal vs. hybrid formation - Crystal engineering of an *E/Z*-butenedioic acid/phthalazine system

A. I. Chamorro Orue¹, C. Schauerte², R. Boese², K. Merz^{2,3}

¹Ruhr-Universität Bochum/solid-chem GmbH, Bochum, Germany

²solid-chem GmbH, Bochum, Germany

³Ruhr-Universität Bochum, Bochum, Germany

The understanding and controlling of proton transfer reactions between acid-base pairs in the solid state is one of the main challenges in the crystal engineering community. The ability to control proton transfer reactions in the solid state enables a more selective preparation of co-crystals and salts, which facilitates the design of solid materials with specific physicochemical properties. In this study, an approach to control proton transfer reactions of an *E*-butenedioic acid/phthalazine co-crystal-salt (hybrid) system is presented, which allows the selective formation of its co-crystal and salt. In this approach the dominant intermolecular interactions between acid-base pairs are identified. Such interactions appear to be crucial for the inhibition or promotion of proton transfers in the solid state. For this, the relationship between these interactions and the so-called ΔpK_a rule has been investigated.

P097

Synthesis and structure of the donor-free potassium silanide $\text{K}[\text{SiPh}_3]$

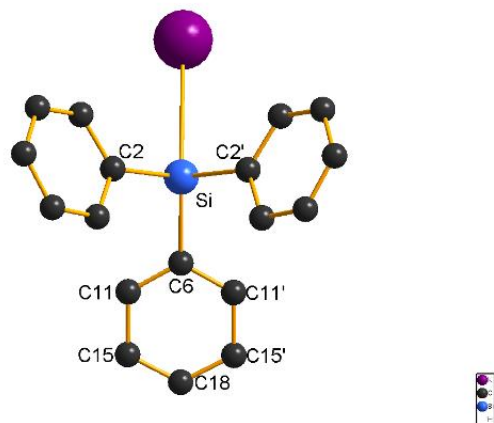
L. Fink¹, E. Alig¹, I. Georg¹, I. Sanger¹, M. Wagner¹, H. W. Lerner¹

¹Goethe-Universität Frankfurt am Main, Anorganische und Analytische Chemie, Frankfurt am Main, Germany

The donor-free potassium silanide $\text{K}[\text{SiPh}_3]$ was prepared by the reaction of hexaphenyldisilane, $\text{Ph}_3\text{Si-SiPh}_3$, with potassium metal in benzene at room temperature. The solid-state structure, determined by powder X-ray diffraction consists of $\{\text{K}[\text{SiPh}_3]\}_2$ units, which interact with adjacent dimers to form an infinite chain along the crystallographic *c* axis (orthorhombic, space group *Cmc*21, *Z* = 4). The structure features short contacts between the π -system of the phenyl rings and the potassium atoms of neighbouring $\text{K}[\text{SiPh}_3]$ units.

Fig.1: Molecular structure of the donor-free potassium silanide $\text{K}[\text{SiPh}_3]$ measured at 298 K. Hydrogen atoms are omitted for clarity.

Figure 1



P098

Crystal Engineering of inorganic-organic hybrid materials with heterobifunctional organic building blocks: interplay of hydrogen bonding and π -system interactions of short chained α,ω -ammonio-phenylalkanes?
M. Lichte¹, F. Freese¹, W. Frank¹¹Heinrich-Heine-Universität Düsseldorf, Lehrstuhl für Material- und Strukturforchung, Düsseldorf, Germany

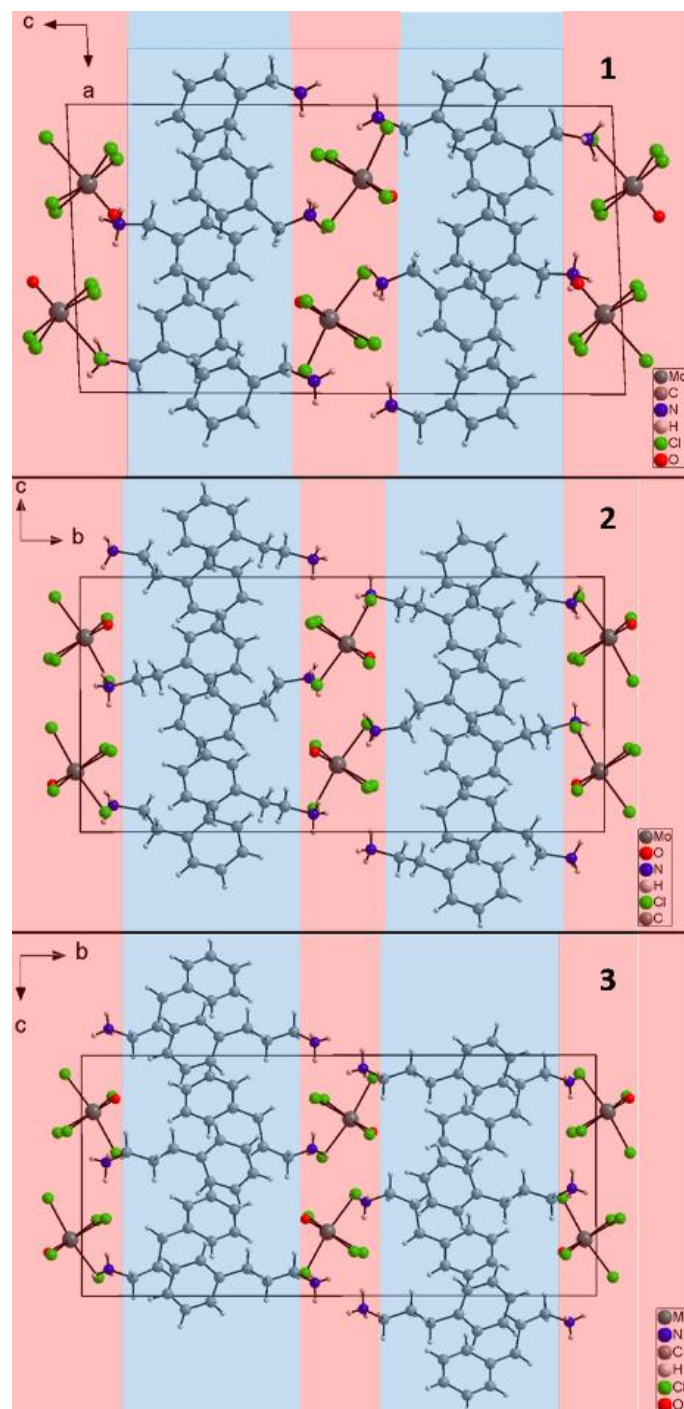
Protonated amines and halogenidometalate^[1-3] or oxidohalogenidometalate^[4] anions are functional moieties for the synthesis of inorganic-organic hybrid materials.

Crystallisation of the compounds $(C_6H_5(CH_2)_nNH_3)_2[MoCl_5O]$ (**1**: $n=1$; **2**: $n=2$; **3**: $n=3$) was achieved by cooling of saturated solutions of the corresponding α,ω -ammonio-phenylalkane chloride and molybdenum(V) chloride in hydrochloric acid. **1** crystallizes in the monoclinic space group $P2_1$ ($a = 11.892(2)$ Å, $b = 7.407(2)$ Å, $c = 22.482(5)$ Å, $\beta = 92.90(3)^\circ$, $Z = 4$, 6950 refl., 419 param., $R_1 = 0.0336$, $wR_2 = 0.0880$). For the homotypic compounds **2** and **3** the monoclinic space group type $P2_1/c$ is found (**2**: $a = 7.3577(10)$ Å, $b = 24.735(3)$ Å, $c = 11.996(2)$ Å, $\beta = 90.838(7)^\circ$, $Z = 4$, 4058 refl., 243 param., $R_1 = 0.0332$, $wR_2 = 0.0760$; **3**: $a = 7.5933(2)$ Å, $b = 26.0733(5)$ Å, $c = 12.2033(3)$ Å, $\beta = 94.37(3)^\circ$, $Z = 4$, 4235 refl., 246 param., $R_1 = 0.0479$, $wR_2 = 0.1049$).

In each case bond lengths (Å) (Mo–Cl (eq.) 2.369(2) - 2.419(2), Mo–Cl (ax.) 2.594(2) - 2.619(1), Mo=O 1.662(4) - 1.670(2)) and the tilt of the equatorial ligands of the distorted octahedral anions are as expected.^[5] In all compounds layerlike hydrophobic regions are formed by the phenylalkyl parts of the cations. Hydrophilic layerlike regions contain NH_3^+ -groups and the $[MoCl_5O]^{2-}$ anions, stacked alternately along $[110]$ (**1**) and $[101]$ (**2,3**). Weak N–H...Cl hydrogen bonds (D–A distances 3.201 - 3.319 Å) connect inorganic and organic moieties along $[001]$ in **1** and $[010]$ in **2** and **3**. In conclusion, an interplay of hydrogen bonding and π -system interactions is recognized but more limited than expected with enhanced contributions of hydrogen bonding in comparison.

[1] J. Graf, W. Frank, *Z. Anorg. Allg. Chem.* **2004**, *630*, 1894.[2] T. Hahn, G. J. Reiß, W. Frank, *Z. Anorg. Allg. Chem.* **2006**, *632*, 2156.[3] W. Frank, T. Hahn, *Z. Anorg. Allg. Chem.* **2008**, *634*, 2037.[4] J. van Megen, A. Heymann, W. Frank, *Z. Anorg. Allg. Chem.* **2014**, 2368.[5] R. A. Isovitsch, J. G. May, F. R. Fronczek, A. W. Maverick, *Polyhedron* **2000**, *19*, 1437–1446.Figure 1: Packing diagram of **1**, **2** and **3** with hydrophobic (blue) and hydrophilic regions (red).

Figure 1



P100

A pyrazole-containing copper coordination framework: an investigation into its Hirshfeld surface analysis, magnetic behavior and biological activity

A. Direm¹, M. S. M. Abdelbaky², O. Abosedo³, S. García-Granda²

¹LASPI2A Laboratory, Faculté des sciences et technologie, University of Khenchela, Khenchela, Algeria

²Universidad de Oviedo, Departamento de Química Física y Analítica, Oviedo, Spain

³Federal University Otuoke, Department of Chemistry, Bayelsa State, Nigeria

The properties of pyrazole-based systems have been widely investigated due to their chelating ability with metallic ions as terminal ligands, bridging ligands and precursors for the design of several multi-nitrogen ligands for coordination, bioinorganic and organometallic chemistry [1], in order to build up new coordination polymeric networks and metal-organic frameworks. Additionally, they are well known for their spin-crossover behavior and their biological and medicinal properties as analgesic, anti-inflammatory agents [2], etc. As a contribution to what has been previously reported, we will be describing herein, for the first time, the magnetic properties and antimicrobial activity of a pyrazole-based copper complex [3]. Furthermore, the Hirshfeld surfaces and the 2D-fingerprint graphics [4] allowing the understanding of the properties and the occurrence of each intermolecular contact around the studied complex molecules will be discussed exclusively in detail.

References:

- [1] a) Montoya, V., Pons, J., Garcia-Antón, J., Solans, X., Font-Bardia, M. & Ros, J. (2007). *Inorg. Chim. Acta.* **360**, 625–637. b) Itoh, T., Fuji, Y., Toda, T. (1996). *Bull. Chem. Soc. Jpn.* **69**, 1265. c) Sun, Y. J., Cheng, P., Yan, S. P., Liao, D. Z., Jiang, Z. H., Shen, P. W. (2002). *J. Coord. Chem.* **55**, 363. d) Lam, M. H. W., Tang, Y. -Y., Fung, K. -M., You, X.-Z., Wong, W.-T. (1997). *Chem. Commun.* 957.
- [2] a) Kahn, O., Martinez, C. J. (1998). *Science.* **279**, 44-48. b) Olguin, J., Brooker, S. (2011). *Coord. Chem. Rev.* **255**, 203-240. c) Gürsoy, A., Demiryak, S., Çapan, G., Erol, K. & Vural, K. (2000). *Eur. J. Med. Chem.* **35**, 359–364. d) Lynch, D. E. & McClenaghan, I. (2005). *Acta Cryst.* **E61**, o2349–o2351.
- [3] Direm, A., Tursun, M., Parlak, C. & Benali-Cherif. N. (2015). *J. Mol. Struct.* **1093**, 208–218.
- [4] a) Spackman, M. A. & Jayatilaka, D. (2009). *Cryst. Eng. Comm.*, **11**, 19–32. b) Spackman, M. A. & McKinnon, J. J. (2002). *Cryst. Eng. Comm.* **4**, 378–392.

Keywords:

Pyrazole-containing complexes, MOFs, magnetic properties, biological activity, intermolecular interactions, Hirshfeld surface analysis.

Small molecules at large facilities

P101
StructureFinder

D. Kratzert¹

¹Albert-Ludwigs-Universität Freiburg, Institut für Anorganische und Analytische Chemie, Freiburg i. Br., Germany

Question

Databases like the Cambridge Structural Database or the Crystallographic Open Database are good at collecting information from crystallographic experiments and making it searchable. But to my knowledge, there is no easy-to-use software to find and present the results of crystallographic experiments for a single workgroup.

Results

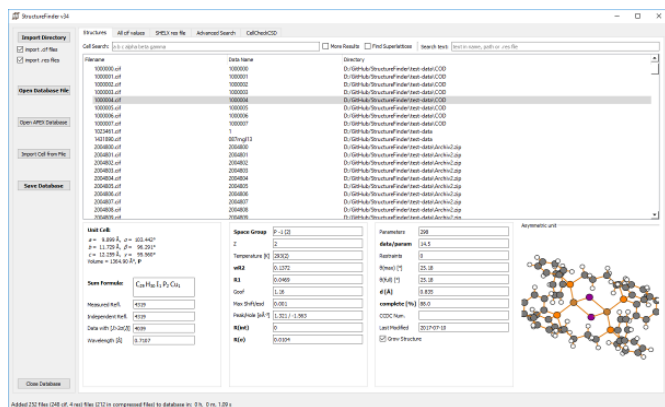
Presented is the computer program called StructureFinder. It creates a database of crystallographic structures on a computer and makes them searchable. The program can search for various properties: unit cell, free text, included atom types, creation date and space group. To build the database, StructureFinder collects all computer information files (cif file format) or res files (from SHELXL) below certain directories on a hard disk. The containing information is stored into a SQLite database. The database can be accessed by two different interfaces. A stand-alone Qt program (Figure 1) to install on a single computer or a web interface to be accesses by a whole work group.

Conclusions

StructureFinder greatly enhances the ability to find old structures in huge collections of crystallographic datasets. The program can easily handle more than 10.000 structures. It can be downloaded at <https://www.xs3.uni-freiburg.de/research/structurefinder>.

Figure 1. Qt interface of StructureFinder.

Figure 1



of molten salt reactor coolants as well as for recycling of used nuclear fuels, and some more. NF₃ is also being currently extensively studied due to its global warming potential, which is ca. 17200 stronger in comparison to CO₂.^[2]

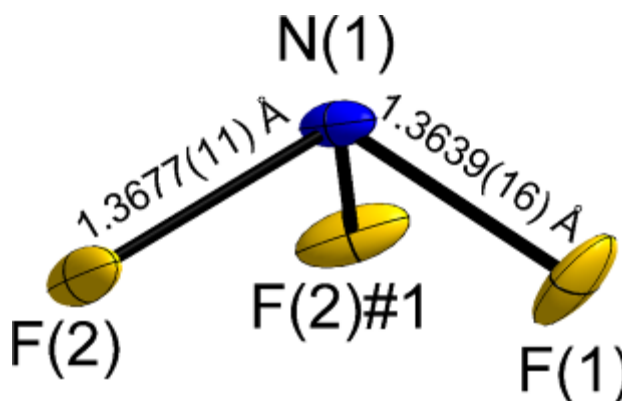
In spite of various analytical data on NF₃ available in literature, it has surprisingly never been characterized by diffraction techniques in the solid state, therefore, its crystal structure remained unknown. Here we will present our results of the crystal structure elucidation of the two polymorphic modifications of NF₃ using powder neutron diffraction on the SPODI powder diffractometer at the Heinz Maier-Leibnitz Zentrum, Garching. The low-temperature α -NF₃, which is stable below 56.62 K,^[3] crystallizes in the PCl₃ structure type, space group *Pnma*. The high-temperature modification is plastic crystalline and forms a Frank-Kasper sigma phase, space group *P4₂/mmm*, considering the positions of the molecular centers.

Figure 1. Structure of the NF₃ molecule of α -NF₃. Displacement ellipsoids are shown at 70 % probability level at 6 K.

References:

- [1] O. Ruff, J. Fischer, F. Luft, Z. Anorg. Allg. Chem. 1928, 172, 417–425.
- [2] A. Totterdill, T. Kovács, W. Feng, S. Dhomse, C. J. Smith, J. C. Gómez-Martín, M. P. Chipperfield, P. M. Forster, J. M. C. Plane, Atmos. Chem. Phys. 2016, 16, 11451–11463.
- [3] L. Pierce, E. L. Pace, J. Chem. Phys. 1955, 23, 551–555.

Figure 1



P102
The Crystal Structures of α - and β -Nitrogen Trifluoride

S. Ilev¹, M. Conrad¹, M. Hoelzel², A. Karttunen³, F. Kraus¹

¹Philipps-Universität Marburg, Fachbereich Chemie, Marburg, Germany

²Technische Universität München, Heinz Maier-Leibnitz Zentrum (MLZ), Garching, Germany

³Aalto University, Department of Chemistry and Materials Science, Aalto, Finland

Nitrogen trifluoride, NF₃, was first synthesized in 1928 by Otto Ruff.^[1] NF₃ is currently used in the semiconductor industry as a cleaning agent for plasma-enhanced vapor deposition chambers. It is also promising in some other areas, for example, as a cathode reactant in metal-gas batteries, in nuclear industry for purification

Solid state physics in crystallography

P103

Magneto-electronic structure of REFe₂ (RE = Ho and Er) intermetallic compounds: Ab initio study.B. Ali¹¹Dr Mouay Tahar University of Saida, Hay Ennasr, Algeria

In this study, the structural, electronic and magnetic properties of the cubic MgCu₂-type binary Laves phases REFe₂ (RE = Er and Ho) compounds. The spin density functional theory (DFT) was used within the generalized gradient approximation (GGA) to estimate the exchange correlation potential and the GGA+U (U: Hubbard parameter) calculations in accurately describing the correlation effects. The lattice parameter and magnetic moments at the equilibrium state are in good agreement with the available experimental data. We have calculated the magnetic moments of RE (RE = Er and Ho) and Fe in their binary compounds, respectively, by using GGA and GGA+U methods, where the magnetic moments value of Fe was found to be larger than that of RE. The obtained results show that the GGA+U method provides the best description of our systems. We also projected the electronic structures and the spin-polarized density of states (DOS) of the RE-4f and Fe-3d orbitals. The REFe₂ compound shows a metallic behavior with a small spin-down electronic density of states at the Fermi level in both the GGA and GGA+U approximations.

P104

Role of particle size distribution and packing density in the SHG powder measurementsL. Bayarjargal¹¹Goethe-Universität Frankfurt am Main, Abt. Kristallographie, Frankfurt am Main, Germany

For nonlinear optical (NLO) applications, crystals with high second-order NLO effects and phase matching conditions are very important. Second harmonic generation (SHG) measurements on powder samples were first performed by Kurtz and Perry [1] and allow a rapid classification of new NLO materials. While powder measurements are very efficient, they suffer from disadvantages such as light scattering and packing density. Recently, an approach to take light scattering into account, has been published [2]. Attempts have been made to determine the role of sample thickness, packing density and particle size distribution [3,4]. However, due to the problems in actual applications it is still difficult to precisely determine SHG coefficients. Therefore, this study aims to take into account the particle size distribution and the packing density of the sample for SHG powder measurements.

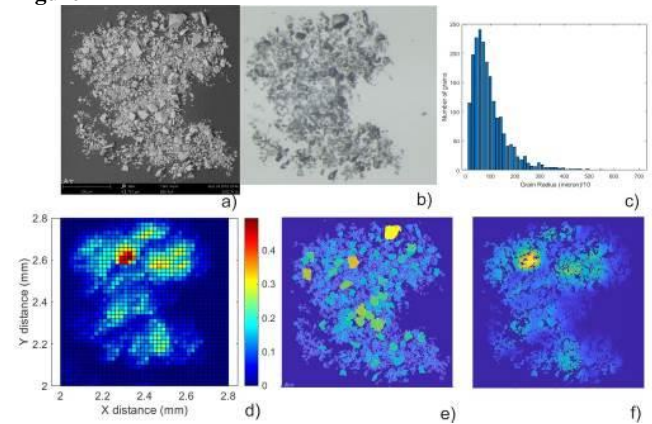
We measured two dimensional SHG intensity maps for commonly used reference crystals (quartz, KDP, ZnO, BaTiO₃). A Nd:YAG laser (1064nm) was used for the generation of the fundamental pump wave. SHG intensities were collected by a photo-multiplier and an oscilloscope. High resolution SEM images have been collected using a Phenom ProX SEM. The particle size distribution was determined using the SEM images and a Matlab code. Typical measurements are presented in Fig 1. Based on our results, we can now correlate the SHG intensities with the particle size distributions and the packing densities.

Fig 1. SEM (a) and optical pictures (b) of quartz. Particle size distributions (c, e). Two dimensional SHG intensities of quartz (d). Correlation between the particles and SHG intensities (f).

Financial support from the DFG (BA4020) is gratefully acknowledged.

- [1] S. K. Kurtz and T. T. Perry, J. Appl. Phys., **39**:3798, 1968
 [2] I. Aramburu et al., Appl. Phys. B, **116**:211, 2014
 [3] A. U. Chowdhury et al., Anal. Chem., **88**:3853, 2016
 [4] I. Aramburu et al., J. Appl. Phys., **109**:113105, 2011

Figure 1



P105

Insulator-half metallic transition by the tetragonal distortion: A first-principles study of strain-induced perovskite RbMnF₃N. Tuvjargal¹, N. Tsogbadrakh¹, C. Feng¹, J. Davaasambu¹¹National University of Mongolia, Department of Physics, Ulaanbaatar, Mongolia

From the spin polarized density functional total energy calculations, we shown that the ground state of cubic perovskite RbMnF₃ is an antiferromagnetic (AFM) insulator due to the super-exchange mechanism, in agreement with the other theoretical and experimental results[1-4].

After tetragonal distortion along the c – axis, keeping the predicted volume, our results indicated that the strain-induced magnetic phase transition from an AFM insulator to a half metallic ferromagnetic (HM– FM) state is available by the tetragonal distortion due to the insulator – half metallic transition.

The predicted electronic and magnetic properties of strain - induced RbMnF₃ show the HM–FM nature, making strain – induced RbMnF₃ suitable for spintronic application.

This work has been done with financial support of the Mongolian Foundation for Science and Technology.

References

- [1]. T. Teaney, M.J. Freiser, and R.W.H. Stevenson, Phys. Rev. Lett. **9**, 212 (1962)
 [2]. L. Melcher and D.I. Bolef, Phys. Rev. **178**, 178 (1969)
 [3]. L. Melcher and D.I. Bolef, Phys. Rev. **186**, 491 (1969)
 [4]. Shapira and N.F. Oliveira, Phys. Rev. B **18**, 1425 (1978)

P106

Phase formation study and crystal growth of cesium cobalt halogenides $\text{Cs}_2\text{Co}(\text{Cl}_{1-x}\text{Br}_x)_4$ and $\text{Cs}_3\text{Co}(\text{Cl}_{1-x}\text{Br}_x)_5$ with $0 \leq x \leq 1$

M. Kloda¹, I. Cisarova¹, I. Nemeč¹, T. Lorenz², O. Breunig², P. Becker³, L. Bohaty³

¹Charles University Prague, Department of Inorganic Chemistry, Faculty of Science, Prague, Czech Republic

²University of Cologne, II. Physikalisches Institut, Köln, Germany

³University of Cologne, Institut für Geologie und Mineralogie, Köln, Germany

Cs_2CoCl_4 is one of the rare materials, which realize the effective 1D XXZ spin-1/2 chain model with strong easy-plane anisotropy XY. A magnetic field of $\sim 2\text{T}$ induces a quantum phase transition described by the spin-chain model above 0.3K [1]. At lower temperature long-range magnetic-order sets in and complex field-induced phases are observed [2]. By substitution of Cl by Br in Cs_2CoCl_4 the magnetic interactions of Co^{2+} via the halide ions are modified and tend to become less 1D. For Cs_3CoCl_5 the possibility for an investigation of a transition from 3D to 2D magnetism is proposed for similar substitution $\text{Cl} \leftarrow \text{Br}$. Detailed studies, however, require homogeneous (large) mixed crystals $\text{Cs}_2\text{Co}(\text{Cl}_{1-x}\text{Br}_x)_4$ and $\text{Cs}_3\text{Co}(\text{Cl}_{1-x}\text{Br}_x)_5$ with $0 \leq x \leq 1$ [3].

In the system $\text{CsCl-CsBr-CoCl}_2\text{-CoBr}_2\text{-H}_2\text{O}$ cesium cobalt halides of the type Cs_2CoX_4 ("214"), Cs_3CoX_5 ("315"), CsCoX_3 ("113") ($X = \text{Cl, Br}$) and $\text{CsCoCl}_3 \cdot 2\text{H}_2\text{O}$ are known so far. For the orthorhombic "214" and the tetragonal "315" compounds the respective chlorides and bromides are isomorphic, but the question of full or only partial miscibility is still open for both cases. With the target of large high-quality single crystals growth in the mixed systems $\text{Cs}_2\text{Co}(\text{Cl}_{1-x}\text{Br}_x)_4$ and $\text{Cs}_3\text{Co}(\text{Cl}_{1-x}\text{Br}_x)_5$ with $0 \leq x \leq 1$ series of crystallization experiments with different solute compositions at three different temperatures were performed to determine the primary phase formation regions and suitable crystal growth conditions. They were complemented by chemical analysis, X-ray powder diffraction and single crystal X-ray structure determination. Depending on crystallization temperature congruent and incongruent solubilities were found. Based on the results large single crystals of Cs_2CoBr_4 , Cs_3CoCl_5 and Cs_2CoCl_4 were successfully grown as well as some mixed crystals of the "214" type.

[1] O. Breunig et al., Phys. Rev. Lett. **111** (2013) 187202.

[2] O. Breunig et al., Phys. Rev. B **91** (2015) 024423.

[3] O. Breunig, Dissertation, University of Cologne 2015.

P107

Energy harvesting with PVDF foils

S. Jankus¹, H. Stöcker¹, J. Hanzig¹, E. Mehner¹, S. Jachalke¹, D. C. Meyer¹

¹Technische Universität Bergakademie Freiberg, Institut für Experimentelle Physik, Freiberg, Germany

Many industrial processes generate waste heat, which cannot be converted into electrical energy by conventional heat engines. A novel method of using waste heat is based on the pyroelectric effect. A material showing this effect is polyvinylidenefluoride (PVDF) in the form of foils. PVDF has several phases depending on the arrangement of the hydrogen and fluorine atoms in the molecule. The α -phase is non-pyroelectric. The β -phase of PVDF is pyroelectric and therefore interesting for the conversion of waste heat.

After foil extrusion, the α -phase is dominant. We subsequently stretch the sample to convert the α -phase into the β -phase. The proportion of the β -phase is determined by X-ray diffraction. The

resulting β -phase is not polarized, i.e. the dipoles in the PVDF molecules are disordered. We therefore polarize the β -phase by Corona discharge making the foil pyroelectric. The pyroelectric coefficient is measured using the Sharp-Garn method. The aim of the PyroFol project is to produce and polarize PVDF foils in order to obtain the largest possible pyroelectric coefficient. Subsequently, a method for inline polarization will be developed.

P108

Water splitting by pyroelectric single crystals

T. Köhler^{1,2}, W. Münchgesang¹, E. Mehner¹, T. Leisegang^{1,3}, H. Stöcker¹, D. C. Meyer¹

¹Technische Universität Bergakademie Freiberg, Institut für Experimentelle Physik, Freiberg, Germany

²Helmholtz-Zentrum Dresden-Rossendorf, Institute of Ion Beam Physics and Materials Research, Dresden, Germany

³Samara National Research University, Samara Center for Theoretical Materials Science, Samara, Russian Federation

The generation of hydrogen through water electrolysis has been understood for a long time and will be used for large-scale conversion of electrical energy into chemical energy in the future. The direct conversion of residual heat into hydrogen is completely new to our knowledge, but feasible when making use of pyroelectric materials. In pyroelectrolysis, a cyclic temperature excitation generates an electric field between the crystal surfaces due to an imbalance between polarization and compensation charges. For water electrolysis, this electric field must exceed the redox potential of water.

For the verification of the water splitting with pyroelectric single crystals an electrochemical measuring cell with optical heating was developed. The electrochemical interaction of LiNbO_3 , LiTaO_3 and $\text{Pb}[\text{Zr}_x\text{Ti}_{1-x}]\text{O}_3$ with aqueous media was investigated, in order to record the surface potential during the temperature change. A sufficient high voltage difference between the opposite crystal surfaces caused by cyclic temperature changes was observed. This satisfies the basic requirement for water splitting on the pyroelectric surface. With this setup, the proof of water splitting has been achieved. We show the calculated reaction rate and compare it with the maximum theoretically achievable H_2 evolution. The work represents a first contribution to new forms of energy conversion using polar materials.

P109

Influence of chloride substitution on the rotational dynamics of methylammonium in $\text{MAPbI}_3\text{-xCl}_x$ perovskites

G. Schuck¹, F. Lehmann^{1,2}, J. Ollivier³, H. Mutka³, S. Schorr^{1,4}

¹Helmholtz-Zentrum Berlin, 14109 Berlin, Germany

²Universität Potsdam, Institut für Chemie, Golm, Germany

³Institut Laue-Langevin, Grenoble, France

⁴Freie Universität Berlin, Institut für Geologische Wissenschaften, Berlin, Germany

We investigated methylammonium (MA) lead halides MAPbI_3 , $\text{MAPbI}_2.94\text{Cl}_0.6$, and MAPbCl_3 using inelastic and quasi-elastic neutron scattering (QENS) with the aim of elucidating the impact of chloride substitution on the rotational dynamics of MA.[1] In this context, we discuss the influence of the inelastic neutron scattering caused by low-energy phonons on the QENS resulting from the MA rotational dynamics in $\text{MAPbI}_3\text{-xCl}_x$. Through a comparative temperature-dependent QENS investigation with different energy resolutions, which allow a wide Fourier time window, we achieved a consistent description of the influence of chlorine substitution in MAPbI_3 on to the MA dynamics. Our results show that chlorine substitution in the orthorhombic phase leads to a weakening of the hydrogen bridge bonds since the

characteristic relaxation times of C3 rotation at 70 K in MAPbCl₃ and MAPbI₂.₉₄Cl_{0.6} are much shorter than in MAPbI₃. For the orthorhombic phase, we obtained the activation energies from the temperature-dependent characteristic relaxation times τ_{C3} by Arrhenius fits indicating lower values of E_a for MAPbCl₃ and MAPbI₂.₉₄Cl_{0.6} compared to MAPbI₃. We also performed QENS analyses at 190 K for all three samples. Here we observed that MAPbCl₃ shows slower MA rotational dynamics than MAPbI₃ in the disordered structure.

References

[1] Schuck et al., submitted to J. Phys. Chem. C, 2019

Spectroscopy

P111

Solid State NMR investigations of cation and anion ordering in the system Lithian muscovite – Trilithionite

M. Fechtelkord¹, N. Becker¹, L. Sulcek¹

¹Ruhr-Universität Bochum, Institut für Geologie, Mineralogie und Geophysik, Bochum, Germany

The lithian muscovite-lepidolite composition series involves the minerals muscovite ($K(Al_2\Box)(AlSi_3O_{10})(OH)_2$), trilithionite ($K(Li_{1.5}Al_{1.5})(AlSi_3O_{10})(F,OH)_2$) and polyolithionite ($K(Li_2Al)(Si_4O_{10})F_2$). Although the principal division into different mineral series succeeds, a more detailed classification based on crystal chemistry is still missing and the detailed mineralogical and petrological relationships are complex. (Fleet 2003).

The main interest of this work focuses on the spectroscopic investigation of the order / disorder of Si and Al in the tetrahedral sheets and of Al, Li, F, and OH in the octahedral sheets of trilithionite and Lithian muscovite. The emphasized analysis method was Solid State MAS NMR spectroscopy, since it enables the characterization and quantification of the different local environments of ²⁹Si, ²⁷Al, ¹H, ¹⁹F, ⁶Li and ⁷Li. Significant questions arising are the transition from trioctahedral polyolithionite-trilithionite to dioctahedral muscovite, alterations in the tetrahedral and octahedral sheets and the correlation between both.

First results show in the ¹H MAS NMR spectra that H-O-AlLi₂ signals only appear only for Li contents ≥ 1.2 . The ²⁹Si MAS NMR spectra show a signal distribution of Si (Q³): 25 % (2Al); 50 % (1Al); 25 % (0Al) which does not change from muscovite to trilithionite. The ²⁷Al MAS NMR spectra indicate only relative changes of the tetrahedral and octahedral signals (probably because of the changes in the octahedral layer). In the ²⁷Al MQMAS NMR the additional phases eucryptite and leucite show visible signals in tetrahedral region. The ⁶Li and ⁷Li MAS NMR spectra show only one resonance which position shifts to lower ppm-values and becomes narrower with decreasing Li-content.

Fleet (2003) Sheet Silicates: Micas. In: Rock-forming Minerals, eds. Deer, W.A., Howie, R.A., Zussman, J., 2nd edition, The Geological Society, Bath, United Kingdom.

P113

Changes of the properties of biogenic and synthetic hydroxylapatite under the influence of external factors deduced by magnetic resonance

V. Radchuk¹, O. Brik², N. Dudchenko²

¹Institute of Telecommunication and Global Information Space NAS of UKRAINE, Environmental Research, Kyiv, Ukraine

²M.P. Semenenko Institute of Geochemistry, Mineralogy and Ore Formation of National Academy of Sciences of the Ukraine, Physics of mineral structures and biomineralogy, Kyiv, Ukraine

It is known that mineral components of bones and tooth enamel consist mainly of hydroxylapatite nanocrystals. The weight of the tooth enamel and bones is determined by these nanocrystals by (95-97) % and (55-75) % respectively. Under the influence of various external factors, the properties of both biogenic and synthetic apatite change significantly, which is important for solving a wide range of applied problems.

Changes of the biogenic hydroxylapatite properties under the influence of radiation exposure are important for solving of retrospective dosimetry problems. These problems were being

solved by us using electron paramagnetic resonance (EPR) method, applied to the tooth enamel. We have studied the influence of caries on the reliability of the retrospective dosimetry results.

With the help of EPR and nuclear magnetic resonance (NMR), it is possible to study the effectiveness of the treatment of bones using implants, made on the basis of hydroxyapatite. It is well known that results of the treatment depend essentially on the properties of the material implanted in the living organism. Using EPR and NMR, we have developed methods for controlling the assimilation processes of the implants by bones of experimental animals.

In the process of evolution, the bone tissues of humans and animals were formed in the presence of the gravitational field of Earth. In the condition of weightlessness, the gravitation field is absent, leading to demineralization of bones. We have investigated the mechanisms of bone demineralization of experimental animals at the level of hydroxylapatite nanocrystals using EPR and NMR. In addition, it has been shown that in weightlessness the phase composition of mineral component of bones changes, namely, the amount of hydroxylapatite decreases, however, the amount of carbonates and bound water increases. The obtained results allow controlling the effectiveness of countermeasures aimed at inhibiting bone demineralization processes.

Structure-property-relationships

P115

Tetragonal mixed system $\text{Cs}_2\text{CuCl}_{4-x}\text{Br}_x$

N. van Well^{1,2}, D. Sheptyakov², E. Canēvet², C. Eisele¹, S. Ramakrishnan¹, T. Shang³, M. Medarde³, A. Cervellino⁴, M. Skoulatos^{5,6}, R. Georgii^{5,6}, C. Rüegg^{2,7}, S. van Smaalen¹

¹University of Bayreuth, Laboratory of Crystallography, Bayreuth, Germany

²Paul Scherrer Institute, Laboratory for Neutron Scattering and Imaging, Villigen, Switzerland

³Paul Scherrer Institute, Laboratory for Multiscale materials experiments, Villigen, Switzerland

⁴Paul Scherrer Institute, Swiss Light Source, Villigen, Germany

⁵Technische Universität München, Heinz Maier-Leibnitz Zentrum (MLZ), Garching, Germany

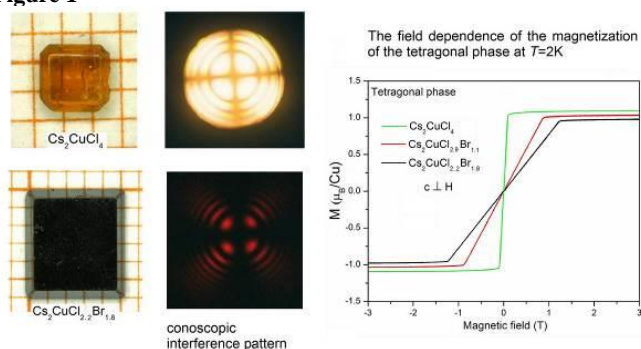
⁶Technische Universität München, Physik Department E21, Garching, Germany

⁷University of Geneva, Department for Quantum Matter Physics, Geneva, Switzerland

In the past, the tetragonal mixed system $\text{Cs}_2\text{CuCl}_{4-x}\text{Br}_x$ was only grown for a Br concentration range of $x=1$ to $x=2$ [1, 2]. The realisation of the new tetragonal phase of Cs_2CuCl_4 is possible using specific crystal growth conditions at a temperature below 281K. For crystal growth a periodically changing temperature profile was used. The susceptibility measurements of Cs_2CuCl_4 show the same magnetic behaviour as the magnetic susceptibility and the magnetisation curves of the tetragonal compounds $\text{Cs}_2\text{CuCl}_{2.9}\text{Br}_{1.1}$, $\text{Cs}_2\text{CuCl}_{2.5}\text{Br}_{1.5}$ and $\text{Cs}_2\text{CuCl}_{2.2}\text{Br}_{1.8}$ and present consistent results for typical quasi 2-D ferromagnets. We have investigated the structure using synchrotron powder diffraction. The structure analysis down to 4K for $\text{Cs}_2\text{CuCl}_{2.2}\text{Br}_{1.8}$ shows no phase transition and the tetragonal symmetry $I4/mmm$, which is also the same for this composition at room temperature. Magnetic reflections are observed for this compound with neutron diffraction experiments below the magnetic phase transition at $T_N = 11.3\text{K}$. The results show that the magnetic order with a temperature-independent positions $(1\ 0\ 0)$, $(0\ 1\ 0)$ and $(0\ 0\ 1)$ below the ordering temperature appears for $\text{Cs}_2\text{CuCl}_{2.2}\text{Br}_{1.8}$.

[1] N. Krüger, S. Belz, F. Schossau, A. A. Haghighirad, P. T. Cong, B. Wolf, S. Gottlieb-Schoenmeyer, F. Ritter, and W. Assmus, *Crystal Growth & Design*. 2010, **10**, 4456–4462

[2] P. T. Cong, B. Wolf, N. van Well, A. A. Haghighirad, F. Ritter, W. Assmus, C. Krellner, M. Lang, *IEEE Transactions on Magnetics* 50, 2700204 (2014)

Figure 1


P116

Synthesis and luminescent properties of Sm^{3+} and Dy^{3+} doped earth alkaline borates MB_2O_4 ($\text{M} = \text{Ca}, \text{Sr}, \text{Ba}$)

C. Otgonbayar¹, H. Pöllmann¹

¹Martin-Luther-Universität, Institut für Geowissenschaften und Geographie Mineralogie/Geochemie, Halle (Saale), Germany

The common way to fabricate white light emitting diodes (W-LED) is to use a blue-emitting GaN chip to pump a YAG: Ce^{3+} phosphor or an ultraviolet InGaN chip to excite blue-, green-, and red-emitting multiphase phosphors. However, there are some drawbacks to these combinations, such as low colour rendering index and low colour reproducibility. The use of two or three different kinds of phosphors leads to a decrease in luminous efficiency. Therefore, a development of single-phased white light emitting phosphors is of big interest. Among these phosphors investigated, borates are good candidates due to their low synthetic temperatures, stabilities, and low costs.[1-3]

A series of MB_2O_4 ($\text{M} = \text{Ca}, \text{Sr}, \text{Ba}$) phosphors doped with Sm^{3+} and Dy^{3+} were prepared by solid state synthesis. The crystal structures of the phosphors were investigated using powder X-ray diffraction (PXRD). The crystal structure CaB_2O_4 and SrB_2O_4 belong to space groups Pnca and Pbcn respectively. The crystal structure of BaB_2O_4 is rhombohedral with space group R3c . The emission and excitation spectra, and decay curves were taken to study the luminescence properties of phosphor MB_2O_4 : Sm^{3+} and Dy^{3+} ($\text{M} = \text{Ca}, \text{Sr}, \text{Ba}$).

Absorption and emission spectra of CaB_2O_4 : 1 mol% Sm^{3+} is shown in Fig 1. The reddish-orange emission from Sm^{3+} is composed of 563, 599, and 646 nm emission peaks, corresponding to the ${}^4\text{G}_{5/2} \rightarrow {}^6\text{H}_j$ ($J = 5/2, 7/2, 9/2$) transitions, respectively. Dy^{3+} ion exhibits two visible emission bands including 474 nm and 572 nm, corresponding to the ${}^4\text{F}_{9/2} \rightarrow {}^6\text{H}_{15/2}$ and ${}^4\text{F}_{9/2} \rightarrow {}^6\text{H}_{13/2}$ transitions, respectively.

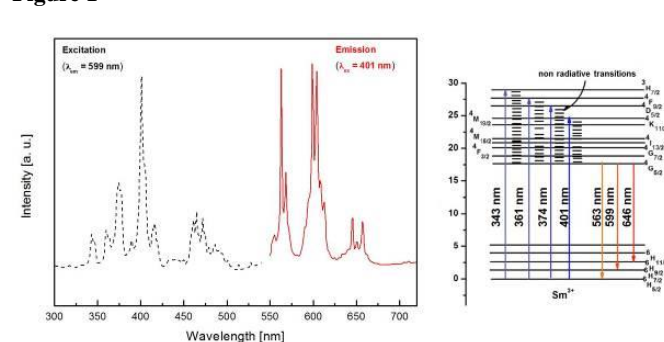
The emissions of all samples consist of two or more colours and the peaks are very sharp, making them attractive candidates for use in optical applications.

 Fig 1:Excitation and emission spectra of CaB_2O_4 : 1 mol % Sm^{3+}

[1] Ye S. et al, *Mater Sci Eng R* 71 (2010) 1–34

[2] T.-W. Kuo, T.-M. Chen, *J. Lumin.* 130 (2010) 483–487

[3] C.F. Guo, Y. Xu, F. Lv, X. Ding, *J. Alloys Compd.* 497 (2010) 21–24

Figure 1


P117

Quantification of stress conditions in quartzite by using RAMAN spectroscopy

K. J. Huenger¹, M. Danneberg^{1,2}, S. Herold^{1,2,3}, J. Acker^{1,2,3}¹BTU Cottbus-Senftenberg, Research & Materials Testing Institute, Cottbus, Germany²BTU Cottbus-Senftenberg, Chair Building Materials&Chemistry, Cottbus, Germany³BTU Cottbus-Senftenberg, Chair Physical Chemistry, Senftenberg, Germany

Introduction

The alkali silica reaction is a problem worldwide in concrete technology. Different mechanisms were postulated to understand this reaction (1,2). An important part is the SiO₂ solubility of aggregates (3). In dense aggregates, the silica release is surface controlled. Therefore, it is necessary to characterize the surface in more details (4). State of the art are mineralogical investigations (quartz content, crystallite size, deformation of crystallites) (5,6). A good differentiation can be realized by using polarisation light microscopy (7,8). Using thin sections, stressed areas in quartzite can be located. However, this method is not suitable for quantitative values on the stress state.

Objective

The aim is to find methods to quantify the deformation state on quartzite surfaces for each grain separately. A combination of polarized light microscopy (for visualization) and Raman spectroscopy (for quantification) is used. With both, maybe, the stress states in different locations could be evaluate more quantitatively.

Results

Fig. 1 shows different areas on a quartzite surface where different stress states are realized. Raman measurements of these areas were made and the expected spectra of quartz with typical signals on 466, 207 and 130 cm⁻¹ (**Fig. 2**) were found. Surprisingly is, that also some unexpected new signals at 1600 and 1300 cm⁻¹ (**Fig. 3**) are found, which could only be measured in stressed areas. Line mappings of these areas show, that a Raman intensity distribution exists over the line (**Fig. 4**).

Conclusion

Wide RAMAN Signals at 1600 and 1300 cm⁻¹ are measured only in areas with stress in the grains of the quartzite surface. A correlation between the intensity of both the Raman peaks and the stress state of quartzite grains can be postulated. Maybe a combination of polarized light microscopy and Raman spectroscopy allows getting deeper information on the surface structure of natural rocks, which are used as aggregates in concrete.

Figure 1

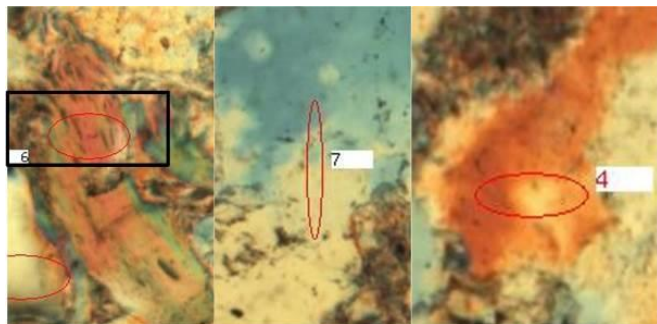


Fig. 1: Polarization micrograph with expected stressed parts on the quartzite surface; the Black box shows the dark field seen in Fig. 4

Figure 2

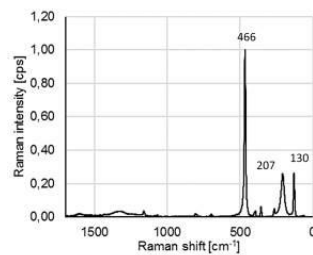


Fig. 2: Raman Spectrum of an unstressed area with typical quartz signals at 466, 207 and 130cm⁻¹

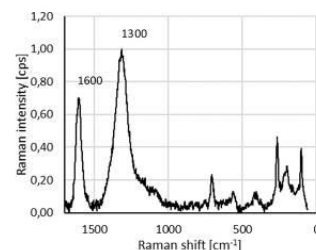


Fig. 3: Raman Spectrum of areas with expected stress, new signals are measured at 1600 and 1300cm⁻¹

P118

Bond lengths in aluminosilicate halide sodalites from 13 K to the decomposition

M. Wolpmann¹, L. Robben^{1,2}, T. M. Gesing^{1,2}¹Universität Bremen, Institut für Anorganische Chemie und Kristallographie, Bremen, Germany²Universität Bremen, MAPEX Center for Materials and Processes, Bremen, Germany

Aluminosilicate halide sodalites (SOD) [Na₈X₂][AlSiO₄]₆ (X = Cl, Br, I) belong to the simplest zeolites. The 3-dimensional framework forms *sod*-cages, containing Na and the halide anions. The interactions between the halide and Na as well as of Na with the framework are decisive for the structure-property relationships, but not yet fully elucidated. Recently, low-temperature anharmonicity was reported for the sodalite with X = I^[1] showing the need for systematic investigations on the template-framework interactions.

Therefore, scattering studies of the halide sodalites were carried out from 13 K to decomposition to determine their structures. It was the overall aim to develop a model describing the temperature-dependent behavior as well as giving insight into changes with respect to the halide anion.

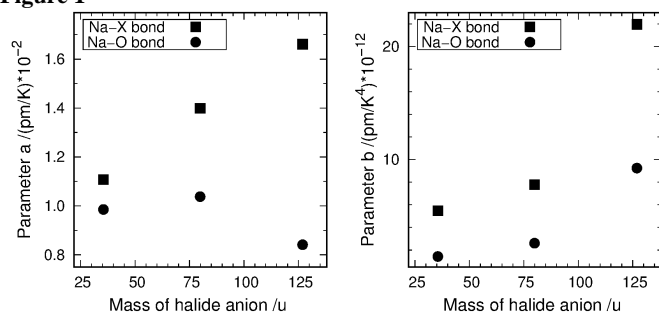
As reported earlier, the I-SOD reaches a state of full framework expansion at high temperatures, corresponding to a phase transition from P-43n to Pm-3n. The thermal expansion behavior was fitted using a Debye-model showing that the Debye temperatures have no simple (i.e. linear) correlation with the templating ion. An equation of the form $R(T) = R_0 + aT + bT^4$ was used to fit the bond-lengths, where the term bT^4 is assumed to describe the anharmonic behavior. For the Na-X bond the factor a increases linearly when plotted against the ionic mass of X while showing only small changes for the Na-O bond. The parameter b shows a distinct jump for X = I for both bonds (Figure 1).

Only the I-SOD shows strong anharmonicity in the bond-lengths behavior. While low-temperature anomalies could only be observed in neutron-diffraction experiments^[1], the general anharmonicity can be seen in the parameters resulting from the fitting of the Na-X and Na-O bond-lengths.

[1] L. Robben; I. Abrahams; M. Fischer; S. Hull; M. T. Dove and T. M. Gesing, Z. Kristallogr. <https://doi.org/10.1515/zkri-2018-2122>.

Figure 1: Parameters a and b resulting from the fitting of the Na-X and Na-O bond-lengths.

Figure 1



P119

Understanding on Microstructure Properties of Additive Manufacturing Ti-Based Alloy Composite Used as Biomedical Implants

J. C. Tseng¹, W. Chang², K. Y. Tseng², S. J. Shih³, N. T. Tsou², P. Y. Tsai⁴, C. C. Huang⁴, W. C. Huang⁵, E. W. Huang²

¹DESY, Photon science, Hamburg, Germany

²National Chiao Tung University, Department of Materials Science and Engineering, Hsin-Chu, Taiwan

³National Taiwan University of Science and Technology, Department of Materials Science and Engineering, Taipei, Taiwan

⁴Industrial Technology Research Institute, Zhudong, Taiwan

⁵Industrial Technology Research Institute, Laser and Additive Manufacturing Technology Center, Hsin-Chu, Taiwan

Ti-based alloy, in particularly Ti-6Al-4V, has developed as biomedical implant since decades because its mechanical property is well adapted to the growth of bones. In addition, Ti-6Al-4V is non-toxic, high anti-corrosive and stable over time in human body. In order to optimize the biomechanical properties for more general use such as on joint, cranial bones, tooth root, a newly porous metallic-ceramic heterogeneous system is developed via additive manufacturing approach. The mixture of bio-glasses and Ti-6Al-4V was prepared as the precursor and subsequently printed with the selective laser sintering technology. A multilayer-like composite can be obtained and tested as implants [1].

Using such manufacturing approach, the understanding on the homogeneity of phases over the printed area is essential because the additive-manufacturing quenching can strongly affect to the microstructure and associated bulk mechanical properties of composites. Therefore, the microstructure analysis and the phase mapping of as-prepared sample are studied using high energy X-ray diffraction and total scattering method. Besides, the theoretical calculation on the correlation of XRD patterns with the presence of bulk defects such as stacking faults and twin is studied.

Reference

[1] Yap, C. Y., et al. "Review of selective laser melting: Materials and applications." *Appl. Phys. Rev.* 2.4, 2015, 041101.

Acknowledgement

Ministry of Science and Technology (MOST) Program- 107-2218-E-009-003.

P120

Curie temperature studies of synthetic titanomagnetite single crystals

S. C. Lappe¹, M. Isenberg¹

¹RWTH Aachen University, Institute of Crystallography, Aachen, Germany

The titanomagnetite (*TM*) solid solution series ($\text{Fe}_{3-x}\text{Ti}_x\text{O}_4$, $0 \leq x \leq 1$) contains some of the most important natural magnetic minerals employed in paleomagnetic studies. To truly understand and utilize

the magnetic information stored within these minerals, it is important to know the exact mechanism responsible for their acquisition and retention of thermal remanent magnetisation (*TRM*). The *TRM* is mainly determined by the Curie temperature (*TC*), which strongly depends on the composition of the *TMs*. However, another factor highly influencing *TC* is the thermal history. This has only recently been discovered, when natural *TMs* showed variations in *TC* of $>150^\circ\text{C}$, when annealed at moderate temperatures (300 - 425°C) for hours to months [1]. It has been shown that the same phenomenon can be observed and reproduced in synthetic *TM* powders [2]. Many paleomagnetic studies rely on precise knowledge of *TC*, which means the observed time- and temperature dependent changes in *TC* could have a huge impact on the accuracy of those studies, such as geomagnetic paleointensity estimates and paleomagnetic paleothermometry. Measurements on natural and synthetic *TM* samples suggest that chemical clustering within the octahedral site might be responsible for the observed changes in *TC* and that the mechanism is likely to be vacancy-mediated [2,3]. To test whether the same phenomenon can be observed in *TM* single crystals, we used optical floating zone technique to grow a large (~ 6.5 mm diameter and ~ 27 mm length) *TM* single crystal. SEM-EDX measurements showed a homogenous composition of $\text{Fe}_{2.64}\text{Ti}_{0.36}\text{O}_4$ over the whole length of the crystal. Several pieces of the crystal were subjected to different annealing treatments and subsequent Curie temperature measurements. We could not detect any systematic changes in *TC* with thermal history, which leads us to conclude that the Curie temperature of stoichiometric single crystals does not show the strong dependency on thermal history as was observed for *TM* powders.

[1] Bowles, J. A., Jackson, M. J., Berquó, T. S., Solheid, P. A. and Gee, J. S. (2013), *Nature Communications*, 4, 1916.

<https://doi:10.1038/ncomms2938>

[2] Bowles, J. A., Lappe, S.-C. L. L., Jackson, M. J. and Arenholz, E. (2018), *in prep.*

[3] Jackson, M. J., and Bowles, J. A. (2018), *J. Geophys. Res.*, 123, 1-20. <https://doi:10.1002/2017JB015193>

P121

FAPbBr₃ – about the influence of deuteration: A temperature dependent neutron diffraction study

A. Franz¹, D. M. Többers¹, F. Lehmann¹, M. Kärgell¹, S. Schorr^{1,2}

¹Helmholtz-Zentrum Berlin, Structure and Dynamics of Energy Materials, Berlin, Germany

²Freie Universität Berlin, Institut für Geologische Wissenschaften, Berlin, Germany

Perovskite materials - which due to their chemical diversity reveal an intriguing amount of physical properties - have recently gained renewed interest following the discovery of hybrid perovskite structures and their high energy conversion efficiencies, making these materials attractive for photovoltaic applications.

Just like the "classic" oxide perovskites with its ABX_3 stoichiometry hybrid perovskites show corner sharing BX_6 octahedra networks. In contrast to the inorganic $\text{A}^{[\text{XIII}]}$ cation in the oxide perovskite the hybrid perovskite's A cation is an organic molecule which is surrounded by 12 halide anions (X). One of the materials with record-breaking solar energy conversion efficiencies of 22.1 % (1) is methylammonium lead iodide ($\text{CH}_3\text{NH}_3\text{PbI}_3$ - MAPbI_3). Solid solutions with either substitution of the organic molecule, the halide anion or both, give the opportunity to further tailor and improve physical properties.

The substitution of the A cation by formamidinium ($\text{CH}(\text{NH}_2)_2$ - FA) and the iodine by bromine leads to formamidinium lead

bromide (FAPbBr₃) which gained interest as a material used as a wide bandgap [2.27eV(2)] absorber material in tandem solar cells. Although thin film synthesis and optoelectronic properties are known only a minor emphasis is put on the influence of crystal structure and the interplay of octahedral tilting and organic unit.

We present a study about the structural determination of FAPbBr₃ over the range of 3 – 300K using neutron- and X-ray diffraction techniques (HZB, BERII – E9 and BESSYII – KMC-2) with emphasis on the different orientational disordering of the formamidinium molecule in dependence of partly deuteration of the formamidinium molecule.

[1] NREL (2018)

<https://www.nrel.gov/pv/assets/images/efficiency-chart.png>

[2] T. J. Jacobsson *et al.* *Energy Environ. Sci.*, 2016, 9, 1706

P122

Investigations on copper iodide as a thermoelectric material

T. Stollenwerk¹, O. Oeckler¹

¹Universität Leipzig, IMKM, Leipzig, Germany

Copper iodide CuI is a wide band gap (3.1 eV) multifunctional p-type semiconductor that has recently attracted attention with respect to several potential applications.[1] At ambient pressure, four polymorphs have been described: α -CuI crystallizing in the rock-salt type, β -CuI in the wurtzite type and γ -CuI in the sphalerite type and a fourth polymorph in the delafossite structure type.[2,3,4] In addition to compelling optoelectronic properties, CuI thin films are among the very few transparent thermoelectric materials. They reach thermoelectric figures of merit up to ZT = 0.21.[5] Experiments to reproduce such ZT values in pristine bulk material are intriguing but have not yet been successful.

Attempts towards such materials include solid solutions Cu_xAg_{1-x}I with 0 < x < 1, because of the closely related structural chemistry of AgI.[6] Compositions were confirmed by X-ray spectroscopy and powder X-ray diffraction yields a Vegard-like relationship for such solid solutions.[7] Thermoelectric properties are still rather poor because of low electrical conductivity. At elevated temperatures, the vapor pressure of iodine leads to changes of the iodine content. This was quantified by DSC and DTA/TG measurements. Compositional changes probably affect the thermoelectric properties in a very pronounced way.

Since syntheses from melts do not provide transparent material, the copper/iodine ratio was altered. Lower iodine contents lead to transparent samples. Reactions between copper and iodine usually afford elemental copper as a side phase next to transparent CuI. Single crystals from such samples were analysed by means of synchrotron radiation at the ESRF (Grenoble). Their structure corresponds to the delafossite structure type.[2]

[1] C. Yang, M. Kneiß, M. Lorenz, M. Grundmann, *Proc. Nat. Acad. Sci.* **2016**, 113, 12929.

[2] D. A. Keen, S. Hull, *J. Phys. Condens. Matter*, **1995**, 7, 5793.

[3] D. A. Keen, S. Hull, *J. Phys. Condens. Matter*, **1994**, 6, 1637.

[4] C. Schwab, A. Goltzené, *Prog. Cryst. Growth & Charact.*, **1982**, 5, 233.

[5] C. Yang, D. Souchay, M. Kneiß, M. Bogner, H. M. Wei, M. Lorenz, O. Oeckler, G. Benstetter, Y. Q. Fu and M. Grundmann, *Nat. Commun.*, **2017**, 8.

[6] J. W. Brightwell, C. N. Buckley and B. Ray, *Phys. Status Solidi A*, **1982**, 69.

[7] M. Johan, T. Leng, N. Hawari und S. Suan, *Int. J. Electrochem. Sci.*, **2010**, 6, 6235.

P123

Comparative study on the axial negative thermal expansion of linear α - and zig-zag chain backboned β -PbAlBO₄.

M. Gogolin^{1,2}, M. M. Murshed^{1,2}, T. M. Gesing^{1,2}

¹Universität Bremen, Chemische Kristallographie fester Stoffe, Institut für Anorganische Chemie und Kristallographie, Bremen, Germany

²Universität Bremen, MAPEX Center for Materials and Processes, Bremen, Germany

Keywords: Lone electron pair, PbAlBO₄, DFT, X-ray and neutron diffraction, thermal expansion

We report a comparative study between the two polymorphs of α -PbAlBO₄ and β -PbAlBO₄ (Fig.). The low-temperature α -PbAlBO₄ phase crystallizes in space group *Pnam* and features mullite-type edge-sharing AlO₆ octahedra. The high-temperature β -PbAlBO₄ phase is described in space group *Pbcn*¹, where the AlO₆ octahedra form a zig-zag chain (Fig.). In both cases, the AlO₆ octahedra are bridged by planar BO₃ groups and the Pb²⁺ cations are located in channels. Based on temperature- and pressure-dependent diffraction studies, both compounds show axial negative linear compressibility (ANLC) in the **b**-direction and axial negative thermal expansion (ANTE) in the **a**-direction. The lattice thermal expansions of these phases are simulated using DFT and the Grüneisen first-order approximation, where the change of the lattice energy is calculated by the Debye-Einstein-Anharmonicity approach²⁻⁴. Raman spectroscopy is used to substantiate the lattice dynamics of the models. The thermal expansion anisotropy is found to be a delicate interplay between the axial Grüneisen parameters and the elastic tensors. The stereochemical activity of the 6s² lone electron pairs of Pb²⁺ is identified to be an important factor in both the ANLC and ANTE.

Figure 1: Crystal structures of α -PbAlBO₄ (left) and β -PbAlBO₄ (right).

References:

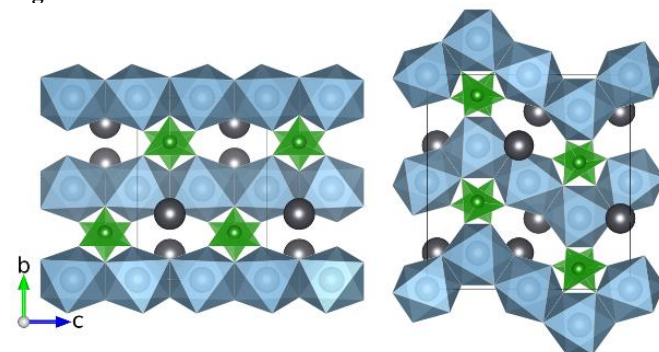
[1] H. Park *et al.*, *Solid State Sci.* **5** (2003) 565–571.

[2] M. M. Murshed *et al.*, *Mater. Res. Bull.* **84** (2016) 273–282.

[3] M. M. Murshed *et al.*, *J. Am. Ceram. Soc.* **100** (2017) 5259–5273.

[4] M. M. Murshed *et al.*, *Z. Anorg. Allg. Chem.* **644** (2018) 253–259.

Figure 1



P124

Synthesis and characterization of $(\text{Bi}_{1-x}\text{R}_x)_2\text{Mn}_4\text{O}_{10}$ ($\text{R} = \text{Nd}, \text{Sm}$ and Eu) for $x = 0.0 - 1.0$ K. Ghosh¹, T. M. Gesing¹, M. M. Murshed¹¹Universität Bremen, Institut für Anorganische Chemie und Kristallographie, Bremen, Germany

Members of the multiferroic $\text{R}_2\text{Mn}_4\text{O}_5$ ($\text{R} = \text{Y}, \text{Bi}$ and rare earth elements) family are well known for their concomitant presence of two or more order parameters at a given temperature [1]. Due to centrosymmetric structure the microscopic origin of the type-I and type-II multiferroic behavior were explained in term of complex interplay between spin-ordering, highly polarizable Bi^{3+} with lone electron pair, $\text{Mn}^{3+}/\text{Mn}^{4+}$ charge-ordering and elastic interaction-led local distortions of the coordination polyhedra. Recently, mixed-phase $(\text{Sm}, \text{Gd})\text{Mn}_2\text{O}_5$ has been demonstrated as an efficient substitute for the commercial Pt-based catalysts, which was claimed to be superior to Pt in terms of cost, thermal durability, and catalytic activity for NO oxidation [2]. Since the crystal-physical properties of mullite-type $\text{R}_2\text{Mn}_4\text{O}_{10}$ greatly depend on the type of R-cation [3], we report on a systematic studies on $(\text{Bi}_{1-x}\text{R}_x)_2\text{Mn}_4\text{O}_{10}$ ($\text{R} = \text{Nd}, \text{Sm}$ and Eu) solid solution using X-ray diffraction, infrared, Raman and UV-Vis spectroscopies and thermal analyses. The compounds were synthesized by the glycerin method followed by conventional solid-state reaction. Where the a - and c -lattice parameters gradually decrease with increasing x in all cases, the b -lattice parameter showed a Gaussian peak-shape change with the maximum value at $x \sim 0.5$ for the $(\text{Bi}_{1-x}\text{Eu}_x)_2\text{Mn}_4\text{O}_{10}$ series. The Wang-Liebau eccentricity parameter describing in this case the stereochemical activity of the lone electron pair of Bi^{3+} cations, as well as the polyhedral distortions (mean quadratic elongation) were analyzed as function of x . Both, the Raman and infrared modes exhibited a global blue-shift associated with the shrinkage of the cell volume with increasing x . Since Nd^{3+} , Sm^{3+} and Eu^{3+} are Van Vleck cation [4], these solid solution would be particularly interesting to demonstrate how the successive dilution of the magnetic cations play roles on the temperature-independent magnetic properties.

Reference

- [1] D. Khomskii, *Physics (College Park, Md)*. **2009**, 2, 20.
 [2] W. Wang, G. McCool, N. Kapur, G. Yuan, B. Shan, M. Nguyen, U.M. Graham, B.H. Davis, G. Jacobs, K. Cho, X. Hao, *Science* **2012**, (80-). 337, 832–835.
 [3] M. Tachibana, K. Akiyama, H. Kawaji, T. Atake, *Phys. Rev. B - Condens. Matter Mater. Phys.* **2005**, 72, 3–6.
 [4] Y. Takikawa, S. Ebisu, S. Nagata, *J. Phys. Chem. Solids* **2010**, 71, 1592–1598.

P125

Ferroelectricity, ionic conductivity and structural paths for large cations migration in $\text{Ca}_{10.5-x}\text{Pb}_x(\text{VO}_4)_7$ single crystals, $x = 1.9, 3.5, 4.9$ D. Deyneko¹, D. Petrova¹, B. Lazoryak¹, S. Aksenov¹¹Lomonosov Moscow State University, Chemistry Department, Moscow, Russian Federation

Crystal structure, thermal, dielectric and optical second harmonic activity were investigated for whitlockite-type $\text{Ca}_{8.6}\text{Pb}_{1.9}(\text{VO}_4)_7$ (**1**), $\text{Ca}_7\text{Pb}_{3.5}(\text{VO}_4)_7$ (**2**) and $\text{Ca}_{5.6}\text{Pb}_{4.9}(\text{VO}_4)_7$ (**3**) single crystals. The refinement of the structure revealed splitting of the $M3$ and $M4$ sites into two and three sub-positions respectively. Splitting of the $M3$ and $M4$ sites strongly enhances nonlinear optical activity, measured on powders, with the effect vanishing at ferroelectric phase transitions at elevated temperatures. Single crystals (**1**) and (**2**) undergo two structural transformations: ferroelectric one between 750–1150 K and a subsequent phase transition at higher temperatures. Structural mechanism of the ferroelectric phase

transition is analyzed with respect to the rearrangement of Ca^{2+} and Pb^{2+} over their positions in the ferroelectric and paraelectric phases. Large Pb^{2+} ions substitution for calcium proceeds unit cell expansion with consequent extending of ion migration channels, thus leading to enhanced ionic conductivity in the Pb-rich materials. It is concluded that in spite of steric hindrances for lead cations, they effectively move between positions $M2 - M4 - M1$ or $M1 - M4 - M2$ together with calcium cations across the crystal. The cations conduction pathways as well as the migration energies of Ca^{2+} and Pb^{2+} cations were calculated by the bond valence energy landscapes (BVLE) method. Among the obtained single crystals, (**3**) demonstrated the highest ionic conductivity, maximum SHG signal and the lowest temperature of ferroelectric phase transition.

Author index

A		
Abdelbaky, M. S. M.	115	
Abdul Azeze, M. S. T.	72	
Abernathy, D. L.	50	
Abosede, O.	115	
Absmeier, E.	4	
Acker, J.	122	
Adam, M.	48	
Ait Haddouch, M.	50	
Akhmetova, I.	87	
Akhmetshina, T. G.	53	
Akselrud, L.	6	
Aksenov, S.	125	
Albrecht, R.	89	
Ali, B.	117	
Ali, S. I.	38	
Alig, E.	9, 113	
Alvaro, M.	43, 81	
Amer, L.	85	
Amjadi, R.	70	
Angel, R.	43, 81	
Anurova, M.	53	
Aprilis, G.	22	
Arimoto, I.	105	
Aroyo, M.	64	
Arzig, M.	65	
Auer, H.	67, 99, 100	
Avalos-Borja, M.	90	
B		
Bächli, A.	64	
Balogh-Michels, Z.	64	
Banchenko, S.	5	
Bareiß, K.	87	
Barkov, A.	92	
Barnett, S.	23	
Barthel, T.	32, 75	
Baruch, P.	31	
Bayarjargal, L.	20, 80, 117	
Beck, T.	15	
Becker, B.	48	
Becker, H.	9, 23	
Becker, N.	49, 120	
Becker, P.	57, 82, 118	
Behrens, M.	33	
Beirau, T.	20	
Benndorf, C.	6, 10	
Benning, M.	105	
Bensch, W.	12	
Bento, I.	74	
Bergh, T.	23	
Bertmer, M.	6, 100	
Bette, S.	36, 52, 65	
Bianga, C. M.	56	
Binck, J.	49, 80, 92	
Binder, J. R.	83	
Bini, R.	43	
Birkenstock, J.	69	
Bismayer, U.	17, 20	
Blake, G. R.	7	
Blanchet, C. E.	74	
Blankenfeldt, W.	29	
Bobnar, M.	6	
Bodach, A.	9	
Boese, R.	113	
Bohatý, L.	118	
Bolormaa, O.	107	
Botti, S.	49	
Bourenkov, G.	74	
Brandstetter, H.	29, 72	
Brantl, J. N.	68	
Breitfeld, S.	112, 113	
Breternitz, J.	23, 103	
Breunig, O.	118	
Bricogne, G.	40	
Brik, O.	120	
Brücher, E.	98	
Brütting, C.	31	
Bubnova, R.	39, 67	
Budzianowski, A.	103	
Bujacz, A.	28	
Burianek, M.	21, 61	
Burkhardt, A.	18, 74	
Burkhardt, U.	6	
Büscher, J.	20	
Buyer, C.	95	
Bykov, M.	22, 76	
Bykova, E.	22, 76	
C		
Canēvet, E.	121	
Caron, L.	44	
Cervellino, A.	121	
Chamorro Orue, A. I.	113	
Chang, W.	123	
Chariton, S.	80	
Chen, P.	102	
Chernikov, R.	49	
Chernyshov, D.	53	
Cisarova, I.	118	
Clausing, A.	109	
Conrad, M.	85, 86, 116	
Cramer, J.	31	
Crosas, E.	74	
Curth, U.	31	
D		
Dahms, S. O.	29, 72	
Dall, E.	29	
Danilevsky, A.	65	
Dankwort, T.	12	
Danneberg, M.	110, 122	
Darma, S.	83	
Daub, M.	88, 101, 102	
Daumke, O.	70	
Davaasambuu, J.	117	
Day, G.	36	
de la Flor, G.	64	
De Negri, S.	53	
Delley, B.	19, 20	
Deng, H.	44, 106	
Dey, S.	101	
Deyneko, D.	125	
Dickmanns, A.	29	
Diederichs, K.	40	
Diehl, L.	36	
Diez, S.	55	
Dinnebier, R. E.	25, 36, 52, 65, 79	
Djendjur, P.	93	
Doert, T.	76, 77, 89	
Doi, T.	105	
Dominik, T.	95	
Doroshenko, M.	86	
Dousza, R.	40	
Dronskowski, R.	17, 50	
Du, X.	44	
Dubrovinskaia, N.	22, 81	
Dubrovinsky, L.	22, 80, 81	
Dudchenko, N.	120	
Dunaeva, E.	86	
Dunzendorfer-Matt, T.	70	
Durst, R.	48	
Dutta, R.	106	
Dziubek, K.	43	
E		
Eckner, S.	49	
Eckold, G.	52	
Effenberger, H.	6	
Eggert, G.	52	
Ehrenberg, H.	83	
Eich, A.	44, 107	
Eisele, C.	53, 101, 121	
Eisenburger, L.	99	
Emmerling, F.	83, 84, 87, 92, 112, 113	
Ende, M.	43, 60	
Ener, S.	67	
Englert, U.	17, 55, 63	
Epple, M.	10, 12, 109, 110	
Eremin, R. A.	53	
Etter, M.	11, 83, 103, 111	
Evarestov, R.	64	
F		
Falk, M.	96	
Fechtelkord, M.	49, 120	
Feddersen, B.	31	
Fedorov, R.	31	
Fedotenko, T.	22	
Fehér, B.	6	
Feiler, C.	32, 41, 75	
Felici, R.	33	
Feng, C.	117	
Fertey, P.	43	
Feulner, F.	53	
Ficner, R.	15, 29	
Filatov, S.	39, 67	
Finger, R.	66, 67	
Fink, L.	9, 113	
Finzel, K.	76	
Fischer, L.	61, 69	
Fischer, M.	55, 56, 122	
Fischer, P.	74	
Fischer, R. X.	21, 61, 68, 69	
Flensburg, C.	40	
Förster, A.	66	
Förster, R.	41	
Förster, S.	33, 34	
Frank, W.	56, 59, 92, 93, 94, 95, 114	
Franz, A.	6, 23, 33, 36, 58, 59, 103, 123	
Freese, F.	114	
Fries, M.	67	
Friese, K.	44, 50, 106	
Fritsch, D.	20	
Fritsch, P.	67	

Author index

Fuchizaki, K.	81	Hausstühl, E.	20	K	
Führung, J.	31	Havlíček, D.	13	Kaercher, J.	48
Funk, C.	98	Hayashi, M.	113	Kärgell, M.	123
G		He, H.	41, 86	Karttunen, A.	116
Gadelmawla, A.	69	Heggen, M.	12, 109	Kasaragod, V.	31
Gajda, R.	43	Heidemann, J. L.	29	Kastner, A.	41
Gallo, G.	65	Heiker, J. T.	72	Katzmann, E.	46
Galluccio, S.	96	Heine, T.	71	Kawata, K.	27
Garbarino, G.	43	Hellmig, M.	41	Kay-Fedorov, P.	31
García-Granda, S.	115	Hennig, C.	47	Keller, P.	40
Gehlhaar, F.	10	Heppke, E.	58	Kemnitz, E.	112, 113
Georg, I.	113	Herath, S.	56	Khadiev, A.	58, 60
Georgii, R.	121	Hergert, W.	33	Khakurel, K.	108
Gerald, G.	95	Hering, P.	44	Khalitov, Z.	60
Gerardy-Schahn, R.	31	Hermann, R. P.	50	Khandarkhaeva, S.	22
Gerlach, M.	32, 41	Herold, S.	122	Kheireddine, A.	90
Germann, L. S.	25	Herrmann, M.	50	Khutia, A.	27
Gesing, T.	102	Herzog, T.	35	Kienle, L.	12
Gesing, T. M.	66, 80, 122, 124, 125	Hierse, W.	27	Kimura, F.	46, 47, 105
Ghoroi, C.	72	Hikita, M.	75	Kimura, T.	46, 47, 105
Ghosh, K.	125	Hilal, T.	15	Kimura, Y.	113
Girard, A.	44	Hilgenfeld, R.	31	Kirkkala, T.	60
Gischkat, T.	64	Hillebrecht, H.	76, 88, 101, 102	Kirsch, A.	66
Glante, S.	65	Hillig, R.	32	Kitaev, Y.	64
Glazyrin, K.	22, 44, 76	Hinrichsen, B.	79	Kitagawa, H.	113
Gless, C.	41	Hirsch, A.	50	Klar, P. B.	77
Glöckner, S.	32	Hoch, C.	91, 92, 97, 100	Klebe, G.	32
Goddard, R.	17	Hoelzel, M.	116	Klein, C.	66
Goerigk, F. C.	93	Hofmann, D. W. M.	34, 63	Kloda, M.	118
Goffinet, C.	31	Hohl, T.	91	Klünemann, T.	29
Gogolin, M.	102, 124	Hollenbeck, L.	57	Knapp, M.	83
Gotthold, C.	5	Hollerweger, J.	29	Koch, C.	12
Gottschalch, V.	85	Holthausen, J.	50	Koemets, E.	22
Götze, A.	12, 13, 67	Horii, S.	105	Kofahl, C.	52
Graf, J.	105, 114	Hornfeck, W.	23, 24, 57	Köhler, J.	76, 98
Greiner, S.	94	Hoser, A.	103	Köhler, K.	86
Grifone, R.	58	Hosseini-Yazdi, S. A.	112	Köhler, T.	118
Grimm, N.	103	Hua, W.	83, 123	Kohlmann, H.	6, 12, 13, 22, 66 67, 99, 100
Grimmer, H.	19, 20	Huang, Y.	15	Kolb, U.	2, 9
Grin, Y.	6	Hübschle, C. B.	26	Kolesnikov, I.	39
Groeneveld, J. D.	61	Huebschle, C.	53	Kositz, M.	110
Grüner, C.	56, 69	Huittinen, N.	50	Kratky, J.	71
Grzechnik, A.	44, 106, 107	Hunger, J.	89	Kratzert, D.	116
Guenther, S.	74	Hutanu, V.	44	Kraus, F.	116
Gunder, R.	20, 49	I		Krauß, N.	16
Günther, D.	99	Ihadjaren, K.	89	Krausze, J.	28
Gurieva, G.	20, 33, 36, 49	Ikeda-Ohno, A.	47	Krautscheid, H.	85, 112
Gurskaya, A. V.	53	Indris, S.	83	Kremer, M.	17, 55
Gutfleisch, O.	67	Inomata, K.	16	Kriegel, M. J.	9
Güthoff, F.	52	Isenberg, M.	123	Krummer, M.	88
H		Ivlev, S.	116	Krupp, F.	5
Habermehl, S.	26	Ivleva, L.	86	Krzhizhanovskaya, M.	67
Hai An Bui, N.	53	J		Kuesel, S.	112
Hakanpää, J.	74	Jachalke, S.	118	Kühn, C.	27
Halasz, I.	36	Jakob, M.	82	Kuleshova, L.	34
Hamdi Ben Yahia, H.	90	Jankus, S.	118	Künzle, M.	15
Hammer, S.	79	Jeffries, C.	74	Küpers, M.	50
Hammerath, F.	67	Jess, I.	25	Kusov, Y.	31
Hanke, S.	72	Jia, J.	4	L	
Hanzig, J.	118	Johnson, D.	12, 44	Lach, M.	15
Hardes, K.	72	Johnsson, M.	38	Lahey-Rudolph, M.	42, 74
Hartmann, M.	65	Juarez-Arellano, E. A.	92	Lamparter, T.	16
Hauß, T.	41			Langenmaier, M.	68

Author index

Layer, G.	29	Meyerheim, H.	33	Peresypkina, E.	18, 25, 26
Lazoryak, B.	125	Mezouar, M.	43	Peschke, I.	88
Lehmann, B.	100	Michael, N.	16	Peters, L.	50
Lehmann, C. W.	107	Michaelsen, C.	105	Petersen, H.	80, 109
Lehmann, F.	23, 59, 118, 123	Mihailova, B.	43, 81	Petrik, M.	23, 24
Leineweber, A.	9, 23	Mikhailova, D.	13, 34	Petrova, D.	125
Leisegang, T.	53, 118	Miletich, R.	43, 60	Pflug, C.	22
Lenz, S.	68	Miller, R. J. D.	40	Pielnhofer, F.	25, 36
Lenzen, D.	111	Mohseni, K.	33	Pietrzyk-Brzezinska, A. J.	4
Li, Y.	2, 23, 39, 44, 90	Möllmer, J.	12, 13	Pippel, J.	72
Lian, H.	7	Mondal, S.	101	Plášil, J.	110
Lichte, M.	114	Moon, D.	17	Plocek, J.	13
Lidin, S.	38	Morgenroth, W.	49, 90, 92	Poddig, H.	77
Liedtke-Grüner, S.	69	Müller, J.	77	Pöllmann, H.	20, 80, 96, 121
Lieske, J.	31	Muller, Y. A.	4	Pompidor, G.	74
Lin, D.	31	Müller-Werkmeister, H. M.	40	Pöthig, A.	25
Lin, Y.	90	Münchgesang, W.	118	Povolotskiy, A.	39
Link, L.	90	Murri, M.	81	Prakapenka, V.	44
Lissner, F.	98	Murshed, M. M.	66, 102, 124, 125	Prakash, O.	31
Litterst, F. J.	66	Murzin, V.	49	Preiß, C.	49
Lohöfener, J.	31	Mutka, H.	118	Prencipe, M.	43
Loitzenbauer, M.	60			Prescher, C.	44
Loll, B.	15	N		Preuß, A.	29
Lorbeer, O.	74	Nagano, S.	16	Prill, D.	26
Lorenz, T.	118	Nallathamby, P. D.	10	Prinz, N.	46
Lösch, H.	50	Naruta, H.	81	Proserpio, D. M.	53
Lotnyk, A.	33, 56, 69	Näther, C.	25	Prots, Y.	6
Lotsch, B. V.	36, 97	Neder, R.	37, 55	Prymak, O.	10
Loza, K.	12, 109	Neder, R. B.	9		
Lübben, J.	26	Neels, A.	64	R	
Luchitskaia, R.	20	Nemec, I.	118	Raabe, J.	58
Lüdicke, M.	76	Nénert, G.	7	Radchuk, V.	120
Lutz, W.	35	Nentwich, M.	106	Radcliffe, P.	105
M		Neumann, P.	15, 29	Radnik, J.	110
Ma, Q.	31	Neumann, T.	25	Radoske, T.	47
Machlus, S.	79	Neumeier, S.	50	Ramakrishnan, S.	53, 121
Majewski, M.	59	Nguyen, T. Y.	83, 84	Rauschenbach, B.	33, 56, 69
Majzlan, J.	110	Niedenzu, S.	33	Redecke, L.	42, 74
Makal, A.	43	Niemann, H.	5	Reichert, D.	109
Maletti, S.	13, 34	Niewa, R.	90	Reime, B.	18, 74
Mändl, S.	47	Noohinejad, L.	112	Reinsch, H.	111
Manfred, W.	95	Nöthling, N.	17, 107	Reissner, C. E.	20
Manolikakes, G.	9	Novikov, D.	58	Rekis, T.	53
Manova, D.	47	Nowell, H.	23	Richter, C.	106
Manstein, D.	31	O		Ritter, K.	49
Marler, B.	61	Oeckler, O.	6, 10, 82, 99, 124	Ritterbach, L.	82
Martin, S.	9	Ollivier, J.	118	Robben, L.	80, 82, 109, 122
Matsugaki, N.	75	Opahle, I.	67	Roder, M.	65
Maurin, G.	111	Orobengoa, D.	64	Roeder, R. K.	10
McDonagh, D.	36	Oswald, S.	34	Roger, D.	105
Medarde, M.	121	Otgonbayar, C.	121	Röhr, C.	68, 86, 92, 96, 100
Meents, A.	74	Ott, H.	26, 105	Routier, F.	31
Mehner, E.	106, 118			Rouvimov, S.	10
Mehrabi, P.	40	P		Royant, A.	41
Mensing, M.	56, 69	Paciorek, W.	40	Ruck, M.	89
Merkelbach, J.	92	Pai, E. F.	40	Rudolph, D.	97
Merker, S.	85	Pakendorf, T.	18, 74	Rüegg, C.	121
Merz, K.	113	Palanisamy, P.	72	Ruf, A.	32
Metz, A.	32	Palatinus, L.	2, 110	Ruf, M.	26
Meutzner, F.	58	Paliwoda, D.	103	Ruiz-Fuertes, J.	44
Meven, M.	17, 44, 106	Panneerselvam, S.	74	Rusinek, D.	103
Meyer, D. C.	106, 118	Papashvili, A.	86	Rutkiewicz, M.	28, 41
Meyer, J.	74	Pappert, K.	12		
Meyer, S. P.	98	Paulmann, C.	90, 101		

Author index

S		
Saccone, A.	53	
Said, N.	15	
Sakagami, T.	81	
Sala, G.	50	
Sänger, I.	113	
Sappl, J.	91	
Sarapulova, A.	13	
Scelta, D.	43	
Schaller, A. M.	53, 76	
Schauerte, C.	113	
Scheer, M.	18, 25, 26	
Scheerer, P.	16	
Scheffzek, K.	70	
Scheinost, A.	47	
Schell, N.	49	
Schellhase, S.	92	
Schierholz, R.	12	
Schindelin, H.	31	
Schleid, T.	85, 87, 93, 94, 95, 97, 98	
Schlesinger, C.	26, 79	
Schmidt, E.	37	
Schmidt, M.	50, 79, 94	
Schmidt-May, J.	105	
Schmuckermaier, L.	41	
Schneider, H.	68	
Schneider, T.	74	
Schnelle, W.	6	
Schnick, W.	90, 99	
Schnohr, C.	49	
Schökel, A.	11, 83, 111	
Scholz, G.	112, 113	
Schönherr, R.	42, 74	
Schorr, S.	20, 23, 33, 36, 49, 59 103, 105, 118, 123	
Schreyer, M.	7	
Schuck, G.	118	
Schulz, B.	97	
Schulz, E. C.	40	
Schulze-Briese, C.	66	
Schumacher, P.	56, 69	
Schumann, F.	33	
Schwarz, B.	83	
Schwarz, T.	109	
Schwarz, U.	6	
Schwefel, D.	5	
Schweininger, J.	4	
Senda, T.	75	
Shablinskii, A.	39	
Shang, T.	121	
Shannon, R. D.	21, 61	
Sharff, A.	40	
Sharma, P.	83	
Sheptyakov, D.	121	
Shpenkov, G.	19	
Simon, E.	67	
Simonov, A.	37	
Sinn, T.	91	
Sisak Jung, D.	36	
Skoulatos, M.	121	
Söhnel, T.	76	
Solokha, P.	53	
Song, J.	49	
Souici, A.	89	
Spahn, C.	5	
Spahr, D.	49, 90	
Spiess, I.	69	
Stachowicz, M.	43	
Stan, C.	43, 81, 92	
Stangarone, C.	43, 81	
Steciuk, G.	110	
Stefanski, J.	44	
Steffien, M.	41	
Steiner, J.	65	
Steinke, N.	31	
Steinmetzer, T.	72	
Stękiel, M.	44, 49	
Stevanovic, I.	64	
Stöber, S.	80	
Stock, N.	111	
Stock, V.	61	
Stöcker, H.	106, 118	
Stoffel, R.	50	
Stöger, B.	53	
Stollenwerk, T.	124	
Stöwe, K.	77, 109	
Sträter, N.	71, 72	
Stroh, J.	83	
Stübe, N.	74	
Stuerzer, T.	48	
Stürzer, T.	105	
Sulcek, L.	49, 120	
Sutula, S.	43	
Svergun, D. I.	74	
Szakáll, S.	6	
T		
Taberman, H.	41, 70	
Takagi, H.	36, 112	
Takayama, T.	36	
Talla, D.	50, 60	
Tamura, N.	92	
Tasci, E.	64	
Tegshbayar, N.	107	
Tellkamp, F.	40	
Terban, M.	79	
Than, M. E.	72	
Thiruvakatam, V.	72	
Thoelen, F.	94, 95	
Thomä, S.	46	
Thorn, A.	57	
Tickle, I.	40	
Tindall, C. A.	72	
Tischler, D.	71	
Többens, D. M.	23, 105, 106, 123	
Tolkiehn, M.	53, 90	
Tovar, M.	103	
Tridane, M.	8	
Truong, K.-N.	17	
Tsogbadrakh, N.	117	
TSookhuu, K.	107	
Tsuboi, C.	46	
Tsukui, S.	46, 47	
Tuvjargal, N.	117	
U		
Ulbricht, D.	72	
V		
Váczí, T.	6	
van Gerven, D. J.	7	
van Smaalen, S.	53, 76, 101, 112, 121	
van Terwingen, S.	63	
van Well, N.	53, 112, 121	
Varentsov, D.	49	
Vaughan, G.	82	
Virovets, A.	18, 25, 26	
Voigt, J.	50	
von Essen, C.	27	
von Stetten, D.	74	
Vonrhein, C.	40	
Voronina, I.	86	
Vullum, P. E.	23	
W		
Wada, M.	105	
Waesermann, N.	43	
Wagner, M.	113	
Wahiduzzaman, M.	111	
Wahl, M.	15	
Wahl, M. C.	4	
Wallacher, D.	32, 75, 103	
Wang, Z.	103	
Warmer, M.	74	
Weber, M.	109	
Weigel, T.	106	
Weirich, T. E.	65	
Weiss, M.	5	
Weiss, M. S.	28, 32, 41, 70, 75	
Weiß, R. H.	71	
Wellmann, P.	65	
Welter, E.	49	
Wendl, S.	99	
Wendschuh, M.	69	
Wendt, M.	11, 111	
Wenz, S.	11, 111	
Werner, J.	65	
Werwein, A.	6	
Wetzel, O.	109	
Wharmby, M.	11, 111	
Wickleder, M. S.	7	
Widdra, W.	33, 34	
Wiedemann, D.	58	
Wieprecht, W.	35	
Wildner, M.	50, 51, 60, 95	
Wilk, P.	41	
Wilke, M.	87	
Winkler, B.	20, 44, 49, 80, 90, 92	
Withers, R.	2	
Wolf, S.	7, 95, 96	
Wollenhaupt, J.	32, 41	
Wolpmann, M.	122	
Wozniak, K.	43	
Wurmehl, S.	67	
Wuttig, M.	12	
X		
Xiao, B.	50	
Y		
Yadava, U.	4	
Yoshida, Y.	113	
Yoshimura, M.	105	

Author index

Z

Zaffiro, G.	81
Zajzon, N.	6
Zegarra Solano, C. A.	92
Zeymer, O.	31
Zhang, H.	67
Zhang, L.	31, 83
Zhao, H.	9
Zhou, X.	31
Zimmer, D.	44, 96
Zimmermann, B.	88
Zizak, I.	105
Zobel, M.	46
Zollner, E. M.	33
Zou, X.	2
Zschornak, M.	106
Zubow, K.	16